University College London

Measurement of Liquid Fuel within the Cylinder of a Spark Ignition Engine

Ph.D. Thesis

Greg Taylor

January 2005

This thesis is submitted in partial fulfillment of the requirements for the degree of Doctor of Philosophy

ProQuest LLC
789 East Eisenhower Parkway
P.O. Box 1346
Ann Arbor, MI 48106-1346

ABSTRACT

It is appreciated that the deposition of liquid gasoline on the wall of the cylinder liner is known to be detrimental to the life of an SI engine. Liquid fuel on the combustion chamber and cylinder liner surfaces may lead to an increase in hydrocarbon emissions, particularly during cold-start operation. In addition, liquid fuel on the cylinder bore may wash the protective oil film from the surface liner, making it vulnerable to increased wear and chemical attack by the corrosive combustion chamber products (the latter particularly true when the liner surface is still cold, promoting the condensation of acids). Finally, liquid fuel on the cylinder wall may pass the piston rings, particularly when clearances are at their largest, causing high rates of 'lost fuel' to the crankcase and dilution of the crankcase oil.

In 1997 BMW admitted they had a problem with their small capacity 6-cylinder engines. BMW was forced to retrofit customer cars with new engines after relatively low mileage and change the design of the engine from Nikasil coated aluminium liners to a more durable cast iron liner. Nikasil coated liners are particularly vulnerable due to the fact that the nickel coating is relatively thin. If wear of the cylinder wall exceeds the 80-micron coating thickness, then the softer aluminium backing material is exposed and wear is accelerated.

The Jaguar AJV8 engine employs Nikasil liners similar to those used by BMW. There has been no published information suggesting that there is a bore wear concern with the Jaguar AJV8. However, being able to evaluate the deposition of liquid fuel of the cylinder wall of an engine during the development process would be extremely valuable. This thesis details the instrumentation, tools and techniques which can be used for such analysis. The results obtained provide an insight into the wall wetting characteristics of a number of four-valve cylinder head designs. There is an absence of such information in the scientific literature. This research suggests that the engine geometries tested in this work should not suffer from any durability concerns related to bore wetting.

ACKNOWLEDGEMENTS

This work was only possible due to the help I received from many individuals. Most importantly, I must thank my supervisor Dr. Paul Williams for his help and support throughout this study.

Thanks go to my second supervisor Dr. Chris Nightingale who provided additional advice and support throughout the duration of my time at UCL.

I am extremely grateful to Dr. Ruthven Evans for his tireless help and commitment in the construction of the LabVIEW data logging software.

Thanks also go to Steve Lewin, Stephen Smith and Steven Pierson at Jaguar Cars Ltd for supplying me with information and engine components.

Special thanks are given to the UCL technicians, especially Kevin Crowley, Phil Jeavons and Dave Hurley for the manufacture of the numerous engine components.

TABLE OF CONTENTS

CHAPTER 7: Conclusions

LIST OF FIGURES

CHAPTER 1

CHAPTER 2

CHAPTER 3

CHAPTER 4

CHAPTER 5

CHAPTER 6

LIST OF TABLES

CHAPTER 2

CHAPTER 3

CHAPTER 4

CHAPTER 6

NOMENCLATURE

AFR	Air Fuel Ratio
BDC	Bottom Dead Centre
bmep	Brake mean effective pressure
CA	Crank angle
CO	Carbon Monoxide
CVI	Closed valve injection
DISI	Direct Injection Spark Ignition
EGR	Exhaust Gas Recirculation
EUDC	Extra Urban Driving Cycle
FID	Flame Ionisation Detection
FTP	Federal Test Procedure
HC	Hydrocarbon
HFS	Heat Flux Sensor
HWA	Hot Wire Anemometer
IC	Internal Combustion
IMEP	Indicated Mean Effective Pressure
LDGV	Light Duty Gasoline Vehicle
LIF	Laser Induced Fluorescence
MBT	Maximum Brake Torque
NO_x	Oxides of Nitrogen
OVI	Open Valve Injection
PCV	Positive Crankcase Ventilation
PEEK	PolyEtherEtherKetone
PFI	Port Fuel Injection
PM	Particulate Matter
PTFE	PolyTetraFluoroEthylene
RPM	Revolutions Per Minute
RTS	Resistance Temperature Sensor
SFC	specific fuel consumption
SOI	Start Of Injection
SCC	Spark Combustion Control

TDC	Top Dead Centre
TTL	Transistor Transistor Logic
UDDS	Urban Dynamometer Driving Schedule
VCT	Variable Camshaft Timing
VI	Virtual Instrument
VTEC	Variable Timing and Event Control
VVA	Variable Valve Actuation
VVC	Variable Valve Control
WOT	Wide Open Throttle
WWMP	World Wide Mapping Point

CHAPTER 1

A LITERATURE SURVEY

1.1 INTRODUCTION

This work aims to investigate wall wetting in V8 gasoline engines, which is an important consideration for automobile manufacturers as it increases fuel consumption and emissions and may eventually lead to cylinder bore wear. Although there is relatively little published information available on this subject, this literature survey covers all of the relevant areas.

After a brief description of some important engine fundamentals, this literature survey describes the phenomenon of wall wetting and how fuel films are produced within an engine. An overview of how computers are used to model such liquid behaviour is also shown here, where modelling of the complex fuel transport systems is an extremely difficult task. This is followed by a thorough description of how in-cylinder motion affects both engine behaviour and fuel film propagation. This information is not only relevant to the formation of fuel films, but is also included because variable camshaft timing and comparing different port geometries forms a large part of the experimental work in this study. Emissions are of extreme importance to automobile manufacturers and this work explores this area with particular emphasis on unburned hydrocarbon emissions, as these are greatly influenced by the presence of fuel wall films. Even though modern Nikasil coated aluminium engines may improve performance in some ways, it is clear that they are more susceptible to bore wear than conventional iron lined engines. Due to this, a section on the tribology of the cylinder and the properties of such cylinder bore materials was included. A basic overview of heat transfer is provided in this literature survey as this will help in the understanding of the experimental results. The heat transfer that occurs within an engine is used as a means of measuring possible liquid fuel films, but whole-cycle engine heat transfer itself is not required to be covered in great detail. From the outset, it was appreciated that wall wetting could be detected by a range of experimental techniques and these are reviewed briefly here. An important aspect of the work was getting sensor wires safely out from the moving piston to a data logger. The various mechanisms available to perform such a task are presented with a discussion on the advantages and disadvantages of each.

1.1.1 Spark Ignition Engine Fundamentals

The internal combustion engine operates on a mechanical cycle that involves compressing and combusting an air/fuel mixture and making use of the expansion work of the combustion products on the piston. This cycle can be observed on a pressure - volume plot and conveniently compared to the Otto cycle on a thermodynamic basis [Stone (1999)]. Figure 1.1 shows both an idealized Otto cycle and a typical cylinder pressure-volume plot from a real engine.

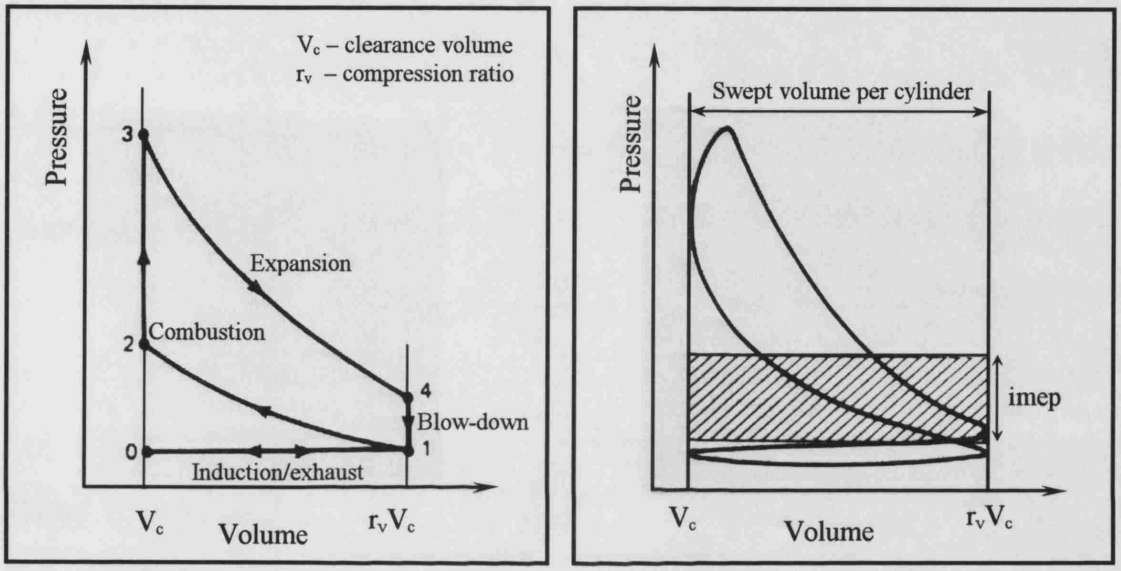

Figure 1.1 Ideal air standard Otto cycle and standard pressure – volume cycle for four-stroke engines [reproduced from Stone (1999)]

In the ideal air standard Otto cycle:

0-1 Induction stroke (With no pressure drop)

1-2 Isentropic compression (Hence adiabatic and reversible)

2-3 Combustion and heat addition at constant volume

3-4 Isentropic expansion

4-1 Blow down (Heat rejection at constant volume)

1-0 Exhaust stroke with no pressure drop

The pressure–volume plot differs from the idealised Otto cycle in several ways. Firstly, it should be noted that the engine pressure–volume plot illustrates that the induction, exhaust and combustion processes occur with a changing working fluid, whereas in the Otto cycle the working fluid is simply recycled with heat addition from an outside source

and rejection to an outside sink. The exchange of fluid gives rise to the so-called pumping loop that gives an indication of pressure losses. Also, the compression and expansion processes are not isentropic because they are neither adiabatic nor reversible and both combustion and blow-down do not occur at constant volume. Peak cylinder pressure usually occurs about 5-20°CA after top dead centre (TDC) of the stroke [Benson *et al* (1979)]. Knowledge of cylinder pressure is of extreme importance to engine designers, since it describes key features such as combustion performance and allows optimization of factors such as filling and emptying of the cylinders.

1.1.2 Compression Ratio

The efficiency (η) of an engine increases with compression ratio of an engine (r_v) according to the Otto cycle.

$$r_v = \frac{V_s + V_c}{V_c} \qquad \eta = 1 - \frac{1}{r_v^{\gamma-1}}$$

Where V_s is the swept volume, V_c is the clearance volume and γ is the ratio of specific heat capacities. The compression ratio of an engine affects the speed of combustion, heat transfer and friction losses. The increase in compression ratio of an engine is limited by the performance of the fuel and the onset of knock as explained in section 1.1.5.

1.1.3 Air-Fuel and Equivalence Ratios

The fuel used in internal combustion engines is conventionally hydrocarbon based. The equation for the complete combustion of a hydrocarbon of molecular composition C_aH_b in air is given by Heywood (1998).

$$C_aH_b + \left(a + \frac{b}{4}\right)(O_2 + 3.773N_2) = aCO_2 + \frac{b}{2}H_2O + 3.773\left(a + \frac{b}{4}\right)N_2$$

This equation describes the stoichiometric ratio of fuel and air that permits complete combustion of fuel resulting with the fuel being converted into fully oxidised products.

The mixture of air and fuel within the engine is described by the air fuel ratio (AFR) and equivalence ratio ϕ.

$$Air\ fuel\ ratio = \frac{Mass\ flow\ rate\ of\ air}{Mass\ flow\ rate\ of\ fuel} \qquad \phi = \frac{stoichiometric\ air\ /\ fuel\ ratio}{actual\ air\ /\ fuel\ ratio}$$

The AFR has a direct influence on the engine performance, economy and emissions. The effect AFR has on specific fuel consumption (sfc) and brake mean effective pressure (bmep) is shown in Figure 1.2. This plot shows that brake mean effective pressure peaks rich of stoichiometric and specific fuel consumption reaches a minimum lean of stoichiometric. The former is explained by the increase in dissociation of CO_2 and H_2O at higher combustion temperatures. This increases the presence of molecular oxygen, allowing more fuel to be burnt than would be suggested by the stoichiometric carbon, hydrogen and oxygen balance in the equation, although this is inefficient with much fuel remaining unburnt. The latter can be explained by the presence of excess oxygen, where for maximum economy, only a weak mixture is needed and all of the fuel is burnt.

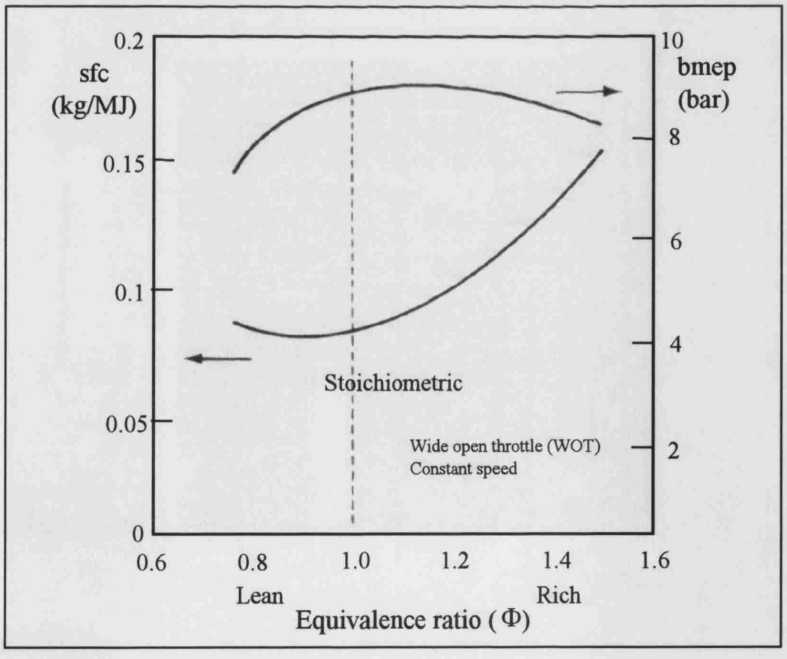

Figure 1.2 Specific fuel consumption and brake mean effective pressure against equivalence ratio [reproduced from Stone (1999)]

An important consideration for the majority of gasoline engines fitted into automobiles at present is that they must operate at stoichiometric AFR in order to obtain maximum performance from the catalytic converter in the exhaust.

1.1.4 Spark Timing

The spark event occurs late in the compression stroke at a point that is intended to generate maximum torque. Early ignition increases the negative work done on the piston during the compression stroke, while late ignition reduces the useful work done on the piston during the expansion stroke due to reduced peak pressure and may result in excessive energy rejection in the exhaust gases. The exact ignition timing will change with engine speed and load. Figure 1.3 shows that the optimum ignition timing is found by incrementally retarding the ignition from the point of maximum output until a drop of only 1% in torque is experienced. This point is called MBT (minimum advance for best torque) [Stone 1999)]. By performing this evaluation, a knock margin is created that guarantees that knock should not be encountered under proper driving conditions.

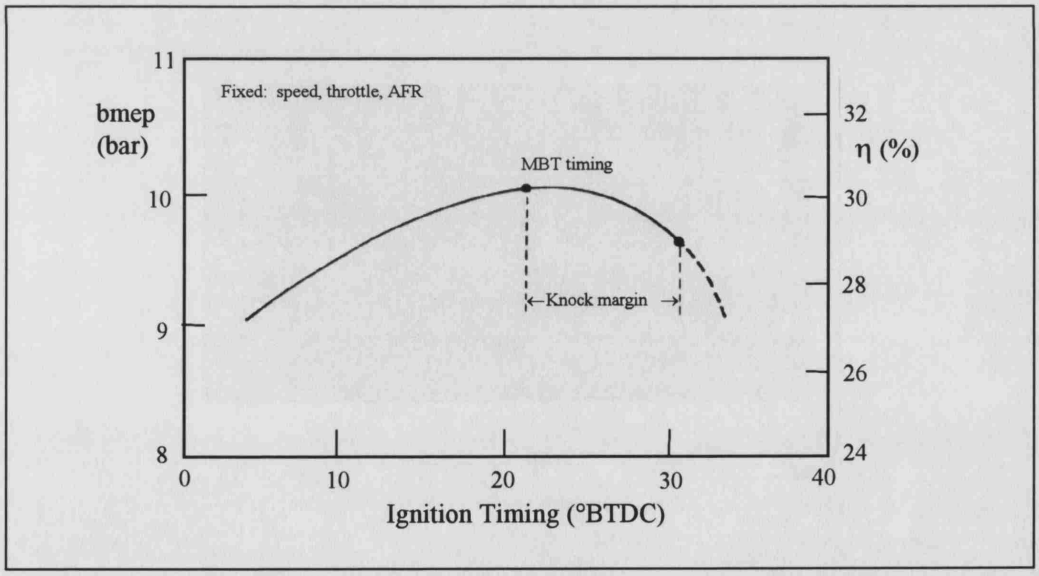

Figure 1.3 Ignition timing and engine output [reproduced from Stone (1999)]

1.1.5 Combustion

In a spark-ignition engine, combustion is initiated by the spark plug just before the piston reaches TDC at the end of the compression stroke. The three stages of combustion that follow are described as the early burn period, fully turbulent combustion and the final burn period. Occasionally, combustion will not be solely initiated by the spark plug as

intended, but by the spontaneous ignition of the end gas at some time after spark if the required conditions such as elevated cylinder pressure and temperature are present. Advanced spark timing can cause these elevated pressures because conventional combustion will start earlier. This pressure adds to the pressure increase from the compression stroke, causing a very rapid pressure rise. The spontaneous ignition of the end gas usually occurs before peak pressure is reached. It should be noted that the end gas is also being heated which also contributes to the likelihood of self-ignition. These increased pressures and temperatures compress and ignite the unburned end gas before the spark induced flame front reaches it. When the spark flame front and the spontaneous ignition flame fronts collide, the damaging superposition of these two pressure waves forms the loud noise called 'knock'. Knock resistance increases with increasing fuel octane number. Surface ignition is similar, except that the ignition source is different and usually comes from a hot spot within the combustion chamber such as an overheated valve. This is a problem that may have been produced when conventional knock disrupted the boundary layer, which normally protects the cylinder surfaces from extreme heat transfers. More extreme pre-ignition and run-on knock are also possible.

Gasoline engines are most efficient when they operate at MBT. Some engines operate with knock limited spark advance systems that are based on feedback from knock sensors. By running the engine with a knock control ignition system in extremely light intermittent knock, optimum efficiency can be achieved, without risking engine damage [Boehm *et al* (1990)]. Typical engine damage caused by knock is erosion of the cylinder head, piston crown and head gasket. The work by Boehm investigated methods of reducing knock in a multi-cylinder engine. It was found that top land clearance and geometry had a great influence on the piston damage incurred by knock, but it should be remembered that the design of these features must also consider blow-by, oil consumption, and scuffing. When one of the pistons was coated with nickel, both piston erosion and piston carbon deposits were reduced. It was interesting to note that nickel coating also reduced piston and cylinder head temperatures. An explanation offered by Boehm was that for these constant speed and load tests, the more robust piston allowed for earlier spark timing (2° to 3°CA) and hence a more efficient engine.

1.2 MIXTURE PREPARATION AND FUEL FILM GENERATION

1.2.1 Introduction

The carburettor used to be the most common means of mixture preparation, but stricter emissions legislation has forced engine manufacturers to use fuel injectors due to their ability to maintain a desired air/fuel ratio, especially during transient conditions. Fuel injection can be either port injection or direct injection. For port injection, the injectors are positioned just before the inlet valves in the inlet port and may use closed valve injection (CVI) or open valve injection (OVI) strategies. Direct injection implies the fuel is injected directly into the cylinder. At the time of writing direct injection was of increasing interest, although port injection was still dominant [Stone (1999)]. Cold start is detrimental to mixture preparation since the cold surfaces reduce evaporation and the required cold start enrichment adds to the build up of liquid fuel.

1.2.2 Port Injection

When using port injection, several different fuel transport mechanisms are observed depending on whether injection is onto an open, closed, hot or cold valve. CVI is the most common strategy because it allows for convenient large-scale evaporation of the fuel in the warm port prior to valve opening, providing excellent mixture preparation. A significant disadvantage of CVI is that during cold start, the evaporation that this strategy relies upon is not present, and large amounts of liquid fuel enter the cylinder. This results in poor combustion and emission characteristics. The OVI strategy relies upon creating a homogeneous (or sometimes stratified) air fuel mixture within the cylinder by injecting during the valve open period. However, depending upon design this may cause significant levels of bore wetting. This is because the injector may have a clear line-of-sight of the cylinder bore through the open valves and the momentum of some of the larger fuel droplets is great enough to not be affected by the direction of the air motion [Ioannou (2000)].

A benefit of OVI is charge cooling through the evaporation of the injected fuel, where the energy required for the latent heat of evaporation of the fuel comes from the incoming air itself, rather than the warm engine surfaces [Kume *et al* (1996)]. Charge cooling is beneficial since it increases the mass of air trapped within the cylinder and

hence increases the volumetric efficiency of the engine. OVI also provides more control over the air/fuel ratio than CVI during transient conditions since it reduces the possibility of forming liquid fuel films [McGee *et al* (2000)]. It may also be beneficial during cold start as it reduces transport delay [Pierson (2002)]. However, McGee found from experiments on a 2.0l engine that HC emissions were higher with OVI than CVI due to the lack of in port fuel evaporation. CVI also had superior combustion stability with retarded spark, which is an important consideration for catalyst "light off" temperature. It should be noted that this could depend on engine geometry.

In a port fuel injector, fuel addition is universally controlled by a solenoid and pintle valve arrangement with the most important part of the injector being the tip design, as this governs the spray quality. A range of injector tip designs is available, each with its own unique 'wetting footprint' [Zhao *et al* (2002)]. In an attempt to further increase fuel atomization, some designs include an air assist mechanism, where high velocity air is passed through the injector tip [Jackson (1997)]. There is limited size variation between injectors in the interests of manufacturers being able to change between brands. Some designs opt for side feed as opposed to end feed because the fuel in the working section of the injector is kept cool by the thicker belt of fuel, limiting undesired internal evaporation of the lighter fuel fractions. Newer injector designs can achieve the same degree of fuel cooling without the complexity of side feed.

1.2.3 The Intake Process and Liquid Fuel Film Generation

The formation of liquid fuel films on engine surfaces is of great importance to engine manufacturers since this affects mixture homogeneity, emissions and drivability due to fuel delivery delay. Miorali *et al* (1998) describe the film as a fuel sink during acceleration and a fuel source during deceleration. To form liquid fuel on the port surfaces, the injected fuel must first travel from the injector tip to the port surface in the form of small droplets, where the magnitude of liquid fuel formation is greatly influenced by the conditions the fuel droplets experience. It is apparent that an initial determining factor is simply the droplet size distribution, which varies depending upon injector type and the pressure drop across it. Variation between the cone angle of different injectors was found to form wetted areas of quite different sizes when tested on a 1.9l engine [Bourke *et al* (1994)].

Liquid fuel film generation will also be greatly affected by the use of either CVI or OVI injection, which will emphasize the above issue [Ioannou (2000)]. In CVI the injected droplets have no option but to impact the port and valve surfaces, but this is actually intended and allows fuel evaporation on the warm port surfaces. However, this effect is greatly reduced during cold start, leaving large quantities of liquid fuel in the port prior to inlet valve opening. In OVI most of the small droplets pass directly into the cylinder following the airflow. Some of the larger droplets may have sufficient momentum to be unaffected by the induction airflow, allowing them to travel directly to the cylinder bore if the design of the port and valve permit this.

When the inlet valves open after CVI, there is an initial backflow of exhaust gas into the inlet manifold which evaporates some of the fuel. Once the flow returns to the forward direction, the liquid fuel in the inlet port is strip-atomized into the cylinder [Meyer *et al* (1999a)]. Meyer *et al* (1999a) also described the mechanism of how strip atomization occurs, where wave type features form on the surface of the wall film and eventually break free, being re-entrained in the airflow. These re-entrained droplets are normally larger than average due to fuel surface tension. At about mid-stroke, strip atomization is increased due to increased flow velocity, leaving fuel of lower volatility on the port surface [Senda *et al* (1999)]. When the inlet valves close, any liquid fuel in the valve seat is squeezed into the cylinder or back into the intake manifold.

An investigation of the circumferential distribution of liquid fuel around the inlet valve was undertaken by Meyer *et al* (1998) using a vertically mounted single cylinder engine and PDA and LIF as explained in section 1.7.3. For OVI, it was observed that as the engine warmed, the amount of liquid fuel entering the cylinder decreased, while for CVI, the amount of liquid fuel entering the cylinder peaked at about 15 seconds after starting due to fuel being held in the cold port during the early stages. The airflow governed where the bulk of fuel entered the cylinder for OVI, while for CVI targeting the injected fuel onto the back of the valve was the more important factor. The wake of the valve stem would also interfere with the size and distribution of fuel droplets for both OVI and CVI. In the case of OVI most fuel entered the cylinder due to the injection contribution, but for CVI it was first forward flow and high speed intake airflow that carried the fuel into the cylinder. Witze *et al* (1997) used LIF to study in-cylinder fuel films under cold

start conditions and found that OVI would wet a greater area in the combustion chamber than CVI. Injector targeting was studied experimentally by Russ *et al* (1998) and the results analyzed using a τ-X model. In these τ-X models, X is the fraction of injected fuel deposited as a film (typically between 0.6 to 0.8) and τ is the time scale for vaporization of the fuel (typically 0.3 to 2.5 s) [Bauer *et al* (1997)]. It was found that targeting the relatively hot inlet valves reduced the fraction of fuel on the port wall (X) by 30-50%. Under cold start conditions the cold engine surfaces reduce fuel evaporation, so to form a combustible mixture, fuel enrichment is used. However, this enrichment adds to the build up of liquid fuel within the engine. Extensive studies of cold start 'fuel loss' to the crankcase by Shayler *et al* (1997) found that after starting, fuel loss would be initially high, but reduce to zero after about 9 minutes. This work was performed at cold conditions between –5°C and 20°C at relatively low engine speeds of 2000rpm to 3000rpm to emphasize the amount of fuel lost.

Shayler *et al* (1996a) also established that the rate of vaporisation was affected by manifold absolute pressure and flow velocity within the intake ports. A high rate of vaporisation was experienced at low manifold pressures and during induction when flow velocities were at their peak.

Koederitz et al (1999) observed fuel film behaviour in the vicinity of the inlet valves of a cold suction rig. This was a basic set-up that was intended to replicate cold start and CVI. At low valve lifts, the usual fuel ligaments and strip atomization was observed, while at higher lifts with higher air flows, droplet and film shear were observed. Fuel film squeezing from the valve seats was absent due to the inlet valves being static.

1.2.4 Computer Models

These are very important in the study of liquid fuel films since they aid in the understanding of experimental results, which may conceal many complex fuel transport mechanisms. The models focus on only a few aspects of mixture preparation simply because there are too many complicated stages involved. An advantage of modelling is that the parameters of the model can be varied to explore which of the influencing factors in a given scenario is of greater importance.

A model to explore methanol wall film evaporation and oxidation in the combustion chamber was created by Oliveira *et al* (2000). It was found that if the wall film thickness was reduced, the rate of evaporation would be greatly accelerated. This model also varied the wall temperature and found that when the wall temperature is lower than the fuel's boiling temperature evaporation is low, although wall temperatures above the fuel's boiling point caused intense evaporation. Senda *et al* (2000) created a model that considered the evaporation of multicomponent fuels which were collectively more simplistic in their properties than gasoline. This provided useful information about the interaction of the different fractions and how this can be extended to gasoline modelling.

Skippon *et al* (1998) modelled fuel using the Major-Component Fuel approach and found that for a cold start at 0°C, only 20 - 30% of the fuel vaporized within the inlet port. The model predicted that under the warm conditions of light load and medium speed, all of the fuel is evaporated within the inlet port. Skippon also provided an overview of fuel movement as shown in Figure 1.4.

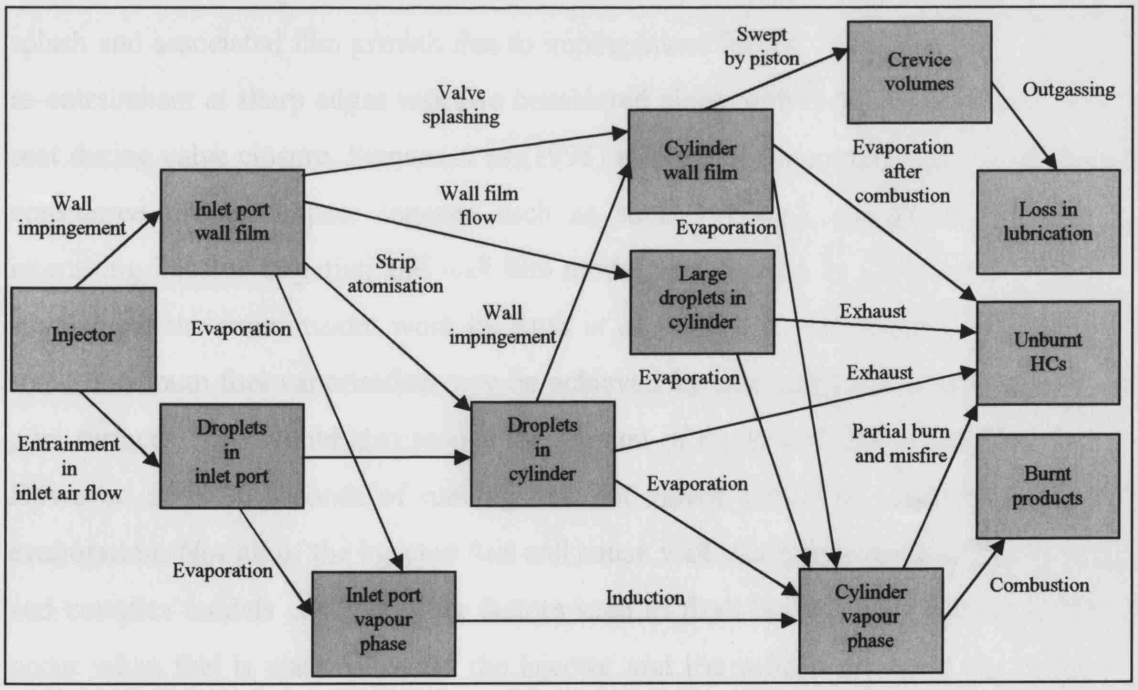

Figure 1.4 Fuel movement in a SI engine [reproduced from Skippon *et al* (1998)]

An excellent review of such models was performed by Lindgren *et al* (2000) who compared various models and went on to describe the terms and considerations of such models. An interesting point was how the surface roughness would influence the outcome of a droplet impacting an engine surface in ways such as the area of splash, amount of fuel re-entrained into the air and impact angle of secondary droplets formed from the first droplet.

The droplet evaporation model of Meyer *et al* (1999b) predicted that OVI allows higher levels of evaporation of airborne droplets than CVI, which is in agreement with the experimental work reviewed. This is mainly because the freshly injected droplets are relatively small and also that they are held in the air for longer prior to impacting the cylinder wall due to the longer flight path promoted by OVI.

O'Rouke *et al* (2000) described a complex model created in the KIVA CFD code. This model considered not only the required fundamental factors such as film heating and vaporisation, but also the numerous factors that can affect the wall film even though they would not have a huge effect alone. One of the considerations in the model was droplet splash and associated film growth due to impingement forces. Splashing, separation and re-entrainment at sharp edges was also considered along with film squeezing in the valve seat during valve closure. Stanton *et al* (1998) also created a complex KIVA model and considered droplet impact regimes such as stick, rebound, spread and splash. An interesting injector targeting and wall film model was created by Curtis *et al* (1998) to supplement the experimental work by Russ *et al* (1998). It was suggested that at cold start, maximum fuel vaporisation may be achieved by increasing the wetted area of the port surfaces. This would also reduce the amount of liquid fuel that enters the cylinder. However, after 30 seconds of running, the hot valves should be targeted to increase evaporation. Not all of the injected fuel will cause wall wetting by large droplets though and complex models consider other factors such as flash boiling. This phenomenon can occur when fuel is warmed within the injector and the sudden decrease in pressure to below the saturation pressure during injection causes a rapid boiling of the fuel Senda *et al* (1994). This was shown to disrupt the normal spray cone and would significantly change the targeting of the fuel.

1.3 IN CYLINDER MOTION

1.3.1 Introduction

The level of turbulence exhibited by the air and fuel mixture is controlled by the intake and exhaust events in addition to the piston motion. Turbulent in-cylinder motion is desired because it ensures thorough mixing of the air and fuel whilst ensuring fast turbulent combustion. Increasing engine speed reduces the time for combustion to occur and the increase in air flow increases the turbulence, which also allows combustion to occur in a shorter time. There are three main mechanisms for turbulence enhancement, being tumble, swirl and squish.

1.3.2 Tumble (Barrel Swirl)

Tumble is the rotation of fluid around an axis parallel to the crankshaft. The tumble motion is usually initiated by the air and fuel mixture passing over the top of the inlet valves and being deflected downwards by the opposite cylinder wall with the flow pattern enhanced by the downward movement of the piston during induction. As the piston rises during compression, the bulk tumble velocity increases until the rotating fluid finally breaks into smaller eddies. High levels of turbulence lead to rapid combustion, which returns low fuel consumption and reduced emissions [Stone (1999)]. Tumble works well even for lean mixtures or those with high levels of exhaust gas recirculation (EGR). Reverse tumble is also possible, but involves the flow passing through the low side of the inlet valves and the rotation of the fluid being in the opposite direction to conventional tumble.

Tumble is a key feature of 4-valve engines. The combination of high flow ports and superior valve flow area of 4-valve engines over 2-valve engines provides better volumetric efficiency at high speeds. Such 4-valve engines are well suited to pent-roof combustion chambers since this combustion chamber permits two relatively large inlet valves within the cylinder. Also, since the spark plug is near the centre of the cylinder the distance that the flame front has to travel is minimized, allowing faster combustion. In recent years, 4-valve engines have become commonplace in automobiles mainly due to their ability to meet the increase in engine performance requirement and tightening of emission legislation as detailed in Section 1.4.

Fry (1994) devised a method of increasing forward tumble in the low speed range of 1500rpm to 2000rpm. By positioning a 'ski slope' in the intake port, the airflow was directed towards the top of the valves, forming tumble within the cylinder as it entered. The ski-slope was lowered flat against the port wall during high-speed operation so as to maintain the maximum possible airflow and volumetric efficiency. Early ski-slope designs showed problems with the flow tumbling within the port, forcing fuel to impact on the low side of the port and becoming trapped under the ski-slope itself. Correction to the design allowed the ski-slope to behave as a superior low-speed tumble generator, although its effect on mixture preparation were not fully decided. If it was proven that the ski slope mechanism produced a good mixture, the tumble motion around the pent-roof close to the spark plug could form the basis of a stratified charge engine design. However, in the interests of increasing tumble by passing flow over the tops of the valves alone, the volumetric efficiency could suffer.

1.3.3 Swirl

Swirl is the rotation of fluid around the axis of the cylinder. It can be formed by the flow entering the cylinder and being forced to follow the curvature of the cylinder bore and is generated most readily when an inlet port meets the cylinder tangentially. It follows that swirl is mostly used in cylinders with a single inlet valve. Shrouding the inlet valves for some or all of their lift is also a common means of producing swirl. In addition, some automobile designers utilize valve or port deactivation mechanisms to achieve swirl at low engine speeds with four valve cylinder heads.

Swirl is very good at producing rapid combustion at part load with lean mixtures. A problem with swirl is that since it requires high velocity flows for it to be formed, the volumetric efficiency is reduced [Endres *et al* (1990)].

1.3.4 Squish

Squish is most commonly used in diesel engines, but is also employed in a range of gasoline engines. In a diesel engine both the cylinder head directly above the piston and the piston itself are usually quite flat, except for a small bowl in the piston that forms the combustion chamber. When the piston is at TDC, the small gap between the flat areas on the piston and cylinder head forms the squish region. During the last stages of

compression the air is rapidly squeezed out from this squish region into the combustion chamber with a high degree of turbulence, ready for the injection of diesel.

In gasoline engines a ring of flat "land" around the perimeter of the piston forms the squish region when it comes close to the cylinder head at TDC. On some cylinder heads that possess valve shrouding, it is this raised area on the cylinder head that forms a squish region with the piston. Having the squish region at the edge of the piston reduces the propensity for knock since this region is close to the cooler cylinder bore and cylinder head.

1.3.5 Deactivation Mechanisms

Under low speed conditions, the benefits of 4-valve engine performance are reduced since the flow through the two inlet valves has a low velocity. This is detrimental since the lack of turbulence leads to poor combustion and increased emissions. To overcome this problem, port deactivation or valve deactivation can be employed at low engine speeds as a means of increasing the net inlet flow velocity.

Port Deactivation

By using a number of possible mechanisms, the flow through one of the ports is stopped, generating a higher flow velocity through the active port. This has the effect of forming high swirl and hence improving turbulence at these reduced speeds.

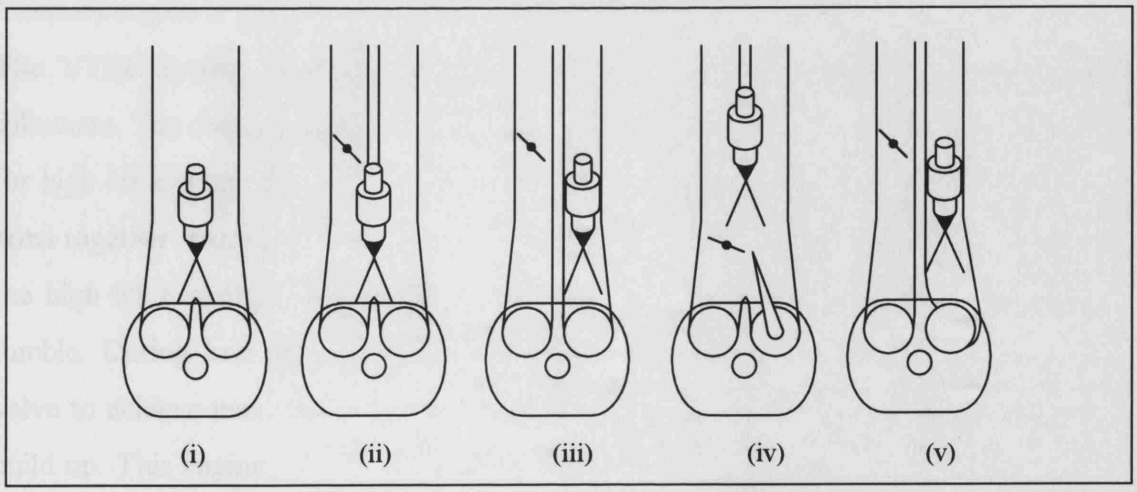

Figure 1.5 Port deactivation alternatives [reproduced from Endres *et al* (1990)]

A design that will perform well at high speeds and loads by promoting a high level of tumble is shown in Figure 1.5 (i), which has no deactivation mechanism. Figure 1.5 (ii) has an inlet manifold runner based deactivation mechanism, with the injector positioned between the ports. This design can lead to excessive fuel wall film build-up in the throttled runner, since it has no airflow to break up the fuel. It is possible to have one port throttled, while the other port has exclusive ownership of the injector, as seen in Figure 1.5 (iii). With this design high tumble can be achieved at high loads, while at low speeds, closure of the throttle produces high swirl and effectively generates a stratified charge allowing combustion of lean mixtures. This combination allows high volumetric efficiency at high speed, while allowing lean combustion at part-load [Pearson (1999)]. A further option is shown in Figure 1.5 (iv), which has a throttle near to the inlet valve with the injector further upstream between the runners. It was thought that this would allow extra time for a homogeneous mixture to form, but instead, the fuel on the back of the throttle would be stripped off and reduce the mixture quality of the other port. Figure 1.5 (v) is a variant of Figure 1.5 (ii). This design provides strong swirl at low speeds during deactivation, however the nature of the port limits the volumetric efficiency at high speeds.

Valve Deactivation

This forms a more powerful swirl ratio than port deactivation because it allows for a completely tangential and single point entry into the cylinder. Probably the most well known valve deactivation system is the Honda VTEC (Variable Timing and Event Control) engine (Figure 1.6), which can effectively close one valve [Horie *et al* (1992)]. The VTEC system uses only one camshaft and a series of rocker arms with roller followers. The deactivation is made possible by there being two camshaft inlet lobes (one for high lift and one for low lift) and the ability to hydraulically lock the two inlet rocker arms together. During high-speed operation, the two inlet rocker arms lock together and the high lift camshaft lobe provides maximum lift for both valves, providing excellent tumble. During low speed operation, the rocker arms act independently allowing one valve to achieve maximum lift, while the other opens by 0.65 mm to prevent liquid fuel build up. This engine also employs extensive squish areas in addition to the tumble and swirl mechanisms.

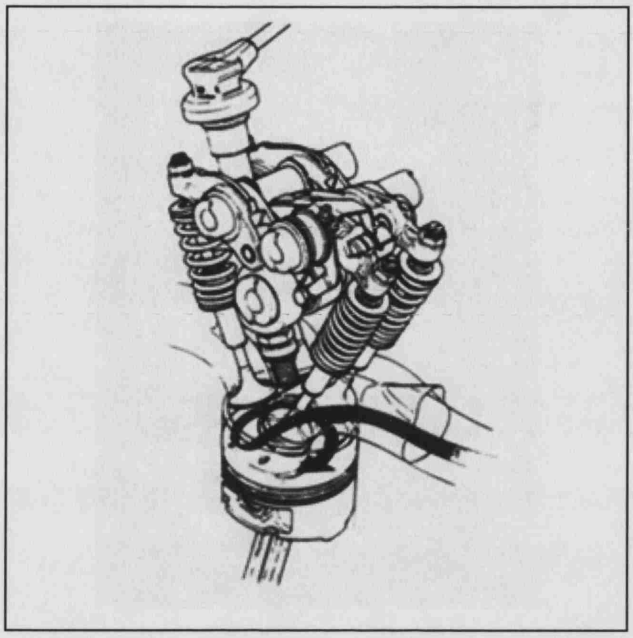

1.6 Honda VTEC engine [Horie *et al* (1992)]

Valve deactivation generates higher swirl velocities than port deactivation, but the mechanism is more complex and difficult to integrate into existing engines.

1.3.6 Variable Camshaft Timing (VCT)

High engine speed conditions

There are positive reasons for adopting either an advanced or retarded camshaft strategy for high-speed conditions (Figure 1.7). The large valve overlap generated by an advanced camshaft creates pressure pulse effects that increase volumetric efficiency. The use of a retarded inlet valve closure is beneficial because the high velocity air in the inlet manifold has great momentum and would continue to fill the cylinder even when the piston is rising during compression in an effect known as dynamic after-charging. Stone (1999) and Heisler (1998) state that the pulse effects outweigh the after-charging benefits, however Baker (1995) states that dynamic after-charging is more important. This illustrates that the ability to control valve event duration would be beneficial, as an increased duration would allow both effects and thus enhance performance.

Low engine speed conditions

This is a trade-off too, between permitting exhaust gas residuals to pollute the fresh charge which inhibits combustion (advanced inlet camshaft timing) or suffering from reduced volumetric efficiency when fresh charge is forced back into the inlet manifold (retarded inlet camshaft timing). In the interests of good combustion, Stone (1999) and Heisler (1998) believed the inlet camshaft should be retarded. However, Baker (1995) believed that it was important to use advanced inlet camshaft operation so as to increase volumetric efficiency and low-speed torque. Ideally, it can be appreciated that a reduced inlet valve duration would be beneficial here. Pressure pulses are not considered since they are not powerful enough to be useful at low speeds.

Idle condition

The main concern at idle is stability, which can be achieved by retarding the inlet event so as to reduce in-cylinder exhaust gas residuals.

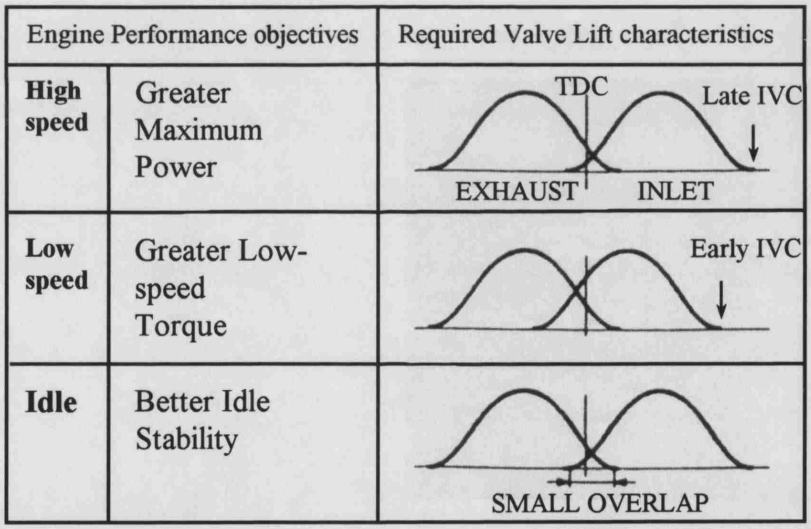

Figure 1.7 Inlet valve event timing [reproduced from Baker (1995)]

The standard approach for camshaft phasing is to use a combination of straight and helical splines. Typically there is a helical spline on the camshaft and a straight spline on the inside of the chain drive. An annular piston with respective straight and helical splines then meshes with the camshaft and drive wheel splines. Varying the oil pressure within the mechanism causes a linear displacement of the piston, which slides linearly along the straight spline and forces the camshaft to rotate relative to its drive wheel due to the helical spline without displacement of the camshaft or drive wheel.

1.3.7 Variable Valve Control (VVC)

This offers more control than camshaft phasing alone since it allows variable valve lift and valve open duration. VVC is often used in combination with camshaft phasing, providing a complete mechanical control over valve behaviour. This type of system has been developed by BMW and is known as their ValveTronic system [Flierl *et al* (2000), Crosse (2001)]. The main benefit of this system is that throttle-less load control can be applied, greatly improving the efficiency of the gasoline engine.

Pierik *et al* (2000) devised a mechanical variable valve actuation (VVA) system that could be used in conjunction with a standard 4-cylinder base engine. The VVA system allowed BSFC improvements of 12% at idle, 7% at low load and 3% at high load over the conventional fixed valve system. It was found that NO_x emissions were reduced, but HC emissions actually increased due to lack of mixture motion caused by early inlet valve closure and low valve lift. A similar mechanism was designed and constructed by Hara *et al* (2000) that was also mounted on a 4-cylinder base engine. Even though a sufficient range of valve lift durations was possible, the author believes that the system was not as mechanically robust as the former system.

1.3.8 Electromechanical Valvetrain

The main benefit of this system is that the valves can be operated exactly when needed for any amount of time during the engine cycle. The control over valve lift and duration by an electromechanical valvetrain would allow a possible 11% reduction in fuel consumption and provide an increase in peak torque of 5% compared to mechanical valve control [Flierl *et al* (2000)]. Electro-mechanical valve control allows for more control than the mechanical fully variable valve train, helping to further increase the efficiency of throttle-less load control.

The current electro-mechanical valve systems under development may allow the valve to operate at any point for a desired period, but the lift is still limited to fully shut or open positions. This gives rise to some interesting valve lift profiles.

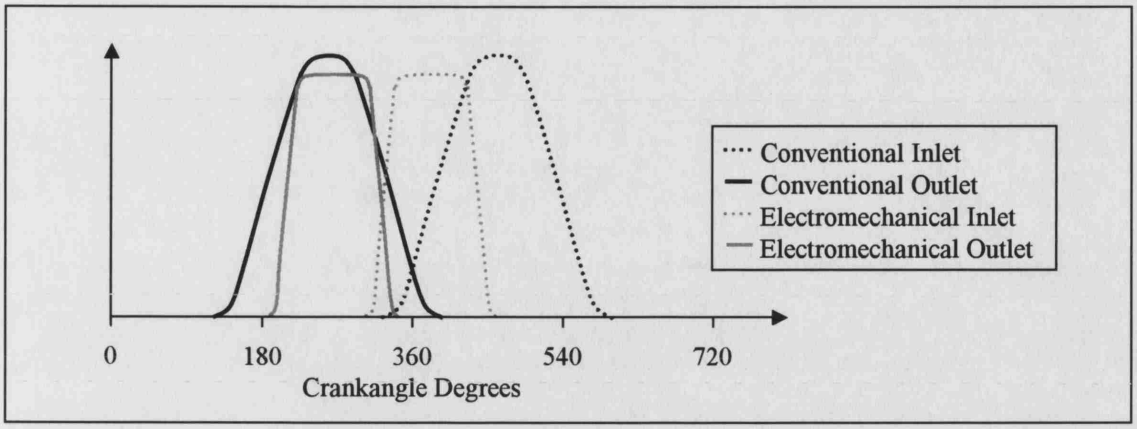

Figure 1.8 Conventional and possible electro-mechanical valve lift profiles [reproduced from Flierl *et al* (2000)]

The idea of an electromechanical valvetrain is not new, but only recently has new technologies made the system feasible. The main problems are coping with the huge acceleration the valves go through and overcoming any unreliability in the solenoid mechanism, since a valve that remains stuck open would collide with the upward moving piston causing massive engine damage. This system also requires a bulky electrical system, including a large battery, starter motor and alternator.

1.4 EMISSIONS

1.4.1 Introduction

Emission legislation is one of the driving factors in the refinement and development of new engine designs and technologies. The main polluting emissions are oxides of nitrogen (NO_x), carbon monoxide (CO), hydrocarbons (HC) and particulate matter (PM), where each of these is briefly described in the following sections. Carbon dioxide (CO_2) has also been seen as a pollutant since it was found to be a 'greenhouse gas'. Reduction in the main emissions is mostly achieved through new engine technologies and use of catalytic converters, however the reduction in CO_2 is only achieved through reducing fuel consumption.

1.4.2 Emission Legislation

In order to evaluate the extent of the pollution caused by a vehicle it is driven on a rolling road in a laboratory and its emissions are measured. FTP-75 is the main US test cycle used, with a duration of 1874 seconds covering 11.04 miles (17.77 km) at an average speed of 21.2 mph (34.1 km/h) [Dieselnet.com (2001)]. FTP-75 is a recent modification of FTP-72, where the last 505 seconds of the cycle is a repeat of the first 505 seconds (Figure 1.9), but with warm re-start after a 10 minute stopped engine period.

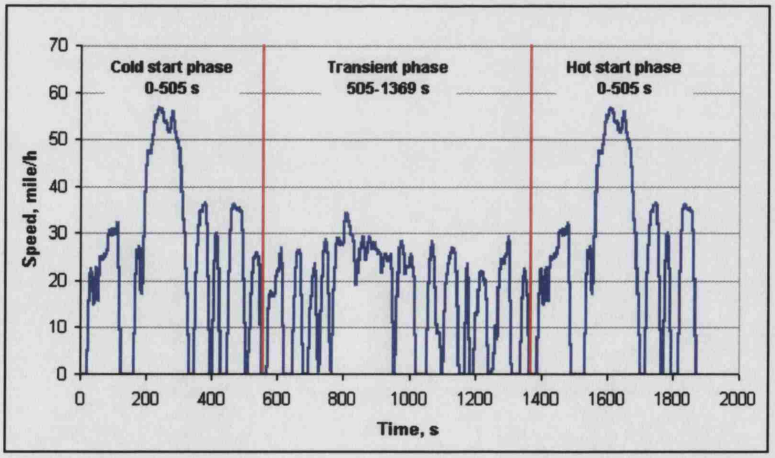

Figure 1.9 Federal Test Procedure 75 [Dieselnet.com (2001)]

Since the FTP-75 cycle does not allow for hard accelerations or air conditioning, the new US06 cycle (Figure 1.10) is employed on vehicles built after 2000 [Ball (1997)].

The US06 is a 600 second test with a highest speed of 80.3 mph and an average speed of 48 mph over its 8 mile distance [Environmental Protection Agency (2001)].

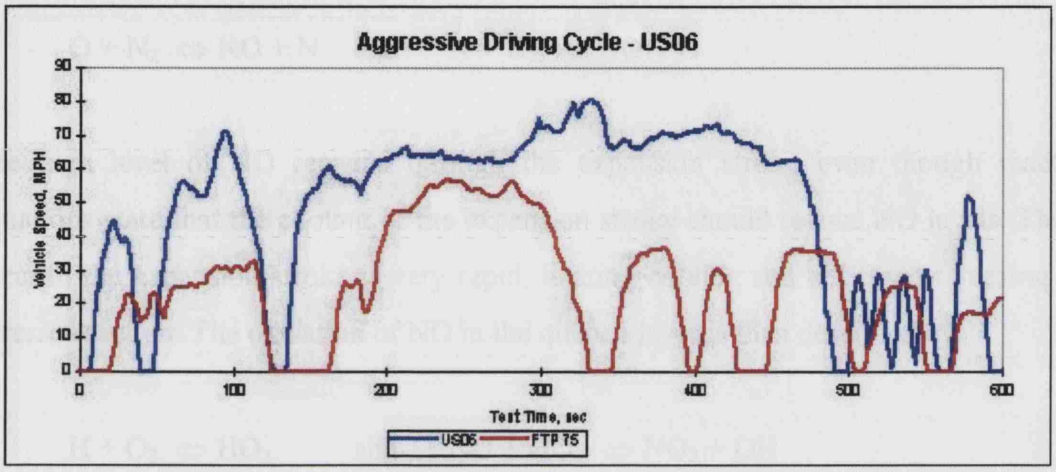

Figure 1.10 The US06 Driving Cycle [Department of Energy – U.S. (2001)]

The equivalent European cycles are the urban ECE-15 (Economic Commission for European) and EUDC (Extra Urban Driving Cycle). Previously, the engine was run for 40 seconds prior to the test commencing, but as of 2000 the test begins when the engine is started. The actual test requires four non-interrupted runs of the ECE-15 test followed by one run of the EUDC test, as shown in Figure 1.11 [Dieselnet.com (2001)].

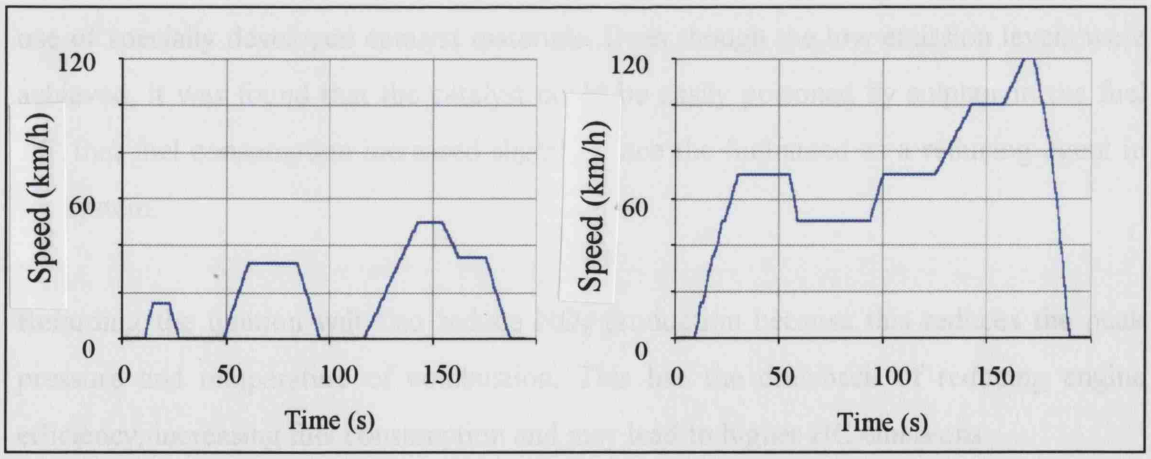

Figure 1.11 The European ECE-15 and Extra Urban Drive Cycles [Dieselnet.com (2001)]

1.4.3 Oxides of Nitrogen (NO_x)

NO_x describes the combination of nitric oxide (NO) and nitrogen dioxide (NO_2). During the high temperatures of combustion NO is formed, although this oxidises to NO_2 as it

cools. Increasing the combustion temperature increases the rate of NO formation, where the Zeldovich mechanism [Stone (1999)] explains the formation of NO_x:

$$O + N_2 \Leftrightarrow NO + N \quad \text{and} \quad N + O_2 \Leftrightarrow NO + O$$

The high level of NO remains through the expansion stroke even though reaction equations state that the cooling of the expansion stroke should reduce NO levels. This is because the expansion stroke is very rapid, limiting cooling and effectively freezing the reverse reaction. The oxidation of NO in the quench layer is then described by:

$$H + O_2 \Leftrightarrow HO_2 \quad \text{and} \quad NO + HO_2 \Leftrightarrow NO_2 + OH$$

NO_x production is affected by air fuel ratio. Even though rich mixtures generate higher cylinder temperatures, NO_x formation is actually reduced by using richer mixtures due to the reduced level of oxygen available. The amount of NO_x production is at a maximum when the AFR is slightly lean of stoichiometric as shown in Figure 1.12. This is especially problematic to lean burn engines that operate in this region because not only does the level of NO_x peak, but conventional catalytic converters fail to operate at this non-stoichiometric condition. Jobson *et al* (2000) have attempted to address this issue by use of specially developed catalyst materials. Even though the low emission levels were achieved, it was found that the catalyst could be easily poisoned by sulphur in the fuel and that fuel consumption increased slightly, since the fuel acted as a reducing agent in the system.

Retarding the ignition will also reduce NO_x production because this reduces the peak pressure and temperature of combustion. This has the drawback of reducing engine efficiency, increasing fuel consumption and may lead to higher HC emissions.

The relative magnitudes of NO, CO and HC emissions against equivalence ratio are shown in Figure 1.12.

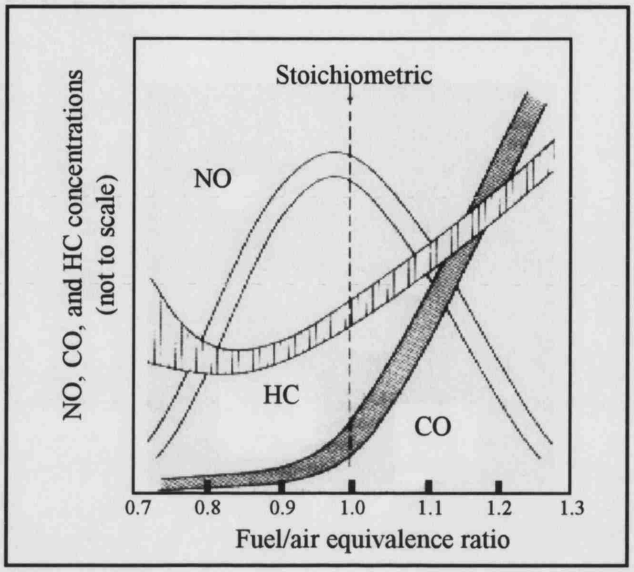

Figure 1.12 Variation of HC, CO and NO concentration against equivalence ratio for a spark ignition engine [reproduced from Heywood (1988)]

Exhaust Gas Recirculation (EGR) is often used as a direct means of reducing NO_x emissions. This is because the exhaust gas lowers the mean gas temperature by acting as a heat sink due to it having a high specific heat capacity. By using 15% to 25% EGR, the maximum temperature and flame speed are reduced sufficiently that the emission of NO_x is reduced by up to a half [Stone (1999)]. If the level of EGR is increased much beyond this in a standard engine, the engine becomes unstable due to slow combustion and misfire. However, Saab claims that its Combustion Control (SCC) system uses 70% EGR in its combustion mixture by using direct injection, variable valve timing and variable spark gap [Birch 2001]. This system operates at stoichiometric AFR with a catalytic converter, which permits low exhaust emissions and 10% fuel savings. EGR reduces the part load fuel consumption because the throttle has to be opened further to admit a certain amount of air, reducing pumping losses.

1.4.4 Carbon Monoxide (CO)

Carbon Monoxide is formed due to incomplete combustion of rich fuel mixtures, although some CO will exist with lean mixtures due to dissociation. Carbon monoxide is created at the flame front and the outer edge of the quench layer when all the local oxygen is consumed and further oxidation to CO_2 is prevented. A weaker mixture will

reduce the production of CO due to the excess oxygen present, which is an added advantage of lean burn engines.

1.4.5 Particulate Matter (PM)

Traditionally these emissions were not considered in conjunction with SI engines and instead associated with Diesel engines, but are now a source of increasing concern. There are three types of particulate matter emission. These are lead, sulphates and organic particulates, under which soot is classified. Particulate matter less than 2.5 μm in diameter is described as fine, while particulates above 10 μm are large [Ball (1997)]. The work by Hall (2000) suggested that material emitted from the engine was deposited in the exhaust system during cool operation, only to be released as particles as the temperature of the exhaust was increased.

A thorough study of particulate emissions from in-use passenger cars in the US was performed by Cadle *et al* (1999). In this study, 361 light-duty gasoline (LDGV) and 49 diesel passenger vehicles made between 1965 and 1997 were tested on the FTP-UDDS (Federal Test Program – Urban Dynamometer Driving Schedule). These vehicles came from Denver, San Antonio and California and special effort was made to also test smoking vehicles, since it was felt they could be major contributors to PM emissions. The average PM emission rates were 3.3, 79.9, 384 and 558 mg/mile for 1991-1997 LDGVs, pre-1981 LDGVs, smoking LDGVs and diesel vehicles respectively. Most of the particulates were found to be less than 2.5 μm.

1.4.6 Hydrocarbon Emissions (HC)

Unburned hydrocarbon emissions are derived from fuel that has escaped the combustion process. The quench-layer and the crevice volume between the piston and cylinder wall are major sources of unburned hydrocarbons. Crevices by the spark plug and valves also contribute to the problem. This problem arises because compression and combustion force a small amount of fuel into these narrow crevice regions, but since combustion cannot properly access these confined spaces, it is free to exit the engine during the exhaust stroke.

The crevice volume between the upper and lower piston rings is also known to be a source of HC due to blowby. Kim *et al* (1999) introduced slits low in the cylinder wall that allowed the trapped gases to escape into the crankcase when the piston is near BDC. This achieved a 23% reduction in HC at speeds of 1250-3500 r/min and loads of 185-556 kPa, bmep without loss of power or efficiency. However, this would dilute oil if the engine were cold.

Liquid fuel contributes to hydrocarbon emissions. This is especially true in port-injection engines where the injection timing will influence the hydrocarbon emission level observed. Closed valve injection (CVI) is currently the most common strategy and relies on the injected fuel evaporating from the hot inlet port surfaces and inlet valves before the valves open. In open valve injection (OVI) the fuel is injected through opened inlet valves into the cylinder [Stone (1999)]. Using either strategy, liquid fuel will inevitably be present within the cylinder.

During cold start, the combination of cold surfaces and fuel enrichment increase hydrocarbon emissions. Emission legislation is tightening to the extent that the first couple of engine cycles provide scope for further emission reduction. Castaing *et al* (2000) found that the piston starting position, ignition timing and amount of fuel injected greatly influenced the likelihood of misfire. Castaing also mentions that only a few misfires are required to generate hundreds of mg of unburned hydrocarbons, forming an alarmingly high percentage of the HC emissions allowed in most test cycles.

Hydrocarbon emissions are also influenced by the flame quench mechanism, which is a two-stage process. In the first stage, the flame is extinguished a short distance from the wall. During the second stage, the quench hydrocarbons diffuse into the combustion gases, where a proportion will oxidize, leaving the remainder to form hydrocarbon emissions. In a cold-start the quench layer is noticeably thicker, helping to raise the emission level [Heywoood (1988)].

Further sources of hydrocarbon emissions are engine deposits and engine oil. Engine oil on the combustion chamber wall adds to unburned hydrocarbon emissions. It has been proven by experiment that adding small amounts of oil to the fuel also increases these

emissions. Surprisingly it was unreacted fuel and not oil components that caused this increase [Heywoood (1988)]. It appears that the increase in emissions with increasing amounts of oil is due to the oil acting as an intra-cycle storage medium, where the fuel is introduced into the cylinder, stored in oil throughout combustion and released during the exhaust stroke.

This complex mechanism of oil layer fuel absorption and desorption is mainly driven by pressures within the cylinder. During the induction and compression strokes the fuel vapour concentration in the cylinder is sufficient that the oil absorbs fuel. The oil will eventually become saturated at low pressure, but will continue to absorb additional fuel at the end of compression due to the increased vapour pressure. The fuel in the oil is completely protected from combustion. The decrease in cylinder pressure and reduction of the concentration of fuel vapour in the cylinder after combustion allows the fuel absorbed in the oil to return to gaseous fuel vapour in the exhaust products, although some of this vapour is oxidised. Shayler *et al* (2000a) provided an excellent description of the HC increase by oil absorption and desorption and reported that this mechanism could cause up to 10% of the total HC emissions under normal operating conditions, but that this would increase under lower operating temperatures.

Under firing conditions, blowby starts to introduce fuel directly into the crankcase. According to Shayler *et al* (2000b), up to 85% of the hydrocarbons from blowby are trapped in the oil below the ring pack. During warm-up from a cold start, a large amount of blow-by hydrocarbons are held within the crankcase, although this amount falls when the oil temperatures rise. When the engine is fully warm and loaded, blow-by still accounts for a larger proportion of crankcase hydrocarbons than desorption of fuel from the sump oil.

A method described by Shayler *et al* (2000b) for studying the desorption level of the fuel is to motor an engine that has a sufficient level of oil dilution by fuel. Any HC detected under motoring originates as fuel from the oil. A motored run with clean oil can calibrate for any HC readings due to vaporisation of the oil itself. Fuel desorption occurs on the cylinder bore and also in the crankcase, implying the crankcase breather is also a source of HC emissions. The breather is usually fed back into the inlet manifold.

The amount of oil dilution is mostly governed by oil temperature and vehicle usage patterns, where frequent cold starts and short journeys greatly increase the dilution. At some point (normally 100hrs of engine operation), an equilibrium between absorption and desorption is reached and the oil dilution level remains constant. This equilibrium will vary depending on oil temperature and vehicle usage patterns. The HC movement within the crankcase is illustrated by Figure 1.13.

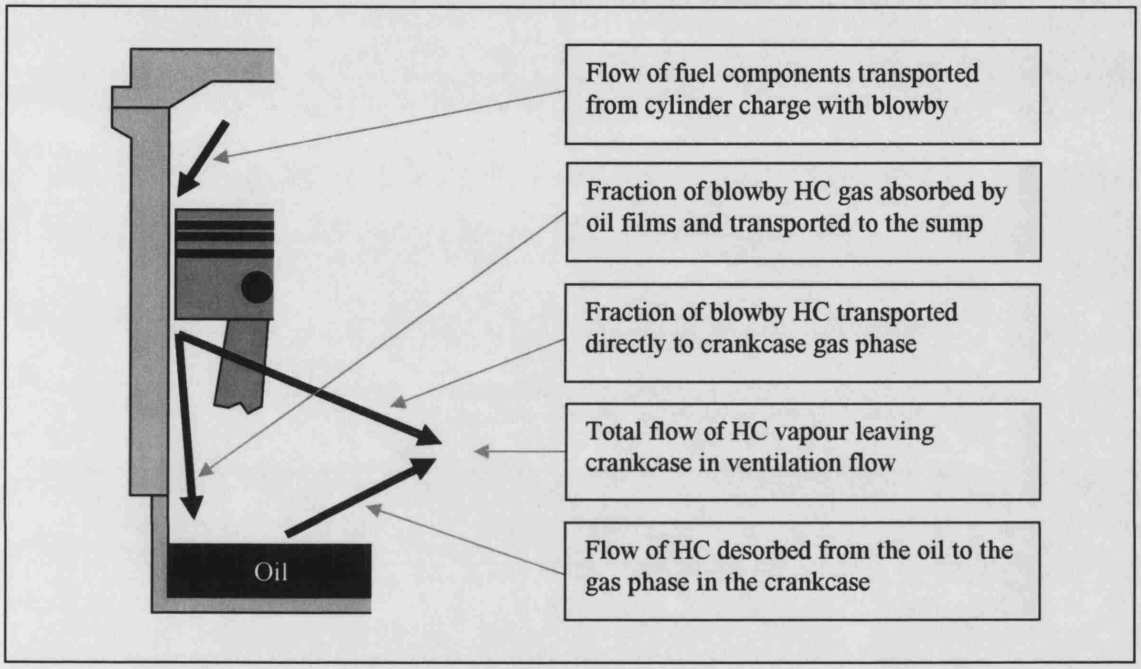

Figure 1.13 Fuel absorption and desorption in the crankcase
[reproduced from Shayler *et al* (2000a)]

Positive Crankcase Ventilation (PCV) is the venting of the crankcase through a valve to the inlet manifold. This can lead not only to increased hydrocarbon emissions, but also increased oil consumption. Froelund (2000) investigated this oil consumption problem in a 4.6l V8 engine by using an SO_2-tracer technique and found that oil consumption increased with engine speed. The average loss of oil through the standard breather valve for all speed and load combinations was 4.4% of the total engine oil consumption. It was found that refining the design of the breather valve could reduce this, with the best design reducing breather losses to 2% of the total oil consumption.

Stanglmaier *et al* [1997] considers that condensation of fuel vapour on cold surfaces of the combustion chamber during cold starts could contribute to HC emissions. During compression, there is an increase in the temperature and pressure of the bulk gas, vaporising droplets in the air, although fluid near the wall will remain at temperatures similar to the wall. Depending on the saturation pressure of the fuel at this wall temperature, it is then possible that vaporised fuel will condense on the wall, since the partial pressure of the fuel vapour in the mixture increases in proportion to the cylinder pressure. Condensation occurs when the partial pressure of the fuel vapour exceeds the saturation pressure at the cooler wall temperature. This condensed fuel is then protected by the boundary layer until the expansion stroke, where it is free to vaporise at the lower pressure and contribute towards HC emissions [Heyward (1988)].

1.4.7 Three-Way Catalyst

The three-way catalyst is the most common means of emission reduction in production automobiles today. Once warmed up, it is very efficient at reducing NO_x, CO and HC emissions. The catalyst must operate at stoichiometric air fuel ratio because it is very sensitive to the availability of oxygen. To maintain stoichiometric operation, a lambda sensor in the exhaust manifold detects oxygen and provides feedback to the engine management system. Due to the nature of this feedback loop, the air fuel ratio oscillates either side of stoichiometric at around 0.5 to 1 Hz. Using a rich mixture causes excess unburned hydrocarbons and carbon monoxide, preventing full oxidation. If however the mixture is too lean with excess oxygen present, NO_x emissions are not fully reduced. This dependence on stoichiometric air fuel ratio for optimum emissions reduction is shown by Figure 1.14. A very important requirement of the catalyst is that it should warm up to its operational temperature of about 300°C quickly. The temperature at which this occurs is known as the light-off temperature. This temperature is lowered to an extent by the addition of rhodium. Several different solutions have been devised to overcome the problem of reducing the light-off time. The simplest method involves using a retarded spark for a short time after starting. Another means of reducing this light-off time is using a combination of electrical heating of the catalyst and an air supply prior to the catalyst. This provides the desired high temperatures due to oxidation reactions of the exhaust gases, but the cost and complexity of this system limit its use.

Instead of heating the catalyst, another means of reducing cold start HC emission considered heating the fuel and vaporising it with an air assisted fuel vaporiser [Jackson (1997)]. This method reduced HC emissions by 48% and required less electrical heating than the heated catalyst.

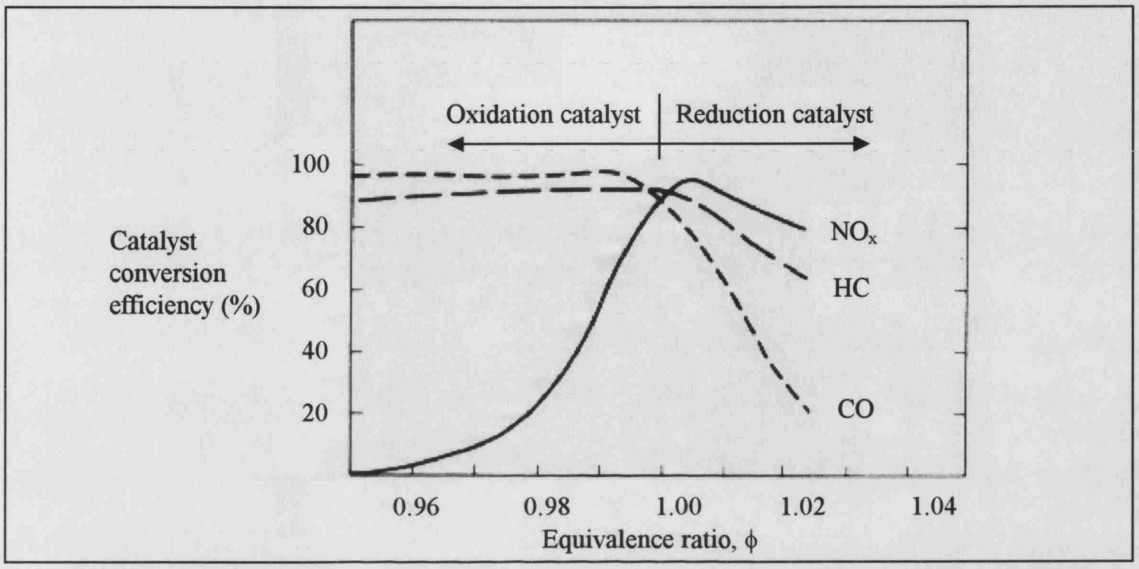

Figure 1.14 Catalyst conversion efficiency [reproduced from Stone (1999)]

Another approach is to use both a small and large catalyst in series. The small catalyst is close coupled to the exhaust manifold and warms quickly. The exothermic reactions of the first catalyst then heat the second larger catalyst. The smaller catalyst is then by-passed after light-off to prevent catalyst ageing and help reduce endurance problems. This approach does reduce light-off time, but its complexity limits its interest.

1.4.8 Carbon Dioxide (CO_2)

This is not seen as a toxic pollutant in the same way as the other emissions mentioned, but is important because carbon dioxide is a 'greenhouse gas' and has the potential to contribute to global warming. Combustion of a hydrocarbon fuel will result in CO_2, so the only ways of limiting its production are to reduce fuel consumption or use an alternative low or zero carbon fuel. Since alternative energy sources such as fuel cells are still in development and unlikely to replace internal combustion engines for some time, engine manufacturers have placed emphasis on reducing fuel consumption. A reduction in fuel consumption will have the added bonus of reducing the other emissions.

Lean Burn and Stratified Charge Engines

A lean burn engine may operate with a homogeneous or non-homogeneous (stratified) charge. Under low load conditions lean burn engines can often operate with AFRs of about 20:1, much leaner than the stoichiometric AFR of 14.7:1, although a strict requirement for the successful operation of lean burn engines is that they must exhibit high turbulence. A problem encountered with these lean burn engines is that effective use of a three-way catalyst is not possible since the mixtures are not stoichiometric. This results in lower tailpipe emissions of CO_2 due to lean combustion, but higher values of NO_x and HC than that of conventional port injected engines because there is no catalyst [Brogan *et al* (2000)]. However, since the combustion temperatures are reduced by use of a lean mixture, the engine out NO_x emissions are lower than that those of a stoichiometrically fuelled engine. During cold start, fuel enrichment is still required, so unburned hydrocarbon emission is still a concern in the same area as conventional engines. For these reasons, lean burn catalyst research is currently an important topic.

Improvements in turbulence generation and combustion chamber design have led to the port fuel injected Honda VTEC-E engine, which achieves an air-fuel ratio of at least 22:1 [Horie et al (1992)]. By injecting late in the intake stroke, a rich mixture is produced near to the spark plug, whereas a relatively weak mixture is present in the lower half of the cylinder. Toyota, like Jaguar, employs a swirl-control flap in one of the two intake runners below 2800 rpm to achieve a lean burn engine [Lumley (1999)].

The ultimate goal of the stratified charge engine is to generate the specific output of a gasoline engine while operating with efficiency similar to that of a diesel engine. The key to achieving this is to create an easily ignitable rich fuel mixture in the vicinity of the sparking plug, while the remainder of the cylinder contains a mixture that is too lean for combustion. If the engine output is controlled by varying the fuel supply and valve timing rather than using a throttle, the efficiency is improved further since the respective throttle and pumping losses are reduced. Injecting during compression has the added benefit that knock is much reduced, allowing a more efficient higher compression ratio.

Direct Injection Stratified Charge Engines

This type of engine is attractive because it allows even greater charge stratification than can be achieved with port-fuelled engines. Most manufacturers have operated at air fuel ratios of up to 48:1, although Toyota claims it has achieved 55:1 [Lumley (1999)]. Creation of a direct injection stratified charge engine involves accurate design of the bowl in the piston crown and the respective positions of the injector and spark plug. This is because the rich pocket must be in the vicinity of the spark plug for all engine conditions, which is extremely hard to achieve. The Toyota design relies on high levels of swirl being created within the piston bowl which is then enhanced by compression to achieve rapid air-fuel mixing. Huang et al (2001) investigated the effect that wall and piston wetting in direct injection engines had on HC emissions at different engine speeds. It was found that when the quantity of impacted fuel was held constant, the level of HC emissions was almost independent of when the fuel was injected, indicating that the mass of impacted fuel had a greater influence than the time for evaporation. Figure 1.15 shows piston wetting is almost unavoidable during typical late injection.

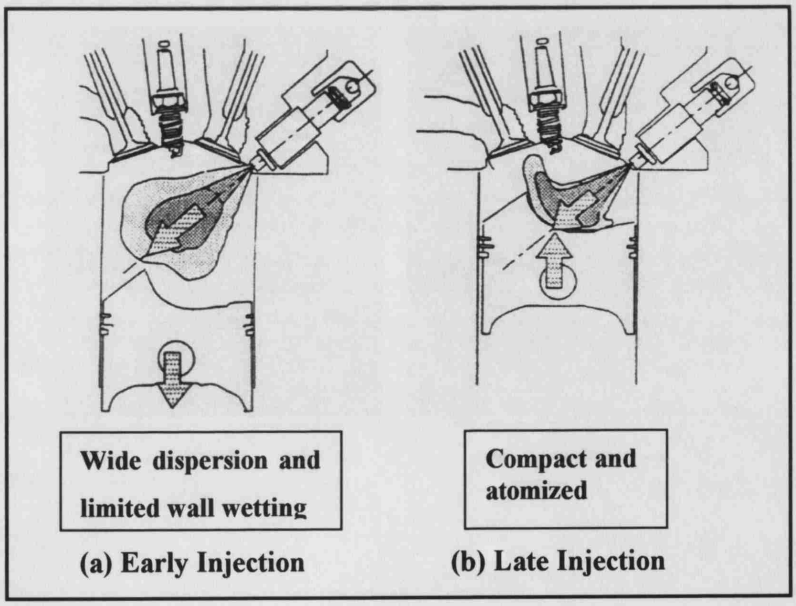

Figure 1.15 Early and late direct injection [reproduced from Kume *et al* (1996)]

Direct injection engines operating at low load also encounter problems with HC levels when the flame is quenched and does not successfully burn all of the fuel beyond the local combustible mixture zone [Zhao *et al* (2002)].

1.5 TRIBOLOGY OF THE CYLINDER AND PISTON

1.5.1 Introduction

Tribology is defined as 'the study of the phenomena and mechanisms of friction, lubrication and wear of surfaces in relative motion' [Schorr (1996)]. Piston friction force is of huge concern to engine manufacturers because it accounts for up to half of the total engine friction. Reduction of piston friction will not only reduce wear, but also create a more efficient engine. This tribology section was included because it highlights how cylinder wall wetting can wear an engine by washing the oil from the bore surface or even result in the chemical attack of the cylinder bore due to the chemical reactions that occur during combustion. The different types of cylinder liner are also discussed, where some of the more recent liner technologies can be more susceptible to wear.

Engine oil serves many purposes. The most obvious requirement is that the oil should provide excellent lubrication so as to reduce engine wear and friction, allowing maximum mechanical efficiency to be reached. The oil also performs an important role in engine cooling and heat dissipation at areas within the engine that exhibit high friction.

1.5.2 Piston Friction

Piston Rings

The cylinder oil film thickness is determined by the action and performance of the piston rings [Basaki *et al* (2000)], where different piston ring profiles can greatly affect the thickness of the oil film. Different profiles can allow a thicker film to be left with the upward or downward movement of the piston. Piston ring flutter and torsional vibration within the piston ring groove, especially at high speeds, further modify the oil film generated, increasing oil consumption. The problem is worsened as the cylinder bore deforms slightly due to pressure, thermal loads, abrasion and head bolt tightening. Proper lubrication of the piston and cylinder is very important because most engine friction originates from piston and bore contact.

A large proportion of the piston friction originates at the piston rings. A possible means of reducing the piston ring friction is to use only two piston rings, relying on a sole compression ring [Pietrobello *et al* (1994)]. This removes the friction of one ring and

allows for a smaller and lighter piston, although an increase in oil consumption was detected. It was found that a special lap-jointed compression ring and larger separation between the two rings improved oil consumption [Yoshida *et al* (1995)].

The tribology of the piston rings is a complex mechanism that consists of many factors as described by Tomanik (2001), who attempted to model the phenomena in the interest of studying engine wear. An initial point is that the profile of the ring leads to non-conforming surfaces, while transient loads and speeds occur at different points in the piston stroke. It is known that the friction appears in either boundary, mixed or hydrodynamic form. Boundary lubrication is experienced when the microscopic peaks of interacting surfaces make contact, whereas hydrodynamic lubrication exists when the working surfaces are separated by a film of oil. The transition between these regimes is called mixed lubrication. The friction effects are further complicated by the presence of abrasive particles in the oil and change in shape of the ring due to thermal deformation. The quality of the oil is affected by other factors such as corrosive combustion by-products and engine starts and stops. Tomanik (2001) also describes how a major influence on the performance of the ring is how the shape of the running profile is modified by wear over time.

Piston ring microwelding is a phenomena that describes the scuffing and sticking of iron piston rings to aluminium pistons. Shuster *et al* (1996) investigated this problem and summarized that it is created by temperature extremes affecting the stability of the metal and can be prevented by piston ring coatings, notably with fluoroplastic materials.

Piston Skirt and Pin Boss

The piston skirt has also been a target for possible means of friction reduction. Nakayama *et al* (1997) used the floating liner technique to investigate skirt lubrication and scuffing. It was found that reducing the diameter of the skirt increased friction force due to reduced contact area and that an eccentric gudgeon pin on the anti-thrust side of the bore could reduce the large friction forces experienced on the thrust side of the cylinder during expansion.

Teraguchi *et al* (2001) investigated piston slap noise and piston friction loss in a diesel engine by varying the amount of oil present between the piston and cylinder bore. An accelerometer mounted on the cylinder block was used to determine the magnitude of the slap noise. The oil was delivered at a known flow rate to the inside of the piston at a range of locations via a Teflon tube that was supported by a special mechanism. It can be appreciated from the work that the gains in lubrication are quite small and definitely not practical for mass production purposes, especially due to the small increase in oil consumption detected with this technique.

The work of Suhara *et al* (1997) on the tribology of the piston pin boss highlighted that despite possible weight savings, the gudgeon pin should become no shorter or thinner due to the increased friction effort and worsened lubrication characteristics. It was found that reducing the surface roughness of the pin could lower its frictional work. Complexity and cost eliminate the possibility of using a fully lubricated pin, but the use of bearing material in the pin boss greatly reduced friction.

1.5.3 Experimental Studies of Piston Friction and Bore Wear

The creation of reciprocating test rigs that allow study of the friction and wear of piston rings was performed by Hartfield-Wünsch *et al* (1993) and Ting (1993a,b), where the results from these tests form useful information for computational models. These rigs employed heaters to warm the oil to representative engine temperatures, in addition to maintaining correct engine dimensions such as stroke and piston size. These test rigs were more flexible than complete engines as they allowed quick changes of test condition. The liner, piston or ring, type or finish can be changed in addition to the type and quantity of lubricant. The addition of fuel for dilution tests was also possible. The shortcomings of the rigs was that they did not allow for the twisting of the piston during extremes of combustion or the action of blowby indicating that running engine tests are still critical for final design choice.

Koch *et al* (1996) used the floating cylinder liner technique to investigate piston friction force in a running engine. This consisted of an axially moveable cylinder liner and special tubular gasket pressurized by gas pressure. The load cell that measured the friction force was mounted on a step on the outside of the liner and connected to the cylinder block.

The cell was positioned in such a way that it was placed in compression or tension by upward and downward movement of the piston respectively. The results of force against crank angle can be seen in Figure 1.16.

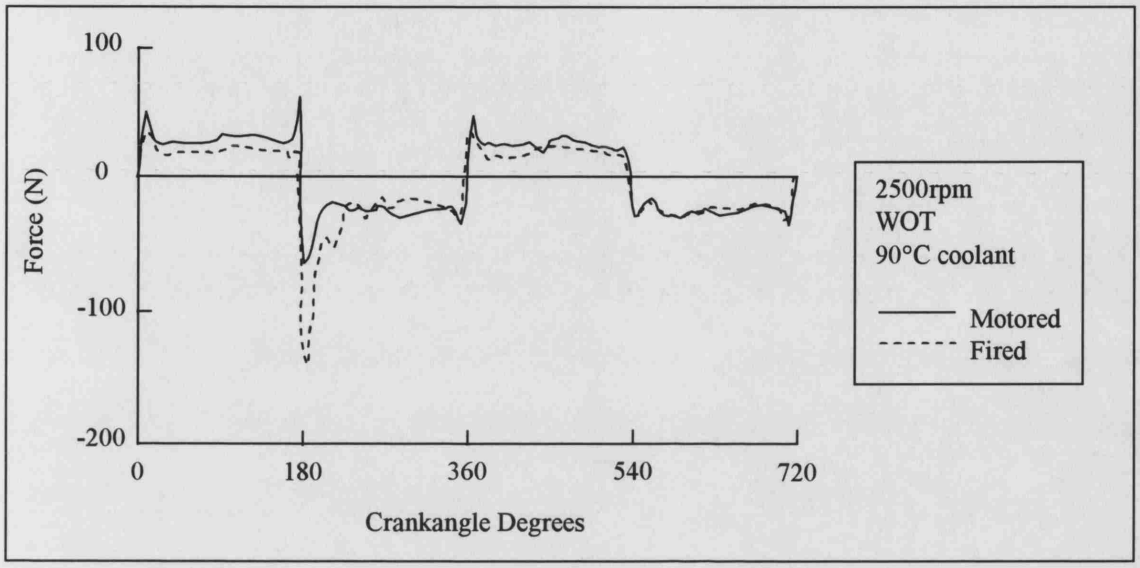

Figure 1.16 Piston friction and crank angle [Koch *et al* (1996)]

This diagram shows the expected positive and negative bulk forces for upward and downward piston movements. An interesting feature is the increase in friction at the early section of the expansion stroke due to the gas forces and lateral piston movement. It is also clear that the magnitudes of the forces increase at the start or end of the strokes due to the slow piston experiencing boundary, rather than hydrodynamic, lubrication. This was confirmed by Radill (1996) who stated that the extremes of piston movement or top ring reversal (TRR) are the most critical points in the engine cycle for piston-induced cylinder wear.

1.5.4 Oil Dilution by Fuel

Shayler *et al* (2000b) detailed the effects cold starts, short journeys and low engine speeds have on oil dilution. In this work, it is described how Kollmann *et al* (1998) managed to achieve an average of 17% oil dilution in five vehicles that were driven solely under certain conditions for 2 years. When one of these vehicles was driven under motorway conditions for 8 weeks, the reduced oil quality resulted in large-scale bore and bearing wear. It was found that the oil was diluted by the heavier fractions of the fuel

since the lighter fractions would have evaporated by the time the fuel could come into contact with the oil.

1.5.5 Formation of Acidic Chemicals

Not all of the fuel absorbed by the oil is desorbed back into the exhaust gases. The remaining fuel either dilutes the oil or forms part of a complex chemical reaction that produces acidic chemicals under the high pressures and temperatures in the cylinder. These acidic chemicals then attack the cylinder wall, resulting in bore wear.

Sulphur is a problematic component in fuel since it is not completely removed from crude oil during the refining process. It can corrode the fuel system and fuel that was absorbed by the oil on the cylinder wall can eventually reach the crankcase, where it forms sulphuric acid [Ferguson (1986)].

The mechanism of sulphuric and sulphurous acid formation within the combustion chamber is given by Caines *et al* (1996).

$$2S + 2O_2 \rightarrow 2SO_2$$

$$2SO_2 + O_2 \rightarrow 2SO_3$$

$$SO_2 + H_2O \rightarrow H_2SO_3 \text{ (Sulphurous acid)}$$

$$SO_3 + H_2O \rightarrow H_2SO_4 \text{ (Sulphuric acid)}$$

Caines *et al* also stated that leaded gasoline contains scavengers that reduce the accumulation of lead salts in the combustion chamber. The scavenger compounds ethylene dichloride and ethylene dibromide can react to produce complex chlorine and bromine oxy-acids in addition to hydrochloric and hydrobromic acids, all of which contribute to engine wear. A further problem with corrosion is that the dissolved metals can actually catalyze oxidation reactions and contribute to deposit formations Owen *et al* (1995). It is common for the corrosive effect of sulphuric acid formed during combustion to be counteracted by the use of alkaline cylinder lubricants.

BMW had problems with premature engine wear in its Nikasil lined engines and blamed excess sulphur compounds in the fuel [Autocar (1998)]. It was thought the damage occurred during cold start when acids generated by combustion attacked the nickel base material. Rival companies that also used Nikasil claimed to have no such wear problems because their engines were intended to warm quicker to reduce catalyst light-off times.

1.5.6 Cylinder Liners

Traditionally, cylinder liners were cast iron and described as wet or dry, depending upon whether the cooling water flowed directly against the back of the liner or whether there was a section of cylinder block between the liner and the coolant. Engine manufacturers are moving towards aluminium cylinder blocks since this provides great weight savings, as already exploited with the piston. However, aluminium is less wear resistant than cast iron, so the cylinder block must either employ cast iron cylinder liners or use special cylinder wall coatings that effectively improve the mechanical properties of the aluminium surface.

Metal-Ceramic Cylinder Liners

The most popular ceramic composite cylinder liner in use today goes by the trade name of Nikasil. Nikasil is an electrochemical dispersion coating of nickel-silicon-carbide applied directly to the cylinder bore. Such coatings are now extremely important in internal combustion engines because a thin coating of this compound effectively changes the mechanical properties of the base metal [Ostermann (1979)]. For instance, a Nikasil coating adds wear resistance to relatively soft aluminium 319 or 390 base metals, making it possible to use aluminium for lightweight cylinder blocks without a separate liner. The Nikasil plating is so tough that it can withstand the forces of several piston scoring "episodes" with virtually no damage to the bore [Ostermann (1979)]. The silicon carbide is beneficial to the formation of the cylinder oil film since these particles form many evenly distributed points that help the oil film cling to the cylinder wall. This helps eliminate the problem of cold-start piston scuffing as described by Xiaohong *et al* (1996). A means of investigating and evaluating the scuff problem was explored by Malaczynski *et al* (1996), who had developed a bench test for comparing scuff in different piston and liner combinations. Ceramic bore coatings also help reduce oil consumption since the coatings have a lower coefficient of friction and a coated

aluminium bore is less distorted than an iron lined bore due to superior heat flow properties. Since Nikasil has a lower coefficient of friction than that of conventional iron or chrome liners, a reduction in the frictional losses by the piston is possible. This advantage has the second benefit of reducing wear of the cylinder bore, piston and piston rings. According to Funatani *et al* (1994), the friction coefficient of Nikasil is only 0.08-0.12, whereas the alternate hard chromium plating has a value of some 0.28-0.48. The ceramic coating would still require the same conventional base and plateau honing process as the conventional cast iron liner [Radil (2000)].

Nikasil cylinder liners also exhibit superior thermodynamic properties in that they can withstand high temperatures and allow for better heat flow to the water jacket. Since the Nikasil plating will expand at the same rate as the aluminium bore and piston, the problem previously encountered of the iron liner expanding at a different rate than the aluminium is removed, allowing tighter clearances between the piston and the bore. The Nikasil layer is also more ductile than the brittle chrome equivalent, reducing the possibility of heat-induced liner damage.

In the interests of optimizing wear performance, the piston rings can be coated with silicon carbide and the piston coated with nickel alone, whilst it has already been mentioned how Boehm explored knock damage limitation by coating the pistons with nickel. According to Rao *et al* (1997a), 30% of piston friction can arise from piston slap. It was found that coating the piston skirt alone reduced friction while also promoting superior oil film formation.

The mechanical properties of Nikasil can be improved with the addition of other compounds [Funatani *et al* (1994)]. For example, the addition of phosphorus to Nikasil increases its high temperature integrity, while silicon nitride (Si_3N_4) increases the wear resistance and lubricity of Nikasil yet further.

A further economic advantage of Nikasil is that it reduces the manufacturing times of cylinder blocks. According to Ostermann, if chrome or Nikasil plating is applied via a traditional chemical deposition means, deposition rates of 0.7 to 1 μm/minute and 0.3 to

0.5 μm/minute are achieved respectively. If however the Nikasil is applied by electrochemical means as developed by Mahle, the deposition rate is 4 to 16 μm/minute. Before electroplating with Nikasil became widespread, a method of impregnating the cylinder bore with silicon carbide alone was used [Tanner (1983)]. This process involved seeding a mineral oil with silicon carbide and then pressing the resulting slurry into the cylinder bore by iron rollers that followed a rotating and reciprocating motion. This process was then repeated with a finer grade of silicon carbide to achieve the required honed surface. A final polish with leathers in the same honing motion finalizes this 'Laystall' silicon carbide process.

It appears that electrochemical coating of Nikasil has become the standard means of application, while a recent variation of the process allows plating of even v-based engines on a high production rate basis. To increase the cost efficiency of engine mass production, methods of cylinder liner application that are faster than electroplating have been devised and implemented [Rao *et al* (1997b)]. The two methods mentioned include plasma transfer wire arc and the plasma powder spray process, which offer application of any material including ceramic powders at rates up to 10 kg/hr.

The latest type of coating to appear is called Keronite. This is based on plasma electrolytic oxidation and could possibly replace plasma spray ceramics, hard anodising and hard chromium plating [Wilks (2000)]. The process works by dipping the alloy in an alkali electrolyte solution while a current is passed through it. Sparks given off around the alloy create a plasma discharge around the component that results in surface oxidation and coating formation at a rate of 1 micron per minute to a maximum coating thickness of 50 to 70 microns. Overall, this process offers low running costs and an electrolyte that is easy to dispose of, making it a viable alternative to previous methods. A possible drawback is that it may not be possible to coat the bore alone, requiring either the entire component to be coated or a selection of masks to be used during dipping.

1.6 HEAT TRANSFER IN ENGINE PORTS, CYLINDER AND PISTON

1.6.1 Introduction

This work is not a study of heat transfer in the engine for its own sake, but uses it to study fuel films. This chapter aims to briefly explain the methods by which the heat transfer is occurring and the basis of the heat flux sensor technology.

There are numerous locations within an engine where heat transfer occurs, with these heat transfers occurring at different points in the engine cycle. During closed valve injection for a warm engine, there will be a heat transfer from the warm port and valve surfaces to the fuel. The induction stroke permits heat to flow from the warm piston and cylinder surfaces to the cool charge as it enters through the inlet valves, while the compression of the mixture generates a heat flow from the increasingly hot gas to the cylinder wall. Combustion causes the largest heat transfer with heat flowing from the hot gas to the piston in addition to the cooled cylinder wall and cylinder head. Cooling is important because it allows a high volumetric efficiency, proper combustion and mechanical reliability [Stone (1999)]. The heat flow from the gas reduces throughout the expansion stroke as the gas expands and remains approximately constant for the remainder of the exhaust stroke.

1.6.2 Modes of Heat Transfer

Heat transfer 'Q' is the rate at which energy moves across a thermodynamic barrier and is measured in watts (W). Heat transfer occurs in three different modes; conduction, convection and radiation [Heywood (1988)]. Heat flux 'q' is the rate of heat transfer per unit area and is measured in W/m^2 or W/cm^2. Conduction is the movement of heat through a solid or stationary liquid due to a given temperature gradient, as shown in Figure 1.17. Heat flow through a material depends on properties such as its conductivity, density and specific heat capacity [Kamo (1989)]. Convection is the transfer of heat in moving fluid or between fluid and a solid wall. Forced convection is common in the engine since factors other than gravity will influence the fluid motion. Heat transfer by radiation implies the emission or absorption of electromagnetic waves and occurs at any engine surface. The highest thermal resistance experienced within an engine is in the boundary layer of the combustion chamber [Stone (1999)].

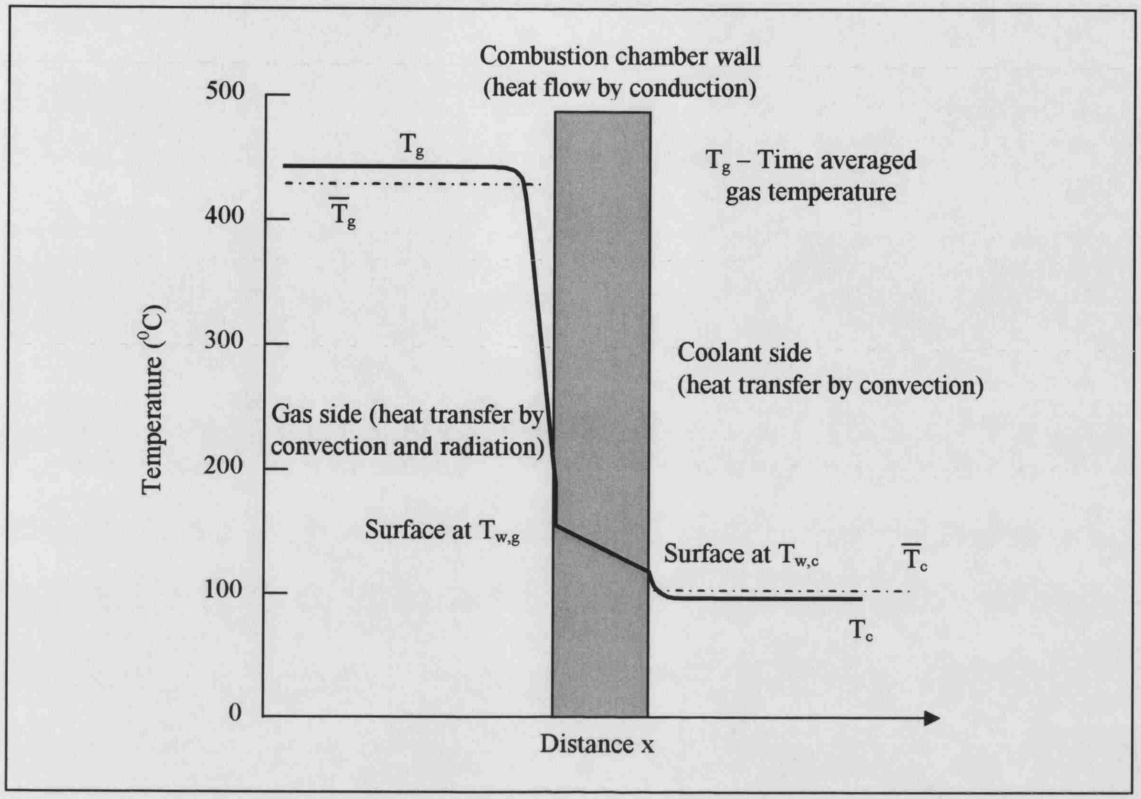

Figure 1.17 Temperature distribution across the boundary layer, cylinder wall and coolant [reproduced from Stone (1999)]

1.6.3 Modelling of Heat Transfer

Completely theoretical prediction of heat release and transfer from combustion is virtually impossible, so models rely heavily on experimental test data. A review of heat release models and some of their fundamental equations, notably those of two-zone models where the burned and unburned gases are treated separately is presented in Guezennec *et al* (1999). The models effectively work backwards by determining the rate of heat release from experimental cylinder pressure data, while exhaust data provides information on the efficiency of combustion [Grimm (1990)]. This process readily allows a study of the burning properties of different fuels or the suitability of an engine's design for optimum combustion. One of the most important factors to be calculated by the model is the gas temperature [Stone *et al* (2000)].

The information generated by the models on items such as burn rate can then be transformed to other useful forms such as a mass fraction burned plot (Figure 1.18).

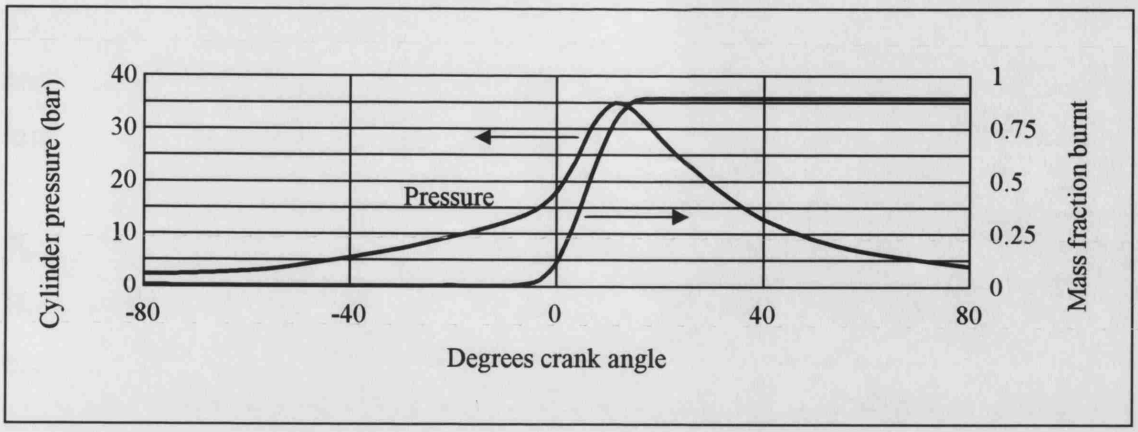

Figure 1.18 Typical mass fraction burned plot [Stone (1999)]

A single zone model uses cylinder pressure traces and considers constant properties found at an average temperature, while the more complex two-zone heat release models use crank angle resolved cylinder pressures and consider variable composition and properties. The single zone method is by far the more common since it is much simpler and can use several assumptions without great loss of accuracy, such as assuming the ratio of specific heats decreases linearly with temperature. A two-zone model can explore what the effects of engine speed, engine load, ignition timing and equivalence ratio have on the burnt mass fraction, which is something that can only be found by modelling and not experiment. Jensen *et al* (2000) created a three-zone model that included the various crevice volumes found within the cylinder. This was performed since these crevice volumes are known to be major sources of unburned hydrocarbons, which is an area of increasing concern among engine designers.

Modelling heat flow through the cylinder wall avoids the usual labour-intensive problems associated with experimental measurement. Also, modelling allows data to be observed for any point in the cylinder, whereas the experimental approach is restricted to finite locations. A further problem with the experimental approach is that the sensors should minimize the disturbance of the heat flux so as to ensure realistic results can be attained [Wimmer *et al* (2000)].

1.6.4 Heat Transfer to Engine Surfaces

The temperature distribution and magnitude of heat flux depend mainly on engine speed and load, although other factors such as equivalence ratio, compression ratio and spark timing are also important.

Port Surfaces

Heat flux sensors were positioned in the intake port of a 1.8l 4-valve cylinder head mounted on a Ricardo 'Hydra' single-cylinder engine by Shayler *et al* (1996), who has used heat flux sensors extensively to measure fuel wall films. This work is similar to that detailed in Section 1.2.3 and is thorough in its description of the various heat transfers that occur within the intake port. Bauer *et al* (1997) performed similar experiments on an almost identical cylinder head and mentioned that the sensors themselves formed a further layer between the port and the fuel, with the effective thickness of this layer being increased by the sensor fixing glue.

Cylinder Wall

The peak burned gas temperature in the cylinder is around 2500 K, however the surface of the cylinder wall must be kept below 180°C to prevent degradation of the oil film [Heywood (1988)]. Fortunately, the boundary layer provides a vast majority of this thermal insulation. Thin cylinder wall coatings allow improved heat flow from the cylinder wall to the cooling water with the added advantages of increasing the volumetric efficiency, improving piston tribological behaviour and increasing erosion and corrosion resistance [Kamo (1989)].

Calculating heat transfer to the cylinder walls requires knowledge of position averaged heat transfer coefficient [Guezennec *et al* (1999)]. This coefficient varies with time and position due to the moving piston, progression of combustion and the turbulent nature of the gas. This coefficient can only be found via experimental means rather than theoretical estimation due to the complexity involved. Ogawa *et al* (2000) studied heat release in a direct injection diesel engine, with part of the work studying the effect of varying the swirl ratios. It was found that heat flow to the cylinder wall was greater with a lower swirl ratio. Although this was due to turbulence affecting the path of the fuel spray and

the place of mixture formation, it is observed that turbulence is an important factor in heat transfer to the wall.

Piston

The piston experiences higher temperatures than the cylinder wall, with the centre of the piston typically being up to 50°C hotter than the edge of the piston. This is because the piston is not cooled by the circulating engine cooling water, it is constantly exposed to the combustion chamber and is less well protected by the thermal boundary layer [Heywood (1988)].

1.6.5 Application of Heat Flux Sensors in an SI Engine

Heat flux sensors are based on thermocouple technology. In this, there are two wires of dissimilar metal that will produce a voltage proportional to the temperature difference between the endpoints of the wires due to the Seebeck effect. It should be noted that the polarity of the heat flux sensor output voltage indicates the direction of heat flow, which is a key factor in determining if the sensor is being impacted by fuel droplets.

Ioannou (2000) successfully introduced heat flux sensors into the cylinder block of a single cylinder engine to monitor the impingement of fuel droplets onto the bore. This is feasible because the difference in the heat transfer coefficient between the cylinder gas and the cylinder wall is different to that of a liquid film and the cylinder wall. Thus if a sensor which was previously exposed to gas becomes covered with a liquid, a detectable difference in heat transfer rate should result [Vatell (2002)]. The work of Ioannou clearly indicated that heat flux sensors can be used to detect the presence of fuel droplets, but had not attempted to quantify the amounts of fuel deposited.

1.7 EXPERIMENTAL METHODS

1.7.1 Introduction

This section describes several experimental procedures that were used or considered in this work, such as the fundamentals of cylinder pressure measurement. Also detailed are the possible methods for liquid fuel detection and measurement in addition to those used by the author. Finally, the mechanism required for extracting a signal from a heat flux sensor in the piston of a running engine is described along with the data analysis software required for signal decoding.

1.7.2 Cylinder Pressure Measurement

Cylinder pressure measurement is achieved by using a pressure transducer. There are two types available that are suitable for this application, being either piezoelectric or strain gauge. Piezoelectric pressure transducers contain a quartz crystal mounted on a bellows that is exposed to the cylinder pressure. As the quartz crystal is compressed it generates a charge proportional to the pressure. A charge amplifier is then used to convert this small charge into an output voltage. Strain gauge pressure transducers also employ bellows, but with strain gauges attached to them. The stretching of the bellows will affect the output voltage of the strain gauge proportional to the cylinder pressure. The piezoelectric type transducer is the preferred choice since it has a faster dynamic response and is hence more appropriate for high speed engine tests. However, piezoelectric pressure transducers measure changes in pressure, whereas strain gauge pressure transducers measure absolute pressure [Amann (1985)].

Calibration of strain gauge transducers can be achieved using a dead-weight pressure tester, whereas piezoelectric transducers require dynamic calibration equipment. The output signal can then be converted into a convenient calibration equation. Cooling of the transducer is important since this will prevent thermal changes affecting the measured pressure, where even fluctuations in the water flow should be avoided since this could affect the output voltage. Ideally, low-pressure pumps integrated with temperature-control systems should be employed [Müller *et al* (1986)]. Traditionally, the diaphragm was coated with silicon rubber to eliminate thermal strain [Lancaster *et al* (1975)], although ceramic heat shields have superceded this technique.

In some circumstances it is not practical to introduce a hole on the combustion chamber surface of a cylinder head for location of a pressure transducer. To overcome this problem, a hybrid spark plug was developed that sparked as usual, but also created an in-cylinder pressure measurement location [McCullough (1953)]. A disadvantage of having a tube from the combustion chamber surface to the transducer itself is that the dynamic gas behavior of the gas in the tube can distort the trace, as shown in Figure 1.19.

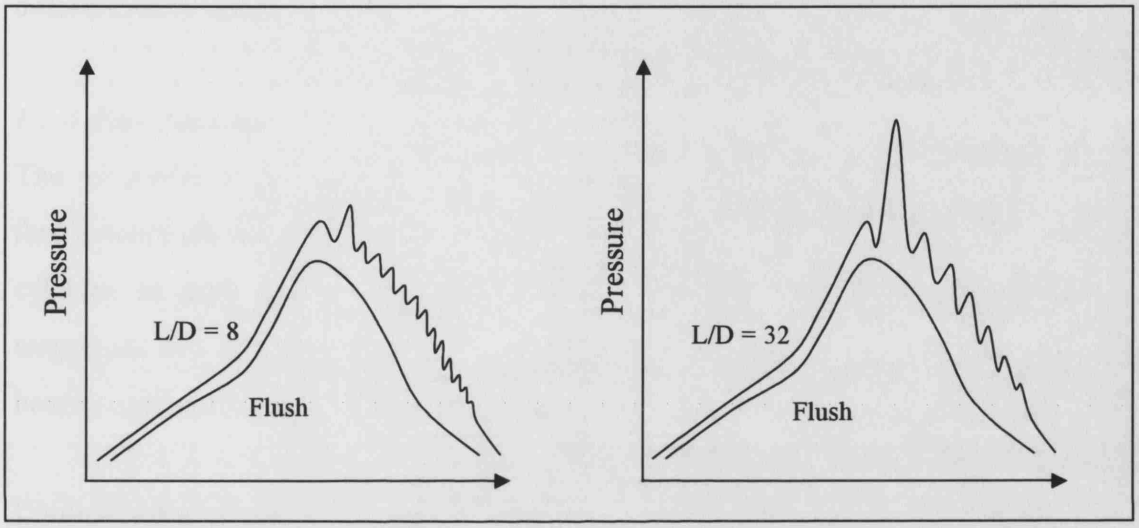

Figure 1.19 Pressure traces from a transducer mounted flush with the combustion chamber surface and via a connecting passage. Passage of length L and diameter D [Recreated from McCullough (1953)]

Boehm *et al* (1990) found that when measuring the cylinder pressure with a quartz pressure sensor on an engine that is running at knock conditions, the reading can be misleading due to cylinder block accelerations caused by the violent knock combustion exciting the quartz crystal. For this reason, in combination with cost and practicality, knock is commonly detected using accelerometers mounted on the outside of the cylinder block as opposed to a cylinder pressure sensor.

1.7.3 Measurement of Liquid Fuel on the Port and Bore Surfaces

Ioannou (2000) presented an exhaustive review of the possible techniques for liquid fuel film measurement. These are summarized as follows:

Porous Liner Technique

This method is discussed in depth in Chapters 2 & 3. The porous liner technique was originally devised by Miller (1992) and uses a porous cylinder liner in combination with a suction rig to create the airflow into the cylinder. There was no piston in this rig, but the inlet camshaft was motored within a production cylinder head while injection occurs as normal. A pressure drop across the porous material forced any fuel on it to pass through the cylinder to be collected in a suitable container. The location of the liquid fuel is determined by which section of the porous material the fuel is drawn through.

Heat Flux Sensors

The remainder of the thesis after Chapter 3 is based on the use of this technique. Heat flux sensors are constructed from an array of thermocouples and can be mounted in the cylinder or port surfaces. The advantage of these sensors is that they allow the magnitude and direction of heat transfer through the surfaces to be determined and are hence superior to conventional thermocouples.

Determination of the location of liquid fuel within the manifold by the use of a heat flux sensor was the work of Shayler *et al* (1996a). This method relied on the evaporation of fuel reducing the local temperature of the manifold surface and causing a change in heat flux through the port surface. The sensor was positioned on the lower surface of the port and an average heat flux of 5 kW/m^2 was recorded throughout the engine cycle, although two peaks above this value were detected. The main peak of 50 kW/m^2 was achieved when the fuel landed on the sensor and the second peak of 30 kW/m^2 was due to convective mass transfer of the fuel to the air during the induction stroke. The injector was inactive at the time of the second peak, removing the possibility of the fuel being in droplet form. The former peak was reduced when the engine coolant temperature was lowered due to the reduction in port temperature while the second peak reduced less since the induction airflow was still present. Shayler *et al* (1996b,c) then positioned heat flux sensors at several positions in the intake port as shown in Figure 1.20. It was found that sensors 4 and 7 experienced the highest heat flux throughout the cycle due to the above reasons. The fact that the second peak exists only for these two sensors indicates that gravity must have been holding the liquid fuel on the lower port surface.

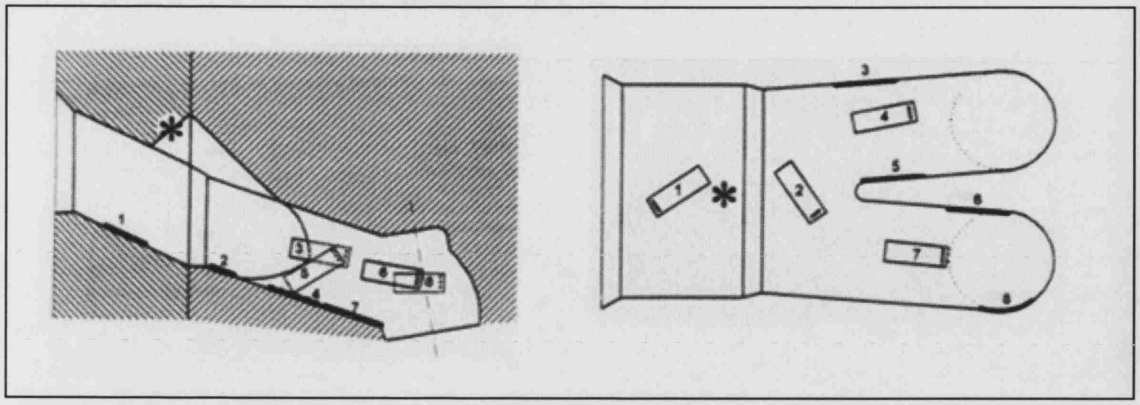

Figure 1.20 Heat flux sensor positions in the intake port [Shayler *et al* (1996b)]

Thermocouples

Attaching thermocouples to the port wall would indicate the presence of liquid fuel because the difference between a dry and a wet thermocouple output trace would be due to the impingement or evaporation of the fuel. This method is not suitable for bore measurements due to possible collision with the piston and the problems of attaching the thermocouples to the cylinder surfaces securely enough that the heat of combustion does not remove them.

Laser Induced Fluorescence (LIF)

This well-established method requires a laser of specified wavelength to illuminate the fuel, which then fluoresces and emits a light. It is assumed that a higher intensity of emitted light indicates a greater amount of fuel being present. It is actually the aromatic fractions of gasoline that emit the stronger fluorescent light when excited by the laser. Since the lighter fractions do not emit as strongly and also evaporate earlier than the heavy fractions, the intensity of light observed could provide a misleading indication of the liquid fuel film thickness. To avoid this, a combination of isooctane fuel and a dopant can be employed [Hentschel (1997)]. The mixture is seeded with particles that fluoresce when targeted with a laser, where a higher intensity represents a thicker fuel film [Dawson *et al* (1998)]. A problem with the LIF technique is that the evaporation of the tracer must coincide with the rate of evaporation of the fuel, with further complications arising from the compatibility of the vapour pressure of the two substances. Hentschel concluded that there would be a fuel wall film in the manifold that could be up to 300 μm

thick. The use of optical engines in the study of wall films can be misleading since methods such as LIF often use fuels other than gasoline, which further affects the air/fuel formation process [Egermann *et al* (2000)].

Laser-Type Optical Method

A laser-type optical sensor is used in this method. The liquid/vapour interface forms the reflecting plane of the laser beam and the intensity of the reflected light is proportional to the liquid fuel film thickness. This method operates on the principle that when the light passes from the high refractive index of the fuel to the lower refractive index of air, the direction of the laser is changed. This technique is therefore based on internal reflection and is forced to operate within many geometrical restraints.

High-Speed Video Recording

This technique employs a transparent cylinder wall and piston for illumination and camera access purposes. High-speed film or digital cameras are used, limited by tape length or available memory. Since this method is limited to slow motored speeds, it is useful for studying fuel films at start-up. Discrimination of the liquid fuel on the engine surfaces can be difficult.

Cylinder Content Isolation and Fuel Vapour Extraction

This technique requires a modified engine that has the inlet and exhaust camshafts replaced with a hydraulic mechanism that shuts the valves at a desired point in the cycle. Flame Ionization Detection then allows determination of the amount of fuel in the cylinder.

In-Cylinder Flame Ionisation Detection (FID)

By disabling the injector while a FID probe is mounted on the cylinder wall, it is possible to examine the amount of fuel that is introduced into the cylinder during the following cycles, although there are many areas for possible inaccuracy in this method.

Ioannou (2000), Miller (1992) and Queenan (1998) used the porous liner technique to determine the locations of surface fuel flows and airborne droplet impactions. Ioannou alone employed the heat flux sensor technique.

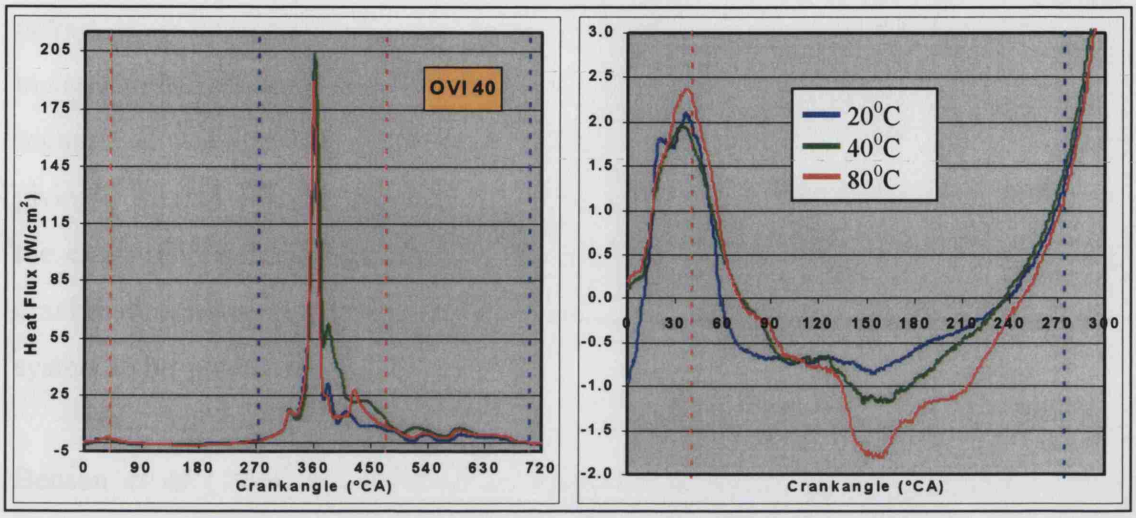

Figure 1.21 In-cylinder heat flux traces [Ioannou (2000)]

Figure 1.21 shows three heat flux traces taken from the firing single cylinder engine used by Ioannou in the heat flux experiments. The first plot shows the heat flux from the entire cycle, while the second looks only at the inlet valve open period, which is of most interest in these fuel film and droplet impaction studies. The three lines are traces obtained from the same sensor location, but at different engine coolant temperatures. The temperature will affect the rate of evaporation of the fuel from the cylinder surface. The time between injection at 40° ATDC and the change in signal at about 120° crank angle is the time of flight of the fuel from the injector tip to the cylinder wall. The cool 20°C coolant will cause limited evaporation of the fuel from the cylinder surface, while the 40°C and 60°C coolant temperatures increase evaporation. The negative heat flux value indicates heat flow from the sensor to the fuel, where the most negative value indicates highest heat flow. The opposite effect is seen during compression and combustion when the heat flux is most positive, indicating heat flow to the cylinder wall from the hot gas. Ioannou proved that heat flux sensors mounted flush with the cylinder bore could be used to detect liquid fuel, but did not attempt to quantify the amount of fuel. A logical progression would be to position heat flux sensors on the piston crown.

1.7.4 Sensor-in-Piston Techniques

It is sometimes desirable to position sensors on the surface of the piston to record information such as piston surface temperatures or heat fluxes. Invariably the problem with performing such a task is not attaching the sensor in the piston, but connecting the sensor to a convenient location outside the engine. The first problem is the rapid movement of the piston where even at only 1500 rpm the piston performs 25 cycles per second. At this speed, if a mechanical linkage were used it should be light and robust giving it a rapid dynamic response. The second problem is the limited free space within the crankcase caused by the relative movements of the connecting rod, crankshaft and crankshaft counter-weights. Finally, the heat and oil within the engine require a robust system to be employed.

Benson *et al* (1979) managed to successfully record the surface temperatures of a conventional piston using the link mechanism shown in Figure 1.22. This illustrates that a small side plate attached below the piston acts as a suitable connection point for a stainless steel tube that carries the sensor wires from the piston to a stationary take-off point.

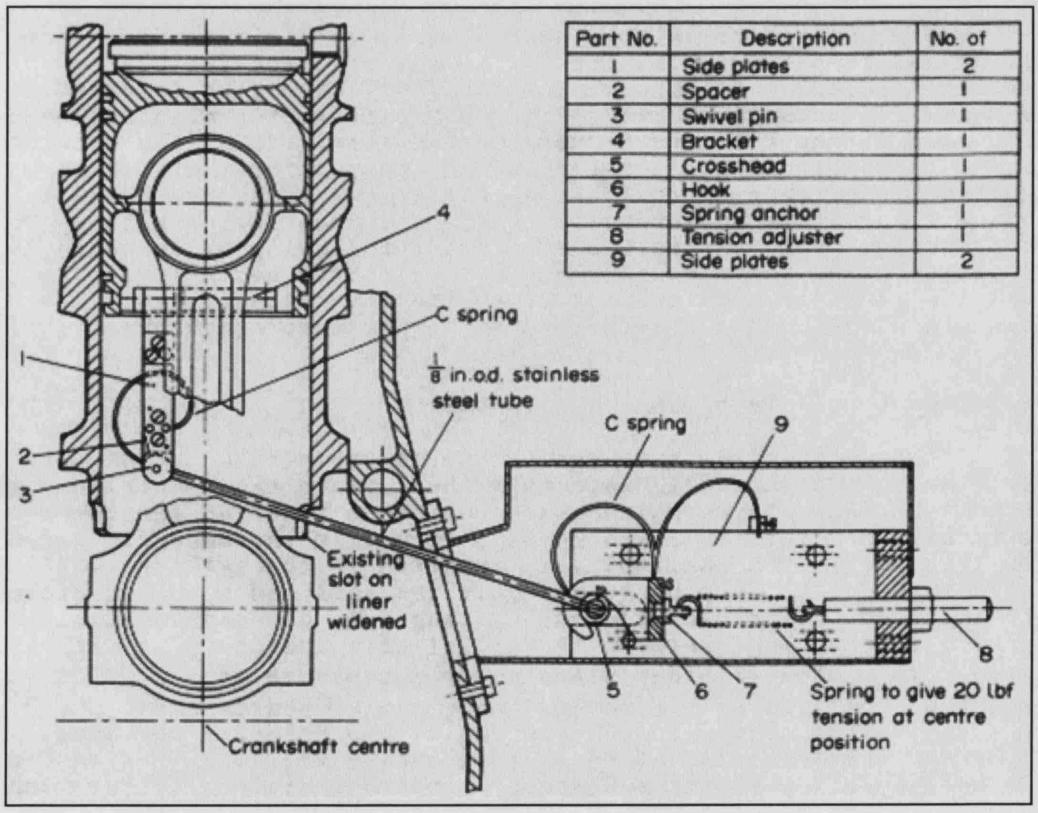

Figure 1.22 Piston surface temperature mechanism [Benson *et al* (1979)]

In a majority of engines this approach would not be possible because when the piston is at bottom dead centre, the raised crankshaft counterweights would occupy the space either side of the connecting rod where the side plate and tube would be. To overcome this space problem other methods such as the commercially available 'grasshopper' or 'L-link' have been devised [Rowe (1998)]. These mechanisms form a 'bridge' from the bottom of the connecting rod to the sump in an area where more space is available. These mechanisms are typically two lengths of hinged tube through which the sensor wires are passed. Finding the correct balance for the relative lengths of the linkage arms is important since this will directly determine the bend radii of the wires. The wires themselves also have to be chosen carefully so as to limit fatigue failure. This was the approach taken by [Mure *et al* (1989)] since other methods were not suitable for the cramped engine under test. Figure 1.23 illustrates the final linkage design.

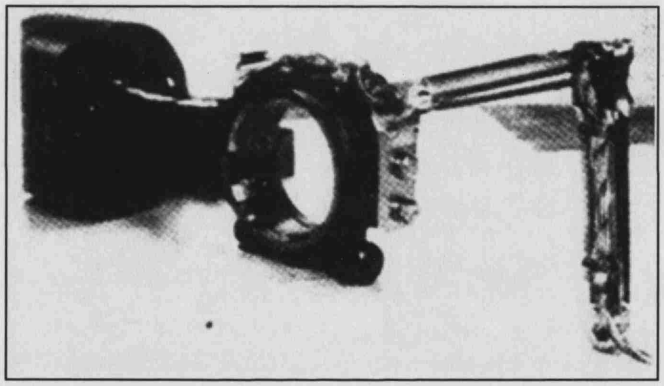

Figure 1.23 Conrod type wires and linkage [Mure *et al* (1989)]

One of the interesting features seen in Figure 1.23 is that the wires are passed through hollow pins rather than looped externally from linkage to linkage so as to support the wires more. A heat transfer study by Wilson *et al* (2002) placed thin film temperature gauges on the piston crown. The sensor wires were bonded to the conrod and sump as in Figure 1.23, but there was no supporting mechanism between. Although the engine provided results up to 3500 rpm, service life would be limited.

Intermittent devices could be considered an option for signal output, where there would be an electronic device within the piston that temporarily stored the data and then gave a data burst at one point in the piston cycle as mentioned by Mure *et al* (1989). This burst could for example be when the piston is at BDC, since this is where the piston would be

closest to the receiver unit in the sump. However, this approach has been superseded by latest developments in infra red telemetry data extraction [IRT (2001)], where this method allows continual transmission. This eliminates the need for data storage in the piston and removes the problem of reduced transmission time at high engine speed. However, excessive heat and vibration can damage the electronics in the piston.

As mentioned earlier, Teraguchi *et al* (2001) investigated piston slap noise and piston friction loss in a diesel engine by varying the amount of oil present between the piston and cylinder bore. The point of interest here is that a two bar linkage connected to the conrod supported a Teflon tube that delivered a known flow rate of oil to the modified piston. The tube and linkage could operate up to 2400 rpm.

In an attempt to measure cylinder bore distortion at 4000 rpm by eddy current sensors, Maassen *et al* (2001) created the linkage mechanism shown in Figure 1.24 for signal removal. The cramped nature of the engine required a mechanism that passed through the block wall, instead of it remaining within the confines of the block and having a signal take-off point on the side of the block. This mechanism is of basic 'grasshopper' design, but carefully utilises curved linkages so as to limit the size of the opening required in the side of the engine block. This was important because a larger hole would have required the removal of the block's stiffening ribs, affecting the engine's deformation characteristics and possibly the results of the study.

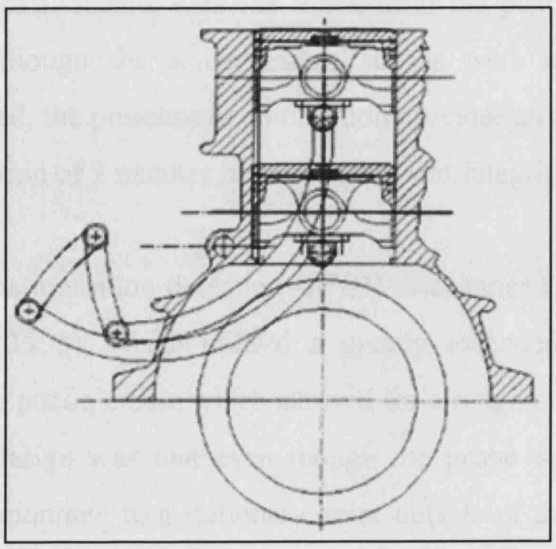

Figure 1.24 Limited access linkage system [Maassen *et al* (2001)]

A study of piston secondary motion or slapping in diesel engines was performed by Offner *et al* (2001). The mechanism employed was very similar to that of Maassen *et al* (2001), although in this engine there was sufficient space for the mechanism to remain within the block, as shown in Figure 1.25.

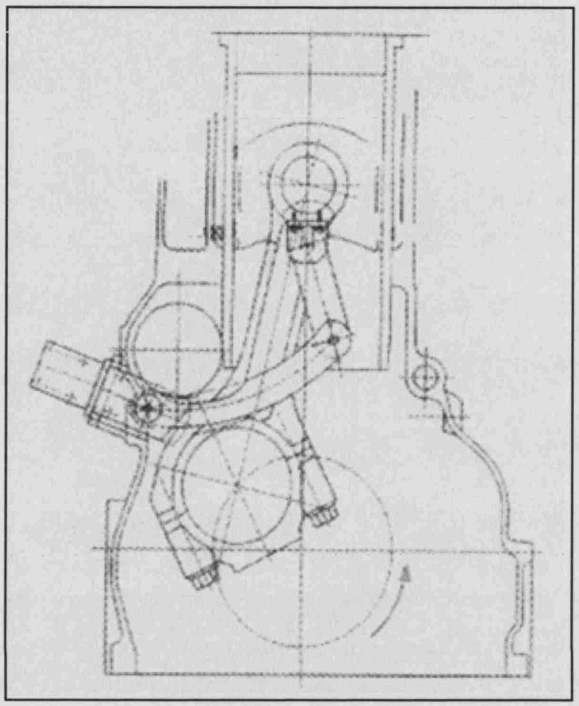

Figure 1.25 Crankcase-contained linkage system [Offner *et al* (2001)]

Steeper *et al* (2000) devised an optical engine to explore combustion and piston temperatures of a DISI engine. Thermocouple placement on the piston crown provided surface temperature measurements with the wires from the piston being supported in Teflon tubing. Even though the actual engine speeds were not provided and the mechanism not described, the presence of combustion provides an idea of baseline engine speed and the test duration of 3 minutes indicates sufficient integrity.

A method for fast flame ionisation detection (FFID) in-cylinder HC measurements was devised by Queenan (1998), which utilised a greatly extended piston containing a selection of holes in the piston crown which allowed for a range of sensor positions. The novel feature of this design was that even though the probe was situated inside the piston, it was actually mounted to a stationary point outside of the cylinder block via a large hole in the side of the piston. This implied that the piston oscillated around the sensor while the sensor sampled a fixed point within the cylinder.

1.8 CONCLUSIONS

Gasoline may be introduced into an internal combustion engine by a variety of methods, but each will generate some amount of wall wetting. Wall wetting is known to be detrimental to the performance of an engine, reducing service life and increasing fuel consumption and emission of unburned hydrocarbons. It appears that the level of wetting may be affected by various means, including injector type, injection timing, valve timing, port deactivation and engine geometry. However, there is an almost total lack of directly measured cylinder wall wetting data in the literature. This work explored to what level these factors influence wall wetting and how they might be optimised to avoid it.

Wall wetting can be detected by a range of techniques, but the porous liner and heat flux methods have the advantage that conventional gasoline may be used in an engine which retains the geometry and metallic surfaces of the donor engine. The porous liner technique gives a very good indication of where fuel impacts the cylinder bore, but does not permit combustion experiments. The fast reaction times of heat flux sensors enable an intra-cycle study of fuel impaction to be performed in addition to quantifying the relative amounts of fuel involved. A range of mechanisms for passing the sensor wires from the moving piston have been presented, although none of these were ideally suited to this engine, implying a novel mechanism had to be designed.

CHAPTER 2

THE POROUS LINER TECHNIQUE

2.1 INTRODUCTION

The rig-based experimental testing was intended to provide an initial indication of the location and relative magnitude of fuel impaction on the cylinder bore, but without knowledge of fuel arrival time. This was performed under 'cold' conditions and a comparison was made between the wall wetting characteristics of two cylinder head variants. The two cylinder heads provided for comparison by the porous liner technique were the production AJ26 head and development AJ33 AP head. The AJ26 head had symmetrical inlet ports without valve shrouding, but the AJ33 AP head was different because it had a dump port, swirl port and shrouding between both the inlet and exhaust valves. The AJ33 AP dump port runner also had a deactivation flap above the point of injection. The injectors provided with the AJ26 and AJ33 AP heads were production Denso side-fed pintle injectors with spray-splitting tip and development Denso 12-hole split-spray injectors respectively. Note that the heat flux work in later chapters only compares this AJ33 AP head to an even later development head classified as AJ33 CP.

The study was performed using a motored rig in which there were no pistons, engine block or combustion. To explore the bore wetting, only one specially designed cylinder was required, where this was used in combination with the cylinder head, inlet manifold and throttle from the conventional engine. Only the inlet camshaft was motored by an electric motor, while a vacuum pump generated the airflow through the cylinder, allowing tests to be performed at the correct air fuel ratio.

The unique cylinder was designed and produced to have a porous insert as the top section of the bore, with pockets behind the porous insert effectively dividing the insert into 8 sectors. A small pressure drop applied across this insert would draw any gasoline that might be on the bore through to be collected and measured, with its location on the bore being determined by which sector it was collected from. There were several advantages of the motored rig tests. This facility allowed the cylinder heads to be compared thoroughly without the need for an entire engine and its management system, which saves on resources and costs. An important part of the work was the endoscope observations of the bore and pent-roof, as these gave visual confirmation of liquid fuel movement within the cylinder. These tests were only possible because there was no combustion within this test rig.

2.2 CYLINDER HEAD AND INJECTOR VARIANTS

The Jaguar AJV8 engine is a modern 4-valve design, first announced in 1994 and the ones used in this work were the AJ26 and AJ33 AP variants.

The AJ26 is a variant of 4.0l capacity with an 86 mm diameter cylinder bore. It uses a conventional pent-roof configuration and is designed to promote the generation of tumble (barrel swirl) in the cylinder, through the use of two straight inlet ports. Both inlet and exhaust valves are unshrouded and port fuel injection is provided in the conventional manner. Fuel pressure is maintained using a common rail with a mechanical spring-type spill regulator.

The AJ33 variant is of 4.2l capacity, but is designed to fit the same cylinder bore of 86 mm as the AJ26 pent-roof. The AJ33 has one straight (dump) and one swirl port, combined with a deactivation device in the runner upstream of the dump port which is intended to deactivate the dump port below 3000 rpm. This combination provides high volumetric efficiency when both ports are in use, but promotes strong swirl airflow to be set up at low speed when deactivation is in use.

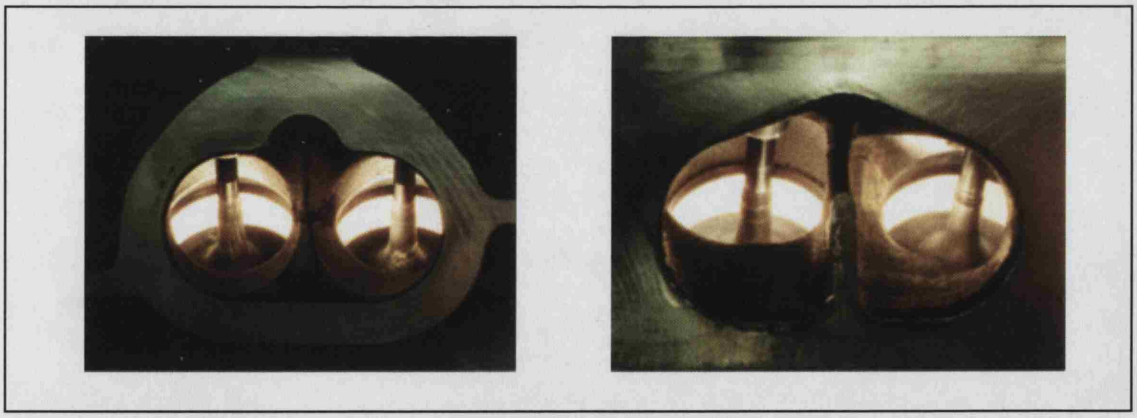

Figure 2.1 AJ26 and AJ33 AP inlet ports

An important difference noted between the AJ26 and AJ33 cylinder heads was that valve shrouding had been provided between both the inlet and exhaust valves on the AJ33 head. This was important in the interests of this work, since these shrouds would divert the incoming air and fuel flow away from the walls. A major reason for the introduction of these shrouds was to produce the correct compression ratio for the

engine while also providing turbulence in the form of squish regions as shown in Figure 2.2.

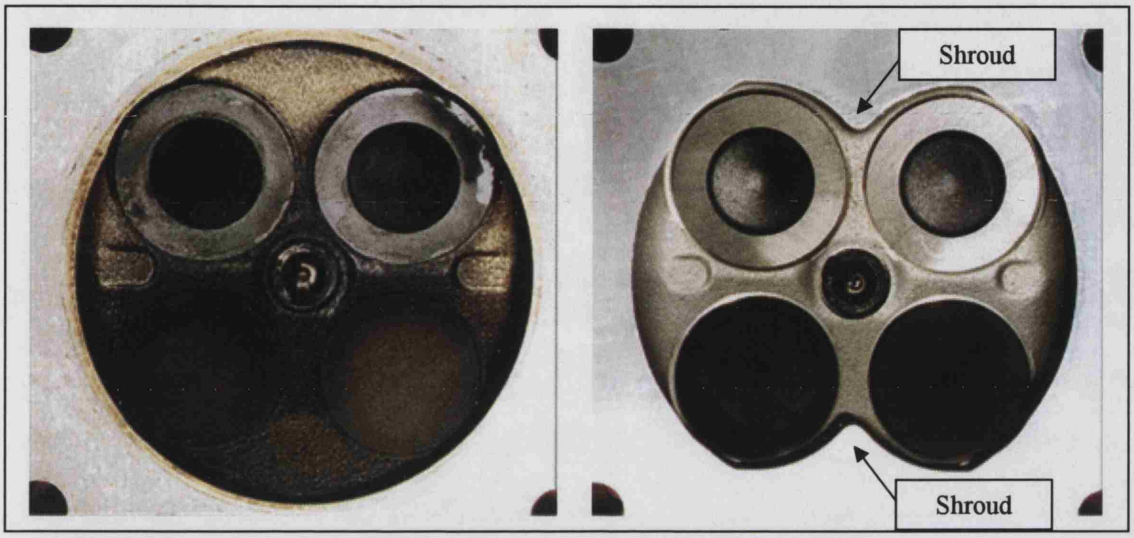

Figure 2.2 AJ26 and AJ33 AP pent-roofs

The AJ26 injector is a Denso side-fed pintle injector, with a plastic two-hole splitter fitted downstream of the metering pintle. This injector is intended to give a twin-spray with equal fuel distribution to both ports. The AJ33 injector is a Denso 12-hole injector designed to operate with 3.8kPa pressure drop across it, slightly higher than in the AJ26 injector. Both injectors provide a split-spray targeted into the ports.

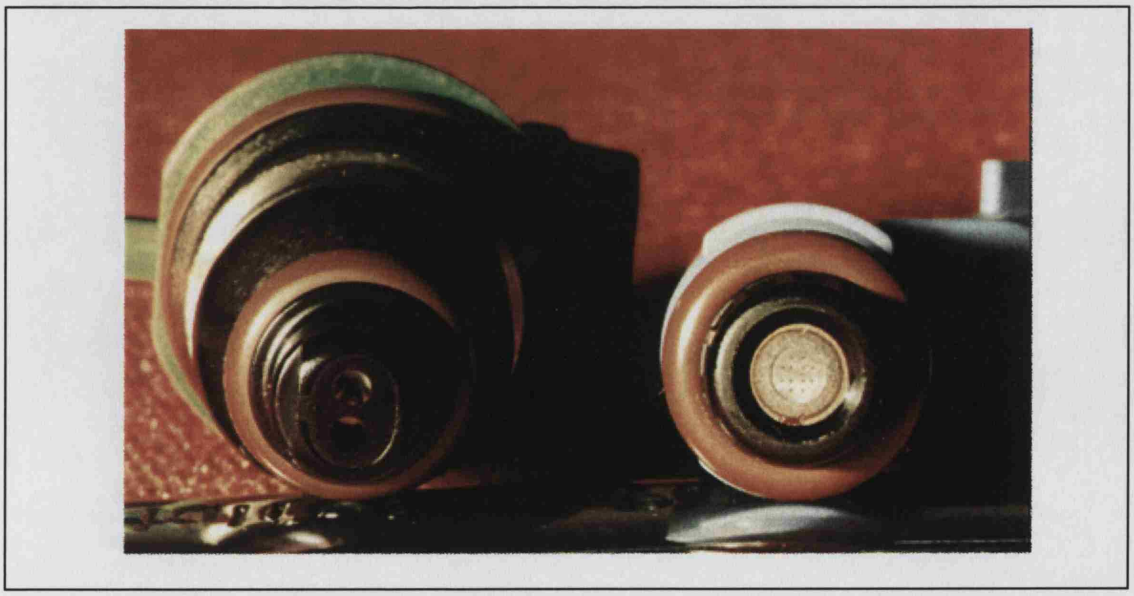

Figure 2.3 The Denso pintle split-spray and 12-hole injector tips

2.3 POROUS LINER MOTORED RIG TEST EQUIPMENT

2.3.1 Dummy Cylinder

The motoring rig used in this work mounted the cylinder head and associated inlet manifold, fuel rail and throttle assembly at the correct 45° angle above a dummy cylinder. The cylinder used in the test rig had the same 86mm bore as the Jaguar engine. The top of the cylinder had a larger bore of 92 mm to accommodate the porous insert and maintain the 86 mm bore of the cylinder, while ensuring the porous ring attained a good seal with the cylinder head gasket. The lower end of the dummy cylinder was attached to a plenum that was evacuated by a vacuum pump, so when the inlet camshaft was motored, a realistic engine airflow was generated through the inlet valves.

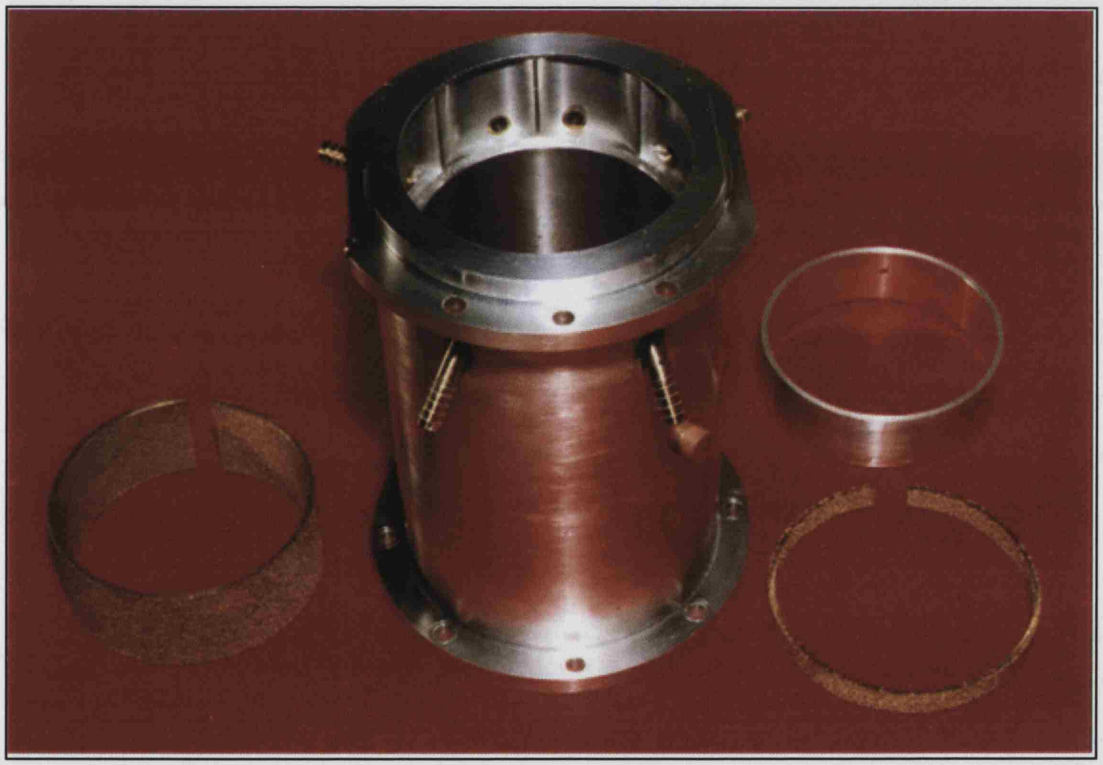

Figure 2.4 Dummy cylinder and porous material inserts

Sampling heights of 37 mm or 10 mm were available, where if the 10 mm ring was used, a 27 mm aluminium ring was used below it in order to seal the lower section of the pockets. Behind the porous material were eight equally spaced collection pockets that permitted radial discrimination of the location of liquid fuel impingement on the porous material. Eight large and equally spaced recesses were milled into this larger

bore so that when the insert was fitted, eight separate cavities were formed behind the porous material. These cavities divided the insert into eight sections to allow accurate determination of the location of liquid fuel impingement on the cylinder bore. A small brass spigot was also introduced at the lowest corner of each of the eight sectors and formed the connection point for the gasoline.

Applying a suitable pressure drop across this porous material allowed liquid fuel on the bore to be drawn through the porous material and collected from the pockets to containers. The schematic in Figure 2.5 shows how the interaction of the insert in the dummy cylinder created the pockets.

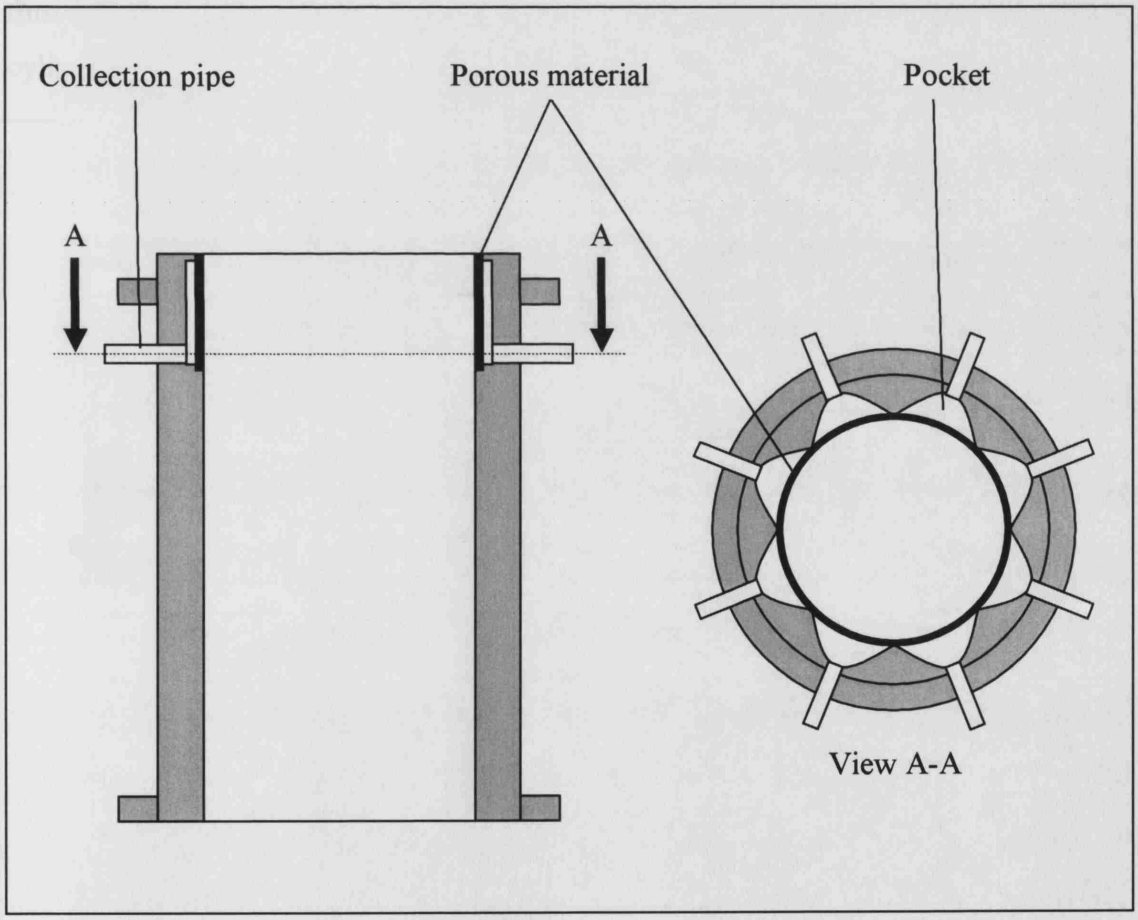

Figure 2.5 Vertical and horizontal section views of the dummy cylinder

At the end of each test the containers were removed and the mass and density of fuel collected at each of the eight locations was measured and then expressed as a percentage of the gasoline injected.

2.3.2 Suction Equipment

Since there was no piston in the dummy cylinder, a constant speed vacuum pump and throttles were used to generate representative flows through the inlet valves. This pump was in fact an integral feature of the Fuel Systems Test Facility at UCL, which enabled the gasoline to be injected at the correct air fuel ratio in safe working conditions.

A schematic of the main rig components is given in Figure 2.6. This highlights that the throttle, inlet manifold, injector, cylinder head and camshaft from the actual Jaguar engine are used. Air is drawn in through the hot wire anemometer, the only point where air may enter the system. The air then passes the engine throttle into the plenum chamber from where it is drawn into either the dummy cylinder when the inlet valves to this cylinder are open. The bulk airflow leaves through the lower end of the dummy cylinder, while some is drawn through the collection pipes with collected fuel.

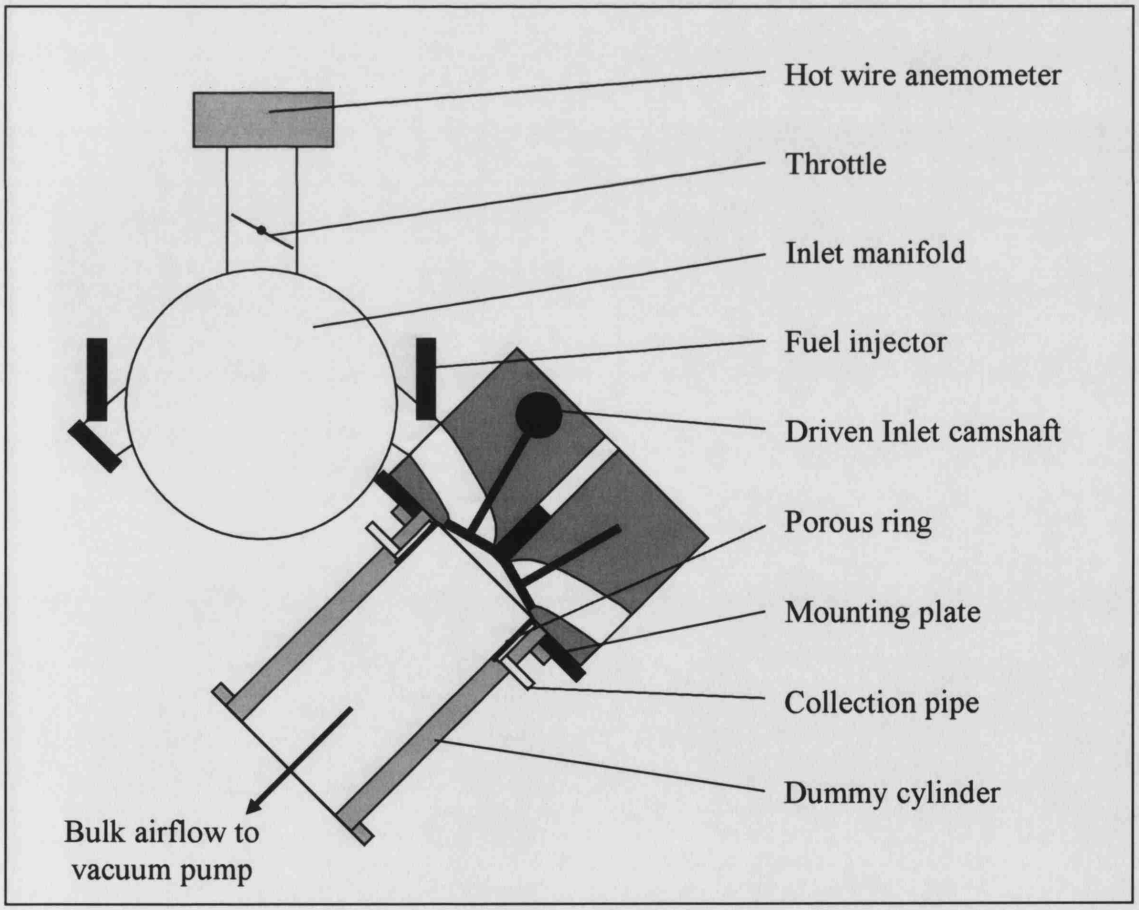

Figure 2.6 View of dummy cylinder and associated components in the rig

Figure 2.7 is a schematic of the rig (Figure 2.8) and primarily shows how a pressure drop could be created across the porous material using the suction tubes and throttles.

Fuel was only injected into the port used by the dummy cylinder, but the air in the intake manifold was intended to flow through the valves of the other three cylinders too. This prevented an unrealistically large depression forming within the lower plenum during the period when the intake valves of the tested cylinder were closed. Such a depression would have generated a large and unrealistic flow through the tested inlet valves when they opened, which would affect the location of fuel impaction on the cylinder wall. All of the suction tubes are shown in Figure 2.7.

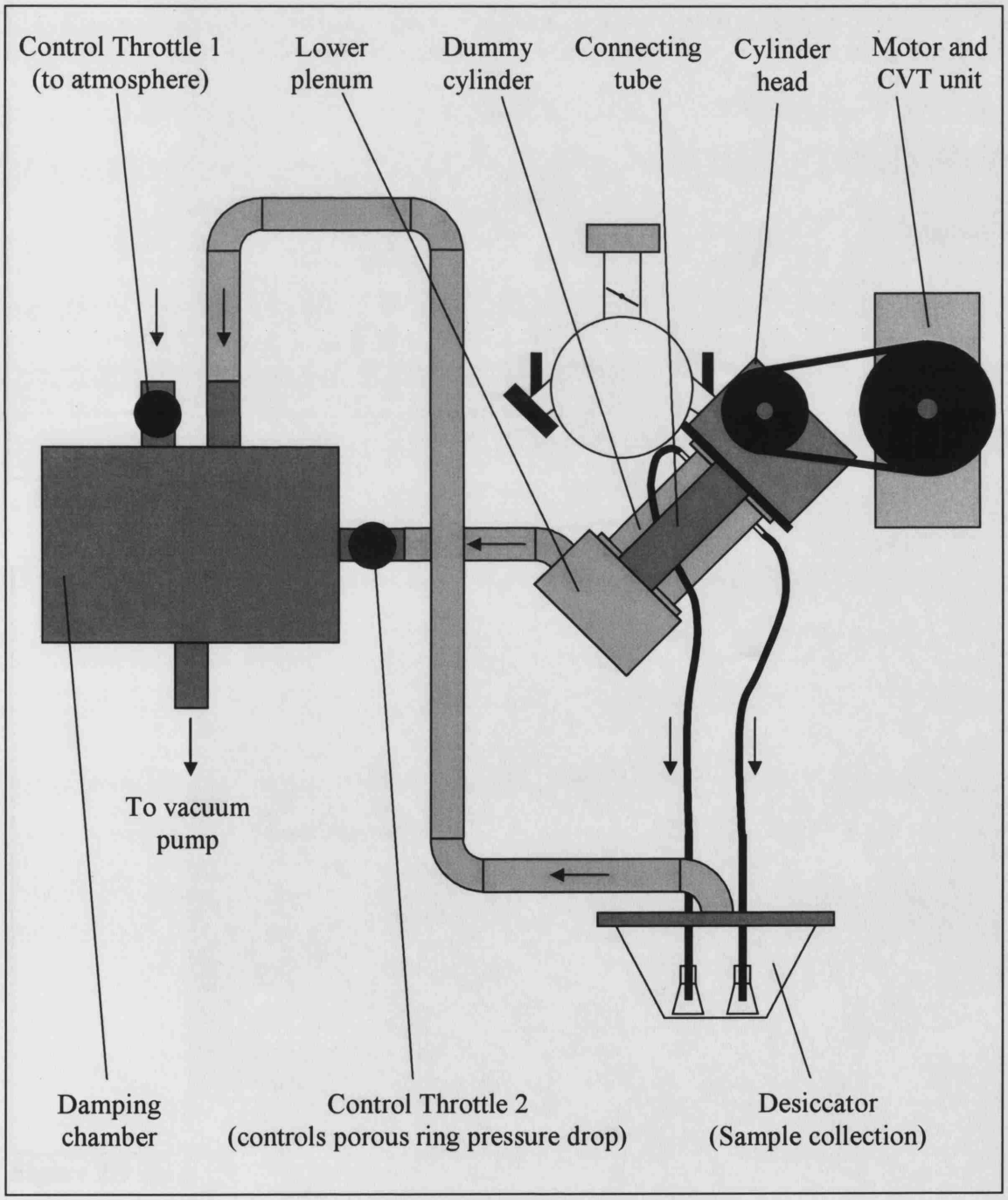

Figure 2.7 Schematic of the motored rig (not to scale)

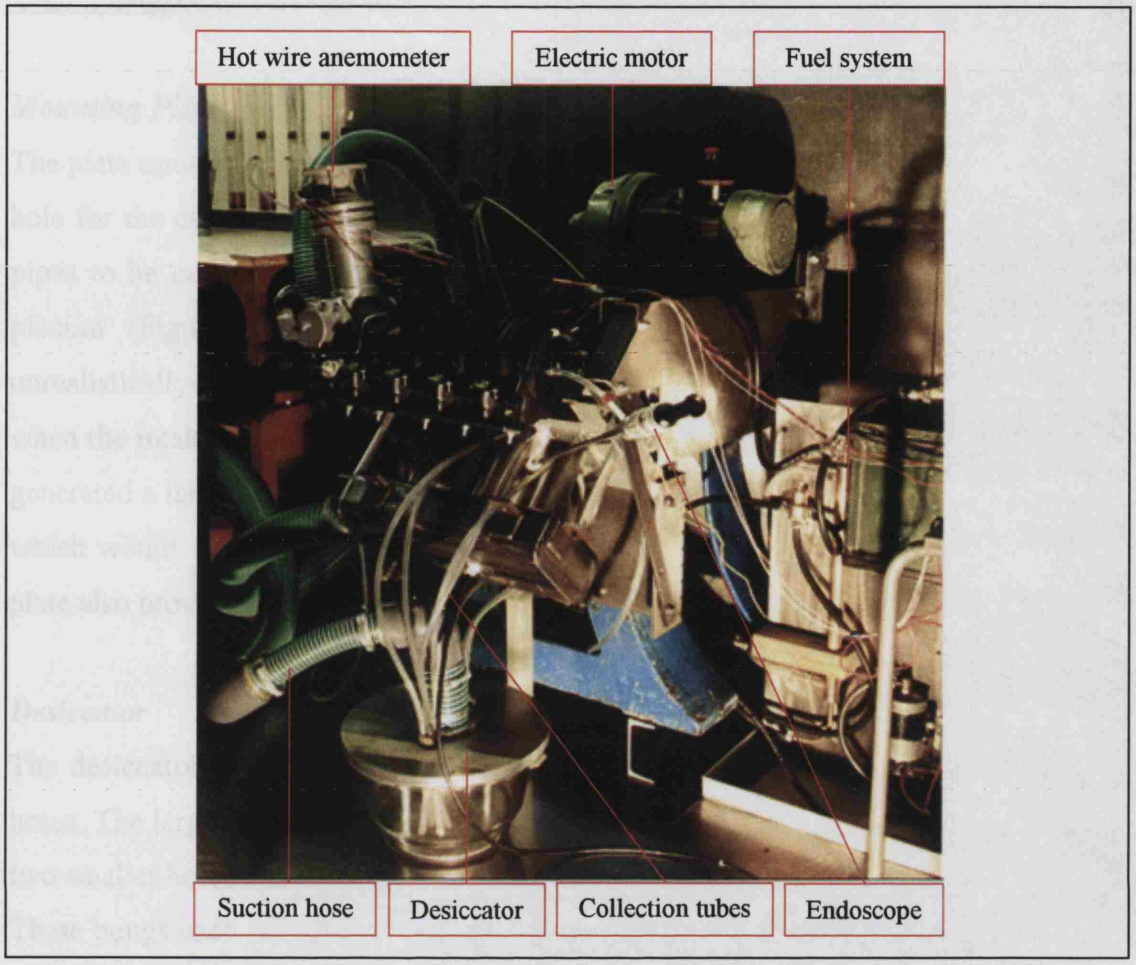

Figure 2.8 The Motored Rig. Note endoscope positioned in the dummy cylinder

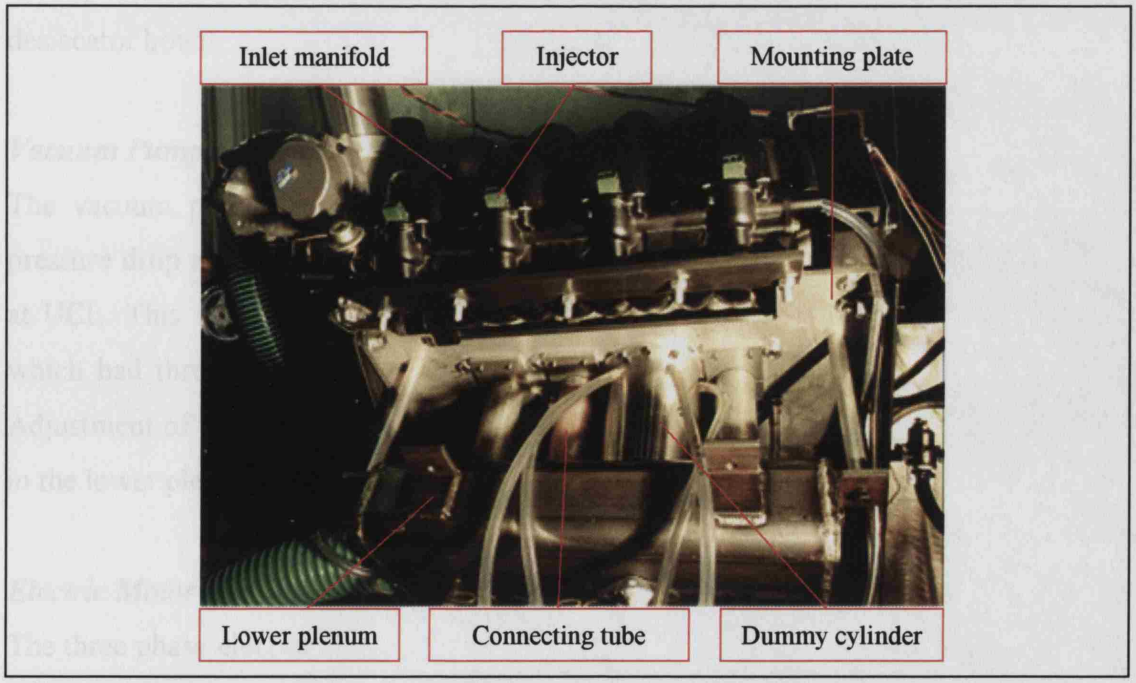

Figure 2.9 Dummy cylinder in position with connecting tubes

2.3.3 Additional Equipment

Mounting Plate and Connecting Tubes

The plate upon which the cylinder block was mounted contained not only the necessary hole for the dummy cylinder, but also three smaller holes, permitting 50 mm diameter pipes to be connected from the head's three 'non-tested' cylinder roofs to the lower plenum (Figure 2.9). This feature was important as these pipes prevented an unrealistically large depression from forming within the lower plenum during the period when the intake valves of the tested cylinder are closed. Such a depression would have generated a large and unrealistic flow through the tested inlet valves when they opened, which would affect the location of fuel impaction on the cylinder wall. The mounting plate also provided a mounting point for the optical switch of the injection system.

Desiccator

The desiccator unit consisted of a glass bowl and a metal top plate containing three holes. The large central hole was for connection of a 3" vacuum pump pipe, while the two smaller holes either side of the main hole allowed for the insertion of rubber bungs. These bungs each provided four secure and airtight attachment points for the collection tubes that ran down from the dummy cylinder collection pipes above. The collection tubes passed through the bungs to the eight individual collection flasks held within the desiccator bowl.

Vacuum Pump and Throttles – Fuel Systems Test Facility

The vacuum pump used to generate the airflow through the dummy cylinder and pressure drop across the porous material formed part of the Fuel Systems Test Facility at UCL. This vacuum pump created a depression within the large damping chamber, which had three 75 mm hose connection points, two of which had control throttles. Adjustment of these throttles and the conventional engine throttle varied the depression in the lower plenum, desiccator and inlet manifold.

Electric Motor and CVT

The three phase electric motor and CVT unit had a speed range of 168 to 1015 rpm. By using timing pulleys with 90 and 56 teeth, the maximum permissible speed was increased sufficiently to perform the 2500 rpm engine speed test (1250 rpm camshaft)

while still being capable of going slow enough to run the 1200 rpm engine speed test (600 rpm camshaft). Speed was adjusted only when the motor was in operation.

Injector Control

A cutter disk was fixed to the pulley end of the camshaft with special attention to its rotational position so that the disk's 'rising edge' would pass an optical sensor at the point of maximum inlet valve lift (Figure 2.10). From this point, the injection delay and pulsewidth could be computer controlled by LabVIEW computer software as discussed in more depth in Chapter 5. The signal from the optical sensor was connected to the computer interface via a 69 pin socket and cable, where the LabVIEW software then allowed the desired injection delay and pulsewidth to be entered. The output of the computer interface was connected to an injector driver unit that converted the TTL logic signal to a high current injector drive signal. The output from the injector driver was then connected to the injector via a switch.

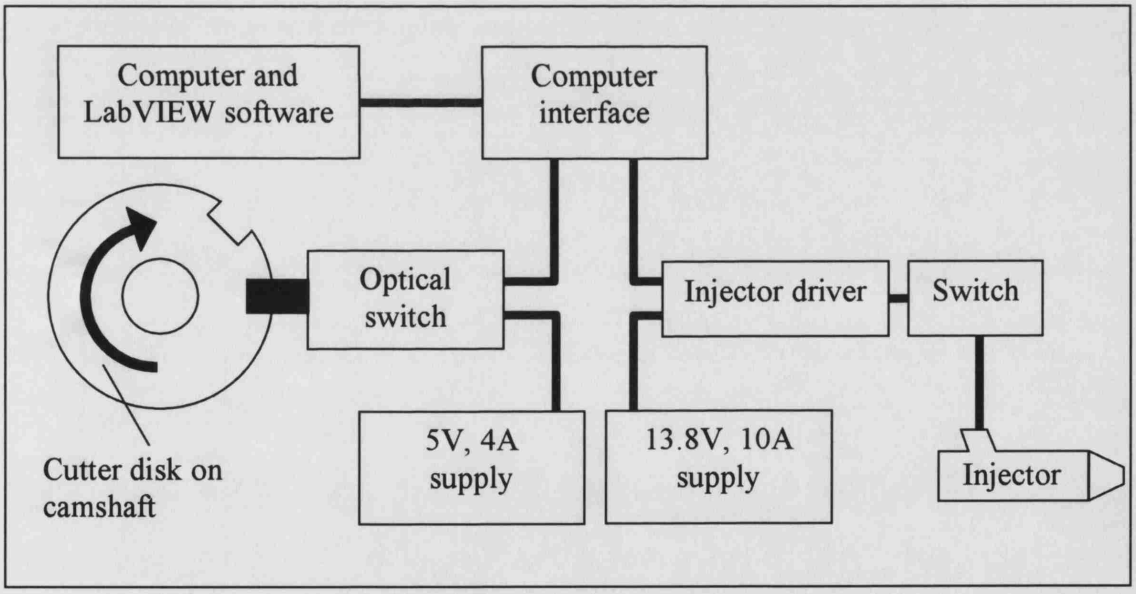

Figure 2.10 Electronic injector control

Fuel Systems

The AJ26 cylinder head employed the mass production inlet manifold, which contained an internal fuel rail and pressure regulator. With the addition of a supply tank, pump, filter and gasoline cooler the AJ26 fuel system was complete (Figure 2.11). Since the real engine used an electronic pressure regulator and the engine management system was not available, a variable mechanical pressure regulator was used in the AJ33 tests.

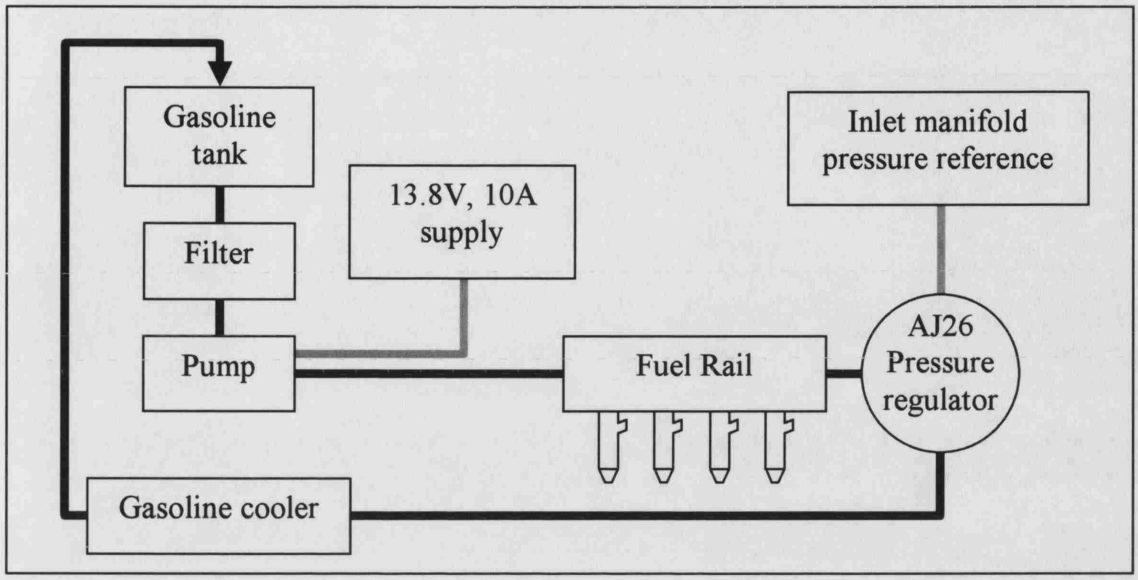

Figure 2.11 AJ26 standard fuel system

To set the correct fuel pressure for the AJ33 3.8kPa Denso 12-hole injector, the inlet manifold depression for the test in question had to be known. The manually variable pressure regulator was adjusted before the test to ensure the pressure drop across the injector was correct (Figure 2.12).

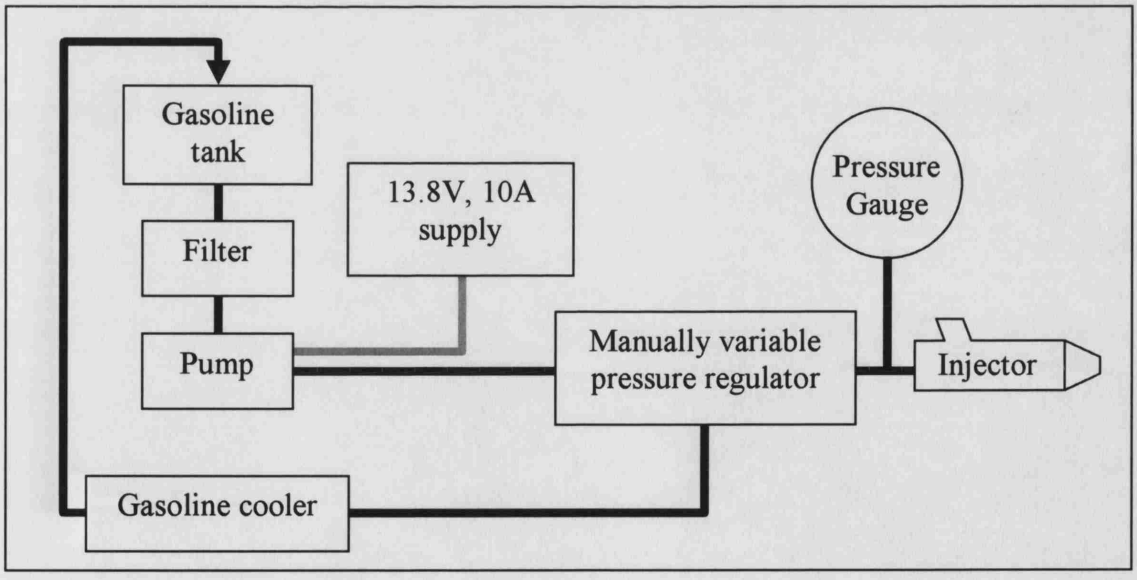

Figure 2.12 AJ33 single ended injector configuration

2.4 RIG CALIBRATION EXPERIMENTS AND REQUIREMENTS

2.4.1 Gasoline Evaporation Tests

During testing, gasoline being collected or even gasoline that was already collected would have lost a measurable amount of its volume through evaporation before the final mass collected was weighed. This resulted in the final quantity of petrol collected being much less than that originally drawn through the porous material, so correction of the results was required.

For the evaporation test, a gasoline sample of known mass and density was left to evaporate freely into the atmosphere. At convenient intervals, the new density and mass of the gasoline were noted. The gasoline used in the measurements was then returned to the container. The percentage reduction in mass could then be calculated and a graph of density against percentage reduction was then plotted with a line of best fit superimposed onto it (Figure 2.13).

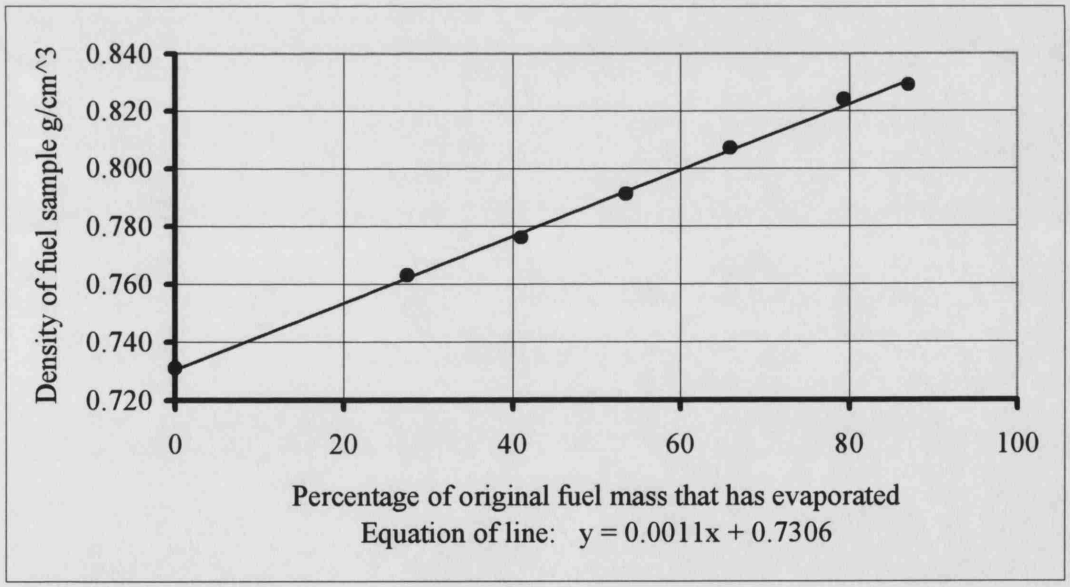

Figure 2.13 Gasoline evaporation curve

By measuring the density of gasoline collected in a test, use of the evaporation equation would reveal the percentage reduction. Knowing the percentage reduction and the total mass of gasoline collected during a test permitted direct calculation of how much gasoline was actually drawn through the porous material.

2.4.2 Fuel Injector Calibration Tests

It was obviously very important to know how much gasoline was actually being injected. In this test, the injector was triggered to inject at a known pulsewidth for a period of 5 minutes. It was decided to run four tests using convenient and representative pulsewidths of 3, 5, 7 and 9 ms.

To perform this test, the camshaft was simply motored at 1500 rpm in order to generate a signal that triggered the injector. A container was then held under the injector to collect the gasoline. At a crankshaft rotation of 1500 rpm, the camshaft rotated at 750 rpm. Since there was one injection per camshaft rotation, and the test lasted for 5 minutes, a total of 3750 injections had occurred. Since the mass of gasoline collected and number of injections were known, the mass per injection could be calculated.

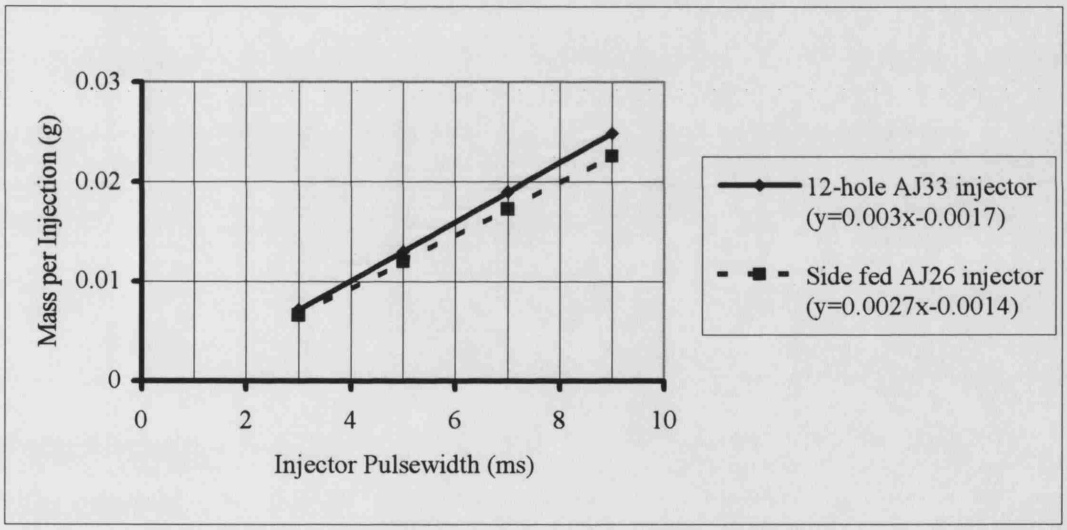

Figure 2.14 Injector calibration plots

The calibration graph of mass per injection versus pulsewidth (Figure 2.14) shows the expected trend of a near-linear relationship between injected mass and pulsewidth, with an offset on the pulsewidth axis at zero mass injected, due to the small initial lag in the injector and its control circuit.

2.4.3 Optimum Pressure Drop across Porous Material

It was noticed that the mass of petrol collected was highest at a small pressure drop, with this amount reducing as the pressure drop was increased. It was also noticed that the density of the petrol collected increased at these higher pressure drops. It is believed that higher pressure drops drew more petrol through the porous material, but the increased airflow in the collection pipes increased its evaporation. Figure 2.15 shows plots of collected and corrected fuel as a percentage of gasoline injected and that according to the corrected line, the optimum pressure drop should be 5 cmH_2O.

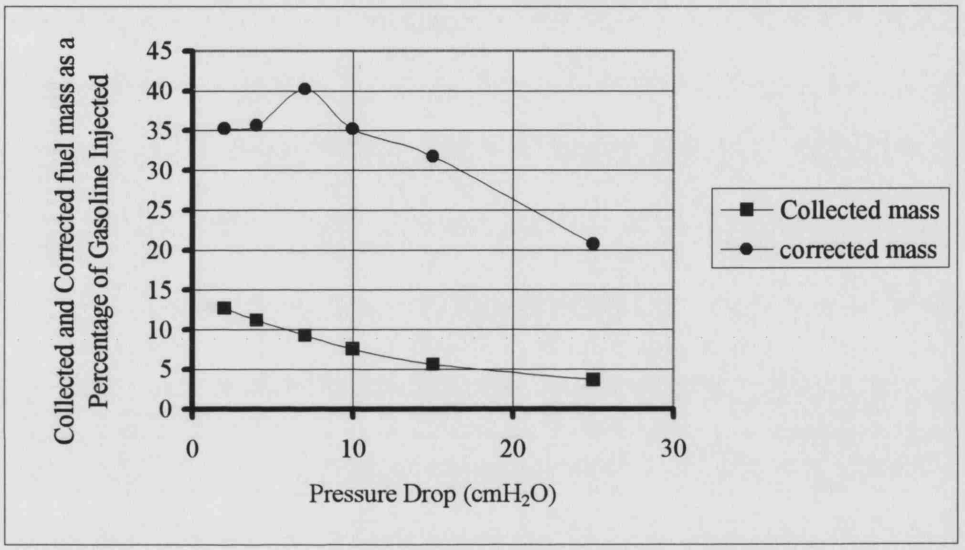

Figure 2.15 Optimum pressure drop across the porous material

Varying the pressure drop across the porous material:

- The camshaft would first be rotating, then the vacuum pump started
- Throttle 1 was slowly closed and the engine throttle position varied to achieve the desired inlet manifold depression. The engine throttle position was then fixed
- Throttle 2 was partially closed to achieve the pressure drop across the porous material
- The initial manifold depression was affected by the position of throttle 2, so both throttles 1 and 2 were then adjusted together to fine tune the manifold depression and pressure drop across the porous material
- Injection began when the desired manifold depression and 5cmH_2O pressure drop across the porous material were achieved

2.4.4 Hot Wire Anemometer Calibration

The hot wire anemometer used was the same unit as used in previous work by Ioannou (2000), so the calibration curve for the unit was already known (Figure 2.16). This curve was established by comparing the output of the hot wire anemometer with the reading on a variable-area rotameter.

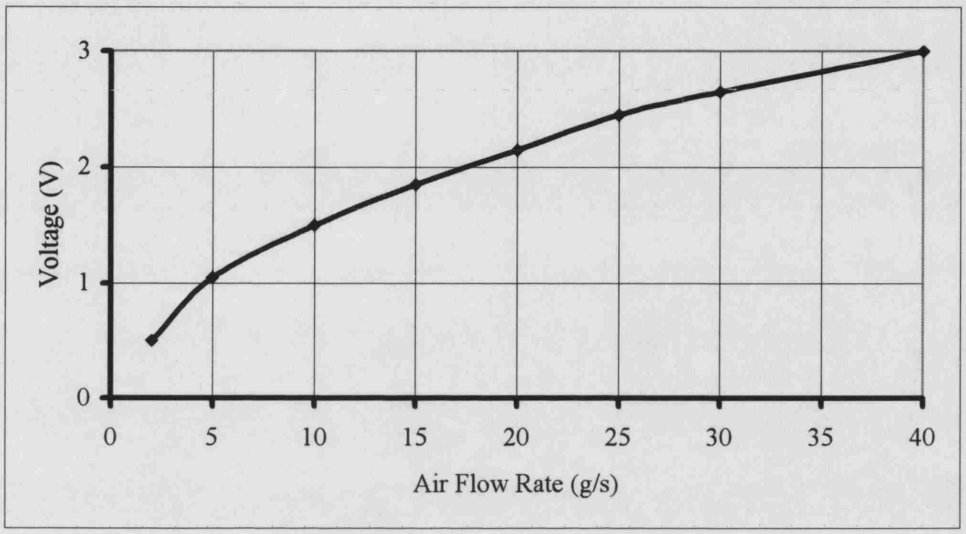

Figure 2.16 Hot wire anemometer calibration

2.4.5 Injection Timing

In the numerous results tables or graphs for this pulsating rig work, it can be seen that the delay between the cutter disc sensor generating a pulse at MOP and SOI is written as a camshaft angle. In performing the tests, these delays were actually in the form of time delays in ms, controlled by LabVIEW software. The times chosen were actually equivalent to multiples of $1/16^{th}$ of a camshaft revolution for continuity of results in the three test speeds explored, remembering that one camshaft revolution takes 100 ms, 80 ms and 48 ms at speeds of 1200 rpm, 1500 rpm and 2500 rpm respectively. This was convenient since injection sweeps at different speeds could be compared more easily.

Since it was desirable to plot the results on a graph with MOP occurring at the centre, the camshaft angle used in the plots was converted into camshaft degrees before and after MOP as shown in the third column of Table 2.1. It can be seen that no injection points occurred at 6, 7, 8, 10, 11 and 12. This was because the inlet valves were still closed at these points, and the results would be identical. The result plots show points 5 and 9 are extremely similar at 1200 rpm and 1500 rpm to prove this.

			1200 rpm	1500 rpm	2500 rpm
16th of camshaft revolution	Delay from MOP (Camshaft°)	Delay from MOP (Camshaft°) (as in plots)	Delay from MOP (ms)	Delay from MOP (ms)	Delay from MOP (ms)
1	-	-	-	-	-
2	22.5	22.5	6.25	5	-
3	-	-	-	-	-
4	-	-	-	-	-
5	90	90	25	20	12
6	-	-	-	-	-
7	-	-	-	-	-
8	-	-	-	-	-
9	180	180 / -180	50	40	-
10	-	-	-	-	-
11	-	-	-	-	-
12	-	-	-	-	-
13	270	-90	75	60	36
14	-	-	-	-	-
15	315	-45	87.5	70	42
16	337.5	-22.5	93.75	75	-

Table 2.1 Injection timings used in tests and results

The result plots show only SOI relative to camshaft position, not the injection period. In order to perceive the sizes of the injection period, the pulsewidth can be expressed as a percentage of the time for one camshaft rotation at 1500 rpm and 2500 rpm (Table 2.2).

	1500 rpm	2500 rpm
Pulsewidth (ms)	4.6	13.9
Time for one rotation of the camshaft (ms)	80	48
Pulsewidth as a percentage of camshaft rotation (%)	5.75	29.0

Table 2.2 Relative sizes of injection pulsewidths

2.4.6 Manipulation of Pulsating Flow Rig Results

During the experiments, the actual readings were noted on specially planned sheets. On the sheets, the term 'flask' described the conical flask used to collect the gasoline and the term 'tube' describes the measuring tube used to measure its density.

Mass of Gasoline Collected in a Flask:

Mass of gasoline (g) = (mass of flask, bung and gasoline) - (mass of flask and bung)

Density of Gasoline:

If a large enough volume of gasoline was collected, a maximum volume of 10cc could be placed in the measuring tube for more accurate density calculation. If less than 10cc was collected, all of the collected gasoline would be poured into one tube.

Density of gasoline (g/cm^3) = (mass of gasoline in tube) / (volume of gasoline in tube)

Percentage Reduction:

This calculation was based on the evaporation equation. To find the percentage reduction, the calculated density of the gasoline was located on the y-axis of the plot and the percentage mass reduction read off the x-axis. This value was found directly by the alternate method of using the equation $y = 0.0011x + 0.731$ on the plot.

Percentage reduction (%) = (Density calculated – 0.731) / 0.0011

Corrected Mass:

To find the corrected mass, the following equation was used:

Corrected mass (g) = (collected mass) x *(100 / (100 - Percentage reduction))*

Percentage of Gasoline Injected:

Once the corrected mass for one of the eight collection points was known, this mass was expressed as percentage of the total mass of gasoline injected. The camshaft rotates at half crankshaft speed and the tests are always performed to the nearest whole minute. Since there was one injection per camshaft rotation and the mass per injection was known, the total mass of gasoline injected was calculated by:

Mass injected (g) = (Crank rpm x 0.5) x *(Mass per injection)* x *(Minutes)*

Percentage of gasoline injected (%) = ((Corrected mass) / (Mass injected)) x *100*

The masses for the inlet and exhaust sectors are added to form the sub totals for convenience of comparison. The grand total is the sum of these two sub totals.

Each of these result sheets had a diagram of the pent-roof, porous material and portion of cylinder wall below the porous material. These diagrams show the movement of petrol within the cylinder as observed with the endoscope, whether in the form of liquid petrol 'wall film' or airborne droplets. In the diagrams, solid lines depict wall film movement from the inlet valves and shaded areas represent the impact of airborne droplets.

2.4.7 Possible Sources of Errors in Density Measurement

During the process of reviewing the results it was found that the density measurements had to be very precise. The scale balance could measure to a $10{,}000^{th}$ of a gram, but the volume measurements were limited to $\pm$ 0.1 cc and sometimes the actual amount of petrol could be less than 1cc. For instance, a small erroneous increase in the calculated density value would increase the perceived level of evaporation. If the level of evaporation is very high, the percentage reduction is accordingly high. When the actual amount of petrol collected is multiplied by the resulting correction factor from above, the level of corrected petrol calculated that allows for evaporation can be unrealistically high. To overcome this problem, the numerous tests were repeated many times and the volume of petrol collected from each set of tests was collected in a container. When a substantial volume was collected for a given test condition, the density could be recalculated with a much higher confidence.

It was found that at 1200 rpm and 1500 rpm conditions, the 10mm insert resulted in a higher density and hence higher level of evaporation than the 37 mm insert. The 2500 rpm speed had the lowest density, implying less evaporation had occurred. It was assumed that the amount of evaporation that took place during the transport of the fuel to the surface of the porous insert was small compared to the evaporation that occurred once the fuel had entered the measurement system. This assumption was justified by the fact that the time of travel of the droplets within the ports and cylinder head would be between a few tens of milliseconds to a few seconds, whereas the liquid fuel would

spend up to 15 minutes in the measuring system. The final density values used are shown in Table 2.3.

	10 mm insert	37 mm insert
1200 rpm / 1500 rpm	0.84 g/cc	0.83 g/cc
2500 rpm	0.8 g/cc	0.8 g/cc

Table 2.3 Density values used in final calculations

2.4.8 Rig Deviations from Reality

The motored rig experiments did generate some deviations from reality.

The exhaust valves were not used in this study so as to reduce rig complexity. This caused a slight deviation from realism in that the opening action of the valves that normally disrupts wall film movement was absent. This meant that having inactive exhaust valves only increased the level of bore wetting.

Some of the gasoline in the form of airborne droplets would have impacted on the piston crown in the real engine, but since the piston was absent in this rig the airborne gasoline is free to cross the cylinder and impact the cylinder bore on the exhaust side.

The lack of combustion implied that the rig was at ambient temperature, so the high level of evaporation usually experienced within the engine did not occur here, further increasing the amount of liquid gasoline collected.

The above points have the effect of increasing the amount of gasoline collected from the bore. This means that the motored rig collected a higher amount of gasoline than would be expected from a real firing engine and that this work generated a worst case benchmark.

CHAPTER 3

THE POROUS LINER TECHNIQUE RESULTS AND DISCUSSION

3.1 INTRODUCTION

The previous chapter described the rig and the various calibration experiments performed with additional details on how the results must be manipulated. This chapter now presents and discusses all of the results, starting with the test conditions used.

3.2 TEST CONDITIONS

In the interest of attaining useful results from the rig tests, a number of test points were identified, in consultation with Jaguar. It was planned to test at three different engine conditions. These represent common conditions of fast cold idle, road load and low speed fast acceleration and are summarized in Table 3.1.

Engine speed (rpm)	Engine Condition
1100 / 1200	Fast cold Idle
1500	World Wide Mapping Point 2.62 bar
2500	Wide Open Throttle

Table 3.1 Basic test conditions

The actual engine 'set-up' values to be used in the AJ26 and AJ33 heads were confirmed with Jaguar and are shown in Tables 3.2 and 3.3 below.

Crank Speed (rpm)	Load	Airflow Engine (g/s)	Airflow Cylinder (g/s)	Manifold Depression (mmHg)	Fuel Pulsewidth (ms)	AFR
1100	No load	16.95	2.12	420	8.25	11.3:1
1500	2.62 bar WWMP	18.06	2.26	410	5	15.0:1
2500	WOT	83.3	10.41	10	15	12.5:1

Table 3.2 AJ26 test conditions

Crank Speed (rpm)	Load	Airflow Engine (g/s)	Airflow Cylinder (g/s)	Manifold Depression (mmHg)	Fuel Pulsewidth (ms)	AFR
1200	No load	16.5	2.12	362	4.5	16:1
1500	2.62 bar WWMP	18.5	2.26	420	4.6	14.7:1
2500	WOT	300	10.41	10	13.9	14:1

Table 3.3 AJ33 AP test conditions

A further test performed on the AJ33 cylinder head had the deactivation flap of the dump port opened at 2500 rpm. In conventional engine operation, the deactivation flap is closed at engine speeds above 3000 rpm.

In the interest of gaining useful results, it was decided during the planned test schedule that several additional fuel collection tests should be performed. These included:

- Testing the AJ33 head at the 1200 rpm and 1500 rpm speeds with the dump port activated while employing OVI. This was simply to see if activation increased or decreased bore wetting at these speeds. OVI was used since the tests had already established that CVI in the AJ33 head generated very little bore wetting

- The AJ26 head was tested using the Denso 12-hole injector from the AJ33 head as a further means of comparison. This batch of additional tests was important because the planned tests showed that the AJ33 head produced a much lower level of bore wetting than the AJ26 cylinder head. It had to be determined if this reduction was due to the improvements in AJ33 cylinder head design or the use of the 12-hole injector.

Every fuel collection test performed had an equivalent endoscope observation test performed at the same engine condition. This was important as it established visibly the liquid gasoline movement within the cylinder. The endoscope was positioned into the dummy cylinder, which was illuminated by a light source inserted through the lower plenum.

The observation tests were not performed at the same time as the collection tests due to practical considerations. These included unnecessary dirtying of the endoscope and light source or holding the endoscope in a position that maintained an airtight seal with the cylinder throughout the duration of a test to ensure consistent airflows within the cylinder.

3.3 RESULTS

All of the numerical results from the motored rig work are plotted on three graphs. These are for tests at 1100 to 1200 rpm, 1500 rpm and 2500 rpm. These plots highlight an important feature of the presentation of results from this work, in that the amount of fuel collected was plotted against camshaft angle with respect to MOP. Since this test rig had a steady flow vacuum pump rather than the usual pistons and crankshaft to draw air through the inlet valves and the exhaust valves were not used, the convention of using degrees crank angle was avoided to limit confusion. This is especially important when it is remembered that the AJV8 engines employ VVT. Since the motored rig had no crankshaft or exhaust camshaft, it was not physically possible to represent the advance or retard of the inlet camshaft position with respect to exhaust camshaft position or crank angle.

The three plots are explained as follows.

Figure 3.1: This shows the 1100 to 1200 rpm results for the AJ26 and AJ33 cylinder heads. The figure clearly shows that the overall magnitude of the fuel collected for the AJ26 cylinder head was much greater than that for the AJ33. For the AJ26 with CVI, approximately 25% of the injected fuel was collected in the upper 10 mm of the cylinder bore, whilst a further 14% was collected between 10 and 37 mm from the top of the bore (i.e. 39% minus 25%). The use of the Denso 12-hole injector in the AJ26 head made very little difference to this result. The amount of fuel collected for the large and small insert have been averaged for the AJ33 cylinder head since the uncorrected quantities of gasoline were so small and similar that it was felt that any difference would only be due to experimental accuracy. The maximum amount of fuel collected for the AJ33 head was approximately 12.5% of that injected and occurred with SOI at MOP. Activation of the dump port made relatively little difference to this result, with the amount collected falling to approximately 10%. Injection during the closed valve period reduced the amount collected to less than 5%.

Figure 3.2: This is the 1500 rpm equivalent of the above. Although the quantities of fuel collected were generally smaller at this speed in comparison to those collected at 1100 to 1200 rpm, the trend observed was identical.

Figure 3.3: This is the 2500 rpm plot showing the AJ26 and AJ33 results. In this plot, the AJ33 10 mm and 37 mm results are not averaged since they were both larger and quite different at this speed. The tests at 2500 rpm yielded the highest amounts of fuel collected. The AJ26 produced the result that for CVI, 60% (corrected) of the injected fuel was collected from the first 37 mm of the cylinder bore. Of this amount, approximately 38% was collected from the top 10 mm of the cylinder bore. These values reduced to 43% and 29% respectively when the Denso 12-hole injector was used in the AJ26 head. In contrast to this, at the same injection timing the results from the AJ33 head yielded 35% and 20% of injected fuel collected with the long and short inserts respectively. When the dump port was active, these amounts reduced to approximately 30% and 16%.

Whilst these figures summarize the overall quantities of fuel collected, the endoscope observations that follow the three result plots are important as they describe the paths that the gasoline actually followed within the cylinder.

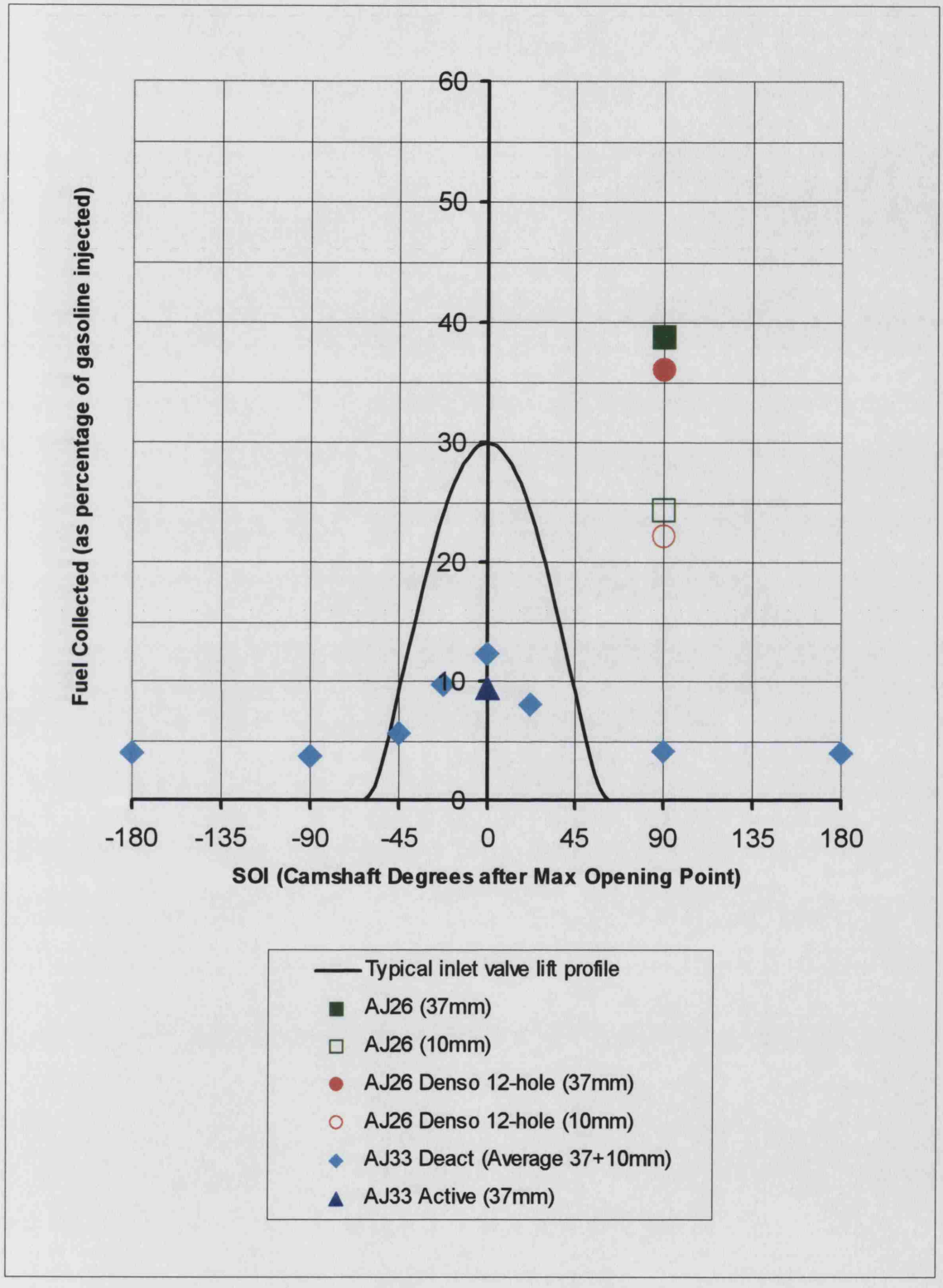

Figure 3.1 Complete result plot for 1100 / 1200rpm

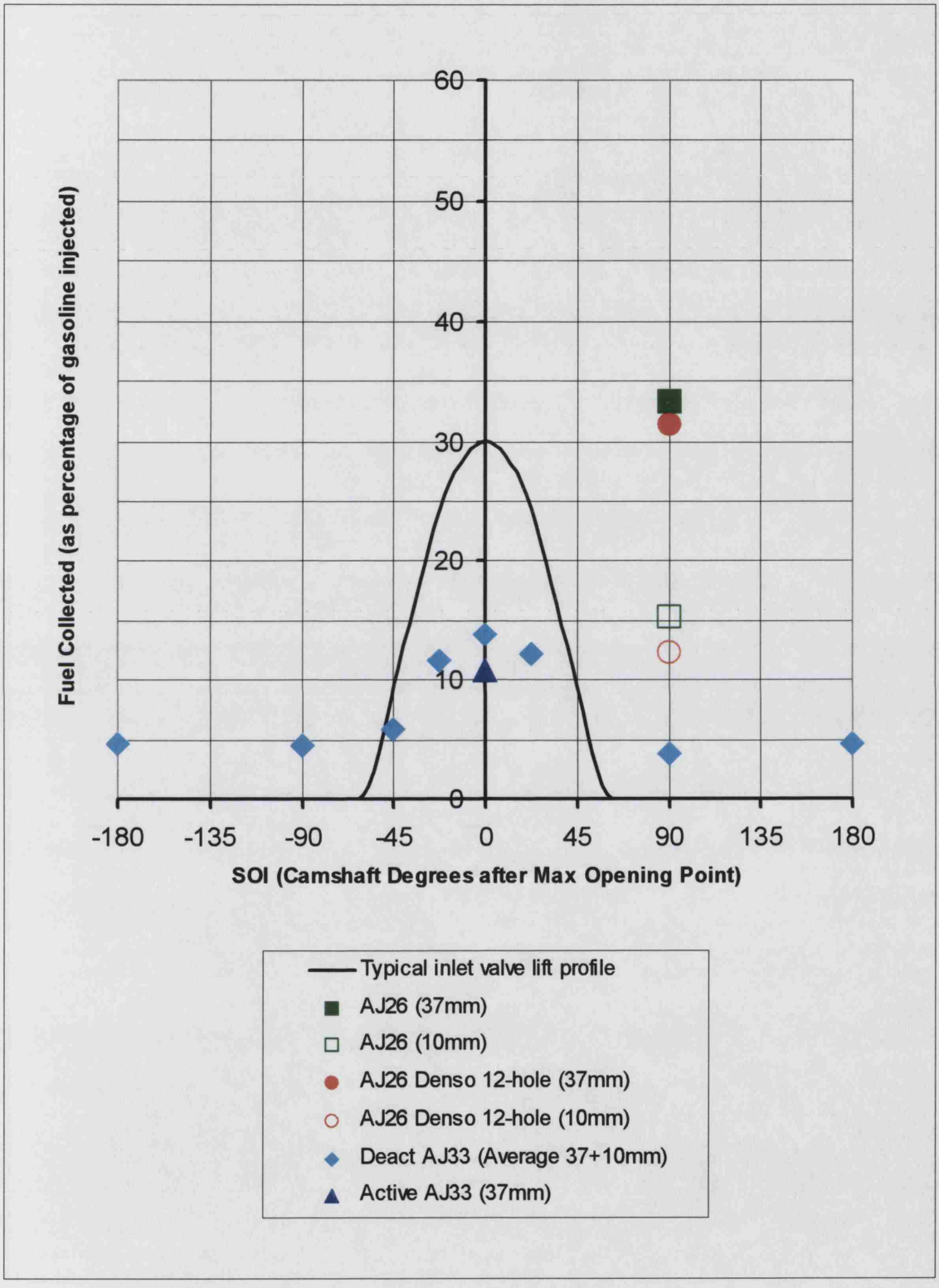

Figure 3.2 Complete result plot for 1500rpm

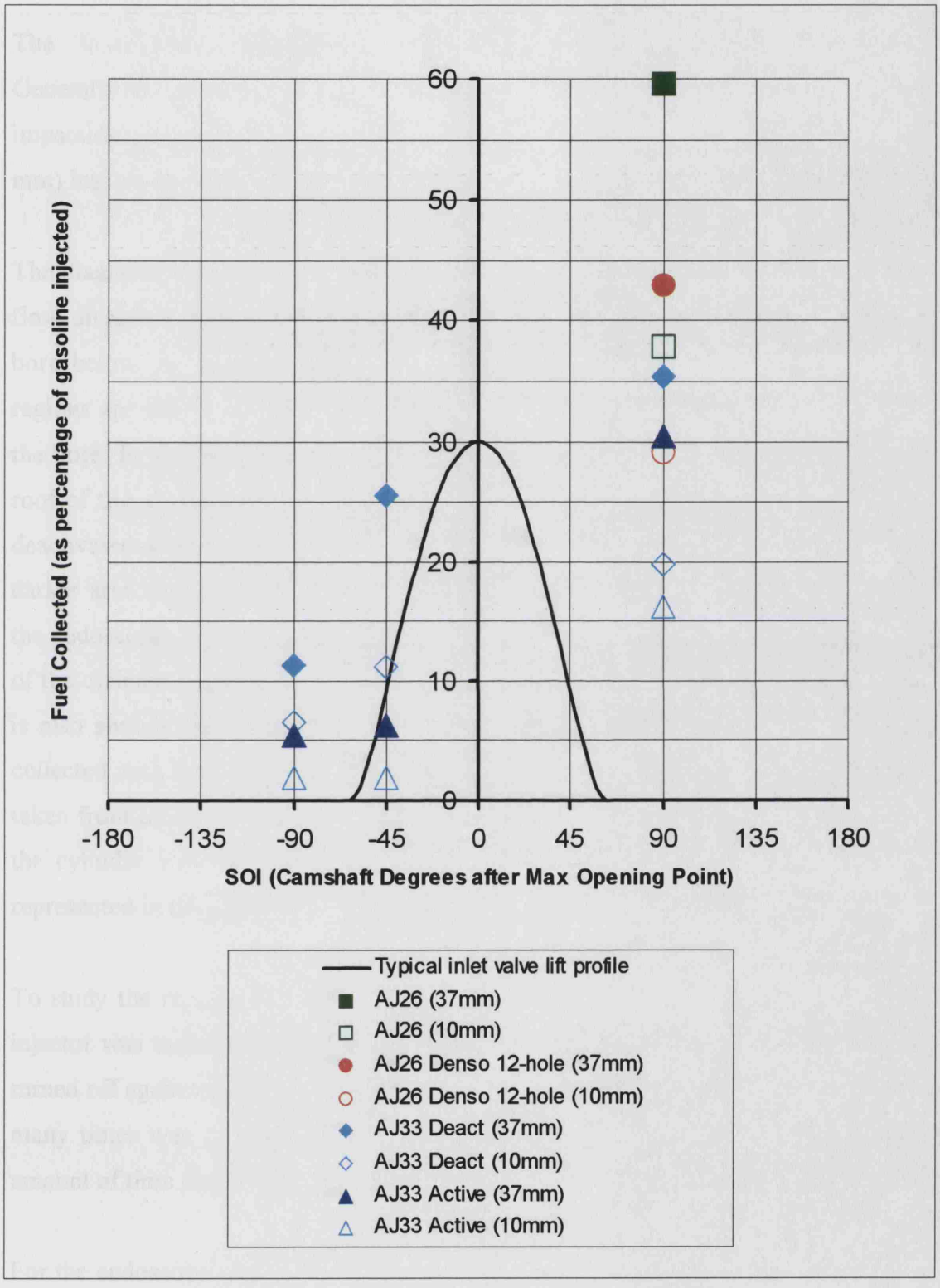

Figure 3.3 Complete result plot for 2500rpm

3.4 ENDOSCOPE OBSERVATIONS

The 'in-cylinder' observations from different tests of interest are shown below. Generally as would be expected, there was not much visible difference in the flow and impaction patterns observed between the tests using the long (37 mm) and short (10 mm) inserts, so only the diagrams for the long insert are shown.

The diagrams show surface flowing wall film as solid lines with arrowheads indicating flow direction, while shaded sections describe the impact location of droplets on the bore below the porous material wherever this was visible. Sometimes these shaded regions are also in arrow form to indicate the direction in which the droplets impacted the bore. In the diagrams, the observer is looking up through the cylinder at the pent-roof of the cylinder head with the pulley end to the right. In the AJ33 diagrams, the deactivated dump port is the valve on the left (marked with a cross when it is shut). The darker area around the pent-roof is the porous material as seen in perspective through the endoscope. The lighter area around the porous material represents the lower portion of the cylinder bore. For convenience, the labelling system used for the sampling tubes is also shown. Below the diagrams are figures for the corrected amount of gasoline collected with both long and short inserts, expressed as a percentage of fuel injected, as taken from tables in Appendix I-1. If these percentages marked for each sector around the cylinder were summed for each insert, then the total would equal those values represented in the plots.

To study the rapid propagation of the wall film a special technique was devised. The injector was turned on, the flow observed through the endoscope and then the injector turned off again to allow the roof to dry quickly. Watching this same wall film develop many times was important as there were several areas of interest and only a limited amount of time since the film developed quickly.

For the endoscope observations to be possible, a bright endoscope inspection light was inserted into the lower manifold in order to illuminate the bore and the cylinder pent-roof.

3.4.1 AJ26 Observations

The wall film seen on the AJ26 pent-roof was generally quite symmetrical on the left and right hand sides. At the lower 1100 rpm and 1500 rpm speeds, the wall film would flow from the inlet valves past the spark plug and be collected mostly at E2 and E3.

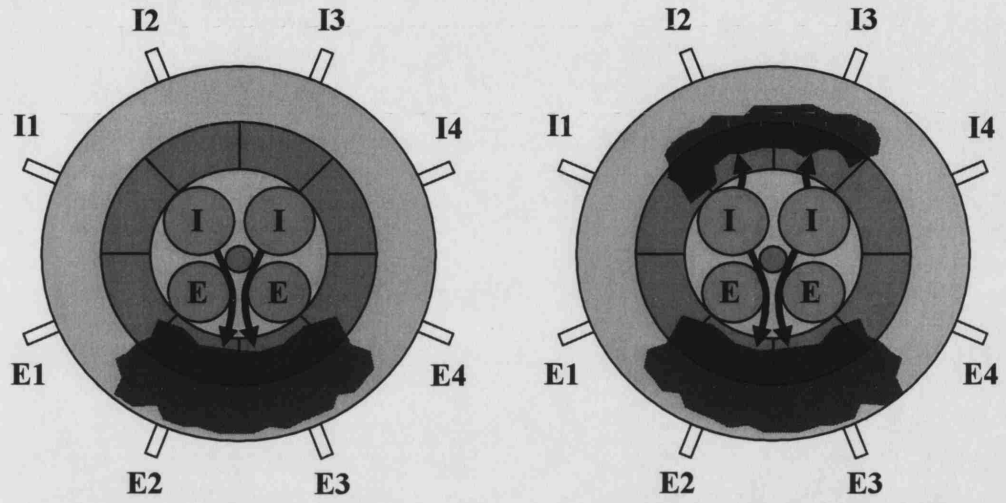

%	10mm	37mm
I1		
I2		
I3		
I4		
E1		
E2	2	5
E3	13	28
E4		

%	10mm	37mm
I1		2
I2	5	6
I3	4	5
I4		
E1		
E2	16	26
E3	13	19
E4		2

Figure 3.4 AJ26 1500 rpm (left) and 2500 rpm (right) observations

Droplets were seen to impact on the heads of the exhaust valves. There were also large droplets impacting on the bore below sectors E2 and E3 (Figure 3.4).

At the higher speed of 2500 rpm, the surface-flowing wall film was also visible flowing uphill from the inlet valves to sections I2 and I3 in addition to the exhaust side sectors. It was quite noticeable how all of the pent-roof quickly became covered in wall film at this speed, making the technique of starting and stopping the injector very useful for observing film formation and flow direction. The main difference between observations made at 2500 rpm and those made at the slower speeds was that wall film formed above the inlet valves, which shows the higher air flow rate forces the gasoline into this new area. It is also true that the greater quantity of gasoline and shorter cycle time may also

be responsible for establishing an upstream wall film around a greater proportion of the valve periphery. Again there was symmetry in this test with similar wall films coming from the two inlet valves. When the Denso 12-hole injector was inserted in the AJ26 head, the location of the fuel impaction was identical to that above, although the quantity of fuel collected did reduce.

3.4.2 AJ33 Observations

The observations for the 1500 rpm tests proved to be very similar to each other visually, even though the AJ33 head provided different wall film patterns to the AJ26 head.

1500 rpm Dump Port Deactivated

At these lower speeds, there was a noticeable difference between the fuel distribution produced by OVI and CVI. For the 1500 rpm tests, the values obtained from the 10 mm and 37 mm inserts were averaged because they were almost identical.

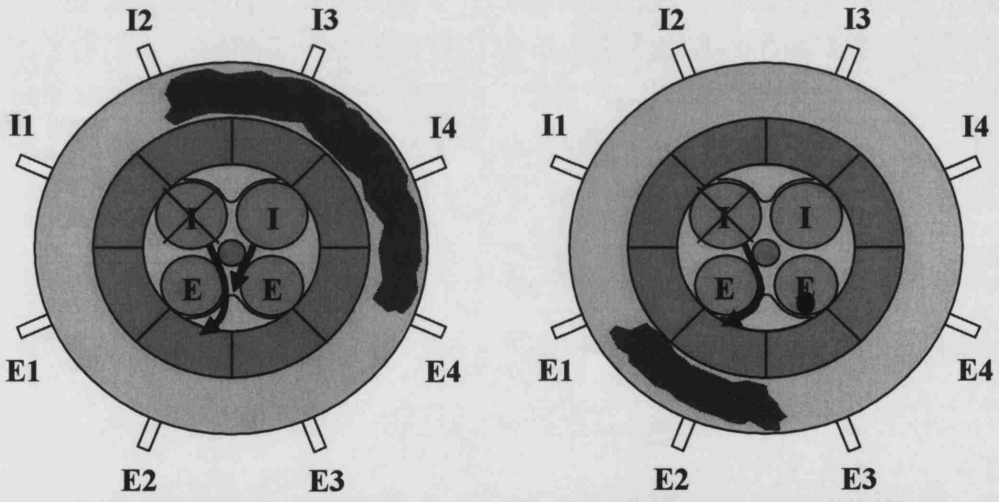

%	10mm	37mm
I1		
I2		
I3		
I4		
E1		
E2		4
E3		
E4		

%	10mm	37mm
I1		
I2		
I3		
I4		
E1		
E2		14
E3		
E4		

Figure 3.5 AJ33 1500 rpm, CVI (left) and OVI (right) with deactivated dump ports

Generally there was only a small amount of bore wetting when using the AJ33 head and CVI (Figure 3.5), with only 4% of the gasoline injected being collected. Under these conditions, the gasoline was always collected at sector E2 on the exhaust side of the bore (dump valve side). Observation with the endoscope showed that there was a small wall film flowing from the deactivated dump port past the spark plug to this sector. Another smaller wall film flowing from the active swirl port added to this.

Observation also showed that the swirl motion within the cylinder forced the wall film to be collected at sector E2 rather than both sectors E2 and E3 for example, was recorded for the AJ26 head which lacked swirl. Observation through the endoscope revealed that there was impaction of fuel on the cylinder wall up to at least 150 mm below the porous material, over an arc of around 120° through sectors I2–E4 (predominantly the high side of the cylinder).

In the case of OVI, more fuel was collected in sector E2, but no measurable quantities of fuel were collected from the other sectors. A noticeable difference from the fuel distribution observed with CVI, was the change in location of fuel impinging upon the lower region of the cylinder wall. In this case, impaction was confined to a region adjacent to sector E2.

The undulating wet area on the exhaust valve opposite the swirl port suggested that fuel was coming from this valve in the form of airborne droplets. This was confirmed when there was no visible wall film flowing from this valve.

1500 rpm Dump Port Activated

When the dump port was reactivated and OVI continued (Figure 3.6), gasoline collection at sector E2 continued, but reduced slightly to 11% of injected fuel. The droplet impact zone below the porous insert was also in a different location moving to a point adjacent to sector E3. The observation for CVI with the dump port activated was the same as that when the dump port was deactivated.

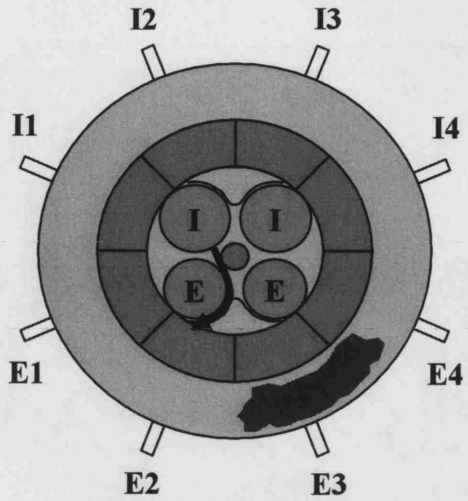

%	10mm	37mm
I1		
I2		
I3		
I4		
E1		
E2		11
E3		
E4		

Figure 3.6 AJ33 1500 rpm, OVI with activated dump port

2500 rpm Dump Port Deactivated

The results obtained at the 2500 rpm test conditions gave quite different fuel distributions, with gasoline collected from most sectors. With CVI and the dump port deactivated (Figure 3.7) fuel was collected in seven out of the eight sectors.

Generally, the amounts collected with the 10 and 37 mm inserts differed. Strong surface fuel flows were observed, particularly originating from the deactivated dump port, whilst droplet impaction below the porous insert was also noted. It was clear that the swirl created by the valve deactivation played a strong role in the distribution of the fuel.

In changing from CVI to OVI at this speed, it was evident that wall wetting was greatly reduced. The high swirl factor remained though, forcing the surface wall film from both inlet valves to be collected at sectors E1 and E2.

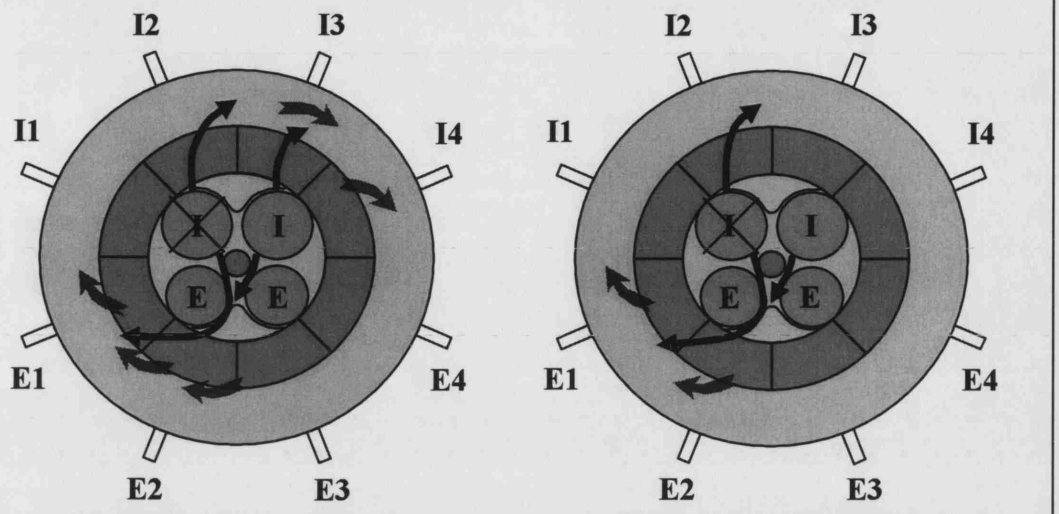

%	10mm	37mm
I1	1	
I2	2	10
I3		1
I4	1	2
E1	12	15
E2	4	7
E3		
E4	1	1

%	10mm	37mm
I1	5	6
I2		10
I3		
I4		
E1	6	10
E2	1	1
E3		
E4		

Figure 3.7 AJ33 2500 rpm, CVI (left) and OVI (right) with deactivated dump ports

2500 rpm Dump Port Activated

Activating the dump port visibly reduced the level of swirl in the cylinder. The quantities of fuel collected were similar to when testing with CVI and dump port deactivation, but with different sectors involved.

The droplet arrows show how the reduced swirl factor caused the droplets to impact the bore at a different angle.

The combination of dump port activation and OVI caused only a very small level of bore wetting to occur at 2500 rpm (Figure 3.8). Even the lower sections of the bore had a low number of droplet impacts for this OVI condition.

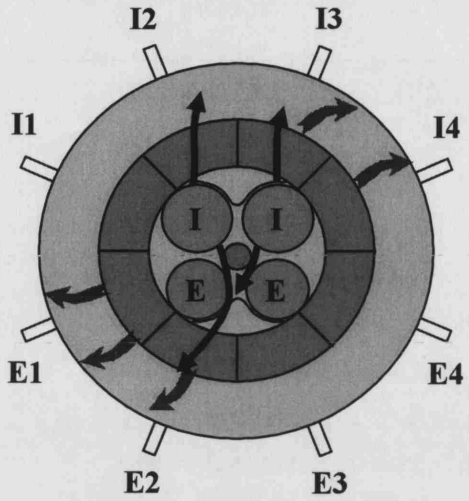

%	10mm	37mm
I1		
I2	6	11
I3	1	3
I4	1	5
E1	1	3
E2	4	7
E3	1	1
E4	2	1

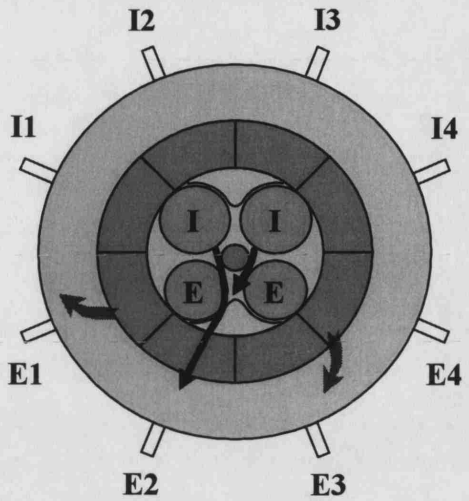

%	10mm	37mm
I1		
I2		
I3		
I4		
E1		
E2	1	2
E3	1	5
E4		

Figure 3.8 AJ33 2500 rpm, CVI (left) and OVI (right) with activated dump ports

3.5 DISCUSSION

The results observed are now discussed. This section aims to explain the results and compare the two cylinder heads.

3.5.1 AJ26 Discussion

The results for the 1100 rpm and 1500 rpm tests were quite similar, while the 2500 rpm tests generally resulted in much more bore wetting due to the larger pulsewidth. All of the tests for the AJ26 head used only CVI.

The AJ26 results will be discussed in the following order:

- 1100 rpm and 1500 rpm
- 2500 rpm

AJ26 1100 rpm and 1500 rpm

The 1100 rpm and 1500 rpm tests resulted in similar bore wetting characteristics, with more wetting at the 1100 rpm speed. The amount of fuel collected at 1100 rpm was 18% and 67% higher for the long and short inserts respectively, when compared with that collected at 1500 rpm. This is likely to be due to the combination of the 9% increase in fuel input (AFR decreased from 16 to 14.7), decreased air velocities through the valves and an increase in the time for gravity-assisted puddle formation upstream in the port at the valve periphery between valve events.

In the observation tests, it was apparent that there was a large wall film flowing from the inlet valves, past the spark plug and exhaust valves to the insert at sectors E2 and E3. No gasoline was collected on the inlet side of the bore. This was almost certainly because during CVI, the petrol had time to move by gravity during the closed valve period and form small puddles behind the inlet valves at the lowest point, not the top edge near the inlet side. When the inlet valves opened, the combination of airflow and gravity carried the gasoline away from the inlet valve to the exhaust side of the bore. In the real engine, this fuel flow path could result in plug fouling under cold start conditions. Since the wall film passed the exhaust valves, it would be likely that under cold start conditions any gasoline surviving combustion (for example in valve seat crevices) would be scoured out of the cylinder through the exhaust valves during blowdown, as seen in other work [Fry *et al* (1995)]. This could increase cold-start HC emissions, but would reduce the amount of surface flowing fuel reaching the cylinder bore. Under fully warm engine conditions, it would be expected that the amount of surface fuel flow reaching the bore wall would be insignificant.

At these test conditions the short insert only collected approximately half of the quantity of fuel which was collected by the long insert (at both speeds). In the observation tests, there was no wall film passing over the short insert (i.e. none escaping), suggesting that this insert was effective in collecting all of the surface flowing wall film. Since the long insert collected nearly twice as much gasoline, it was fair to assume that this additional amount must have been in the form of airborne droplets impacting on the lower portion of the long insert. This lower portion of the long insert occupies the area normally blocked by an aluminium ring when the 10mm insert is used. In fact, when using the short insert there was a large droplet impaction zone observed on the aluminium ring,

which confirms this theory. The distinction between wall film flowing over the surface of the cylinder head and impaction of airborne droplets directly onto the cylinder bore wall is an important one. Although the surface flow of fuel will only exist when the engine is cold, it is the airborne droplets that may continue to be generated even as the engine warms up. These airborne droplets may then be a source of concern over a wider range of engine operating conditions. An interesting fact was that at 1100 rpm, sector E2 collected a vast majority of the gasoline, while at 1500 rpm, it was sector E3 that collected more. This was very repeatable and could suggest some asymmetry with a change-over in flow distribution between the two inlet ports.

AJ26 2500 rpm

At this test condition, gasoline was collected at sectors E2 and E3 on the exhaust side and at sectors I2 and I3 on inlet side. The amount of wetting at E2 and E3 was much larger in this 2500 rpm case than that at the slower 1500 rpm condition. This was a rich condition with an AFR of 12.5:1. It is believed that the gasoline built up behind the inlet valves and created a large surface wall film when the valves opened. The amount of bore wetting in this test was higher than in any other test in this work. It is useful to note that between one-third and one-half of the measured fuel is still arriving directly at the cylinder bore wall as airborne droplets. Because only CVI was tested, this must be from port fuel films re-entrained or strip-atomised at the inlet valves.

3.5.2 AJ33 Discussion and Comparison with AJ26

The results for 1200 rpm and 1500 rpm cases were again very similar for the AJ33 cylinder head as observed with the AJ26 head. The 2500 rpm tests also resulted in more bore wetting than the 1200 / 1500 rpm cases due to the large pulsewidth and short residence time. The most important fact is that the relative level of bore wetting for the AJ33 head was much less than that of the AJ26 head.

The results are explained in the following order:

- 1200 rpm and 1500 rpm CVI and OVI
- 1200 rpm and 1500 rpm OVI with activated dump port
- 2500 rpm CVI and OVI
- 2500 rpm CVI and OVI with activated dump port

AJ33 1200 rpm and 1500 rpm CVI and OVI

It was noticed at this speed that the long and short inserts collected similar and small quantities of gasoline. Due to this the long and short insert values for the AJ33 at the slow speeds were averaged. The non-averaged individual values are available in the tables of Appendix I. Obtaining such similar results for the two inserts indicated that the fuel collected must be primarily wall film flowing from the inlet valves or droplets with a high angle of approach to the cylinder wall. The small amount of fuel could be explained by the shrouds in the AJ33 head promoting most gasoline to be in the form of airborne droplets that passed down the central area of the cylinder. As with low speed AJ26 tests, no gasoline was collected on the inlet side of the bore, probably due to the same effects of gravity and airflow. Since the main points of interest are the differences between CVI and OVI, these are discussed as follows.

CVI - There was only a small amount of bore wetting when using CVI with the AJ33 head, with only 4% of the gasoline injected being collected. In these conditions, the gasoline was collected at sector E2 and endoscope observations showed that there was a wall film flowing from the deactivated dump port past the spark plug to this sector. Another smaller wall film flowing from the active swirl port added to this. Observation also showed that the swirl motion within the cylinder forced the wall film to be collected at sector E2 rather than both sectors E2 and E3 as with the AJ26 head which lacked swirl. In the real engine, these surface films would be expected to dry up quite quickly as the engine warmed up. The path of the wall film, which is similar to that in the AJ26, suggests that any surviving liquid fuel could cause plug fouling and exit the cylinder via the exhaust valves causing high HC emissions under cold start conditions. The observation test was especially useful as it showed droplets of gasoline impacting very low on the bore, at least 150 mm from the top of the dummy cylinder. In the real engine these droplets would almost certainly impact on the piston. These droplets were probably formed when the inlet valves opened and the airflow removed most of the gasoline present from the back of the valves and port walls stripping it into the air. The remaining gasoline forms the wall film observed above.

OVI - Observation with the endoscope showed that during 1200 rpm and 1500 rpm OVI tests, the active swirl valve had no visible surface wall film coming from it, suggesting all gasoline entering from here would be in the form of airborne droplets. The

undulating damp area that formed on the opposite exhaust valve also suggested the presence of the airborne droplets. The deactivated dump valve was always the source of the surface wall film during tests at these two speeds, following the usual path past the spark plug and exhaust valves to be collected on the exhaust side of the bore. The reason for this surface wall film forming under OVI conditions was believed to be the result of two influencing factors. The first was that the dump port was deactivated and the only air that flowed through the dump valve are the trace flows that leak past the deactivation flap or from the swirl port through the small aperture between the tip of the injector and septum of the cylinder head. The second factor was the positioning of the injector, which was aimed favourably towards the swirl port. This positioning would result in some of the injected petrol making contact with the septum on the dump port side, forming a wall film immediately. When the dump port was deactivated, there would have been a lower pressure in this port than the swirl port at part load conditions as the engine is sucking from both. Some of the injected fuel may be deflected or drawn into the dump port through this small aperture that connects the ports. It should also be noted that the tip of the injector is aimed directly at the leading edge of the septum. Due to the distance from the injector tip to this leading edge being less than a centimetre and the leading edge being quite 'blunt' at two millimetres wide, the proportion of the spray that impacts upon this division may be quite high. This would be especially true if the fine spray produced by the 12-hole injector is deflected towards the division wall by the airflow through the aperture.

AJ33 1200 rpm and 1500 rpm OVI with Activated Dump Port

In the interests of determining whether the surface wall film emerging from the deactivated dump port at 1200 rpm and 1500 rpm was created as a result of port deactivation with its associated loss of airflow or a result of the injector positioning, a further test was conducted at each of these two speeds with the dump port activated. It was decided to perform the tests with OVI as it was already established from previous tests using OVI with port deactivation that any wall film would always come from the deactivated dump port, not the swirl port. In this activated condition, there was the usual pent-roof wall film and at best a 20% reduction in the amount of gasoline collected, suggesting it was the injector positioning and/or spray targeting rather than the port deactivation that was the main source of the dump port surface wall film.

When the inlet manifold was removed with the inlet valves fixed at MOP, it was clear to see that the injector was directed (through the open valves) at the exhaust side of the cylinder bore. In fact, the porous material could be observed easily through the opened inlet valves. This unobstructed path from the injector to the exhaust-side porous material was present in both the AJ26 and AJ33 cylinder heads. The similar quantities of gasoline collected by the long and short inserts during CVI suggested that the two inserts were either collecting the same level of wall film or the same level of wall film and airborne droplets. Of the entire sweep when still using a deactivated port, the injection timing at MOP showed a slight increase in the amount of fuel collected by the long insert over the short insert. This could be due to the 'line-of-sight' effect allowing airborne droplets to impact on the insert at sector E2 in addition to the fuel arriving there in the form of wall film. For all the other points in the sweep, the difference between the amounts of gasoline collected by either insert was so small it was believed that the difference between the inserts falls into the realms of experimental accuracy and repeatability rather than determining between wall film and airborne droplets. It is for this reason that the 1200 rpm and 1500 rpm result plots use the average of the long and short insert values, instead of being considered separately as in the AJ26 head.

AJ33 Deactivated 2500 rpm CVI and OVI

These results were quite different from those measured at 1200 rpm and 1500 rpm. The increased pulsewidth increased the level of wetting, while the increased airflow and decreased residence time had allowed gasoline to be collected in different places. In this 2500 rpm test, CVI caused more fuel to wet the bore more than OVI, reversing the trend observed at the slower speeds. It is believed that at 2500 rpm, the larger wall film generated under the CVI condition outweighs the 'line-of-sight' effect experienced by airborne droplets during OVI conditions. A characteristic of this speed was that there was a difference between amount of fuel collected by the long and short inserts. This suggests that a greater proportion of the fuel arrived at the wall as airborne droplets. Even though the level of bore wetting has increased, it is still much less than that experienced with the AJ26 head.

CVI - Most of the gasoline collected here was on the exhaust side to the dump side of the head as with the lower speeds, indicating this to be wall film again. It was also clear that the swirl was sufficient to blow some of the gasoline round the bore, where at this

higher speed the wall film is collected at sector E2 and even sector E1. A large amount of gasoline was also collected on the inlet side of the bore. This could be explained by the long pulsewidth producing a wall film that is blown upwards to the top edge of the inlet valve by the higher airflow at this 2500 rpm condition. Upon opening, this gasoline would leave the valve in the form of wall film or bulky airborne droplets. At point I2, the long insert collected much gasoline, but the short insert collected almost nothing, suggesting that fuel collected at this sector was entirely made up from the impaction of airborne droplets at a distance greater than 10 mm from the top of the bore. The downward deflection of the fuel may be due to the action of the inlet valve shrouding on the AJ33 head. In comparison, the AJ26 head collected a vast amount of gasoline with the short insert at this test speed.

OVI - In this test some gasoline was collected at sectors E1 and I1. This shows the trend of the wall film being blown around the bore enough to reach these two points. In the observation tests, it was clear to see that there was less wall film with OVI than CVI and that there were no major droplet impacts on the bore. The amount of gasoline collected by the short insert was less than the long insert, but the locations of impact had not changed. This shows the collected fuel was in the form of both airborne droplets and wall surface film. This OVI test was similar to the CVI test at sector I2 because the long insert collected much more gasoline than the short insert. This was again expected to be due to the inlet valve shrouding on the AJ33 head.

A third injection timing was investigated where its value ensured that SOI was during the closed valve period and EOI was during the open valve period. This ultimately means that the inlet valve would open during the injection period. This was interesting as less gasoline was collected at this injection timing than when injection occurred as completely CVI or OVI. The sectors that collected the petrol at this point were the same as for the other injection timings, but the difference was in the reduction in the quantity of gasoline collected on the inlet side. It was thought that the opening of the valve removed much of the gasoline that built up in the port around the inlet valves during the closed valve period and the initial airflow through the valves was not strong enough to carry the gasoline up to the inlet side of the bore.

AJ33 Activated 2500 rpm CVI and OVI

Generally in these tests, activation of the dump port reduced the amount of gasoline collected during OVI, but had little effect in reducing that collected with CVI. The amount of swirl present reduced noticeably though.

CVI - During the CVI tests, the amount of gasoline collected was only slightly smaller than when the dump port was deactivated. This shows a similar trend to that observed for the 1500rpm test, where activation reduced the bore wetting only slightly. The most noticeable difference in this test was the visible reduction in swirl. During one of the observation tests, the deactivation flap was closed and opened at regular intervals. Any large wall film droplets that were gliding down the bore in a spiral motion under deactivation conditions would continue to follow a spiral pattern, but in a more vertical manner as the swirl effect was reduced. The short insert collected approximately half of that collected by the long insert in this test, showing that there was still a wall film and airborne droplet combination.

OVI - During OVI with an activated dump port only sectors E1 and E2 collected small amounts of gasoline. The long insert collected more than the short insert, showing that there was a wall film and airborne droplet combination as in the CVI case. The third injection timing that spans the opening of the inlet valve showed a reduction in gasoline collected. This was attributed to two factors. The first was the opening action of the valve forcing wall film into airborne droplets. The second simply being that the second half of the injection occurs during OVI with both valves active, reducing wall film formation.

3.5.3 AJ26 Cylinder Head and Denso 12-Hole Injector

One feature of the test work was to insert the AJ33 Denso 12-hole injector into a slightly modified AJ26 manifold. It was hoped that this would help to determine if the reduction in bore wetting experienced by the AJ33 head during CVI at all three speeds was due to the new cylinder head design or the use of the new injector.

Details of the characteristics of the two injectors were later determined by Van Romunde [2003] and are included at Appendix V. These indicated a substantial difference in the droplet sizes produced by the two injectors. The 12-hole injector

produced an Smd and dv,90 of less than 50 μm and 100 μm respectively for much of the injection duration. The side-fed injector produced droplets that were too large to be adequately characterised by the available equipment (implying Smd droplet sizes of several hundred μm). This is also apparent in the spray photographs in Appendix V.

The results indicated that there was only a small reduction in wetting with the AJ26 head and Denso 12-hole injector combination. It was expected that this was due to the more sophisticated 12-hole injector wetting the back of the closed inlet valves and ports in a different way to that of the AJ26 injector. When the inlet valves opened, this gasoline was distributed from the opened valve in a slightly different distribution to that obtained with the AJ26 head and side-fed split-spray injector combination.

It was therefore decided from the above set of tests that the reduction in bore wetting in the AJ33 and Denso 12-hole injector combination was due almost entirely to the redesign of the AJ33 cylinder head (including valve shrouding) and the respective changes in injector position and targeting, rather than being primarily function of injector refinement.

3.5.4 Comparison with Results from Ford 4.6 Litre Modular V8

In previous work [Ioannou (2000)], Ford 4.6l 2 and 4-valve heads were compared on a somewhat similar test rig. The two valve design had a more direct and short fuel path from injector to cylinder wall than the 4-valve heads and the 4-valve heads had similar valve shrouding to the AJ33 cylinder head.

For the 2-valve case at 1500 rpm, the total amount of fuel collected was nominally 90% (corrected) of the fuel injected for CVI, reducing to 66% for OVI. The 10mm inset helped establish that during CVI, 91% of this collected fuel was in the form of liquid surface films, whereas for OVI, 64% of this collected fuel was due to wall films.

At the same speed, the Ford 4-valve head would usually collect about 60% of the fuel injected with the 37 mm insert, showing only little difference between CVI and OVI. The 10 mm insert was not used for this head as the endoscope observations indicated that there were not many fuel droplet impactions on the cylinder wall.

The comparable 37 mm CVI values for this work would be 33% and 4% for the AJ26 and AJ33 designs respectively as shown in Figure 3.9. This implies that the design features in the Jaguar cylinder heads significantly reduce the amount of fuel impacting with progressive improvement from the AJ26 to the AJ33 head.

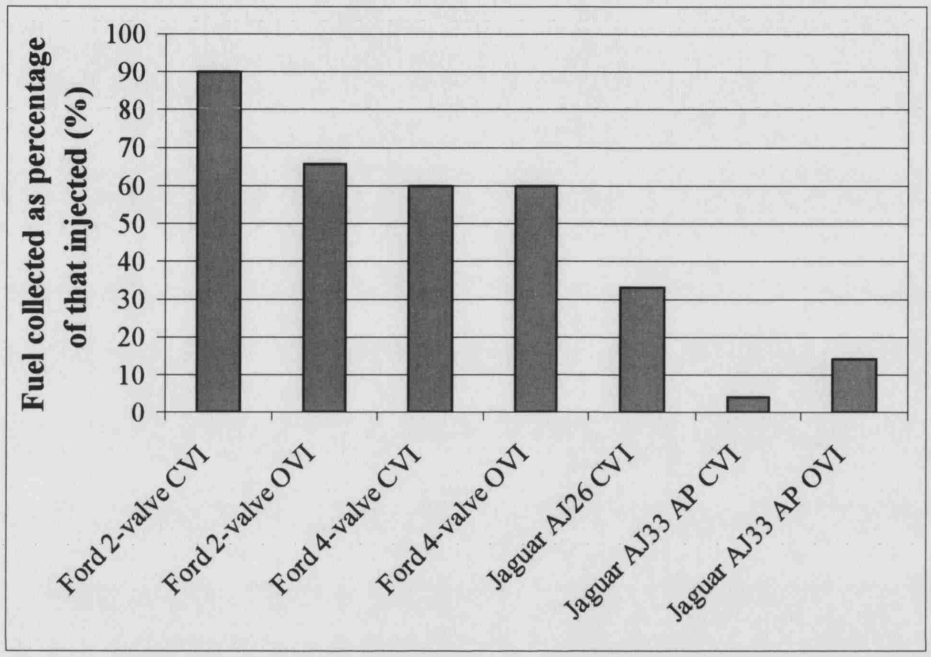

Figure 3.9 Comparison of wall wetting of the different cylinder heads

3.6 CONCLUSIONS

The motored rig proved to be a useful means of comparing the two cylinder heads and their injectors, with the confidence that the tests were very repeatable. When Ioannou tested a 2-valve design on a similar test rig, the measured fuel impaction on the cylinder wall was very large. This reduced when he used a 4-valve pent roof design, but still remained relatively high. Both the cylinder heads tested in this study and documented in this thesis produced significantly lower levels of measured fuel wall film in comparison to the work of Ioannou.

The main finding from the motored rig work was that the combination of AJ33 cylinder head and 12-hole injector caused much less bore wetting than the AJ26 cylinder head and its side-fed injector. Under CVI conditions, the results for the AJ26 cylinder head indicated both wall film and airborne droplets had been collected by the porous material, but when using a CVI strategy with the AJ33 cylinder head almost no fuel was

collected, immediately indicating that this cylinder head was not as prone to wall wetting as the AJ26. The AJ26 head was not tested with OVI, but the AJ33 head showed a slight increase in wall wetting with this strategy.

In the AJ26 head, there was little difference in the quantity of fuel collected between the 1200 rpm and 1500 rpm tests, but the faster 2500 rpm test was quite different and generated more wetting than any other test in this study. At this faster speed of 2500 rpm with wide open throttle and longer injection pulsewidth, the amount of wall wetting with both heads increased as expected. Of the three injection timings used, the CVI condition caused the AJ26 head to wet the bore twice as much as the AJ33 head. The remaining two injection timings returned similar levels of wall wetting for the AJ33 head, where both liquid wall film and airborne droplets were experienced.

The most important conclusion that can be made from the motored rig work was that the cylinder head design and injector targeting appeared to be the dominant factors in determining the likelihood of liquid fuel impaction upon the cylinder wall. This was confirmed when the 12-hole injector and AJ26 cylinder head were tested together under CVI conditions, where the wall wetting did reduce, but not to the extremely low levels experienced on the AJ33 head.

The design features of the cylinder heads that are thought to affect wall wetting are now described. Injector targeting involves not only the line-of-sight of the injector, whether to the cylinder wall (for OVI) or back of valve and port area (for CVI), but also the distance from the injector tip. Both of these are important design factors and the values used by the engine manufacturer will be determined by which injection strategy is chosen, where the interaction of the spray and local airflow are critical [Pierson (2002)]. Generally, a long path (as is common for 4-valve pent roof designs) and avoidance of a direct path to the cylinder wall provide measurable benefits.

Valve shrouding is often varied during engine design to provide the correct compression ratio for the engine. However, its role in the fuel delivery system should not be overlooked. The results presented here suggest that the valve shrouding applied to the AJ33 AP head were a key factor in the reduction of wall wetting in comparison to the AJ26 design. The primary benefit of shrouding was at low lift, where strip atomisation

of collected fuel may occur. It is therefore very effective at redirecting fuel from part load CVI away from the bore on the AJ33 AP design. At higher load, the air may initially succeed in carrying the fuel away from the cylinder bore, but the amount of re-entrained fuel from CVI port films may still enter the cylinder at higher valve lifts (as much larger droplets) and dominate the cylinder wall film generation. The shrouding will have less affect on OVI, due to the direct path from injector to wall when the inlet valves are well open. This was confirmed when by the AJ33 1200 rpm and 1500 rpm tests, when it was observed that OVI produced more wall wetting than CVI.

The endoscope observations confirmed the belief that the head design was chiefly responsible for the difference in results for the two cylinder heads, as the fuel impactions observed for the AJ33 AP cylinder head were further down the cylinder below the porous material and further around the circumference of the cylinder in a spiral pattern. This was because the inlet ports of the AJ26 cylinder head were straight and symmetrical, but the inlet ports on the AJ33 AP head were quite different, where the port without deactivation approached the cylinder more tangentially and was designed to promote axial swirl within the cylinder.

When the dump port deactivation flap of the AJ33 AP head was opened, the amount of fuel reduced slightly, but such a small change indicated that port deactivation alone could not account for the noticeable difference between the AJ26 and AJ33 AP under CVI conditions. In fact, it could be argued that opening the port deactivation flap during OVI should have made the AJ33 AP head behave more like the symmetrical AJ26 head, but this action reduced the wall wetting rather than increase it, further indicating the core difference between the designs on the two cylinder heads.

Generally, the AJ33 head generally showed not only a much lower total amount of bore wetting than that for the AJ26, but also a reduction in the amount of airborne droplets impacting the bore. This is important because the wall film observed flowing along the surface of the cylinder head would probably evaporate quickly in a warm engine and impaction from airborne droplets may persist in a warm engine.

The porous liner did have several disadvantages in the study of wall film. The most notable was that the rig could only run cold and was not heated to promote fuel

evaporation. The exhaust valves were static in this work and it was not possible to study what affect they would have on wall wetting. Since no piston was present, no backflow from the cylinder into the intake port was created, where in a real engine this backflow would disrupt the formation of liquid fuel films. The lack of piston also caused the in-cylinder motion to behave in a different way to the normal engine and any impactions that may have normally occurred on the piston would go un-detected. This technique generally presented a worst case scenario due to the cold nature of the rig and how some of the mechanisms for wall film generation that are normally inhibited by normal engine operation were not stopped here. These drawbacks are addressed by application of the heat flux technique, as described in the remainder of this thesis, where heat flux sensors are used to detect liquid fuel in a firing single-cylinder engine.

CHAPTER 4

ENGINE DESIGN AND INSTRUMENTATION

4.1 INTRODUCTION

It was decided to construct a single cylinder engine, capable of fired operation under 'warmed-up' conditions, in order to examine the impaction of liquid fuel from the AJ33 AP cylinder head in more detail and contrast this with the next generation AJ33 CP head. This chapter is devoted to the description of the engine and instrumentation. From the outset, the engine was designed to accommodate heat flux sensors on the piston crown in addition to the cylinder bore, unlike the work of Ioannou (2000). This implied that a key aspect of the design was how to pass the signal from the moving piston to a PC-based data logger outside of the engine. This required an integrated design of the piston, cylinder block and the system that would pass the signal from the piston-based sensors to the data logger. The design of this engine also considered cooling, lubrication and modification of standard engine parts for use with the unique cylinder block.

Figure 4.1 Photograph of the single cylinder engine

The bottom-end of a Lister Diesel engine provided a convenient crankcase and crankshaft unit. The same 86 mm bore as the production engine and an 88 mm stroke (which was only 2 mm shorter than that of the AJ33 engine) were used. A 160 mm long modified Lister conrod (8 mm longer than the production conrod) was also used.

4.2 ENGINE INSTRUMENTAION

4.2.1 Heat Flux Sensors

The heat flux sensors used in this work are based on thermocouple technology and essentially join many such thermocouple pairs in series to form a flat-plate differential-thermopile as shown in Figure 4.2. This plate actually consists of a ceramic thermal resistance layer. Since the thermocouples are arranged in series, the total output voltage 'V_t' of the thermopile is proportional to the number of thermocouples.

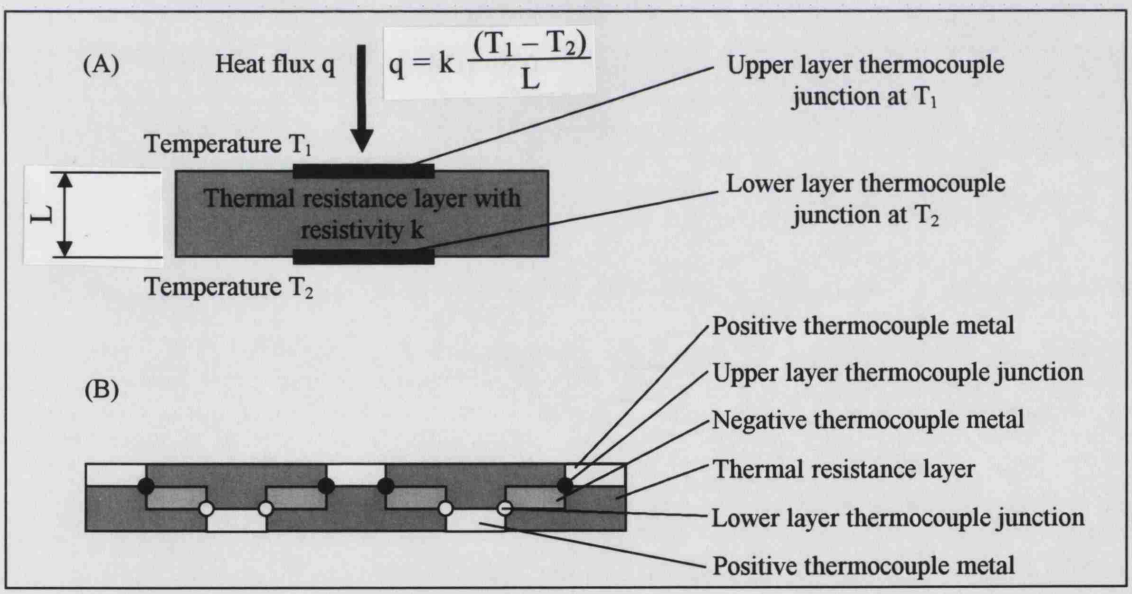

Figure 4.2 Thermocouple and resistance layer [reproduced from Vatell]

The temperature difference across this thermopile then allowed the heat flux to be determined, where the heat flux was proportional to the ceramic material's thermal conductivity 'k' and the temperature difference, but inversely proportional to thickness of the resistance layer 't' as observed in equation 1.1.

$$q \propto (k / t) * V_t \qquad ...(4.1)$$

Since the thermal conductivity of the ceramic material is a function of temperature the sensors were initially calibrated at the factory. A platinum resistance temperature sensor (RTS) was used to measure the temperature at the sensor's face as shown in Figure 4.3.

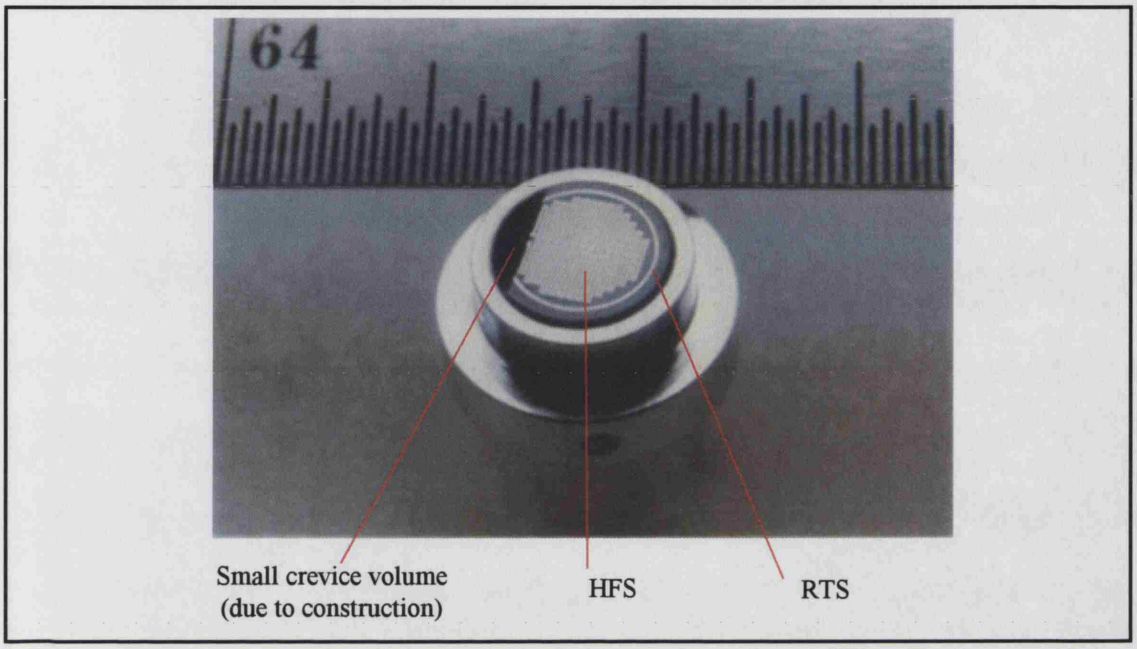

Figure 4.3 Face of heat flux sensor. Note HFS and RTS features [Vatell (2001)]

The face of the heat flux sensors is only 2 microns thick and permits response times of only 6±2 microseconds (for an uncoated sensor) [Vatell (2001)]. This surface temperature reading was then used to correct the heat flux signal by allowing for any variation in conductivity of the thermal resistance layer. This implied that a second output from the sensor was continually required, where both of these outputs were amplified by an AMP-6 unit (Figure 4.4).

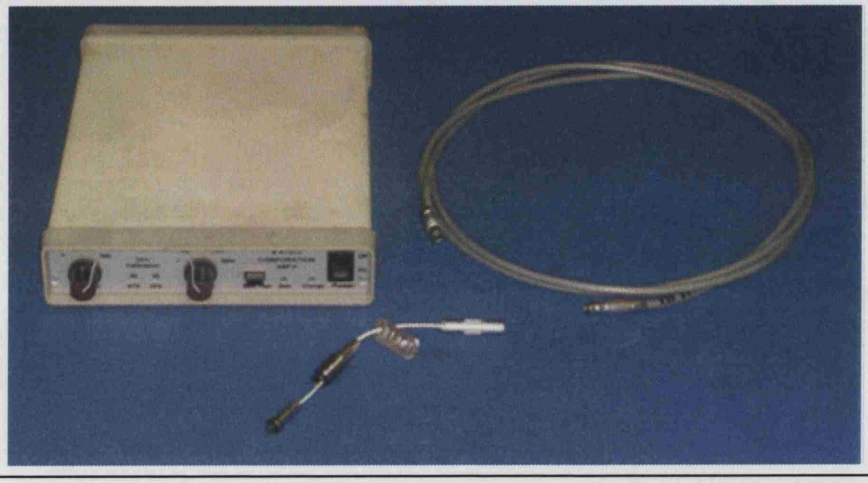

Figure 4.4 Heat flux sensor, amplifier and grey extension cable

When the sensors were located on the curved bore, small pockets were formed where fuel could collect, as shown in Figure 4.5. However, these pockets were extremely small and unlikely to influence the results. The performance of the sensors is detailed in Table 4.1 and the details of the AMP-6 unit are provided in Table 4.2.

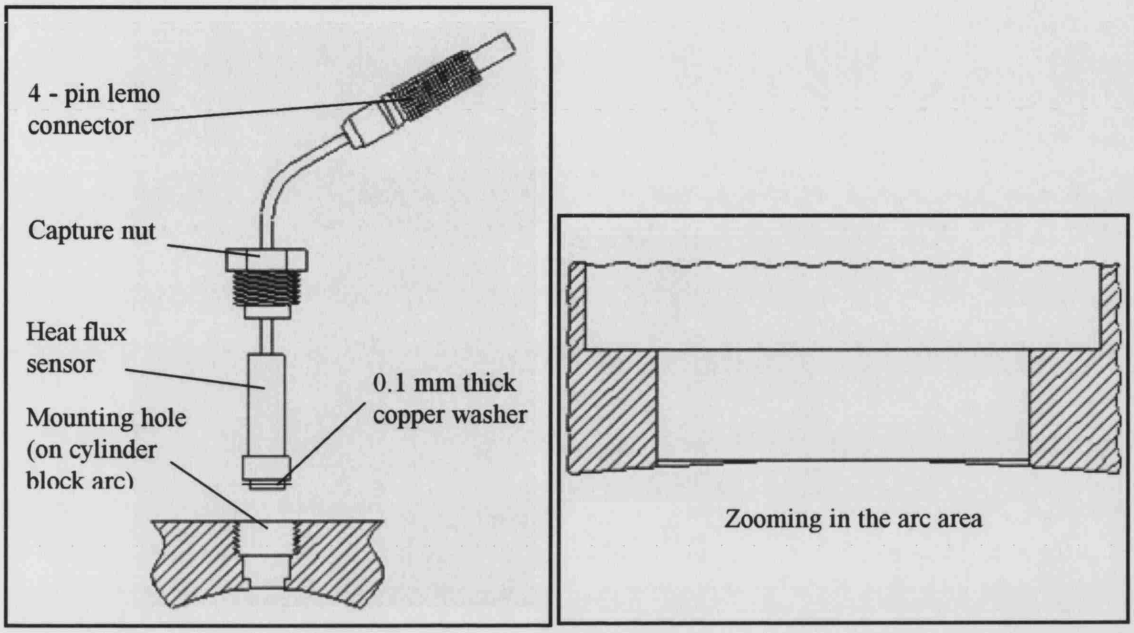

Figure 4.5 Heat flux sensor mounting [reproduced from Ioannou (2000)]

HFS model	HFM –7 E / H
Max. Face Temperature (°C)	700
Min. Detectable Heat Flux (W/cm^2)	0.01
Uncoated Response Time (μs)	6 ± 2
HFS sensitivity (μV / W / cm^2)	150 ± 10
HFS source impedance (Ω)	2500
RTS sensitivity (Ω / °C)	0.25 - 0.35
RTS resistance (Ω)	100 – 200
Thermocouples	Chromel / Constantan
RTS metal	Platinum
Housing	Nickel
Wiring (max. Temperature)	Mineral sheath (350°C)

Table 4.1 Heat flux sensor specifications [Vatell (2001)]

	Heat Flux Channels	Temperature (RTS) Channel
Gain Settings:	1, 100, 500, 1000, 5000	1, 100, 200, 500
Gain Accuracy (%)		
Gain = 1	± 0.6	± 0.6
Gain = 100	± 1.5	± 1.5
Gain = 200, 500	± 1.5	± 1.5
Gain = 1000	± 2.1	-
Gain = 5000	± 3.6	-
Bandwidth		
Gain = 1	1 MHz	1 MHz
Gain = 100	150 kHz	150 kHz
Gain = 200		100 kHz
Gain = 500	50 kHz	50 kHz
Gain = 1000	25 kHz	-
Gain = 5000	5 kHz	-
Input Impedance	10^9 Ohms	10^9 Ohms
Input Noise	0.2 μV	0.2 μV
Full Scale Output	6 Volts	6 Volts

Table 4.2 AMP-6 specifications [Vatell (2001)]

Calibration of the heat flux sensors was required to ensure accurate results. At lower temperatures (0°C to 250°C) the relationship between temperature (T) and resistance (R) was linear, although, the characteristic up to the maximum operating temperature (700°C) was best described by a cubic polynomial with coefficients a, b, c, and d (equation 4.2). These coefficients were evaluated by Vatell.

$$T = a R^3 + b R^2 + c R + d \qquad \ldots(4.2)$$

Where:

T (°C) – temperature of the RTS

R (Ω) – resistance of the RTS

a, b, c, d – coefficients of the cubic polynomial

Zeroing the heat flux and temperature output voltages of the AMP-6 unit was required at the start of each session when the sensor was not exposed to any change in heat flux. This implied that the heat flux sensors had to be zeroed in free air before insertion into the engine, where the room temperature was recorded. This temperature was known as the reference temperature 'T_o'. The linear relationship between temperature and resistance at the low temperature range of 0°C to 250°C was expressed in equation 4.3. Since the reference temperature was always between these limits, equation 4.3 was used to calculate the corresponding reference (offset) resistance R_o.

$$R_o = e\,(T_o) + f \qquad \ldots(4.3)$$

Where:

T_o (°C) – RTS reference (offset) temperature

R_o (Ω) – RTS reference (offset) resistance

e, f – coefficients describing the linear temperature/resistance relationship

Equation 4.2 could be applied to find the actual temperature in terms of the reference resistance plus the change of resistance due to temperature change. The change of resistance can be expressed in terms of the change in output voltage of the amplifier, gain and current. To find the actual temperature, the offset resistance was then added to the output resistance of the sensor. The resistance of the amplifier was expressed by equation 4.4.

$$R = \left(\frac{\Delta V_{RTS}}{I \times G_{RTS}} \right) + R_o \qquad \ldots(4.4)$$

Where:

ΔV_{RTS} (v) – output from amplifier

G_{RTS} – gain for RTS signal

I (A) – current with which the amplifier drives the RTS

The amplified RTS signal was found by substitution of equation 4.4 into 4.2.

$$T_{act} = a \times \left[\left(\frac{\Delta V_{RTS}}{I \times G_{RTS}} \right) + R_o \right]^3 + \; b \times \left[\left(\frac{\Delta V_{RTS}}{I \times G_{RTS}} \right) + R_o \right]^2 + \; c \times \left[\left(\frac{\Delta V_{RTS}}{I \times G_{RTS}} \right) + R_o \right] + d \qquad \ldots(4.5)$$

Since the actual temperature was now known, the heat flux could be calculated.

$$q = \frac{\left(\frac{V_{HFS}}{G_{HFS}} \right)}{g \times T_{act} + h} \qquad \ldots(4.6)$$

Where:

q (W/cm^2)	– heat flux
T_{act} (°C)	– sensor temperature from RTS signal (measured simultaneously)
V_{HFS} (v)	– amplified voltage signal received from HFS
G_{HFS}	– gain for HFS signal
g, h	– coefficients for linear relationship between sensitivity and temperature

It should be noted in the above that the polarity of the heat flux sensor voltage indicates the direction of heat flow. Coefficients were also provided by Vatell on the same calibration certificate as the other coefficients mentioned earlier.

4.2.2 Cylinder Pressure Transducer

The cylinder pressure was monitored by a Kistler 6001 pressure transducer with a pressure range of 0 to 250 bar and a temperature range of -200 to 350°C. The pressure transducer was connected to a specially modified spark plug via a thin steel tube. This could cause some changes to the dynamic pressure reading, but this was not considered a problem because the readings were not intended to be used for detailed mean effective pressure or burn rate calculations. The output of the sensor was amplified by a Kistler 566 charge amplifier and the resulting voltage was logged throughout the engine cycle by LabVIEW.

4.2.3 Inlet Manifold Pressure Transducer

A Druck PMP 4010 1.5 bar absolute pressure transducer was used to measure the pressure in either the inlet manifold or inlet port. The pressure reading was logged by LabVIEW throughout the engine cycle.

4.2.4 Shaft Encoder

In order to provide a triggering system for the LabVIEW logging software, a shaft encoder (Hohner W4C10R) was mounted on the Lister engine accessory drive shaft. This shaft rotated at camshaft speed and provided 720 5V TTL pulses per revolution or one every degree of crank rotation. The shaft encoder also provided one large pulse per cycle, which was referenced to TDC of the exhaust stroke.

4.2.5 Hot Wire Anemometer

The same hot wire anemometer was used to measure the air flow into the engine as used in the motored rig work. This data was not logged, but provided an accurate means of ensuring that the correct mass flow rate of air entered the engine.

4.2.6 Universal Exhaust Gas Oxygen Sensor

This sensor was used to ensure that the engine operated at the correct air fuel ratio, and was controlled by an AFM1000 air-fuel ratio combustion monitoring unit as produced by Engine Control and Monitoring. The UEGO sensor was inserted into the exhaust pipe of the engine approximately 300 mm from the exhaust valves. This data was not logged, but allowed the correct throttle and load conditions to be set before logging began.

4.3 MODIFICATION OF STANDARD ENGINE COMPONENTS

4.3.1 Cylinder Heads

The previous porous liner work compared the production level AJ26 cylinder head with a prototype AJ33 AP head. The heat flux sensor (HFS) work in the remaining chapters concentrated on the newer AJ33 CP cylinder head, which was expected to become the main production variant. However, tests were also performed using the same AJ33 AP cylinder head type from the porous liner work to provide continuity.

Although standard cylinder heads were used, they had to be extensively modified before they could be used in this work. The first step was to generate more access for the belts and pulleys that would power the camshafts, as shown in Figure 4.6. This was achieved by completely removing the casting flanges at the end of the cylinder head that once formed the chain and sprocket housings. The numerous unwanted entrances to oil galleries were blocked by threaded taper plugs.

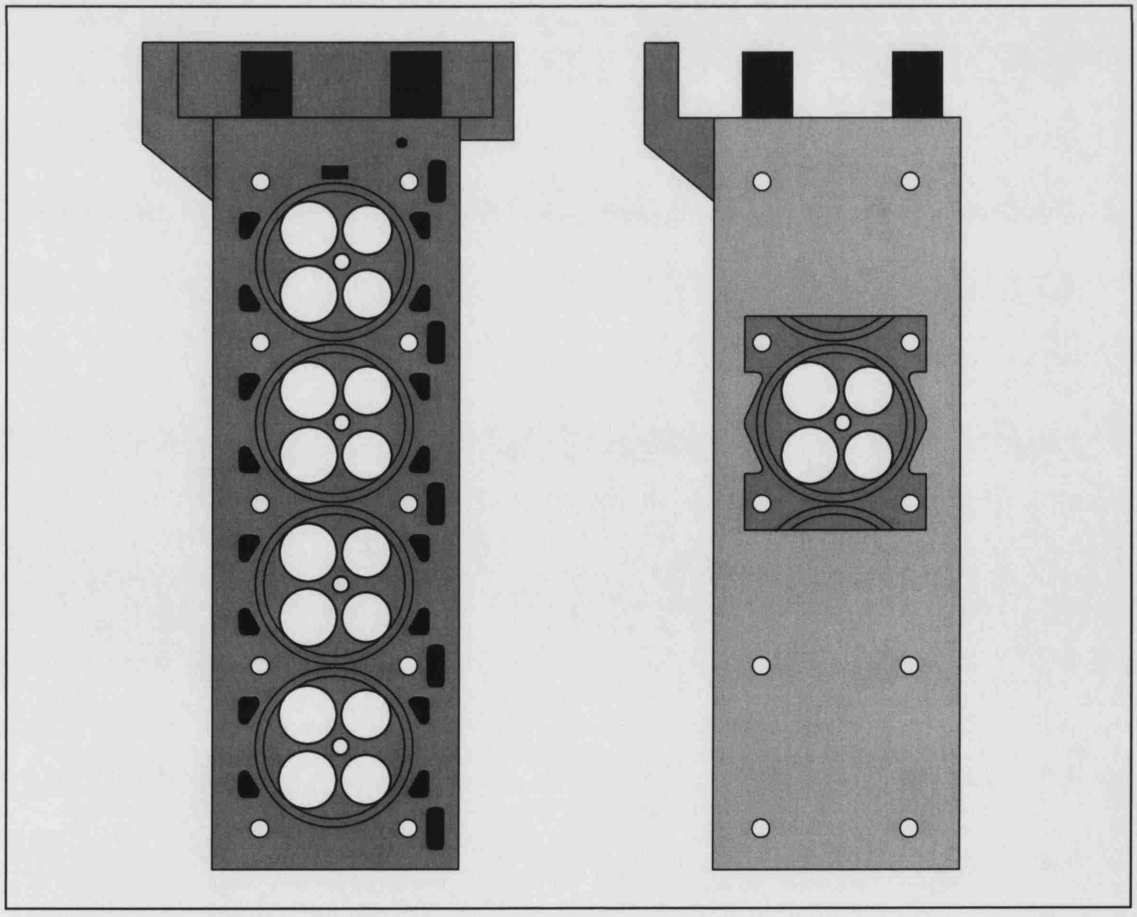

Figure 4.6 Underside of standard (left) and modified (right) cylinder heads

The most difficult modification to achieve was blocking the lower water passages that would have led to the standard cylinder block below. These holes were large, numerous and quite irregular in size and shape preventing conventional taper plugs and sealing putty from being used. The blocking was achieved by completely milling away the lower 6 mm of the cylinder head, except for a complex rectangular section located immediately around the four cylinder head bolt holes of the tested cylinder. A 5mm thick aluminium plate the same length and width as the cylinder head containing a matching complex rectangular hole for location of the protruding cylinder head section was then positioned onto the newly milled surface and permanently connected by careful application of sealant. Additionally, all of the valves and associated hardware from the 3 unused cylinders was removed and great care was taken to remove any swarf generated from the machining.

4.3.2 Inlet Manifolds and Throttle

Since the flow of air through the other seven pairs of inlet valves was absent and the volume of the inlet runner was small during operation of the single cylinder engine, the pressure recovery within the inlet manifold during the closed valve period would be much greater than normal. To limit this recovery noting also that the engine was to be operated at only 1500 rpm, the volume between inlet valves and throttle was massively increased and a smaller and more controllable throttle was used. The use of a larger inlet plenum would also help damp the rapid pressure drop experienced when the inlet valves opened. This larger plenum was fabricated from a steel tube of bore 290 mm and length 610 mm, with a 13 mm thick steel plate sealing each end. This provided a volume of 0.04 m^3, which was about 4 times that of the production V8 plenum. The plenum was mounted on its end since this provided a convenient flat surface for mounting the throttle, pressure gauge and 50 mm diameter spigot for the pipe that fed the air to the engine. This vertical arrangement also reduced the length of the 50 mm diameter pipe between plenum and port which improved airflow characteristics and saved space.

Both of the standard inlet manifolds were extensively modified, effectively leaving only a short 100 mm approach section upstream of the injector mounting location, into which was placed the pressure transducer. Great care was also taken in the manufacture of the

adapter connecting the round 50 mm diameter pipe from the large plenum to the arch-shaped approach section of the standard inlet manifolds in order to ensure smooth flow transition near to the injector.

Figure 4.7 shows a comparison between port and plenum pressures at an engine speed of 1200 rpm. A valve lift profile has been inserted at the correct location for comparison. The use of the large plenum is seen to be successful since the pressure recovery during the closed inlet valve period is limited and the pressure fluctuations are small. This is desired as the flow through the hot wire anemometer 300 mm upstream of the throttle will be more constant, providing a more reliable reading for the airflow into the engine.

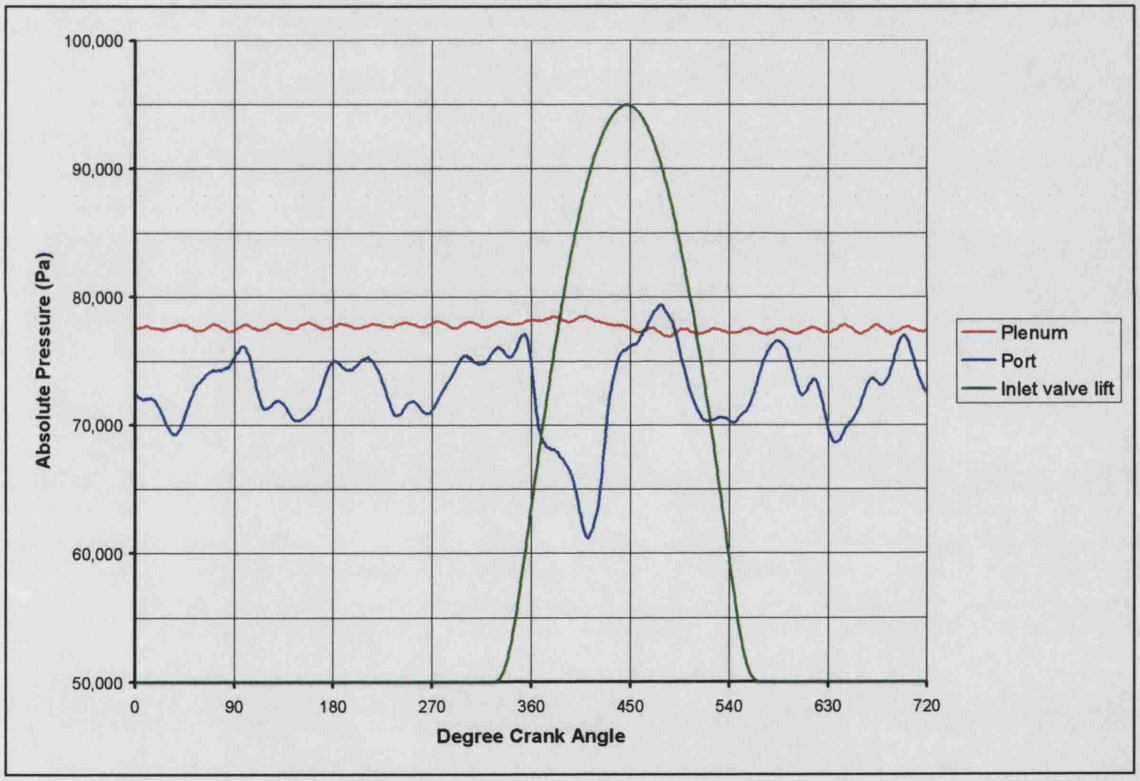

Figure 4.7 Plenum and port pressures

The average pressure recorded in the plenum is higher than that recorded in the port as expected due to the pressure drop experienced between the two sensor locations along the 50 mm bore inlet pipe. The pressure recorded in the port was used to calculate the flow through the inlet valves rather than that recorded in the more distant plenum as this gave much more realistic values.

4.4 ENGINE DESIGN

4.4.1 Design Strategy

The main influence in the design of the cylinder block and piston for this engine was how to pass the signal from the heat flux sensors in the moving piston to an external data logger. The two possible options were to either use a special wire-carrying mechanism or use an Infra-Red or radio-wave based transmitter and receiver system. The wire-carrying method was the preferred option, mainly because such mechanisms have been widely used before by researchers for other applications. Additionally, Ioannou (2000) found the extension wires used with the heat flux sensors to be robust and relatively impervious to electrical noise, where the sensors were used in what was a very electrically noisy environment.

This implied the wire mechanism was already feasible, while the transmitter method could potentially introduce unforeseen noise or durability problems that would not be a concern in the wire mechanism. Furthermore, the piston and block would require an open-side for in-situ access to change the piston sensors, so there was an aperture available out of which the cables could pass. Both methods would require a mounting device and small support clips for the smaller sensor wires within the piston and external mounting points for either the receiver or other end of the mechanism. Due to the above reasons the wire-carrying method was decided to be the superior option for this work. The next decision to be made was which type of wire-carrying mechanism should be used to carry the sensor wires from the piston-based sensors to the data logger. There were two options.

1. Develop a grasshopper mechanism based on existing designs as shown in Chapter 1.
2. Develop a new design based on an elongated piston, as found in an optical engine.

The second option was chosen due to three main reasons:

1. Problems with the conventional Grasshopper linkage

There was only a very limited space within the Lister Diesel crankcase in which to locate a grasshopper mechanism. This option would also have required extensive machining of

the Lister crankcase for the grasshopper connection to be possible. The linkages of the grasshopper mechanism would also have to go through comparatively large angles to fit within the Lister unit, greatly accelerating sensor wire fatigue. The angle between the grasshopper arms could have changed by as much as 150°, whereas the equivalent angle in the side-arm mechanism was only 12°. The side-arm mechanism could also be removed much more rapidly than the grasshopper linkage for tests that did not require piston crown sensors.

2. Advantages of the long piston

The larger piston immediately provided the longitudinal space required for the heat flux sensors and their removal by hand. Since it was desired that only cheap extension wires and not the fragile 100 mm integral sensor wires were to be passed over the flexing mechanism, the long piston would also provide adequate housing for the lengthy 'Lemo' electrical connectors between the two wire types. These connectors could then be easily fastened to the piston to prevent any wire movement and damage during piston motion.

3. Time savings in sensor relocation

For access to the sensors with the grasshopper method, the cylinder head and cylinder block would have to be removed in order to gain access to the underside of the piston. The associated engine rebuild and re-timing processes would then waste vast amounts of time and since the grasshopper method would require the cylinder head timing belts to be repositioned every rebuild, inconsistency of results would occur, which would not be the case for the side-arm mechanism. Since the side-arm mechanism had only a minimal number of components (Figure 4.8), it could be removed from the piston quickly and easily allowing access to the inside of the piston for sensor cleaning and relocation. This was achieved by releasing the two wire clips and simply removing four securing screws, avoiding the need to dismantle the mechanism. Once the mechanism type was decided upon, the piston, cylinder block and mechanism were designed in parallel.

4.4.2 Piston

It was decided that the piston should be made of high strength aluminium alloy 7075t651, which had a tensile strength of 580 MPa. The high strength of this alloy permitted thinner sections to be used throughout the piston than would have been

possible with other alloys, in order to help save weight. The expansion of the piston due to the high temperatures of combustion was an important part of the design, since failure to consider this expansion would result in the piston seizing within the cylinder block. Given the 85.5 mm diameter of the top of the piston and that the thermal expansion coefficient of aluminium is 23×10^{-6}/°C, a 200°C increase in piston crown temperature would increase the diameter of the piston crown by 0.4 mm.

It was decided at an early stage that this engine design should accommodate only two piston sensors at any given time due to weight considerations and the limited available space for the sensor wires, clips and mechanism within the piston. The ability to readily access these sensors was also an important design requirement.

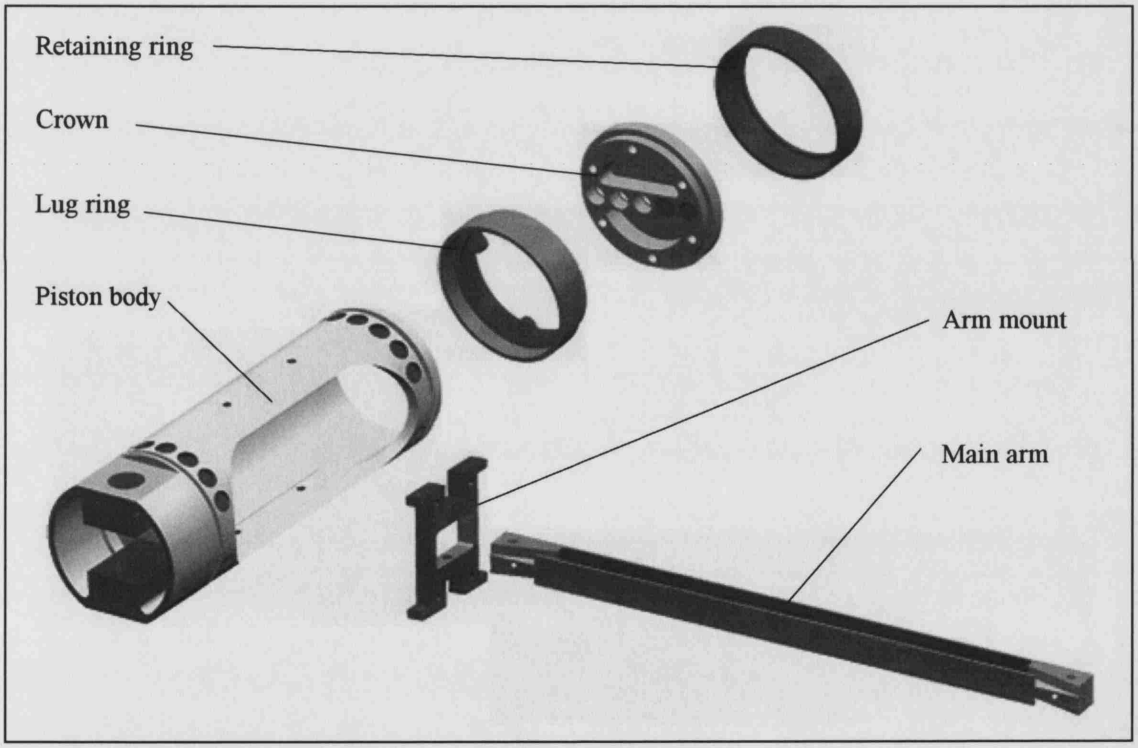

Figure 4.8 Piston body, lug ring, crown and mechanism mount with main arm

Piston Mass and Effect on Engine Dynamic Loadings

The cumulative mass of the piston and its contents was important in this design, with the vibrational analysis in Appendix III ensuring acceptable loading on the Lister bottom-end. Even though the mass of the piston and internal components was slightly greater than the mass of the Lister piston, the resultant force on the crank bearings at 1500 rpm were found to be about one third those of the Lister operating at its maximum speed of

3000 rpm. Despite the size of these loadings being acceptable, vibration was still a concern, since the Lister bottom-end would be mounted at 45° to match the half v-angle of the donor engine and the piston and block would be relatively long. So, as a form of safety in continuity, it was desired from the outset of this design work that the combined mass of the piston, mechanism and sensors should be no greater than the piston successfully used by Ioannou (2000).

Rotatable Piston Crown

The restriction of being able to use only two sensors in the piston simultaneously and the desire to study the entire piston surface soon gave rise to the idea of a rotatable piston crown that possessed only three available sensor locations (Figure 4.9). It was decided that the rotatable piston crown should contain 3 sensor locations, with one location at the centre of the crown and the other two in alignment on one side at distances of 14 and 28 mm from the centre respectively. When a sensor was absent from a sensor location, a blank filled the remaining sensor location. Since the piston crown had three sensor locations and could be rotated to 6 different positions, 13 different sensor locations were possible. The crown had 6 equally spaced tapped holes around its lower surface so it could be fixed to a lug-ring by three screws in the desired position (Figure 4.10).

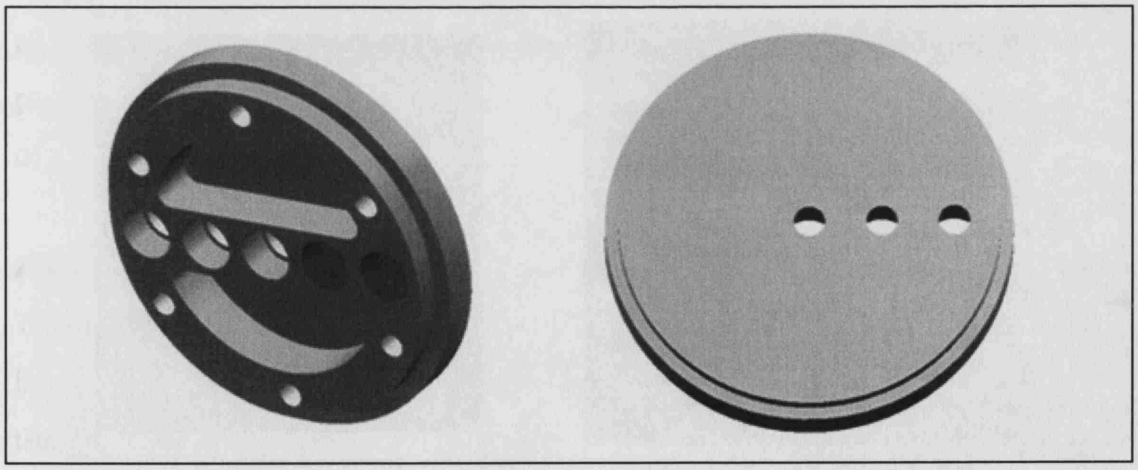

Figure 4.9 Piston crown underside and top views

The lug ring was itself permanently screwed and pinned to the piston body. If the 3 screws were removed, the piston crown could be freely rotated by hand from below due

to the access provided by the extended piston, although the outermost sensor had to be removed to avoid collision with the lugs on the lug-ring.

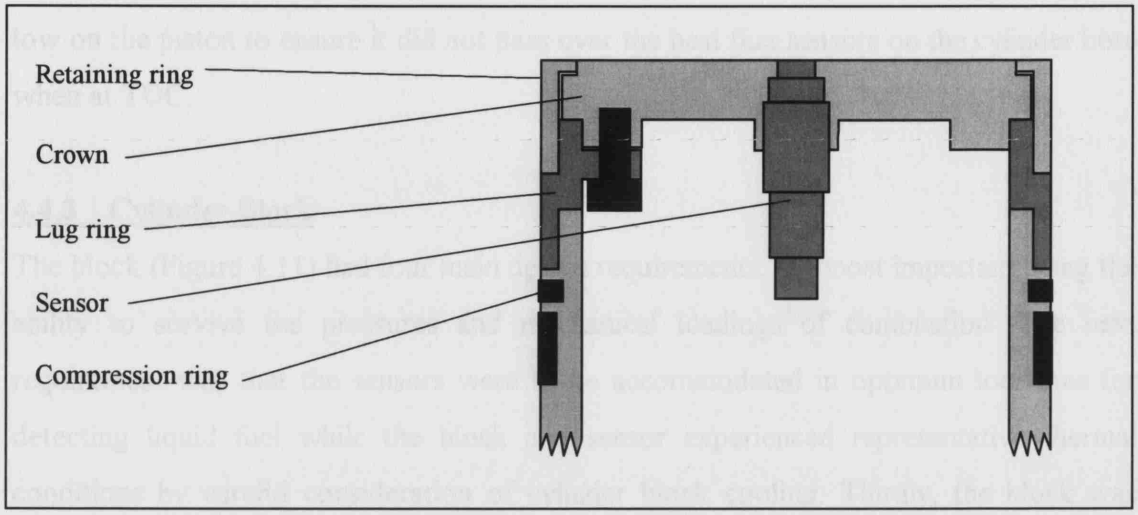

Figure 4.10 Piston lug ring and retaining ring final assembly

Although the engine would be operating at the production half-vee V-angle of 45° to the vertical with the mechanism protruding from the upward side of the cylinder block, relocation of the sensors and rotation of the piston crown would still be almost blind and in a confined space. This required that the piston crown could be rotated with the minimum effort with zero risk of it falling from its seating into the combustion chamber, as retrieval would be extremely difficult given the available access. So, to prevent such problems, a retaining ring was devised that screwed onto the lug ring over the periphery of the piston crown. The retaining ring was then pinned permanently to the lug ring.

Piston Tribology

The bottom end of the piston was very similar to a conventional piston, with oil lubrication and oil scraper rings from the production piston. To avoid the possibility of the heat flux sensors becoming polluted with oil and returning meaningless data, dry lubricant pads were used at the top of the piston instead of relying on conventional oil lubrication. The pads had to be robust and possess a low coefficient of friction while operating at the high temperatures experienced at the top of a piston. An ideal solution came in the form of a high performance bearing plastic called PEEK (Poly Ether Ether Ketone). The grade used for the pads and compression ring was PEEK 450FC30. This

was a plastic resin containing 10% carbon fibre, 10% PTFE and 10% graphite, where the carbon fibre provides strength and the PTFE and graphite provides lubrication. The 450 denotes the maximum temperature in degrees C. The lone compression ring was placed low on the piston to ensure it did not pass over the heat flux sensors on the cylinder bore when at TDC.

4.4.3 Cylinder Block

The block (Figure 4.11) had four main design requirements, the most important being the ability to survive the pressures and mechanical loadings of combustion. The next requirement was that the sensors were to be accommodated in optimum locations for detecting liquid fuel while the block and sensor experienced representative thermal conditions by careful consideration of cylinder block cooling. Thirdly, the block was required to have a large hole in one side to allow access to the piston and allow operation and removal of the wire-carrying mechanism. The length of the piston allowed the rectangular access hole in the side of the cylinder block to be a few millimetres wider than the piston and protrude much further back behind the piston into the block. This provided an additional measure to prevent engine oil from passing up the gap between the cylinder block and the piston, which could pollute the sensor faces and result in incorrect heat flux readings. The final requirement of the cylinder block was that it should fit correctly with the cylinder heads under test and the Lister engine base unit.

Sensor Positions on the Cylinder Block

The positions of the sensors on the cylinder block were decided independently of the piston and mechanism designs. The heat flux sensors were restrained in the cylinder block by capture nuts and individually tuned 0.15 mm thick copper washers ensured the flat sensor faces fitted flush to the cylinder bore.

The final sensor positions chosen within the cylinder block were governed by several factors, including the cylinder head bolt positions and cooling channels. The main dictating factor though was the results of the motored rig work, where this initial study highlighted the areas of the cylinder bore that were expected to suffer from wall wetting even in this firing engine. The 12 sensor positions used in this design were arranged to

provide 6 possible locations on both the inlet and exhaust sides of the cylinder block. These groups were then divided into upper and lower levels of 3 positions respectively.

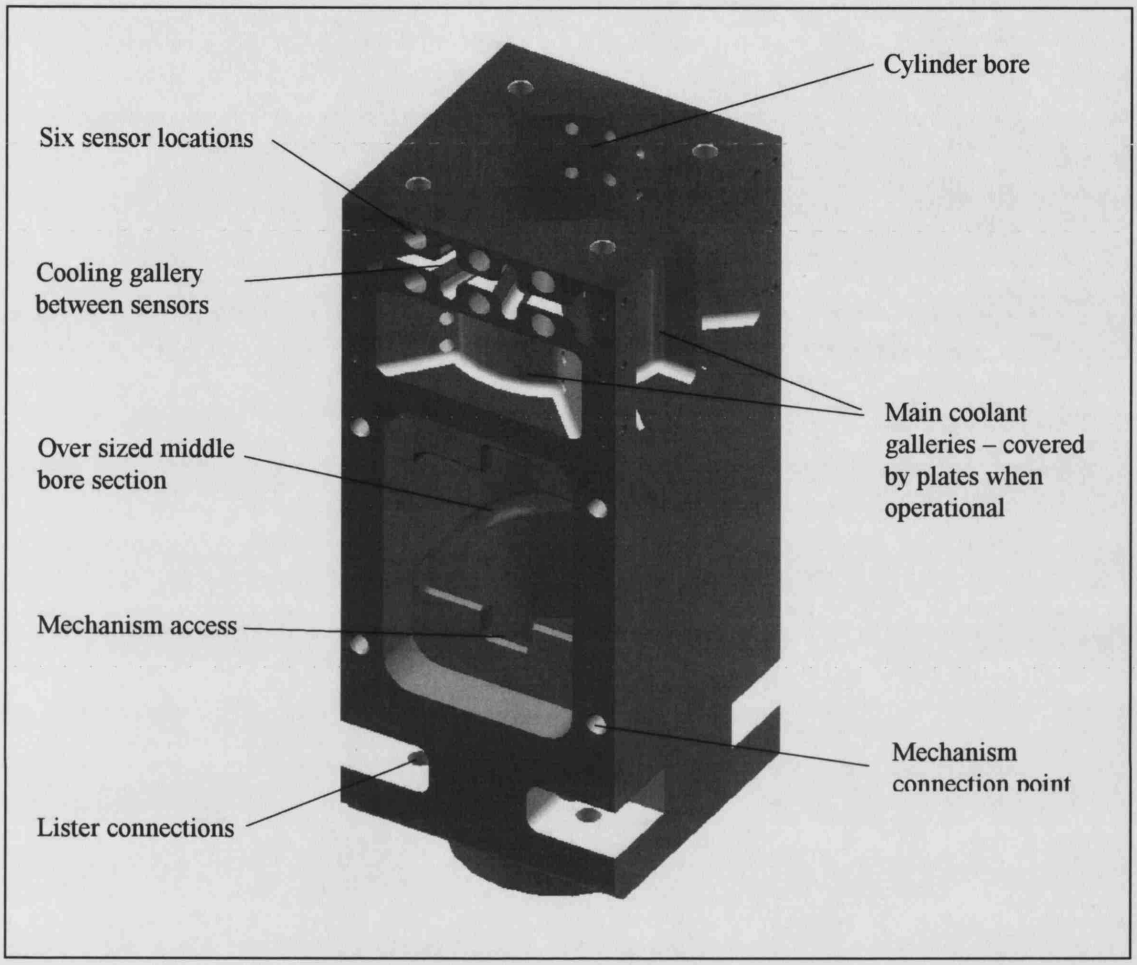

Figure 4.11 Cylinder block

The sensor positions in this design did differ from those used by Ioannou (2000). Firstly, the outer sensor positions were spread further around the bore from 17° to 25° to provide a wider sensing area (Figure 4.12). This used all of the available space between the cylinder head bolts, while still permitting adequate cooling channels around all of the sensor positions. The second difference was the vertical positioning of the sensors at 8mm and 32 mm from the top of the block, rather than 7.5 mm and 27.5 mm as used by Ioannou in order to accommodate an additional horizontal cooling passage between the upper and lower sensor rows. Despite the separation of the sensor positions, the gaps between the sensors remained small enough that no fuel droplet cloud larger than about 10 mm in diameter could impact the bore without being detected by a sensor.

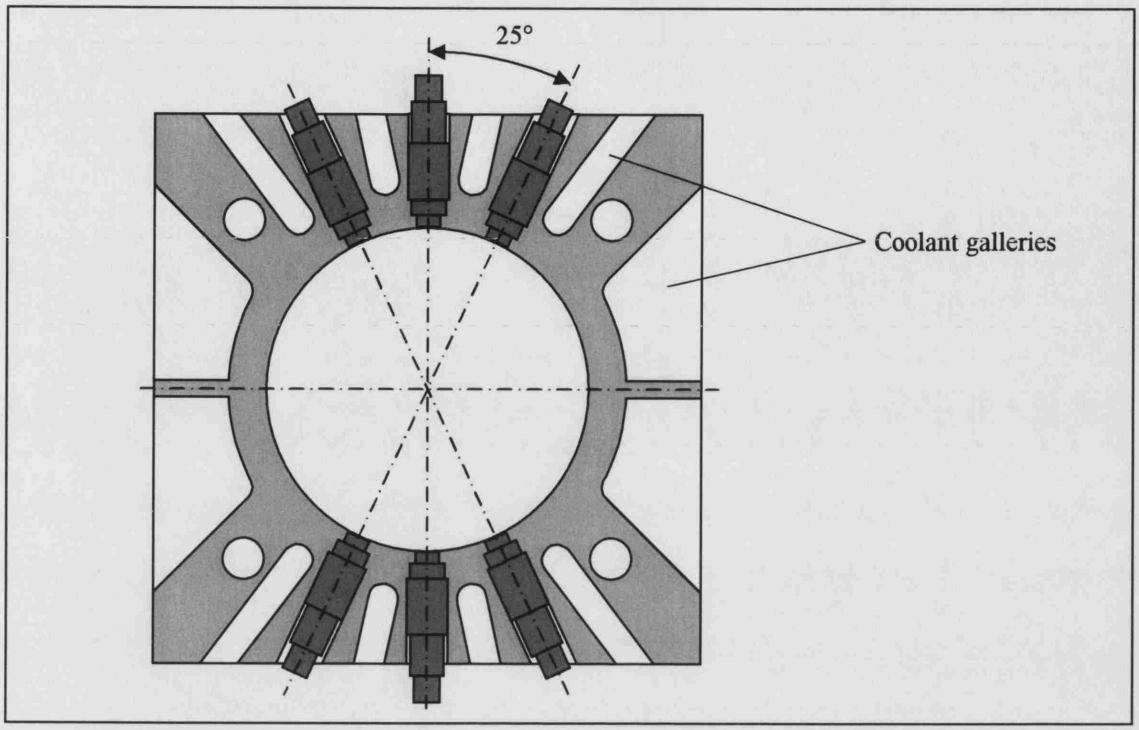

Figure 4.12 Sensor positions in the cylinder block

Cylinder Block Cooling Channels

As with the block used by Ioannou (2000), this cylinder block had a separate cooling passage around either side of the cylinder, implying it required two water supply and outlet spigots on the non-sensor faces of the block. The main advance from the cooling passage design used by Ioannou (2000) was that the new sensor locations in this work permitted an additional cooling passage between the upper and lower rows of sensors on either side of the block. This new central passage also had vertical side branches to provide additional cooling between the upper and lower sensors. The provision of air bleed holes in the covering plates also permitted any trapped air to be vented when the coolant was added, reducing the risk of air pockets forming within the cooling passages. The block cooling water was supplied by a recirculating system as described in section 4.5.1

4.4.4 Wire Carrying Mechanism

It was already established that the mechanism should be in the form of a long arm that extended from one side of the piston through the cylinder block to a shorter external linkage that was attached to a fixed base at the other end. The smaller linkage

accommodated the small lateral movement generated by external end of the long arm as it oscillated. Initially it was believed that a simple aluminium tube could act as the perfect long arm, but it was decided a more dedicated solution was required because there would be problems with the wires moving within the tube and it would be difficult to introduce proper bearings and wire-grips.

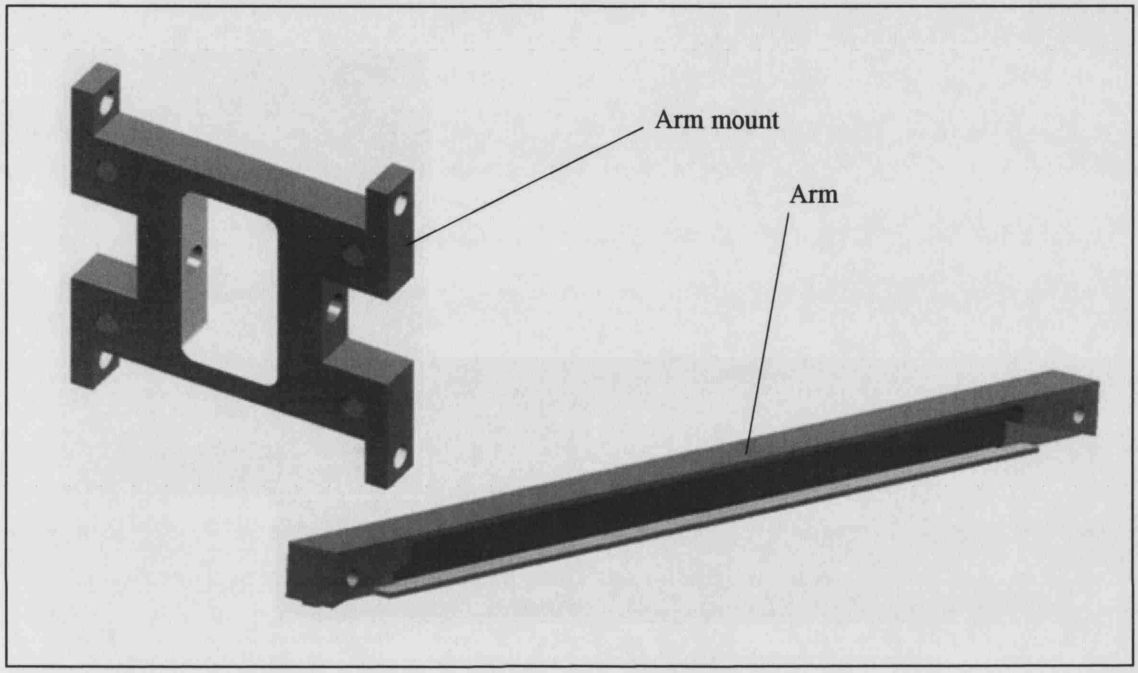

Figure 4.13 Piston arm mount and main arm

The main arm was effectively an I-beam machined from a square section bar of high strength 7075t651 aluminium alloy for optimum weight and strength characteristics, where the recesses on the sides formed ideal wire location sites (Figure 4.13). The arm remained square section at the ends to allow for insertion of phosphor bronze bushes to permit smooth action and prohibit damage to the aluminium linkages. All of the joints in the mechanism had such phosphor bronze bushes. Even though a longer main arm would reduce the angle through which the wires were bent, space limitations and the excessive lateral deflection of the arm due to its own inertial loading limited the arm to a length of 400 mm. The thicker square sections at the ends of the main arm also had tappings for wire grips to ensure the correct length of wire was used in the loops to achieve the optimum bend radii for a long life. The design considered that only the relatively cheap extension wire and not the short and fragile wire of the expensive sensor would be passed through the flexing mechanism.

Arm Mount and Wire Clips

The arm mount within the piston had to be strong enough to support the dynamic loading from the long arm, while being light, easy to remove and of a shape that did not affect the moving loop of extension wire (Figure 4.14).

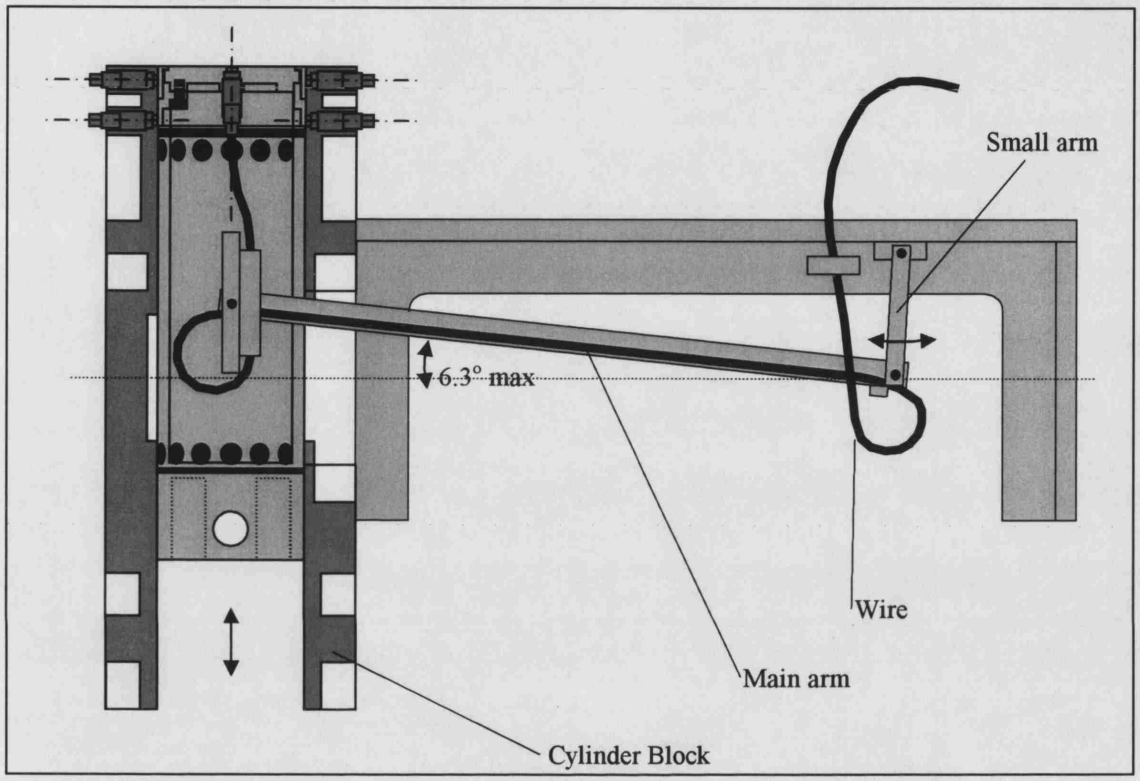

Figure 4.14 Mechanism positioned in the piston while at TDC

The final arm mount was also made from aluminium alloy 7075t651 and was secured into the piston by 4 screws. Wire clips were needed to ensure that the Lemo connectors that connected the fragile sensor wire to the extension wire remained connected during the violent accelerations of the piston. These simple clips also acted as wire grips that secured the loop of sensor extension wire as it passed from the piston to the wire grips of the main arm. Two screws fixed each of the two wire clips onto the arm mount.

Mechanism support and Safety cage

Either side of the large access hole in the side of the cylinder block were two M8 tapped holes that allowed the large mechanism support and safety cage unit to be attached. This unit consisted of two 'C' sections, an end plate and a top plate (Figure 4.15).

The smaller linkage of the mechanism was mounted onto the top plate via a small block. The top plate had two holes for the heat flux wires to pass through, while the two 'C' sections housed the stationary wire grips for the heat flux wires. This 'C' design readily allowed unrestricted upward insertion of hand, forearm and tools into the under piston cavity when the mechanism was not in use.

Figure 4.15 Mechanism support and arm (safety cover removed).

The open nature of the unit also made it easy to access the screws when fixing the mechanism into the piston. The components of the unit were made from ½" thick aluminium plate for ease of construction and rigidity to avoid vibration caused by the mechanism. The final safety cover was 'U' section made from steel sheet that completely covered the mechanism and joined the tips of the 'C', further ensuring rigidity.

4.5 ENGINE ANCILLARY SYSTEMS

4.5.1 Water System

Water could be heated up to 100°C by a thermostatically controlled water column before being pumped to the cylinder block from where it returned to the column. Since the engine could increase the temperature of the water, a water mains-cooled heat exchanger helped maintain the desired temperature. The water temperatures used in the tests were 60°C or mains water temperature of approximately 20°C, depending upon the test in question. A range of head and block cooling and heating combinations were achieved as shown in Figure 4.16.

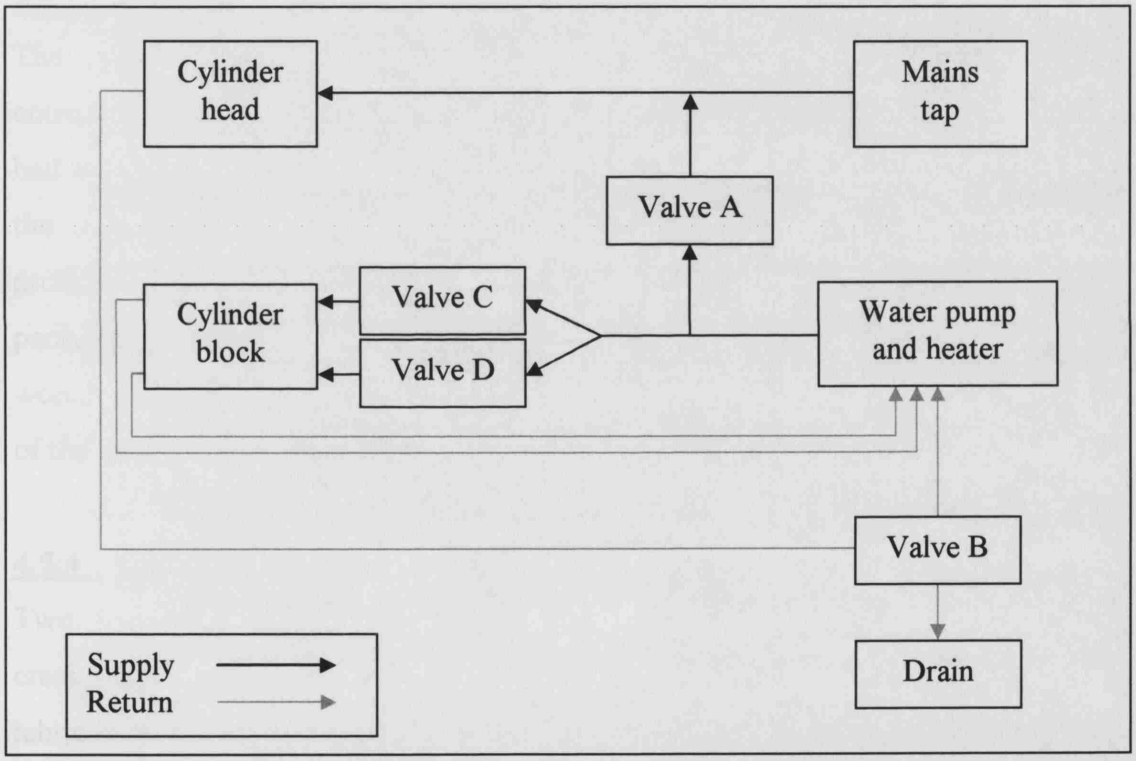

Figure 4.16 Engine water system

The cylinder head and cylinder block temperatures could both be set at 60°C (or 20°C if the heater was turned off). Most tests used a head temperature of 20°C and a block temperature of 60°C to ensure minimal fuel evaporation in the port and strong heat flux signal when the fuel evaporated from the hotter bore surface. This meant that the water mains acted as a 20°C water supply and had to run water to waste, as controlled by the mains tap, valve A and three-way valve B. Valves C and D simply ensured a balanced

flow around the inlet and exhaust side of the cylinder block. Engine cooling water temperatures and atmospheric air temperature were monitored using K-type thermocouples and displayed on a Comark display unit.

4.5.2 Fuel System

The fuel system used on this engine was the same as that used in the single-ended injector configuration used in the porous liner work and is shown in Figure 2.12. The same LabVIEW program and camshaft mounted cutter disk controlled the Denso 12 hole injector, which was set to operate with the standard 3.8 bar pressure drop across it.

4.5.3 Ignition system

The system used was a Luminition opto-electronic ignition system, which was a commercially available form of replacement ignition system for automobiles. The system had a fixed optical switch that was used in combination with a cutter disk mounted on the camshaft of the engine. A small 60° slot in the disk allowed the optical switch to produce an uninterrupted infra-red beam for a short time once per engine cycle, permitting the ignition coil to charge. When the disk again interrupted the beam, the coil would discharge to the spark plug. Spark timing was readily adjusted by slight rotation of the cutter disk relative to the camshaft.

4.5.4 Lubrication System

Two separate systems were employed for crankshaft and camshaft lubrication. The crankshaft and lower end of the piston were lubricated by a combination of splash lubrication from the wet sump and the standard Lister oil pump mounted within the bottom-end. In order to lubricate the camshaft bearings, an external oil pump powered by the Lister bottom-end pumped oil from a reservoir into the conventional oil galleries of the production cylinder head. The excess oil in the cylinder head was then free to drain back to the reservoir via conventional oil drain tubes in the cylinder head.

4.5.5 Drive Systems and Dynamometer

The Lister bottom end was mounted at 45° to provide the same cylinder vee-angle as used in the Jaguar engine. The crankshaft of the Lister bottom-end was directly

connected to an AC motoring and absorbing dynamometer unit (Laurence Scott and Electromotors Ltd., model NS 1962, serial # 261601). The torque loads experienced by the dynamometer were measured using a load cell (Maywood, series U-4000) that had been calibrated accordingly (Figure 4.17).

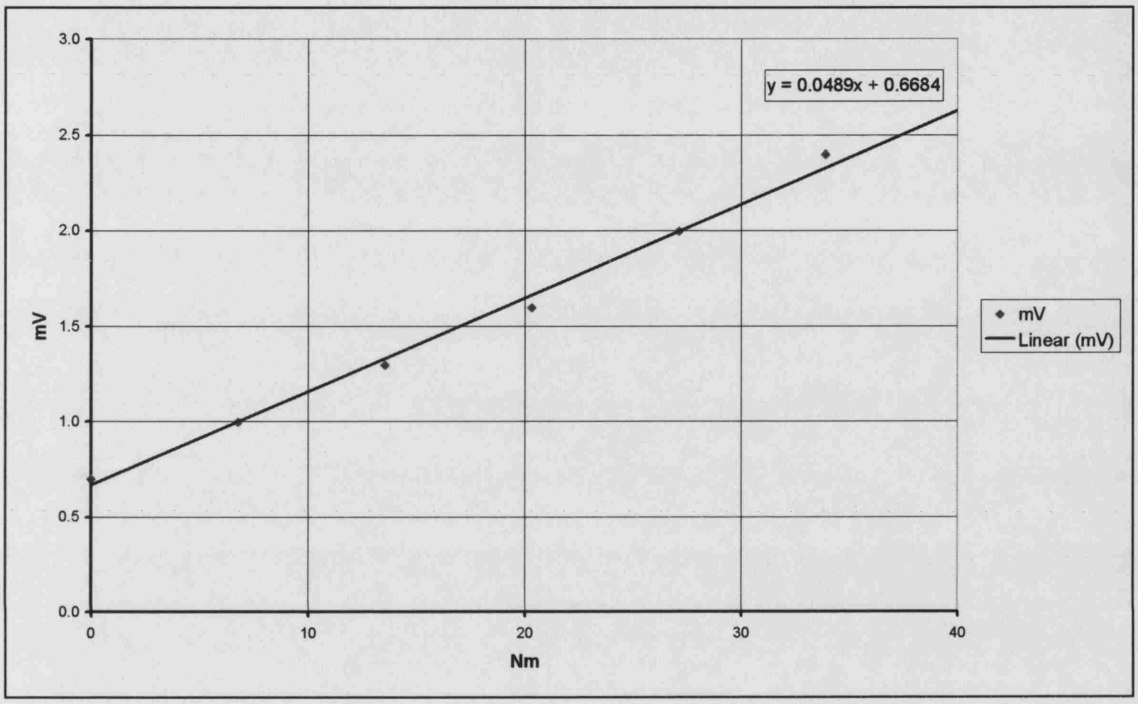

Figure 4.17 Calibration of load cell

4.6 CAMSHAFT TIMING MECHANISM

Camshaft timing would affect both engine performance and results. Both of the camshafts had an off-centre slot at the free end which would allow for the insertion of a special timing tool, but no accurate means of adjusting their rotational position was available. To overcome this problem, a special steel plate that could be fastened to available tapped holes on the cylinder head was devised (Figure 4.18). This plate possessed two 180° protractors for accurate positioning and two slots for locking the timing arms for when belt and taper-lock pulley tightening was performed. To prevent the timing arms from clashing, the camshaft's slot angle, valve incline and possible valve timings were considered in their design.

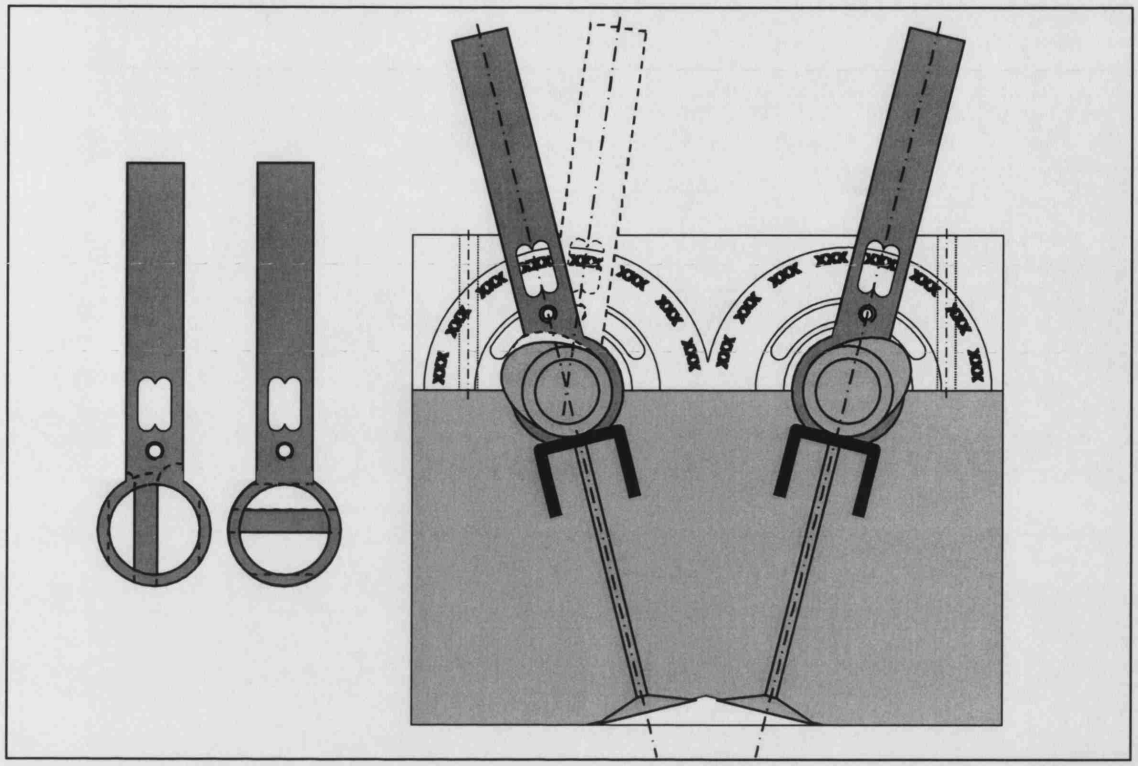

Figure 4.18 Camshaft timing arms and plate mounted on the cylinder head

The actual valve timings that were employed on the firing single-cylinder engine are shown in Table 4.3 below. The fully advanced and fully retarded inlet valve timings used for the CP cylinder head replicated what was possible with the VCT of the donor engine, while the inlet valve timing was fixed in this work when using the AP head.

		Lift duration (°CA)	Valve opens (°CA)	Maximum Opening Point (°CA)	Valve closes (°CA)
AJ33 AP	Exhaust valve	220	150	260	370
	Inlet valve	230	327	442	557
AJ33 CP	Exhaust valve	230	140	255	370
	Inlet valve (advanced)	240	327	447	567
	Inlet valve (retarded)	240	375	495	615

Table 4.3 Valve timings used on the single cylinder engine. Note zero degrees represents TDC of the firing stroke

CHAPTER 5

ENGINE DATA LOGGING AND ANALYSIS SOFTWARE

5.1 INTRODUCTION

In order to analyse the data from the heat flux sensors, the data initially had to be logged by a combination of specialist hardware connected to the engine and software stored on a personal computer. The logged data was then analysed and presented in an appropriate way that assisted in the understanding of this complex phenomenon. For this work, National Instruments LabVIEW (Laboratory Virtual Instrument Engineering Workbench) was the perfect tool for logging the information, while Microsoft Excel was ideal for the analysis and graphical presentation of the results. This chapter describes the hardware and software used for this task. The first part of the chapter will discuss the data logging arrangements. Then the required analysis will be discussed and the implementation of these analyses presented.

5.2 DATA LOGGING WITH LABVIEW

5.2.1 Introduction

LabVIEW is a graphical programming language that permits data acquisition, analysis and control via both analogue and digital inputs and outputs. Programs are not textual, but presented in the form of icon blocks connected by 'wires', the type of which depends on what type of data flows along them. A basic program is called a VI (Virtual Instrument) and has a front panel with which the user controls the program and a back panel that contains the program script, which is in the form of icons and connecting wires. If a more complex program is written, VI's can be connected on the back panel to become sub-VI's in a similar way to subroutines in other programming languages.

There are a number of important factors in data logging as summarized by Bendat *et al* (2000). A basic consideration is whether the sensors provide an analogue or digital signal and whether the sensors are correctly calibrated. The dynamic range or ratio of the maximum to minimum data value of the acquisition system should also be adequate so as to limit distortion. Background noise such as 50Hz 'mains hum' may interfere with the signal if proper wire shielding and insulation is not provided. A bandpass filter can remove most of these undesired frequencies [Lynn et al (1994)], but only if these

frequencies are sufficiently distinct from the signals being measured and the signal to noise ratio is adequate. The signal to noise ratio describes how large the signal of interest is compared to the background noise. Conversion of data from analogue to digital format is important since the storage and analysis of the data will be performed digitally (Figure 5.1). If the sampling rates are inadequate, aliasing errors occur during the analogue to digital conversion. Theoretically, the sampling rate should be at least twice the frequency of the original signal. It is often much higher than that in practice [Ifeacher *et al* (1995)]. If the signal had contained significant energy at frequencies larger than half the sampling frequency, an anti-alias filter would have been required.

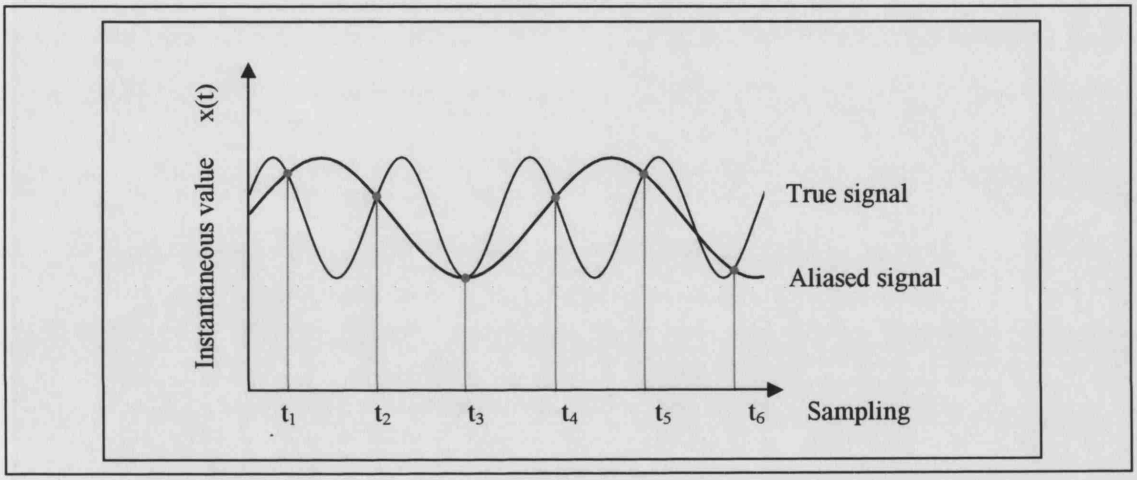

Figure 5.1 Frequency aliasing due to inadequate sampling rate [reproduced from Bendat *et al* (2000)]

5.2.2 LabVIEW Hardware

To connect the various sensors to the PC, a National Instruments interface board PCI-MIO-16E-4 was used [National Instruments (2002)]. Full use was made of all 16 available input channels on the LabVIEW board. Since 6 heat flux sensors were available and it was known that the sensors had a finite service life before they needed refurbishment and recalibration, a rotation was devised where 3 sensors would be used while 3 were held in reserve or being repaired. An AMP-6 amplifier unit was used with each sensor and had BNC outputs for both heat flux and temperature. This implied 6 differential channels were needed for the heat flux sensors and a further 2 channels for the inlet manifold pressure and cylinder pressure, which were treated as single-ended inputs.

5.2.3 LabVIEW Software

The logging software used in this work was National Instruments LabVIEW 6.1 (2002). The LabVIEW program [Evans, Taylor (2002)] was called Main.vi and consisted of several sub-VI's connected together. The front panel in this program actually consisted of 2 separate panels called 'Setup' and 'Display' (Figure 5.2).

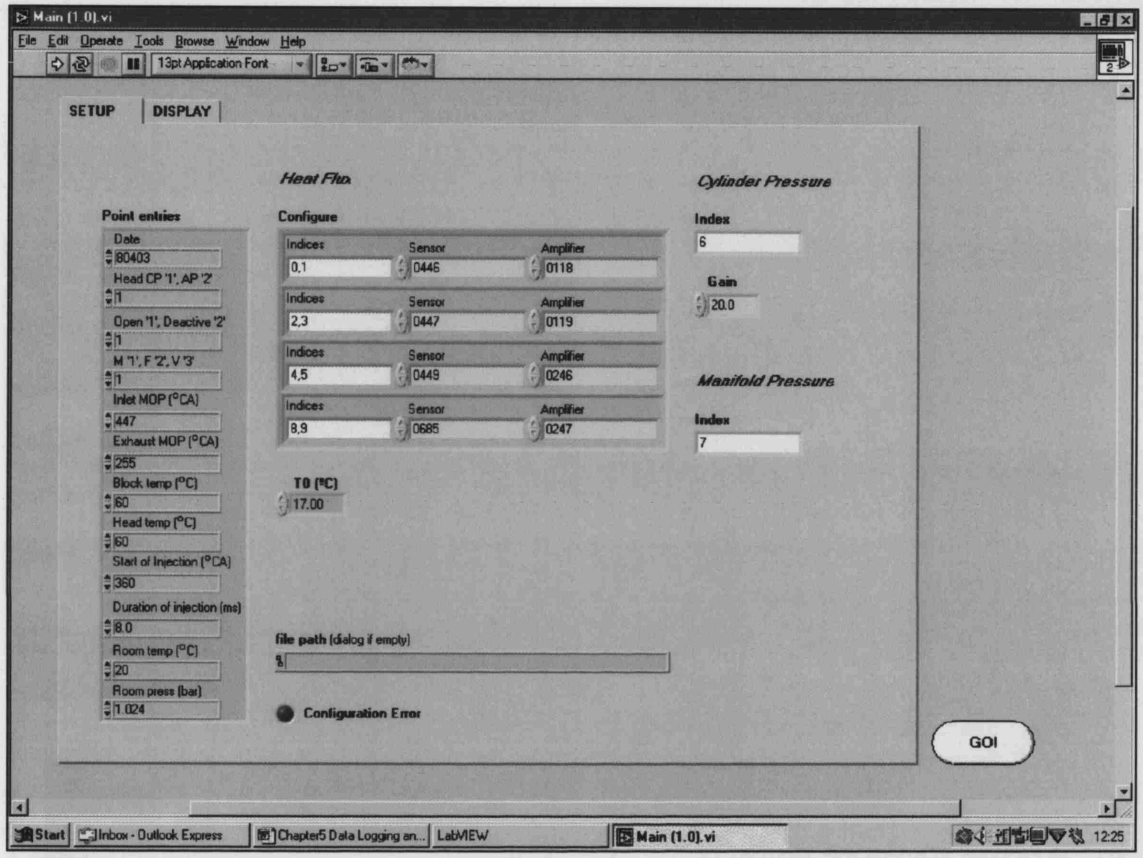

Figure 5.2 Setup front panel in LabVIEW

The main feature of the Setup panel was the Index system. For correct readings to be taken, specific calibration coefficients were required by the PC where each of the 6 heat flux sensors and 4 AMP 6 amplifier units possessed a series of 9 multi-digit calibration coefficients. The Index system conveniently allowed the user to enter into the PC using simple mouse clicks which sensor and amplifier combinations (and hence coefficients) were being used at the time. The gain setting on the cylinder pressure charge amplifier, room temperature and several important experimental point values were also entered here, in order to retain these values with the logged data. The point values on the Setup panel were presented as boxes, each with its own label that asked for either a numerical option of '1' to '3' or actual test values to be entered. The terms 'CP' or 'AP' refer to

the two cylinder heads under investigation, while 'open' and 'deactive' refer to the port deactivation mechanism on cylinder head 'AP'. Terms 'M' and 'F' refer to whether a motoring or firing test was performed. As with all the crank degree values used in this work, zero degrees refers to TDC exhaust. 'MOP' implies the maximum opening point of the inlet or exhaust valves. The start of injection, duration of injection and cylinder block and cylinder head water temperatures were also recorded.

The first step in running the program was to configure the PC memory buffer by clicking on the run icon at the top of the screen with the mouse. When the engine condition had been set and logging was required, the large 'Go' button at the bottom of the Setup panel was selected using the mouse and logging began. Logging was usually complete within 5 seconds, during which time the 'Go' button would instead say 'Going' and turn green. There was then a period of similar duration when any remaining data held in the buffer was stored to file. Upon completion of this, a prompt asked for a suitable file name for the new Excel file. The actual events can be followed by observing the back panel, shown in Figure 5.3.

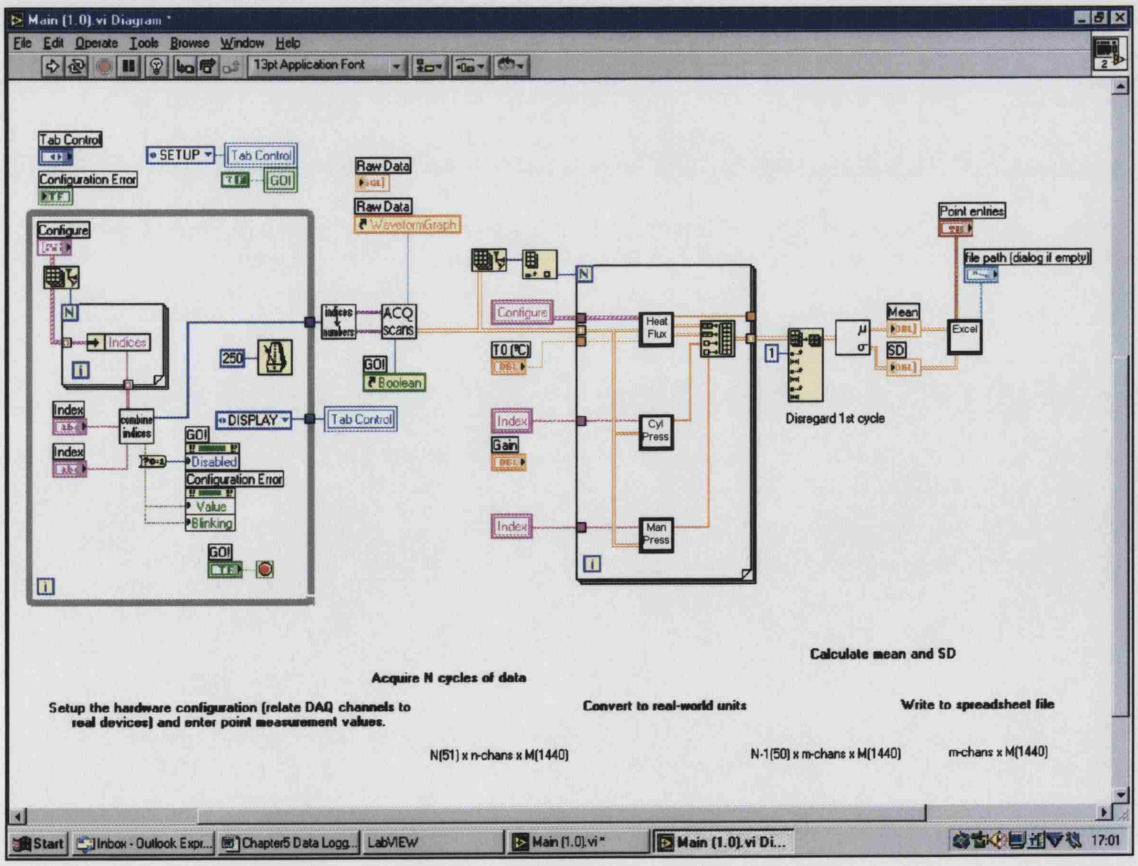

Figure 5.3 Main.vi back panel in LabVIEW

The Indices were brought together in the 'Combine Indices' VI, within the large while loop box on the left and converted into meaningful values in the 'Indices to Channel Numbers' VI just after the loop. The main logging occurred in the 'Acquire Scans' VI, where the data was temporarily stored in the buffer. The next step was to convert the heat flux voltages into actual heat flux values in the 'Heat Flux' VI. These conversions had to be performed in the LabVIEW program since this is where the relevant coefficients were held. The cylinder pressure and manifold pressure were not converted here since this operation could be preformed later in Excel, where further manipulation of the data by the user was allowed.

The mean and standard deviation of the different heat fluxes and pressures were calculated in the 'Mean and Standard Deviation' VI using the logged data temporarily stored in the PC memory buffer. In order to calculate the mean or standard deviation of any of these values, the software would start by using the first data value (which represented the first crank angle) from each of the stored cycles. This process would then be repeated with the next data value (which represented the second crank angle) from each engine cycle until all of the 720 data points for the cycles were used. Using this method implied that logging more cycles would generate a larger population from which the statistical values could be calculated. The averaged cycle and respective standard deviation values were stored in the new data file and the respective raw data for the logged engine cycles was discarded. The standard deviation was important as it indicated the repeatability of the test results, where a lower standard deviation implied a more consistent reading from cycle to cycle. Standard deviation can be calculated as follows:

$$SD = \sqrt{\frac{\sum\left(x_i - \bar{x}\right)^2}{n-1}} \qquad \ldots(5.1)$$

In equation 5.1 x_i is the value of the measured parameter at a particular crank angle cycle 'i' and $\bar{x}$ is the mean value of the measured parameter at a particular crank angle for the number of cycles n. The results were written to file in the 'Save to Spreadsheet File' VI.

When the data logging was complete, a display panel automatically appeared and gave a basic preview of the logged data. This was especially useful when the program was under construction, since the logged voltages were shown before conversion into the appropriate units.

The format in which the data was saved in the Excel data file was important because the Excel analysis program needed to know the specific cell locations of the various logged items. The data files were saved in a format where single point values such as the date were stored in rows across the top of the data file, while the continuous data such as heat flux and cylinder pressure were stored in the columns below. A typical data file is shown in Figure 5.4, where the single point values at the top of the spreadsheet are the same as those entered on the 'setup' front panel of the LabVIEW. The columns of data below are seen to be the continuously logged values of heat flux and pressure and the respective standard deviations.

	A	B	C	D	E	F	G	H	I	J	K	L	M	N	O	P	Q	R	S	T	U
1	Date	Head CP	Open T. D	M 'T, F 'Z,	Inlet MOP	Exhaust N	Block tem	Head tem	Start of In	Duration c	Room tem	Room pressure [bar]									
2	280303	1	1	1	447	255	60	60	360	8	20	1.024									
3	Eff. Heat f	EIC Heat	EIR Heat f	Heat flux [	EIL Temp	EIC Temp	EIR Temp	Temperat	Cylinder P	Manifold	SD Heat f	SD Heat fl	SD Heat fl	SD Heat fl	SD Temp	SD Temp	SD Temp	SD Temp	SD Cylind	SD Manifold	Pressur
4	22.48008	16.44855	19.47046	0	68.91899	69.38823	68.47194	17.00029	4.191802	1.916648	1.002246	0.842914	0.983007	0	0.141495	0.12906	0.095549	0	0.015029	0.001827	
5	22.3098	16.24708	18.98416	0	68.87843	69.40415	68.47194	17.00029	4.188672	1.91582	1.050357	0.787594	1.042612	0	0.138945	0.145434	0.095549	0	0.01505	0.00141	
6	22.0993	16.0155	18.68618	0	68.85502	69.43598	68.45774	17.00029	4.174805	1.917188	1.036297	0.817391	0.941821	0	0.143003	0.158979	0.069082	0	0.009294	0.000977	
7	21.76217	15.72592	18.02955	0	68.83161	69.40415	68.47194	17.00029	4.144922	1.921289	1.110564	0.827692	0.923553	0	0.143003	0.145434	0.095549	0	0.009835	0.001619	
8	21.41194	15.41935	17.56073	0	68.91355	69.40415	68.50004	17.00029	4.100781	1.926367	1.157109	0.798252	0.925794	0	0.124276	0.145434	0.129836	0	0.008588	0.00249	
9	20.95789	15.11305	16.96655	0	68.92526	69.38823	68.48594	17.00029	4.041992	1.931445	1.163252	0.799676	0.865906	0	0.116557	0.12906	0.114332	0	0.009995	0.002325	
10	20.44086	14.68317	16.33618	0	68.92526	69.43598	68.48594	17.00029	3.976562	1.936719	1.201564	0.726556	0.926571	0	0.116557	0.158979	0.114332	0	0.010556	0.00249	
11	19.9818	14.30045	15.79609	0	68.91355	69.40415	68.47194	17.00029	3.906836	1.941376	1.22102	0.745624	0.835176	0	0.124276	0.145434	0.095549	0	0.01202	0.002238	
12	19.30056	13.86684	15.09388	0	68.94867	69.38823	68.45774	17.00029	3.829102	1.951953	1.212653	0.687758	0.863894	0	0.094918	0.12906	0.069082	0	0.010827	0.003127	
13	18.63656	13.3957	14.26533	0	68.91355	69.43598	68.45774	17.00029	3.746094	1.955273	1.176625	0.67591	0.836789	0	0.124276	0.158979	0.069082	0	0.01262	0.002392	
14	17.95078	12.90548	13.7428	0	68.90185	69.42006	68.47194	17.00029	3.667773	1.956641	1.179848	0.71892	0.795624	0	0.130452	0.158483	0.095549	0	0.012995	0.002325	
15	17.21162	12.39907	13.00469	0	68.92526	69.46782	68.44364	17.00029	3.594531	1.955273	1.179209	0.739134	0.784947	0	0.116557	0.163961	0	0	0.013147	0.001619	
16	16.4622	11.84808	12.23002	0	68.93697	69.40415	68.45774	17.00029	3.525586	1.953516	1.166682	0.718121	0.80161	0	0.10696	0.145434	0.069082	0	0.012969	0.001619	
17	15.68099	11.26524	11.4013	0	68.96038	69.43598	68.47194	17.00029	3.455078	1.950195	1.139864	0.757093	0.634934	0	0.079324	0.158979	0.095549	0	0.011617	0.002238	
18	14.91129	10.75963	10.78521	0	68.91355	69.40415	68.44364	17.00029	3.379688	1.942773	1.087736	0.72127	0.617684	0	0.124276	0.145434	0	0	0.011276	0.001993	
19	14.1828	10.16188	10.0686	0	68.94867	69.42006	68.45774	17.00029	3.303516	1.934766	1.02351	0.675233	0.535719	0	0.094918	0.158483	0.069082	0	0.011427	0.001827	
20	13.43405	9.610436	9.330237	0	68.90185	69.38823	68.44364	17.00029	3.228711	1.925	1.002824	0.644425	0.596778	0	0.130452	0.12906	0	0	0.009614	0	
21	12.74797	9.119502	8.663664	0	68.91355	69.43598	68.45774	17.00029	3.15293	1.91543	1.001236	0.622518	0.467895	0	0.124276	0.158979	0.069082	0	0.010559	0.00141	
22	12.01944	8.598968	7.961091	0	68.93697	69.37231	68.47194	17.00029	3.073828	1.902344	0.865636	0.640165	0.492214	0	0.223418	0.107857	0.13813	0	0.009879	0.002238	
23	11.31306	8.06235	7.312888	0	68.89014	69.38823	68.44364	17.00029	2.991211	1.89043	0.875404	0.583291	0.440051	0	0.135295	0.12906	0	0	0.009967	0.002325	
24	10.58475	7.572012	6.64634	0	68.90185	69.37231	68.45774	17.00029	2.907227	1.877733	0.874156	0.519654	0.418868	0	0.130452	0.107857	0.069082	0	0.010262	0.002325	
25	9.993348	7.066045	5.998009	0	68.92526	69.38823	68.44364	17.00029	2.826172	1.86543	0.746189	0.519899	0.465109	0	0.116557	0.12906	0	0	0.010779	0.003814	
26	9.381713	6.575459	5.439636	0	68.90185	69.40415	68.44364	17.00029	2.746094	1.853906	0.690748	0.464128	0.380651	0	0.130452	0.145434	0	0	0.009531	0.007812	
27	8.769493	6.146412	4.917287	0	68.91355	69.38823	68.44364	17.00029	2.667187	1.844531	0.662821	0.478999	0.356304	0	0.124276	0.12906	0	0	0.010269	0.00249	
28	8.169174	5.840761	4.250841	0	68.89014	69.35639	68.44364	17.00029	2.590039	1.835547	0.643209	0.45593	0.352962	0	0.135295	0.07798	0	0	0.009959	0.001619	
29	7.566107	5.165589	3.818552	0	68.96038	69.35639	68.44364	17.00029	2.514844	1.825586	0.60849	0.383227	0.329139	0	0.079324	0.07798	0	0	0.009316	0.002238	
30	7.017873	4.690337	3.332227	0	68.89014	69.37231	68.44364	17.00029	2.441211	1.816016	0.570871	0.347271	0.298389	0	0.135295	0.107957	0	0	0.009778	0.002325	
31	6.426738	4.322403	2.773854	0	68.91355	69.38823	68.44364	17.00029	2.370312	1.810742	0.525976	0.347302	0.380651	0	0.124276	0.12906	0	0	0.010157	0.008611	
32	5.909797	3.801444	2.603643	0	68.89014	69.34047	68.45774	17.00029	2.301367	1.807031	0.504612	0.337295	0.284487	0	0.135295	0	0.069082	0	0.010133	0.001993	
33	5.319815	3.43345	2.089397	0	68.89014	69.37231	68.44364	17.00029	2.233789	1.805469	0.422331	0.280071	0.352962	0	0.135295	0.107957	0	0	0.010764	0.001619	
34	4.822676	3.019695	1.657083	0	68.93697	69.34047	68.45774	17.00029	2.167773	1.805664	0.419032	0.28658	0.244089	0	0.10696	0	0.069082	0	0.010541	0.001953	
35	4.379492	2.651813	1.278655	0	68.91355	69.34047	68.44364	17.00029	2.105469	1.807813	0.40566	0.306435	0.269769	0	0.124276	0	0	0	0.009655	0.001993	
36	3.904765	2.29926	0.954639	0	68.89673	69.34047	68.44364	17.00029	2.045313	1.811914	0.394552	0.271206	0.220025	0	0.141495	0	0	0	0.010312	0.001827	
37	3.440471	1.992692	0.720492	0	68.85502	69.34047	68.44364	17.00029	1.986914	1.817383	0.357405	0.253875	0.244096	0	0.143003	0	0	0	0.009358	0.00249	
38	2.986615	1.696124	0.540373	0	68.89673	69.34047	68.42953	17.00029	1.929883	1.825391	0.32515	0.253875	0.262612	0	0.141495	0	0.069082	0	0.009955	0.002325	
39	2.532707	1.419213	0.252181	0	68.91355	69.34047	68.41543	17.00029	1.874414	1.834961	0.289219	0.25824	0.252269	0	0.124276	0	0.095549	0	0.00956	0.001827	
40	2.152904	1.088317	-0.12609	0	68.86673	69.34047	68.41543	17.00029	1.820508	1.843945	0.269225	0.229593	0.298395	0	0.141495	0	0.095549	0	0.009895	0.002441	
41	1.751697	0.843062	-0.28821	0	68.85502	69.34047	68.35903	17.00029	1.768359	1.855664	0.288448	0.229593	0.375298	0	0.143003	0	0.149636	0	0.009104	0.002776	
42	1.361451	0.659133	-0.50434	0	68.83161	69.32456	68.42953	17.00029	1.719531	1.868164	0.245607	0.187248	0.375276	0	0.143003	0.07798	0.069082	0	0.009663	0.002645	
43	1.044848	0.444524	-0.90061	0	68.80819	69.34047	68.42953	17.00029	1.671094	1.88125	0.272479	0.216398	0.217703	0	0.138945	0	0.069082	0	0.009531	0.002409	
44	0.770427	0.306568	-0.90063	0	68.83161	69.34047	68.41543	17.00029	1.625195	1.891992	0.229935	0.177151	0.176507	0	0.143003	0	0.095549	0	0.010289	0.008524	
45	0.517127	0.193275	-1.09881	0	68.84331	69.32456	68.37313	17.00029	1.580664	1.902148	0.217464	0.242072	0.311724	0	0.143502	0.07798	0.140398	0	0.00956	0.000977	
46	0.432697	0.091982	-0.77452	0	68.85502	69.29272	68.44364	17.00029	1.536523	1.913672	0.284184	0.223657	0.336765	0	0.143003	0.12906	0	0	0.010453	0.001993	

Sheet1

Figure 5.4 Typical Excel data file

5.3 MICROSOFT EXCEL

5.3.1 Introduction

In order to provide the most comprehensive understanding of cause-and-effect on wall wetting behaviour a flexible software tool was required and considerable effort was made to develop a Microsoft Excel based Analysis program. This program could manipulate the data, calculate various derived values and present a graphical representation of the results with minimal user intervention. The program was also designed to be easily adapted for future similar projects. Multiple channels of heat flux, temperature and cylinder and manifold pressure data were logged from the engine and stored in numerous data files. The signals from each of these channels were dependant upon crank angle and were influenced by the timing of various engine events, such as inlet and exhaust valve timing and lift profile, piston position and port deactivation, where all of these were considered by the program. The program also calculated derived events such as the crank angle period during which the heat flux sensors on the cylinder wall were shielded by the piston and the crank angle at which the inlet valve shrouding was likely to affect the flow from the valves. In an attempt to further understand wall wetting, values for the likely time of flight of the fuel droplets from the injector tip or valve curtain to the cylinder wall were also deduced. Excel version 2002 was chosen for this work due to several distinct reasons. Firstly, it was the most common and readily available form of spreadsheet package available. This software was also excellent at reading specific data from any cell in any worksheet of any workbook. Excel had the useful ability of sorting data, where rearranging the contents of a column into size order was easily achieved and was especially useful for when grouping specific data types prior to analysing them. A vital role for Excel was to perform the numerous calculations of the Analysis program, where this was made possible by some of the available logic functions such as IF, AND and OR. The nature of this study required the results to be displayed in a graphical way and Excel was very capable at showing results in a wide range of graphs which were easily adjusted by the user for optimal presentation. The Excel model contained six worksheets called 'Lifts', 'Tests', 'Data', 'Main', 'Plotting', 'Quantity' and one results display plot called 'Chart'. These worksheets will now be discussed individually and the actual equations entered in Excel are shown in Appendix IV.

5.3.2 Worksheet 'Lifts'

This was simply a 5 column data sheet containing a counter from 1 to 720 to represent crank angle degrees and the inlet and exhaust valve lift profiles for the two different cylinder heads. Such valve lifts are usually described in terms of MOP (Maximum Opening Point) where in this worksheet, the data was stored conveniently in the columns so that the four MOP values all occurred at crank angle 360, with the remaining cells containing zeros to represent a closed valve. The analysis program would later observe the inlet and exhaust MOP values held within the chosen data file and then reposition the valve events so that they were presented at the correct times in the engine cycle in relevant worksheets. This valve lift data was stored within the analysis workbook because this gave faster computer access times.

5.3.3 Worksheet 'Tests'

This was effectively a chronological test matrix that was updated every time a new batch of tests was performed (Figure 5.5). In worksheet 'Tests' columns A to J simply showed the test condition data as held in the individual cells at the top of the Excel data files. A descriptive sensor-location system was used on the engine and is detailed in section 6.3.4, but for convenience in the Excel work each sensor location was given a number. When this sensor location number was entered into columns K, L and M, columns N to AN looked to see if the sensor location number they represent had been entered and would show this number in the appropriate cell. This was a visually useful tool as it showed which tests had been performed using these sensor locations. Column AO showed the file names that the data is stored in, where the text of these data file names was generated automatically by joining the text from the other cells. This sheet performed a further task in that it would allow the user to sort the test information into a convenient order for display in worksheet 'Data'. It should be noticed that this file name column also contained the word "BLANK" at the top. This will be described in the 'Data' worksheet section. Since the sorting could lead to the tests being left in an unusual order, column AP effectively assigned a unique identification number to each test to allow rapid reordering back to the original (default) chronological test order. Column AQ was simply a counter to monitor the number of tests performed. This structured data management facility was vital for handling the 400 data files.

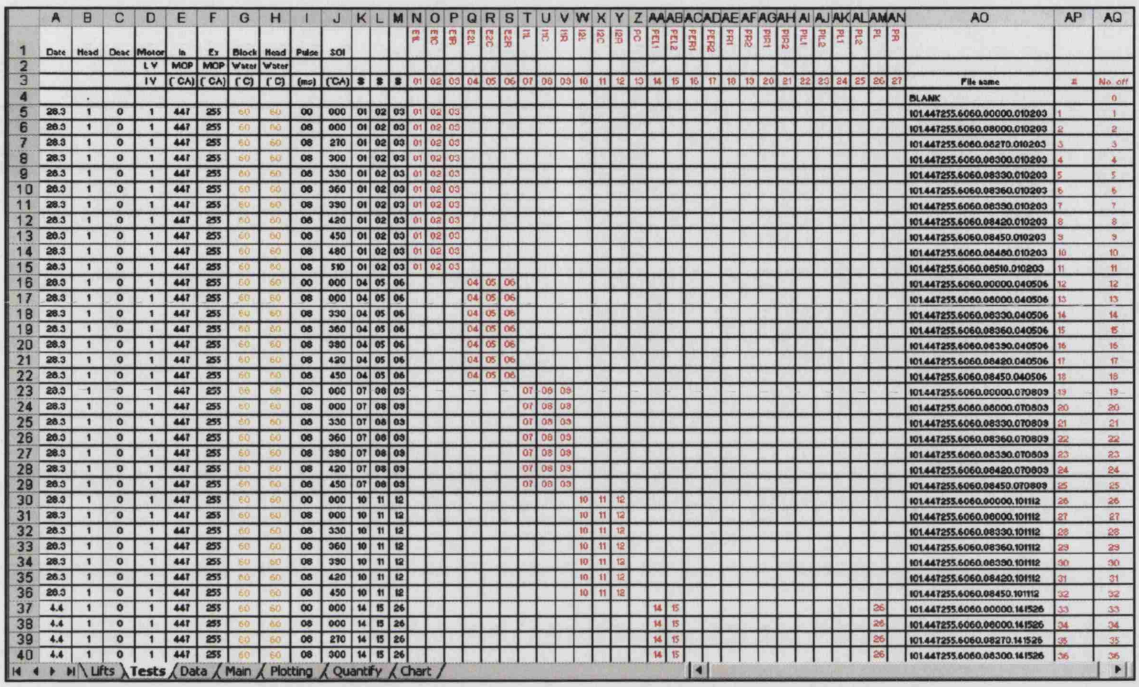

	A	B	C	D	E	F	G	H	I	J	K	L	M	N	O	P	Q	R	S	T	U	V	W	X	Y	Z	AO	AP	AQ
1	Date	Head	Desc	Motor	In	Ex	Block	Head	Pulse	SOI																			
2				LV	MOP	MOP	Water	Water																					
3				IV	(°CA)	(°CA)	(°C)	(°C)	(ms)	(°CA)	S	S	S	01	02	03	04	05	06	07	08	09	10	11	12	13	14	15	16	17	18	19	20	21	22	23	24	25	26	27	File name	#	No. off
4																																							BLANK		0
5	28.3	1	0	1	447	255	60	60	00	000	01	02	03	01	02	03																							101.447255.6060.00000.010203	1	1
6	28.3	1	0	1	447	255	60	60	08	000	01	02	03	01	02	03																							101.447255.6060.08000.010203	2	2
7	28.3	1	0	1	447	255	60	60	08	270	01	02	03	01	02	03																							101.447255.6060.08270.010203	3	3
8	28.3	1	0	1	447	255	60	60	08	300	01	02	03	01	02	03																							101.447255.6060.08300.010203	4	4
9	28.3	1	0	1	447	255	60	60	08	330	01	02	03	01	02	03																							101.447255.6060.08330.010203	5	5
10	28.3	1	0	1	447	255	60	60	08	360	01	02	03	01	02	03																							101.447255.6060.08360.010203	6	6
11	28.3	1	0	1	447	255	60	60	08	390	01	02	03	01	02	03																							101.447255.6060.08390.010203	7	7
12	28.3	1	0	1	447	255	60	60	08	420	01	02	03	01	02	03																							101.447255.6060.08420.010203	8	8
13	28.3	1	0	1	447	255	60	60	08	450	01	02	03	01	02	03																							101.447255.6060.08450.010203	9	9
14	28.3	1	0	1	447	255	60	60	08	480	01	02	03	01	02	03																							101.447255.6060.08480.010203	10	10
15	28.3	1	0	1	447	255	60	60	08	510	01	02	03	01	02	03																							101.447255.6060.08510.010203	11	11
16	28.3	1	0	1	447	255	60	60	00	000	04	05	06				04	05	06																				101.447255.6060.00000.040506	12	12
17	28.3	1	0	1	447	255	60	60	08	000	04	05	06				04	05	06																				101.447255.6060.08000.040506	13	13
18	28.3	1	0	1	447	255	60	60	08	330	04	05	06				04	05	06																				101.447255.6060.08330.040506	14	14
19	28.3	1	0	1	447	255	60	60	08	360	04	05	06				04	05	06																				101.447255.6060.08360.040506	15	15
20	28.3	1	0	1	447	255	60	60	08	390	04	05	06				04	05	06																				101.447255.6060.08390.040506	16	16
21	28.3	1	0	1	447	255	60	60	08	420	04	05	06				04	05	06																				101.447255.6060.08420.040506	17	17
22	28.3	1	0	1	447	255	60	60	08	450	04	05	06				04	05	06																				101.447255.6060.08450.040506	18	18
23	28.3	1	0	1	447	255	60	60	00	000	07	08	09							07	08	09																	101.447255.6060.00000.070809	19	19
24	28.3	1	0	1	447	255	60	60	08	000	07	08	09							07	08	09																	101.447255.6060.08000.070809	20	20
25	28.3	1	0	1	447	255	60	60	08	330	07	08	09							07	08	09																	101.447255.6060.08330.070809	21	21
26	28.3	1	0	1	447	255	60	60	08	360	07	08	09							07	08	09																	101.447255.6060.08360.070809	22	22
27	28.3	1	0	1	447	255	60	60	08	390	07	08	09							07	08	09																	101.447255.6060.08390.070809	23	23
28	28.3	1	0	1	447	255	60	60	08	420	07	08	09							07	08	09																	101.447255.6060.08420.070809	24	24
29	28.3	1	0	1	447	255	60	60	08	450	07	08	09							07	08	09																	101.447255.6060.08450.070809	25	25
30	28.3	1	0	1	447	255	60	60	00	000	10	11	12										10	11	12														101.447255.6060.00000.101112	26	26
31	28.3	1	0	1	447	255	60	60	08	000	10	11	12										10	11	12														101.447255.6060.08000.101112	27	27
32	28.3	1	0	1	447	255	60	60	08	330	10	11	12										10	11	12														101.447255.6060.08330.101112	28	28
33	28.3	1	0	1	447	255	60	60	08	360	10	11	12										10	11	12														101.447255.6060.08360.101112	29	29
34	28.3	1	0	1	447	255	60	60	08	390	10	11	12										10	11	12														101.447255.6060.08390.101112	30	30
35	28.3	1	0	1	447	255	60	60	08	420	10	11	12										10	11	12														101.447255.6060.08420.101112	31	31
36	28.3	1	0	1	447	255	60	60	08	450	10	11	12										10	11	12														101.447255.6060.08450.101112	32	32
37	4.4	1	0	1	447	255	60	60	00	000	14	15	26													14	15											26	101.447255.6060.00000.141526	33	33
38	4.4	1	0	1	447	255	60	60	08	000	14	15	26													14	15											26	101.447255.6060.08000.141526	34	34
39	4.4	1	0	1	447	255	60	60	08	270	14	15	26													14	15											26	101.447255.6060.08270.141526	35	35
40	4.4	1	0	1	447	255	60	60	08	300	14	15	26													14	15											26	101.447255.6060.08300.141526	36	36

Lifts | Tests | Data | Main | Plotting | Quantify | Chart

Figure 5.5 Top rows from the 'Tests' worksheet

5.3.4 Worksheet 'Data'

User Options Section – Columns A to D

Column A was simply a convenient repeat of the ordered file name column generated in column AO of the previous 'Tests' worksheet. Column B allowed the user to choose up to 12 data files of interest (as observed in column A) by clicking on the 12 dedicated cells under the heading "Files" and scrolling down the pop-up list (Figure 5.6). Since there were hundreds of tests to choose from, it was convenient that the tests of interest were already grouped together at the top of the file list due to the sorting operation performed in 'Tests'. This pop-up list was generated by the "VALIDATION" command and used column A as its source data. This command required the source data to be on the same page, hence the duplication of column AO from the 'Tests' worksheet. An option of "BLANK" was given in column B, since it was not always desired to read the maximum of 12 data files. If the user had chosen the "BLANK" file name option, the cell would have simply presented a zero in the cell. The user could then choose which column to read from the data file by clicking on the neighbouring cell in column C under the heading "File Columns". The source data for this VALIDATION command was the contents of the block below which reminded the user about the contents of each column in the LabVIEW data file. Column D simply informed the user what data had been found in the column as a check.

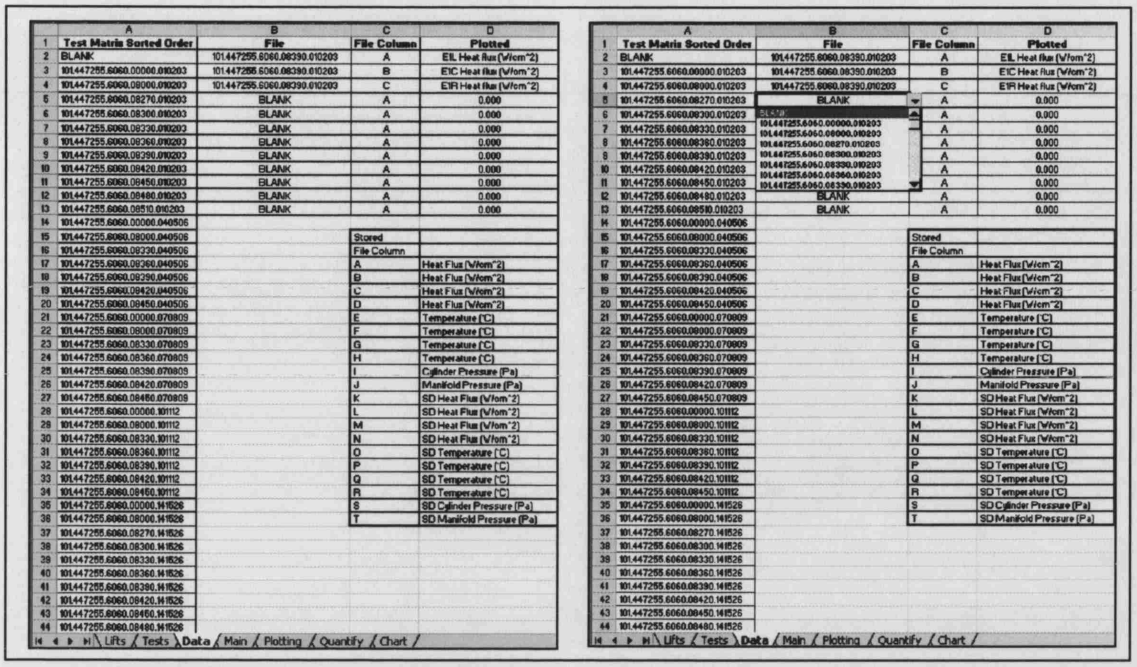

	A	B	C	D
1	Test Matrix Sorted Order	File	File Column	Plotted
2	BLANK	101447255.6060.08390.010203	A	EIL Heat flux (W/cm^2)
3	101447255.6060.00000.010203	101447255.6060.08390.010203	B	EIC Heat flux (W/cm^2)
4	101447255.6060.08000.010203	101447255.6060.08390.010203	C	EIR Heat flux (W/cm^2)
5	101447255.6060.08270.010203	BLANK	A	0.000
6	101447255.6060.08300.010203	BLANK	A	0.000
7	101447255.6060.08330.010203	BLANK	A	0.000
8	101447255.6060.08360.010203	BLANK	A	0.000
9	101447255.6060.08390.010203	BLANK	A	0.000
10	101447255.6060.08420.010203	BLANK	A	0.000
11	101447255.6060.08450.010203	BLANK	A	0.000
12	101447255.6060.08480.010203	BLANK	A	0.000
13	101447255.6060.08510.010203	BLANK	A	0.000
14	101447255.6060.00000.040506			
15	101447255.6060.08000.040506		Stored	
16	101447255.6060.08330.040506		File Column	
17	101447255.6060.08360.040506		A	Heat Flux (W/cm^2)
18	101447255.6060.08390.040506		B	Heat Flux (W/cm^2)
19	101447255.6060.08420.040506		C	Heat Flux (W/cm^2)
20	101447255.6060.08450.040506		D	Heat Flux (W/cm^2)
21	101447255.6060.00000.070809		E	Temperature (°C)
22	101447255.6060.08000.070809		F	Temperature (°C)
23	101447255.6060.08330.070809		G	Temperature (°C)
24	101447255.6060.08360.070809		H	Temperature (°C)
25	101447255.6060.08390.070809		I	Cylinder Pressure (Pa)
26	101447255.6060.08420.070809		J	Manifold Pressure (Pa)
27	101447255.6060.08450.070809		K	SD Heat Flux (W/cm^2)
28	101447255.6060.00000.101112		L	SD Heat Flux (W/cm^2)
29	101447255.6060.08000.101112		M	SD Heat Flux (W/cm^2)
30	101447255.6060.08330.101112		N	SD Heat Flux (W/cm^2)
31	101447255.6060.08360.101112		O	SD Temperature (°C)
32	101447255.6060.08390.101112		P	SD Temperature (°C)
33	101447255.6060.08420.101112		Q	SD Temperature (°C)
34	101447255.6060.08450.101112		R	SD Temperature (°C)
35	101447255.6060.00000.141526		S	SD Cylinder Pressure (Pa)
36	101447255.6060.08000.141526		T	SD Manifold Pressure (Pa)
37	101447255.6060.08270.141526			
38	101447255.6060.08300.141526			
39	101447255.6060.08330.141526			
40	101447255.6060.08360.141526			
41	101447255.6060.08390.141526			
42	101447255.6060.08420.141526			
43	101447255.6060.08450.141526			
44	101447255.6060.08480.141526			

Lifts / Tests \ Data / Main / Plotting / Quantify / Chart /

Figure 5.6 Columns A to D in 'Data' worksheet. Note pop-up list in column B

Data Extraction – Columns G to T

The actual act of extracting the data from data files occurred in columns G to T (Figure 5.7). If a filename other than BLANK was chosen from the file options list, a function INDIRECT.EXT would be invoked in all of the cells in 'Data' that contained it.

This "add-in" command was not normally found in Excel and was created by Laurent (2003). Its advantage over the standard Excel function INDIRECT was that it could take data from closed Excel files in addition to open ones.

Data extraction would take the form of single point value cells, direct drag down value cells and optional drag-down cells, where the equations entered in Excel were quite different.

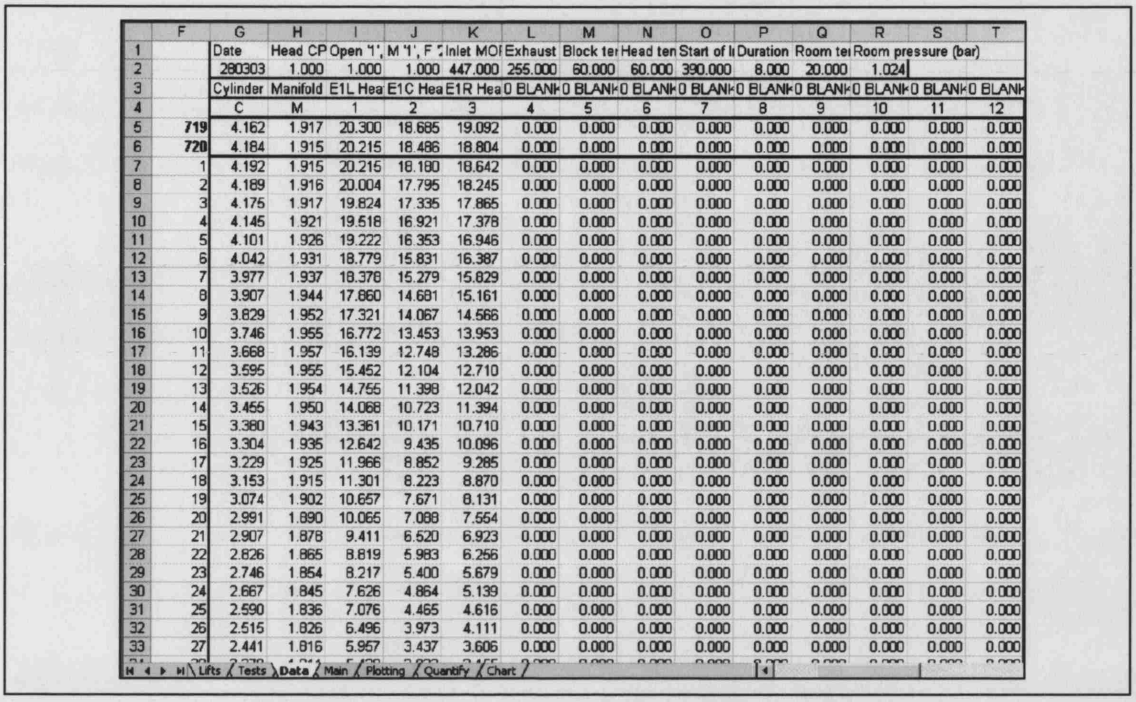

	F	G	H	I	J	K	L	M	N	O	P	Q	R	S	T
1		Date	Head CP	Open '1',	M '1', F	Inlet MOI	Exhaust	Block ter	Head ten	Start of Ir	Duration	Room tei	Room pressure (bar)		
2		280303	1.000	1.000	1.000	447.000	255.000	60.000	60.000	390.000	8.000	20.000	1.024		
3		Cylinder	Manifold	E1L Hea	E1C Hea	E1R Hea	0 BLANK	0 BLANK	0 BLANK	0 BLANK	0 BLANK	0 BLANK	0 BLANK	0 BLANK	0 BLANK
4		C	M	1	2	3	4	5	6	7	8	9	10	11	12
5	719	4.162	1.917	20.300	18.685	19.092	0.000	0.000	0.000	0.000	0.000	0.000	0.000	0.000	0.000
6	720	4.184	1.915	20.215	18.486	18.804	0.000	0.000	0.000	0.000	0.000	0.000	0.000	0.000	0.000
7	1	4.192	1.915	20.215	18.180	18.642	0.000	0.000	0.000	0.000	0.000	0.000	0.000	0.000	0.000
8	2	4.189	1.916	20.004	17.795	18.245	0.000	0.000	0.000	0.000	0.000	0.000	0.000	0.000	0.000
9	3	4.175	1.917	19.824	17.335	17.865	0.000	0.000	0.000	0.000	0.000	0.000	0.000	0.000	0.000
10	4	4.145	1.921	19.618	16.921	17.378	0.000	0.000	0.000	0.000	0.000	0.000	0.000	0.000	0.000
11	5	4.101	1.926	19.222	16.353	16.946	0.000	0.000	0.000	0.000	0.000	0.000	0.000	0.000	0.000
12	6	4.042	1.931	18.779	15.831	16.387	0.000	0.000	0.000	0.000	0.000	0.000	0.000	0.000	0.000
13	7	3.977	1.937	18.376	15.279	15.829	0.000	0.000	0.000	0.000	0.000	0.000	0.000	0.000	0.000
14	8	3.907	1.944	17.860	14.681	15.161	0.000	0.000	0.000	0.000	0.000	0.000	0.000	0.000	0.000
15	9	3.829	1.952	17.321	14.067	14.566	0.000	0.000	0.000	0.000	0.000	0.000	0.000	0.000	0.000
16	10	3.746	1.955	16.772	13.453	13.953	0.000	0.000	0.000	0.000	0.000	0.000	0.000	0.000	0.000
17	11	3.668	1.957	16.139	12.748	13.286	0.000	0.000	0.000	0.000	0.000	0.000	0.000	0.000	0.000
18	12	3.595	1.955	15.452	12.104	12.710	0.000	0.000	0.000	0.000	0.000	0.000	0.000	0.000	0.000
19	13	3.526	1.954	14.755	11.398	12.042	0.000	0.000	0.000	0.000	0.000	0.000	0.000	0.000	0.000
20	14	3.455	1.950	14.068	10.723	11.394	0.000	0.000	0.000	0.000	0.000	0.000	0.000	0.000	0.000
21	15	3.380	1.943	13.361	10.171	10.710	0.000	0.000	0.000	0.000	0.000	0.000	0.000	0.000	0.000
22	16	3.304	1.935	12.642	9.435	10.096	0.000	0.000	0.000	0.000	0.000	0.000	0.000	0.000	0.000
23	17	3.229	1.925	11.966	8.852	9.285	0.000	0.000	0.000	0.000	0.000	0.000	0.000	0.000	0.000
24	18	3.153	1.915	11.301	8.223	8.870	0.000	0.000	0.000	0.000	0.000	0.000	0.000	0.000	0.000
25	19	3.074	1.902	10.657	7.671	8.131	0.000	0.000	0.000	0.000	0.000	0.000	0.000	0.000	0.000
26	20	2.991	1.890	10.065	7.088	7.554	0.000	0.000	0.000	0.000	0.000	0.000	0.000	0.000	0.000
27	21	2.907	1.878	9.411	6.520	6.923	0.000	0.000	0.000	0.000	0.000	0.000	0.000	0.000	0.000
28	22	2.826	1.865	8.819	5.983	6.256	0.000	0.000	0.000	0.000	0.000	0.000	0.000	0.000	0.000
29	23	2.746	1.854	8.217	5.400	5.679	0.000	0.000	0.000	0.000	0.000	0.000	0.000	0.000	0.000
30	24	2.667	1.845	7.626	4.864	5.139	0.000	0.000	0.000	0.000	0.000	0.000	0.000	0.000	0.000
31	25	2.590	1.836	7.076	4.465	4.616	0.000	0.000	0.000	0.000	0.000	0.000	0.000	0.000	0.000
32	26	2.515	1.826	6.496	3.973	4.111	0.000	0.000	0.000	0.000	0.000	0.000	0.000	0.000	0.000
33	27	2.441	1.816	5.957	3.437	3.606	0.000	0.000	0.000	0.000	0.000	0.000	0.000	0.000	0.000

Lists / Tests / Data / Main / Plotting / Quantify / Chart /

Figure 5.7 Columns G to T in 'Data' worksheet

Point Value Cells - Some values such as the date only required a single cell and the data in such a cell was readily replicated directly into worksheet 'Data'.

Direct Drag-Down Value Cells - A vast majority of the cells were of the drag-down type with each cell in the column relating to a specific engine crank degree.

Optional Drag-Down Value Cells - A further complication to the drag-down cell type was to allow for when the user chose one or a number of the 12 File Columns from column C in the 'Data' worksheet. To permit such flexibility, the basic drag-down Excel line was modified. An interesting feature of columns G to T seen in worksheet 'Data' was that the first two rows were effectively duplicates of the data in the last two rows in the data file, while conversely the last two rows in worksheet 'Data' were duplicates of the first two rows of the data file. This was done because the final values presented later in columns W to AK were actually an average over 5 crank degrees, with these being the current row, two rows above and two rows below. This averaging procedure over 5 crank degrees did not affect the trends, but eliminated any spike points due to noise.

Final Cell Calculation and Averaging – Columns W to AK

Cells W to AK performed three functions, namely the conversion of voltages to pressures in columns W and Y, the matching of the cylinder pressure to the inlet manifold pressure at a desired crank angle in column X (Figure 5.8) and data averaging.

Column W - This column performed the averaging task and also converted the average logged cylinder pressure voltage to a pressure in Pascal, where the sensitivity of the pressure transducer was 15.1 pC /bar and the charge amplifier setting was 20 mV/pC .

$$P = \frac{1x10^8 \overline{V}}{15.1 \times 20}$$

Column Y - This column performed the averaging task and also converted the average logged inlet manifold pressure voltage to a pressure in Pascal, where the linear relationship between output volts and applied pressure was given by the manufacturer.

$$P = \left(\frac{\overline{V} + 0.0189}{3.3374} \right) x\ 1x10^5$$

	V	W	X	Y	Z	AA	AB	AC	AD	AE	AF	AG	AH	AI	AJ	AK
1																
2																
3		Cyl press	Cylinder	Manifold	E1L Hea	E1C Hea	E1R Hea	0.000	0.000	0.000	0.000	0.000	0.000	0.000	0.000	0.000
4			C	M	1	2	3	4	5	6	7	8	9	10	11	12
5																
6			540													
7	1	1384197	1244391	57974	20.11	18.10	18.53	0.00	0.00	0.00	0.00	0.00	0.00	0.00	0.00	0.00
8	2	1383058	1243252	58001	19.96	17.74	18.19	0.00	0.00	0.00	0.00	0.00	0.00	0.00	0.00	0.00
9	3	1377535	1237729	58068	19.76	17.32	17.82	0.00	0.00	0.00	0.00	0.00	0.00	0.00	0.00	0.00
10	4	1367627	1227821	58169	19.47	16.85	17.36	0.00	0.00	0.00	0.00	0.00	0.00	0.00	0.00	0.00
11	5	1353580	1213774	58294	19.14	16.34	16.88	0.00	0.00	0.00	0.00	0.00	0.00	0.00	0.00	0.00
12	6	1335834	1196028	58453	18.75	15.81	16.34	0.00	0.00	0.00	0.00	0.00	0.00	0.00	0.00	0.00
13	7	1314919	1175113	58637	18.31	15.24	15.78	0.00	0.00	0.00	0.00	0.00	0.00	0.00	0.00	0.00
14	8	1291430	1151624	58810	17.82	14.66	15.18	0.00	0.00	0.00	0.00	0.00	0.00	0.00	0.00	0.00
15	9	1266847	1126841	58961	17.29	14.05	14.56	0.00	0.00	0.00	0.00	0.00	0.00	0.00	0.00	0.00
16	10	1241347	1101541	59072	16.71	13.41	13.94	0.00	0.00	0.00	0.00	0.00	0.00	0.00	0.00	0.00
17	11	1216098	1076293	59131	16.09	12.75	13.31	0.00	0.00	0.00	0.00	0.00	0.00	0.00	0.00	0.00
18	12	1191329	1051523	59120	15.44	12.09	12.68	0.00	0.00	0.00	0.00	0.00	0.00	0.00	0.00	0.00
19	13	1167063	1027257	59045	14.75	11.43	12.03	0.00	0.00	0.00	0.00	0.00	0.00	0.00	0.00	0.00
20	14	1142940	1003134	58914	14.06	10.77	11.39	0.00	0.00	0.00	0.00	0.00	0.00	0.00	0.00	0.00
21	15	1118714	978908	58733	13.36	10.12	10.71	0.00	0.00	0.00	0.00	0.00	0.00	0.00	0.00	0.00
22	16	1094036	954229	58505	12.67	9.48	10.07	0.00	0.00	0.00	0.00	0.00	0.00	0.00	0.00	0.00
23	17	1068786	928980	58218	11.99	8.87	9.42	0.00	0.00	0.00	0.00	0.00	0.00	0.00	0.00	0.00
24	18	1043059	903253	57904	11.33	8.25	8.79	0.00	0.00	0.00	0.00	0.00	0.00	0.00	0.00	0.00
25	19	1016815	877009	57564	10.68	7.67	8.15	0.00	0.00	0.00	0.00	0.00	0.00	0.00	0.00	0.00
26	20	990157	850351	57207	10.05	7.10	7.55	0.00	0.00	0.00	0.00	0.00	0.00	0.00	0.00	0.00
27	21	963214	823408	56838	9.43	6.53	6.91	0.00	0.00	0.00	0.00	0.00	0.00	0.00	0.00	0.00
28	22	936284	796478	56491	8.83	5.97	6.31	0.00	0.00	0.00	0.00	0.00	0.00	0.00	0.00	0.00
29	23	909716	769911	56163	8.23	5.45	5.72	0.00	0.00	0.00	0.00	0.00	0.00	0.00	0.00	0.00
30	24	883731	743925	55849	7.65	4.94	5.16	0.00	0.00	0.00	0.00	0.00	0.00	0.00	0.00	0.00
31	25	858237	718431	55553	7.07	4.43	4.63	0.00	0.00	0.00	0.00	0.00	0.00	0.00	0.00	0.00
32	26	833351	693545	55294	6.52	3.95	4.13	0.00	0.00	0.00	0.00	0.00	0.00	0.00	0.00	0.00
33	27	809124	669318	55069	5.98	3.51	3.63	0.00	0.00	0.00	0.00	0.00	0.00	0.00	0.00	0.00

Lifts | Tests | Data | Main | Plotting | Quantify | Chart

Figure 5.8 Columns W to AK in 'Data' worksheet

Since the cylinder pressure transducer only provided a signal when a change in pressure occurred, the cylinder pressure had to be referenced to a known pressure at some point in the cycle. The chosen point was 540° (BDC) when the inlet valves were open since the independently measured inlet manifold pressure would be approximately equal to the cylinder pressure at this point [Stone (1999)].

Columns Z to AK - These columns simply performed the described averaging procedure over the five rows of the extracted data as described earlier.

5.3.5 Worksheet 'Main'

This worksheet was the most important part of the Analysis software because it contained all of the analysis equations. This worksheet consisted of information and data in an upper table at the top left of the worksheet in column A (Figure 5.9) and a large table below that contained the bulk of the calculations (Figure 5.10).

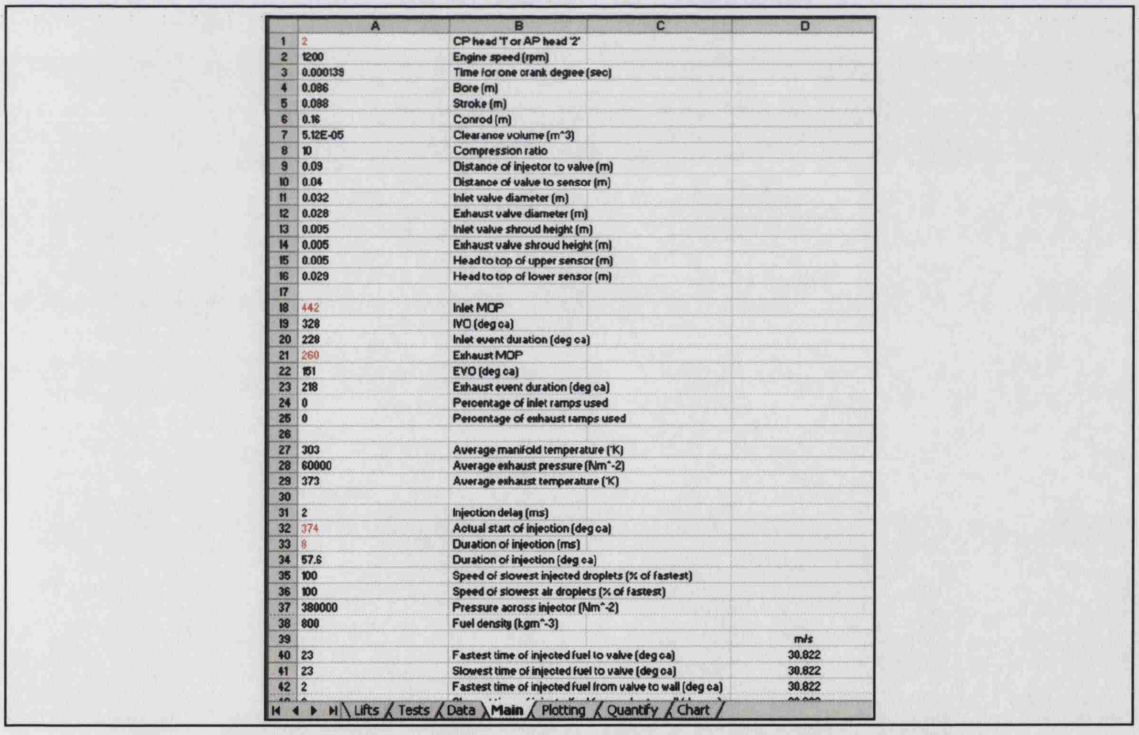

	A	B	C	D
1	2	CP head '1' or AP head '2'		
2	1200	Engine speed (rpm)		
3	0.000139	Time for one crank degree (sec)		
4	0.086	Bore (m)		
5	0.088	Stroke (m)		
6	0.16	Conrod (m)		
7	5.12E-05	Clearance volume (m^3)		
8	10	Compression ratio		
9	0.09	Distance of injector to valve (m)		
10	0.04	Distance of valve to sensor (m)		
11	0.032	Inlet valve diameter (m)		
12	0.028	Exhaust valve diameter (m)		
13	0.005	Inlet valve shroud height (m)		
14	0.005	Exhaust valve shroud height (m)		
15	0.005	Head to top of upper sensor (m)		
16	0.029	Head to top of lower sensor (m)		
17				
18	442	Inlet MOP		
19	328	IVC (deg ca)		
20	228	Inlet event duration (deg ca)		
21	260	Exhaust MOP		
22	151	EVO (deg ca)		
23	218	Exhaust event duration (deg ca)		
24	0	Percentage of inlet ramps used		
25	0	Percentage of exhaust ramps used		
26				
27	303	Average manifold temperature (K)		
28	60000	Average exhaust pressure (Nm^-2)		
29	373	Average exhaust temperature (K)		
30				
31	2	Injection delay (ms)		
32	374	Actual start of injection (deg ca)		
33	8	Duration of injection (ms)		
34	57.6	Duration of injection (deg ca)		
35	100	Speed of slowest injected droplets (% of fastest)		
36	100	Speed of slowest air droplets (% of fastest)		
37	380000	Pressure across injector (Nm^-2)		
38	800	Fuel density (kgm^-3)		
39				m/s
40	23	Fastest time of injected fuel to valve (deg ca)		30.822
41	23	Slowest time of injected fuel to valve (deg ca)		30.822
42	2	Fastest time of injected fuel from valve to wall (deg ca)		30.822

Lifts / Tests / Data / Main / Plotting / Quantify / Chart /

Figure 5.9 Basic data in the upper table on the 'Main' worksheet

The cells in the upper table of the worksheet contained either information entered by the user such as geometric engine values, data that was replicated from worksheet 'Data' or additional basic calculations that helped in the operation of the large table on the worksheet.

The additional calculations performed at the top of the worksheet include the velocity of the injected fuel droplets and the associated flight times within the engine.

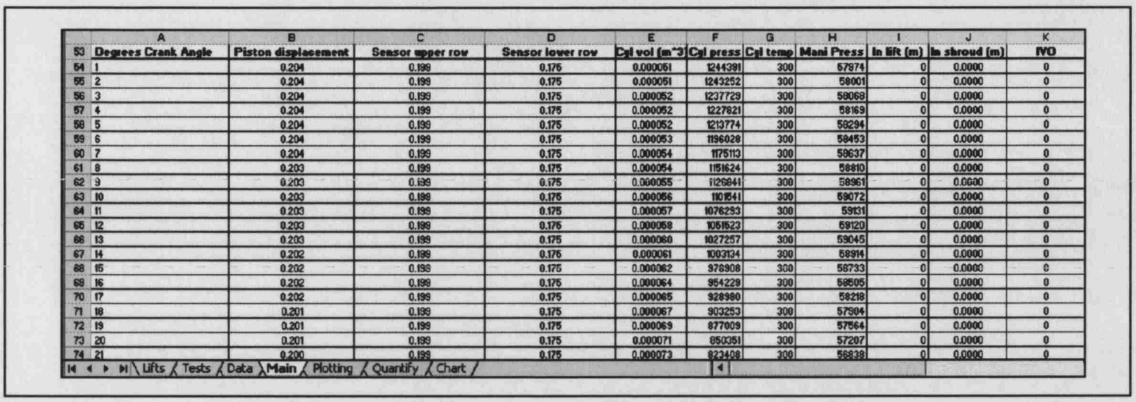

	A	B	C	D	E	F	G	H	I	J	K
53	Degees Crank Angle	Piston displacement	Sensor upper row	Sensor lower row	Cyl vol (m^3)	Cyl press	Cyl temp	Mani Press	In lift (m)	In shroud (m)	IVO
54	1	0.204	0.199	0.175	0.000051	1244391	300	57974	0	0.0000	0
55	2	0.204	0.199	0.175	0.000051	1243252	300	58001	0	0.0000	0
56	3	0.204	0.199	0.175	0.000052	1237729	300	58069	0	0.0000	0
57	4	0.204	0.199	0.175	0.000052	1227821	300	58169	0	0.0000	0
58	5	0.204	0.199	0.175	0.000052	1213774	300	58294	0	0.0000	0
59	6	0.204	0.199	0.175	0.000053	1196028	300	58453	0	0.0000	0
60	7	0.204	0.199	0.175	0.000054	1175113	300	58637	0	0.0000	0
61	8	0.203	0.199	0.175	0.000054	1151624	300	58810	0	0.0000	0
62	9	0.203	0.199	0.175	0.000055	1126941	300	58961	0	0.0000	0
63	10	0.203	0.199	0.175	0.000056	1101541	300	59072	0	0.0000	0
64	11	0.203	0.199	0.175	0.000057	1076253	300	59131	0	0.0000	0
65	12	0.203	0.199	0.175	0.000058	1051522	300	59120	0	0.0000	0
66	13	0.203	0.199	0.175	0.000060	1027257	300	59045	0	0.0000	0
67	14	0.202	0.199	0.175	0.000061	1003104	300	58914	0	0.0000	0
68	15	0.202	0.199	0.175	0.000062	978908	300	58733	0	0.0000	0
69	16	0.202	0.199	0.175	0.000064	954229	300	58505	0	0.0000	0
70	17	0.202	0.199	0.175	0.000065	929980	300	58219	0	0.0000	0
71	18	0.201	0.199	0.175	0.000067	903253	300	57904	0	0.0000	0
72	19	0.201	0.199	0.175	0.000069	877009	300	57564	0	0.0000	0
73	20	0.201	0.199	0.175	0.000071	850351	300	57207	0	0.0000	0
74	21	0.200	0.199	0.175	0.000073	823408	300	56839	0	0.0000	0

Lifts / Tests / Data / Main / Plotting / Quantify / Chart /

Figure 5.10 Typical calculations in the big table on the 'Main' worksheet

The single cell calculation of the injected fuel velocity used the pressure across the injector and the fuel density as shown in Equation 5.2 [Williams (1994)].

$$\text{Fuel velocity} = \sqrt{\left(\frac{2\Delta P_{\text{across injector}}}{\rho_{\text{fuel}}}\right)} \qquad \ldots(5.2)$$

Knowledge of the fuel velocity was important because it could be used to calculate the flight time of the fuel from the injector to the valves or cylinder wall and allow the user to examine if changes in the heat flux trace were due to droplet impaction. Cells containing the time of flight calculations can be seen at the bottom of Figure 5.9.

The contents of the columns on the 'Main' worksheet are now described, giving details on why the calculations were performed and what equations they used.

Crank angle position – Column A

Column A simply contained a counter representing crank angle from 1 to 720°.

Instantaneous Piston Position – Column B

Knowledge of the piston position was important because it allowed calculation of the instantaneous cylinder volume and information on when the heat flux sensors on the cylinder wall were shielded from the combustion chamber by the piston.

The piston position was calculated for every degree of crankshaft rotation throughout the cycle. This was achieved by finding x, the displacement of the piston from the rotational axis of the crankshaft as shown in Figure 5.11 [Stone (1999)].

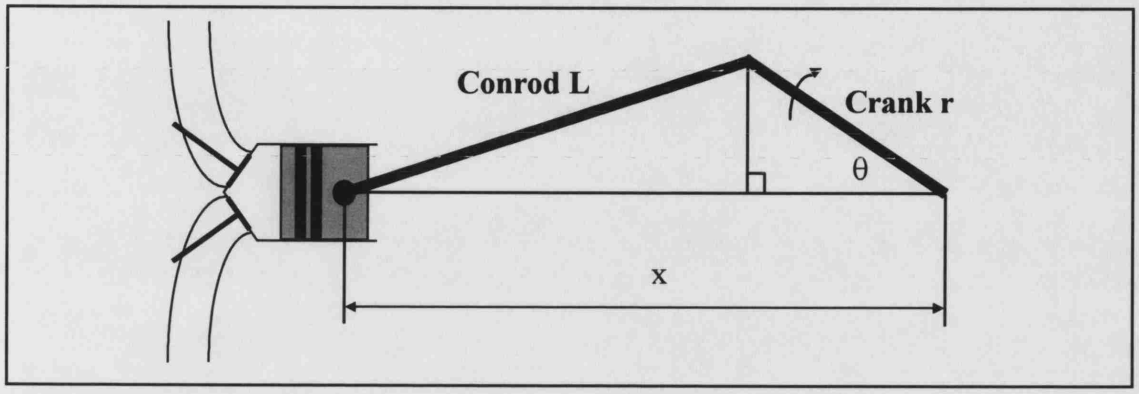

Figure 5.11 Instantaneous piston position

The appropriate equation [Stone (1999)] is written:

$$x = r\left(\cos\theta + \frac{L}{r}\left[1 - \tfrac{1}{2}\left(\frac{r}{L}\right)^2\left(\tfrac{1}{2} - \tfrac{1}{2}\cos 2\theta\right)\right]\right) \qquad \ldots(5.3)$$

To find the distance of the top of the piston from TDC this value of x was then subtracted from the sum of the conrod length and half the stroke.

Sensor Covering – Column C and D

An important consideration when viewing the results from the sensors on the cylinder bore was that the sensors were passed by the piston when it approached TDC. Since there was an upper and lower row of sensors, two plot lines and hence two columns were required in Excel. The distance from the top of the cylinder block to the top of the sensor was entered in each case since the heat flux readings would change when the retreating piston first exposed part of the sensor face to the combustion chamber.

Cylinder volume – Column E

The distance of the piston from TDC was multiplied by the cross sectional area of the cylinder to find the instantaneous swept volume of the cylinder. The clearance volume (5.245×10^{-5} m^3) was added find the total instantaneous cylinder volume.

Cylinder pressure – Column F

This was already calculated in worksheet 'Data', but was duplicated in this worksheet for convenience. The cylinder pressure was important for when calculating the flow through the inlet and exhaust valves.

Cylinder temperature – Column G

The main reason for requiring a cylinder temperature was to enable a more accurate estimation of the flow through the valves using the compressible flow equations. During a motoring test, it was assumed the cylinder temperature remained constant at approximately room temperature of 300 K. The temperatures experienced during compression would increase the cylinder temperature, but this could be ignored since the valves would be closed at this time and calculating the flow was not needed. For the firing tests, a temperature of 800 K was assumed up until the point of IVO and a temperature of 300 K assumed from IVC onwards. The Excel equation simulated a linear transition between these temperatures to represent the cooling effect on the cylinder contents due to the incoming fresh charge.

Inlet manifold pressure – Column H

This was already calculated in worksheet 'Data', but was included on this worksheet for convenience. Knowledge of this allowed the flow through the inlet valves to be calculated.

Inlet valve lift – Column I

As mentioned previously, the basic inlet valve lift profile was stored in worksheet 'Lifts'. However, the inlet valve event could be advanced or retarded on the real engine and the MOP values used were entered in LabVIEW at the time of the experiment in order to obtain the correct valve timing in the analysis program. Due to experimental variation and the time between tests, the temperature of the cylinder head and valves could vary and this would slightly affect the valve lift and duration. To allow for this in a real engine, there is a small linear ramp before and after the main curved lift profile on the camshaft. The Excel simulation catered for the ramps by allowing the user to choose what percentage of the ramp should be included with the main valve lift. The change in cylinder pressure at the start of compression indicated what ramp setting was required.

Inlet valve shrouds – Column J

In the engine studied there were squish zones between both of the inlet valves and the exhaust valves, as shown in Figure 2.2. This feature also acted as valve shrouding which affected the air flow into the cylinder through the inlet valves, as strongly suggested by the motored rig work. This feature was included in the chart to act as a visual reminder for the user to examine the data for any correlation between time of fuel impact and point at which valve shrouding ceased to be effective. The setting used for this feature could be tuned by the user, although it was difficult to find an ideal value in this work.

IVO – Column K

This column searched the inlet valve lift column for when the inlet valve first opened, which was an event influenced by the cylinder head used and simulated ramp value chosen by the user. The crank angle at which IVO occurred was then detected and recorded in the relevant cell in this column. This value of IVO was then presented at the top of worksheet 'Main'.

IcdA – Inlet Coefficient of Discharge and Flow Area – Column L

This column primarily calculated the curtain area of the valve using both the valve diameter and lift. The "1" in the equation is where real lift-dependant values of discharge coefficient could be included by the user at a later date to increase the functionality of the program, although it was believed the benefits of including this in this work were limited. The compressible flow equations were also designed to cope with these coefficients. This coefficient is considered because the flow in the real engine can separate from the valve seats and the duct wall and also experience various boundary layer effects and friction, which result in the actual flow area being smaller than the geometric area.

Inlet f/r c/u – Forward or Reverse, Choked or Un-choked Flow – Column M

This column used the inlet manifold and cylinder pressures along with the critical pressure ratio to determine the nature of flow through the valves, rather than magnitudes. This was a useful checking tool when creating the Excel model. If the valves were closed, there would be no flow through them. Depending upon the pressures and temperatures encountered either side of open valves the flow would be either forward or reverse and un-choked or choked. When the exhaust valve is nearly closed, the cylinder

pressure is at approximately atmospheric pressure, so when the inlet valves open, the cylinder pressure will be greater than the inlet manifold pressure. This will cause a brief period of reverse flow through the inlet valves before the downward movement of the piston induces forward flow through the inlet valves. This point of forward flow was of interest in this work as it indicated when any fuel in the inlet port or on the inlet valve could potentially be re-entrained into the forward flow to cause cylinder bore wetting.

The nature of the flow could be established using the compressible flow equations [Stone (1999)]. These equations were used for calculating the mass flow rates across the inlet and exhaust valves, which are effectively poppet valves. They are based on isentropic flow of a compressible fluid through an orifice and are derived from the application of the General Flow Energy Equation to compressible flow in a duct. The driving force for this mass flow rate is the difference between the upstream and downstream pressures. In all of the equations, a subscript 1 represents upstream conditions, while a subscript 2 represents downstream conditions. The flow is subsonic throughout most of an engine cycle, but if the downstream pressure drops below a certain level, the flow becomes sonic, where the critical pressure ratio determines whether the flow is subsonic or sonic. The actual equation entered in Excel would assume the flow was zero if the valve was closed or the pressure difference across the valve was zero. The equation then calculated whether the flow was forward or reverse (f/r) and then if it was a choked or un-choked (c/u) flow.

Critical pressure ratio [Stone (1999)]:

$$\left(\frac{p_2}{p_1}\right)_{crit} = \left(\frac{2}{\gamma_1 + 1}\right)^{\frac{\gamma_1}{\gamma_1 - 1}} \qquad \ldots(5.4)$$

Inlet m f/r c/u – Forward or Reverse, Choked or Un-choked Mass Flow – Column N

This equation used the same logic as the previous column, but calculated actual values of mass flow instead of simply presenting the relevant flow type.

Subsonic flow [Stone (1999)]:

$$\frac{dm}{dt} = C_d\ A_2\ p_1 \sqrt{\left\{\left(\frac{2\gamma_1}{\gamma_1 - 1}\right)\frac{1}{RT_1}\left[\left(\frac{p_2}{p_1}\right)^{\frac{2}{\gamma_1}} - \left(\frac{p_2}{p_1}\right)^{\frac{\gamma_1+1}{\gamma_1}}\right]\right\}} \qquad \ldots(5.5)$$

Sonic flow [Stone (1999)]:

$$\frac{dm}{dt} = C_d\ A_2\ p_1 \sqrt{\left\{\frac{\gamma_1}{RT_1}\left(\frac{2}{\gamma_1 + 1}\right)^{\frac{\gamma_1+1}{\gamma_1-1}}\right\}} \qquad \ldots(5.6)$$

In fact, the downstream pressure should be the pressure at the throat, but since this was not known, the pressure of the turbulent downstream volume, i.e. the cylinder was used on the reasonable assumption that no significant pressure recovery took place. In using the compressible flow equations, γ was assumed to have a constant value of 1.4, since the gas present was taken to be air, with c_p and c_v being 1005 J/kgK and 718 J/kgK respectively [Rogers and Mayhew (1992)]. These equations are also seen to contain discharge coefficient 'C_d' and valve curtain area 'A' as already calculated in column L.

The trace representing inlet valve flow on the final display chart does not show the magnitude of flow through the valves, but rather a simplified representation that denotes no flow, forward flow and reverse flow. If the user wanted the actual values, they would be clearly presented in the 'Main' worksheet.

Inlet gas velocity – Column O

There was a small possibility that some fuel could remain on the back of the inlet valves and that it could become re-entrained into the flow at some time after injection was complete. By knowing the gas velocity, an estimate could be made on how long it would take for such fuel stripped from the valves to reach the cylinder wall.

The mass transfer equations for compressible flow can be modified to find the flow velocity through the valve throat C_2. The equations were simplified when the upstream velocity C_1 was assumed to be zero. The flow velocity equation was similar in nature to the mass transfer equation.

Subsonic flow [Stone (1999)]:

$$C_2^2 - C_1^2 = \left[\left(\frac{2\gamma_1}{1-\gamma_1}\right)RT_1\left\{\left(\frac{p_2}{p_1}\right)^{\frac{\gamma_1-1}{\gamma_1}} - 1\right\}\right] \quad \ldots(5.7)$$

Sonic flow [Stone (1999)]:

$$C_2^2 - C_1^2 = \left(\frac{2\gamma_1}{1+\gamma_1}\right)RT_1 \quad \ldots(5.8)$$

Exhaust lift, Exhaust shroud, EVO, EcdA, Exhaust f/r c/u and Exhaust m f/r c/u – Columns P to U

These are identical to their inlet equivalents with the only difference being which cells are observed for lift, MOP and percentage of ramps used.

Injection – Column V

This column was the first in a series of logic-based columns that used the values from the top of column A in worksheet 'Main' to calculate possible fuel impaction event times within the cylinder. To calculate whether injection was occurring, the values of SOI and the duration of injection were used, where in the column, injection was represented by a "1" and no injection was represented by a "0".

All direct wall – Column W

Columns W, X and Y were logic-based and used in combination to calculate when an event might occur in crank angle degrees. Column W calculated a window in crank degrees from when the first to the last of the injected fuel could possibly impact the cylinder bore. In this, it was imagined that the valves were fixed fully open. The crank angle of the earliest impact would be the sum of the crank angle for start of injection, the

shortest fuel flight time from injector to valve and shortest fuel flight time from valve to wall. The latest the injected fuel could impact the bore was the sum of the crank angle for the start of injection, the injection duration, the longest flight time from injector to valve and the longest flight time from valve to wall. To create longer flight times, the user could enter a speed reduction factor to cater for droplets that might be travelling slower, where this was expressed as a percentage of the fastest injected fuel.

Direct window – Column X

This column calculated the largest possible impact window that could occur considering the fuel flight times and when the inlet valves were open. The earliest impact time was the sum of the crank angle for IVO and shortest flight time from valve to wall. The latest impact time was the sum of the crank angle for IVO, valve lift duration and longest flight time of fuel from valve to wall.

Direct impact – Column Y

This column simply considered if the above two cases were true, where fuel was injected and the valves were open. So, this column allowed for the valve event, injection timings and all fuel velocities.

Gas forward – Column Z

This logic-based column searched for when there was the first forward flow into the cylinder. This required knowledge of if the inlet valves were open and the inlet manifold and cylinder pressures. The crank degree at which the first forward flow occurred was presented in the appropriate cell in this column.

Gas impact – Column AA

This logic-based column considered how any fuel that may have been on the inlet valves could have been sucked from the valve and re-entrained in the flow into the cylinder at the flow velocity. The point of first forward flow was found by column Z and for convenience, the forward flow velocity used by the analysis programme at this point was the highest velocity found during the entire valve event. This assumption presented the largest possible window when such forward flow re-entrainment could cause bore wetting. The earliest time the flow could impact the wall was the sum in crank angle of

when forward flow occurred and the shortest time of flight from the valves to the cylinder wall at this velocity. The latest point at which the flow could impact the wall was the sum of the crank angle for IVO, inlet lift duration and longest time of flight from the valves to the wall at the lowest flow velocity, as tuned by the user as a percentage of the fastest flow velocity.

5.3.6 Worksheet 'Plotting'

The main purpose of this worksheet was to allow the manipulation of the numerous calculated data sets to allow them to be presented on one chart with scaled arbitrary units on the secondary y-axis in Excel. The heat flux traces chosen by the user were plotted on the primary y-axis with the correct heat flux units.

5.3.7 Chart

This Excel sheet (Figure 5.12) showed all of the heat flux and calculated values of interest. It was this sheet that formed the basis of the graphical results display in Chapter 6 and the features seen on these charts are explained as follows. The geometric values such as the position of the piston, times when the sensors were covered and the valve lifts are shown at the top of the chart. The actual magnitude of flow through the inlet valves is not shown in the chart, but rather a simplified representation where forward and reverse flows are denoted by linear deviations above and below the zero flow line respectively. The charts show when injection was occurring in addition to the two types of possible bore impaction, these being 'direct OVI bore impact window' and 'forward flow re-entrainment window'. The first comes from the column 'direct impact' in worksheet 'Main' and indicated when fuel could possibly impact the bore directly after exiting the injector at the injection velocity. The second type of impaction was based on column 'gas impact' in worksheet 'Main' and indicated when fuel pulled from the valves could possibly impact on the cylinder bore, regardless of the injection timing. It was only the first of the twelve user plot options in worksheet 'Data' that enabled the injection timing calculations to be performed, so if the user desired to compare two tests on this chart, a test with injection occurring should be opted for in the first option box. These two impaction windows are not shown on any piston based results plots since it was deemed too complex to estimate when such impactions might occur.

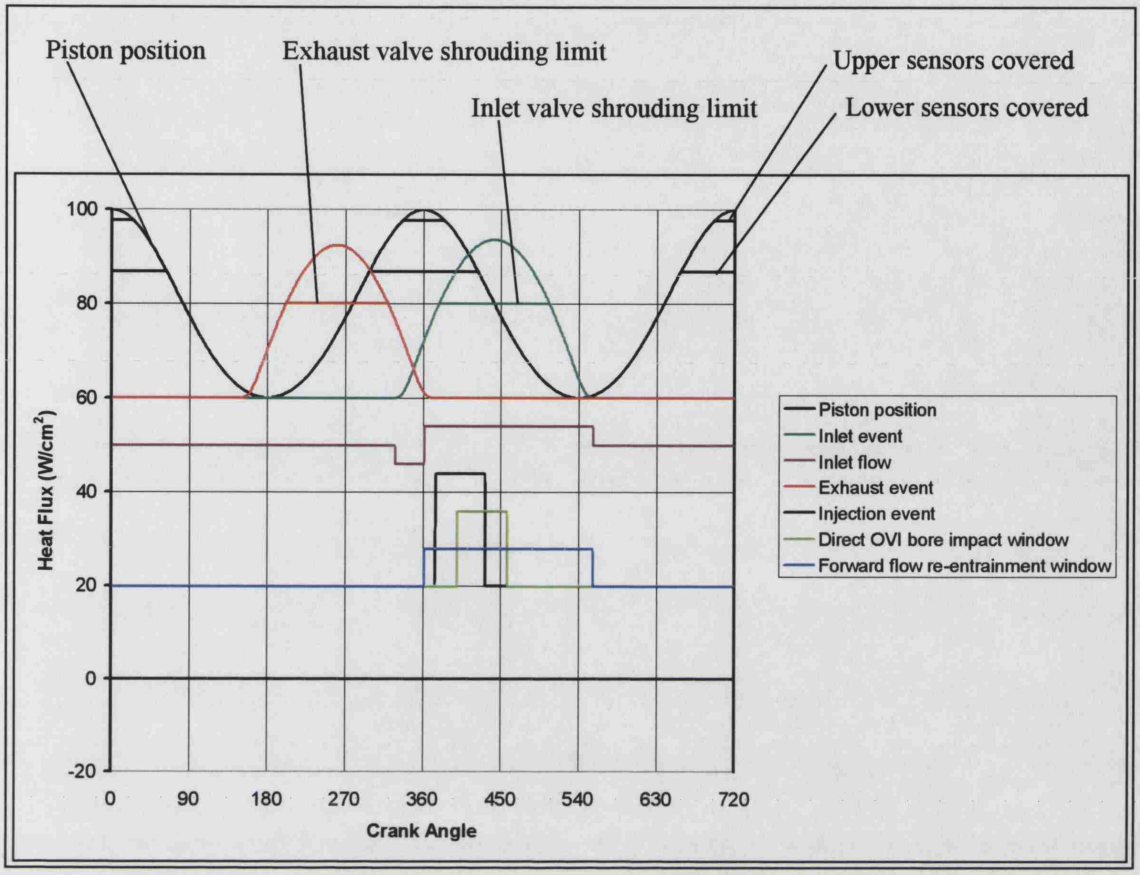

Figure 5.12 Chart layout showing the calculated values and no heat flux traces

The heat flux traces themselves were positioned at the bottom of the chart for convenience, since the area of interest here was the negative values below the x-axis. In a vast majority of the charts, the peak heat flux which started at the onset of compression was clipped from the charts to enable an expanded view of the negative heat flux section.

5.3.8 Worksheet 'Quantity'

This worksheet aimed to provide an estimate of how much fuel was impacting and evaporating from the sensor face. However, because of the strong relationship between these calculations and the measured results, the description of the calculations performed is deferred until Chapter 6.

CHAPTER 6

ENGINE TEST RESULTS AND DISCUSSION

6.1 INTRODUCTION

This chapter commences by describing the experimental variables and calibration tests, together with a discussion on heat flux sensor performance. It then provides all of the important findings and results from the engine equipped with heat flux sensors. The logging and analysis of results were completed using the hardware and software detailed in the previous chapters. It should be noted that the measurements were performed just prior to the demolition of the 1950's built engine test facility at UCL. This meant that the engine was actually moved between test cells part-way through the programme. In addition, there were continuous problems with ingress of water and debris into the test cell which led to the construction of a polythene 'tent' around the engine. Finally, before the results could be analysed, the engine was removed and the laboratory demolished. Thus analysis largely took place without any opportunity to repeat test-points.

6.2 EXPERIMENT VARIABLES

This section briefly highlights the main experiment variables such as the mechanical settings on the engine or numerical settings on the logging computer and how these influenced the discrete sections in which the results are presented.

6.2.1 Inlet Valve Timing, Port Deactivation and Engine Speed

An interesting aspect of this work was the investigation of how inlet valve timing and port deactivation influenced wall wetting. When testing the CP cylinder head the inlet valve timing was set to either fully advanced or fully retarded to generate the largest possible variation in the results. The valve timings used in this work are shown in Table 4.3. The AP cylinder head was tested with and without the dump port deactivated, where in the production engine the dump port was deactivated below 3000 rpm. The engine used in this work was operated at 1200 rpm in all of the experiments (instead of 1500 rpm) due to the lack of speed control on the dynamometer and the possible dangers presented if over-speed occurred. This was not thought to have a major influence on the results since the data from the porous cylinder rig showed that such speed variation did not affect the amount of fuel collected. A manifold depression of 45 kPa and an air mass flow rate of 3.2 g/s were used.

6.2.2 Injection Timings

Identical injection timings were used for both the CP and AP cylinder heads. Motoring tests were performed with a range of start-of-injection (SOI) timings, including 0° CA SOI to represent CVI and a sweep of 270° to 510° CA SOI in 30° CA increments to provide a range of OVI results. It was also standard practice to perform motoring tests with no injection for comparative purposes. The timings used in the firing tests were 0° CA SOI for CVI and 360° and 390° CA SOI for OVI. Sometimes in the results, an injection timing of 360° or 390° CA SOI is shown as the sole OVI timing simply because that timing produced the strongest fuel impaction heat flux signal.

6.2.3 Injection Duration

The Denso 12-hole split-spray injector design was used for all engine tests. It was found that the engine operated most reliably without misfire with an 8ms pulsewidth, so this was used for all of the motoring and firing tests and a stoichiometric air-fuel-ratio was maintained with a load of 2.62 bar BMEP. However, the injection duration was varied in a set of experiments as detailed in Section 6.4.1.

6.2.4 Sensor Location

All of the sensor locations used in this work are shown in Figure 6.1.

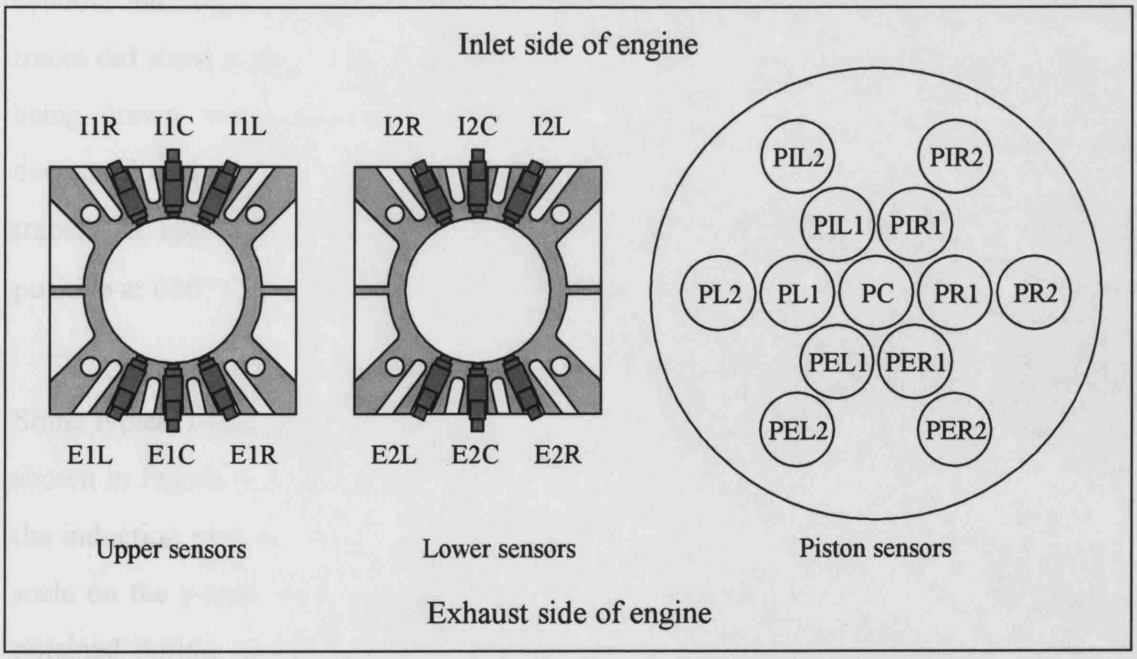

Figure 6.1 Sensor locations in the cylinder block and piston

6.2.5 Typical Motoring and Firing Heat Flux Traces

Figure 6.2 shows typical motoring traces for no injection and both 0° and 390° CA SOI timings at sensor location E1L (exhaust side of bore, top row, left side). All three heat flux readings were at a maximum at 0° CA due to compression heating of the cylinder gases and decreased similarly throughout the expansion stroke during the period that the sensors were not covered by the piston. The piston rings never passed over the sensors, which were instead exposed to a relatively large crevice volume when the piston was near TDC. Over expansion of the cylinder gas, almost certainly caused by slight leakage at the compression ring during the high-pressure part of the cycle was likely. As the gas cooled rapidly during expansion, it is likely that the cylinder wall retained its heat for longer and caused the negative heat flux up until EVO at about 135° CA. Reverse flow of relatively cool air through the exhaust valves into the cylinder then caused a strong negative heat flux of -4 W/cm^2 where this cooling effect was enhanced by forced convection. The heat flux returned close to zero up until IVO, where there were some small undulations due to air motion in the cylinder. Up to this point, the shape of the trace had been independent of the fuel injection event. An extremely important difference occurred just before 450° CA, where the OVI heat flux reading dipped to approximately -3 W/cm^2, whereas both the CVI and no injection heat flux readings were not affected. This was evidence that fuel injected during OVI conditions was capable of crossing the cylinder and impacting directly on the heat flux sensor at this location. The other two traces did show a slight negative heat flux during the inlet period due to the cold inlet air being drawn across the sensors. As the rate of fuel evaporation from the sensor decreased in the OVI test, the trace returned to coincide with both the CVI and no-fuel traces. At approximately 570° CA the inlet valves closed and the heat flux became positive at 630° CA with the cylinder pressure increasing during compression.

Some typical firing traces for sensor location E1L with 0° and 390° CA SOI timings are shown in Figure 6.3. The heat flux readings were seen to be very similar except during the induction period when injected fuel impacted the cylinder bore. In this example, the scale on the y-axis was changed in the recognition of the much higher heat flux values obtained during combustion. This would make discrimination of the traces during the induction stroke more difficult, however the magnitudes of heat flux experienced at this

point were similar to that of the motoring tests as described previously. The heat flux traces remained positive throughout the expansion and exhaust stroke due to the hot combustion products being hotter than the cylinder wall. The heat flux readings during the expansion and compression strokes were not of interest in this work since they did not concern fuel impaction on the bore. In addition, the cylinder sensors were covered by the piston for some time during these periods. For this reason, in the study the peak heat flux values observed during compression was ignored and the y-scale optimised to give best discrimination between the traces during the induction period.

6.2.6 Cylinder Head Temperature

In this work the cylinder block was always kept at 60°C to ensure a strong heat-flux signal when the relatively cool fuel impacted the hot sensor surface. Experiments were performed with an 80°C cylinder block, but the results were identical to that of the 60°C block. However, when tests were run with cylinder head coolant temperatures of 20°C and 60°C, it was found that using a 20°C coolant slightly increased the wall wetting for OVI conditions. Due to this stronger signal, a cylinder head coolant at 20°C was used in all of the logged tests. Figure 6.4 compares the heat flux traces obtained when using OVI and both cylinder head temperatures.

6.2.7 Number of Cycles Logged

Figure 6.5 shows the heat flux traces generated by tests performed using 1, 10, 25 and 50 cycles, where a group of four tests was performed for each number of cycles. The groups for each number of cycles were artificially offset from one another by one heat flux unit in this plot to aid clarity. Logging one cycle alone was of little value since cycle to cycle variation and the digital steps incurred during logging were still observed. Logging ten cycles was an improvement and twenty-five cycles gave even better consistency. Although fifty cycles gave the best repeatability, it was not much better than logging twenty-five cycles and the shear bulk of data caused problems with the logging hardware. Twenty-five cycles also complied with the 95% confidence limit, where there was 95% confidence that the standard deviation of the data fell within recognised upper and lower limits, as calculated from statistics theory [Hoel (1984)] and using the mean, standard deviation and number of cycles logged for this data set.

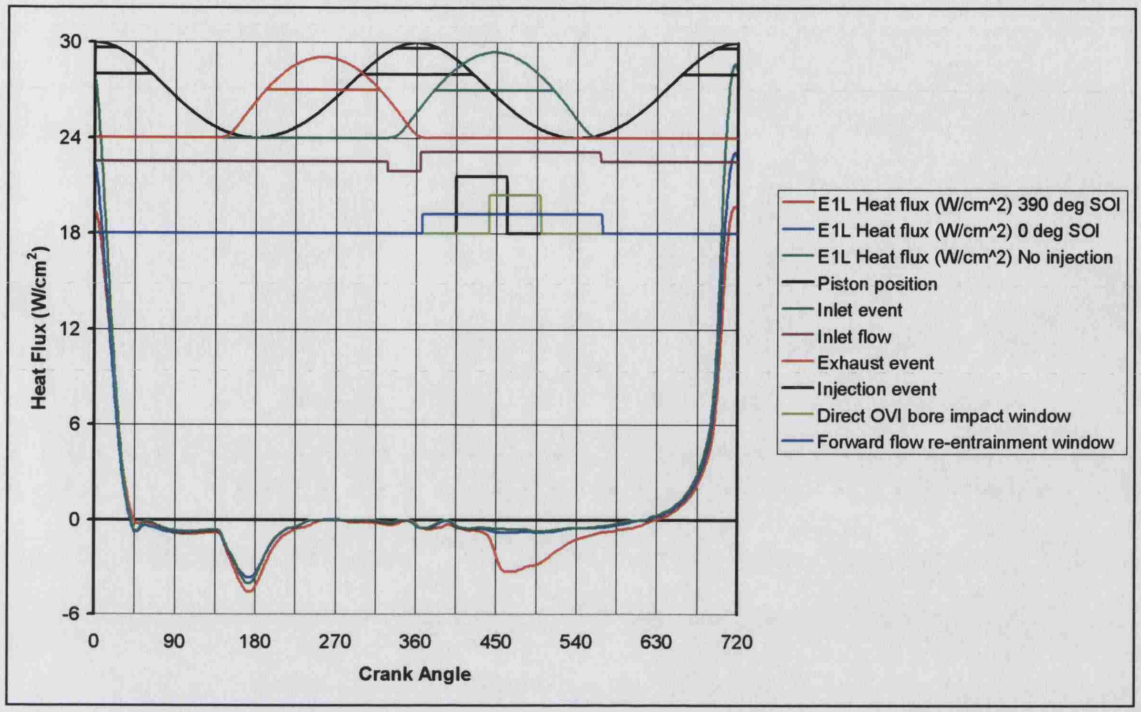

Figure 6.2 Typical motoring heat flux traces from location E1L comparing OVI (390° CA), CVI (0° CA) and no injection

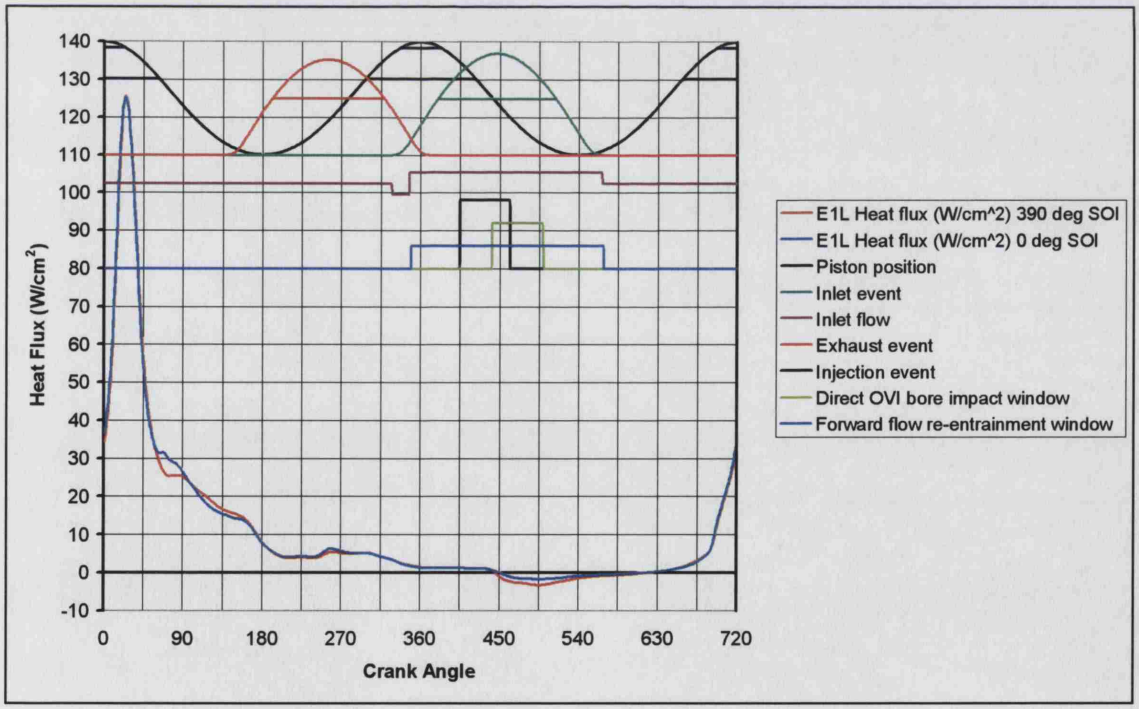

Figure 6.3 Typical firing heat flux traces from location E1L comparing OVI (390° CA) and CVI (0° CA)

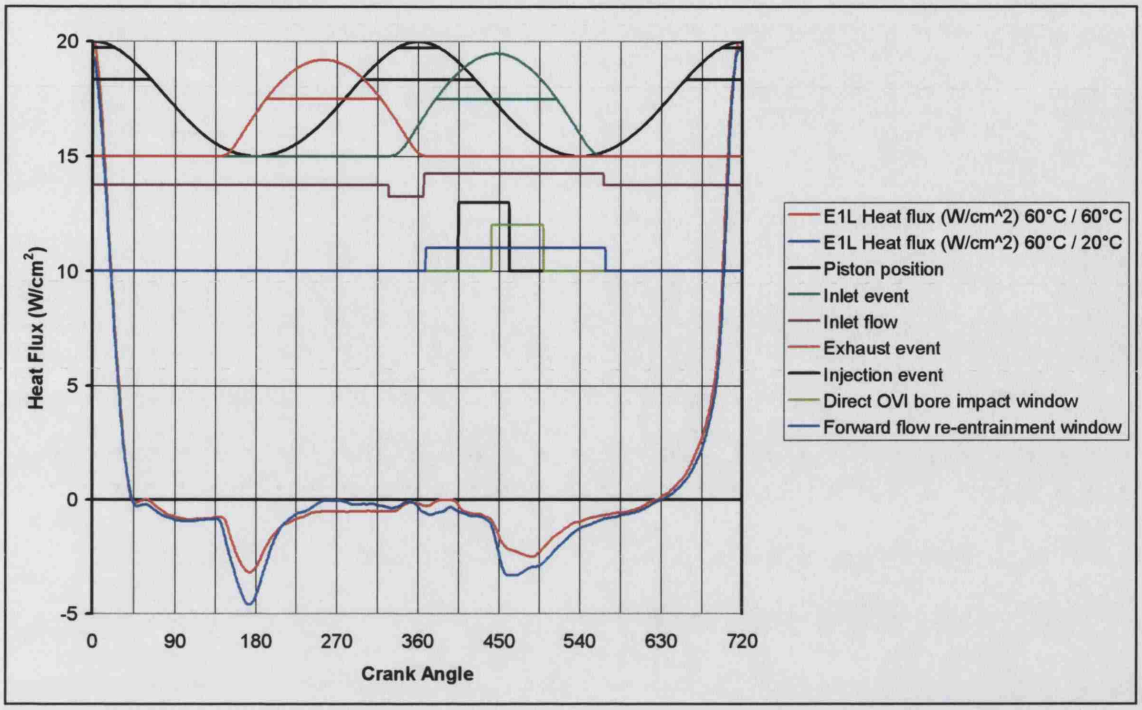

Figure 6.4 Motoring heat flux traces from location E1L with cylinder head coolant temperatures of 60°C and 20°C with a 60°C cylinder block coolant

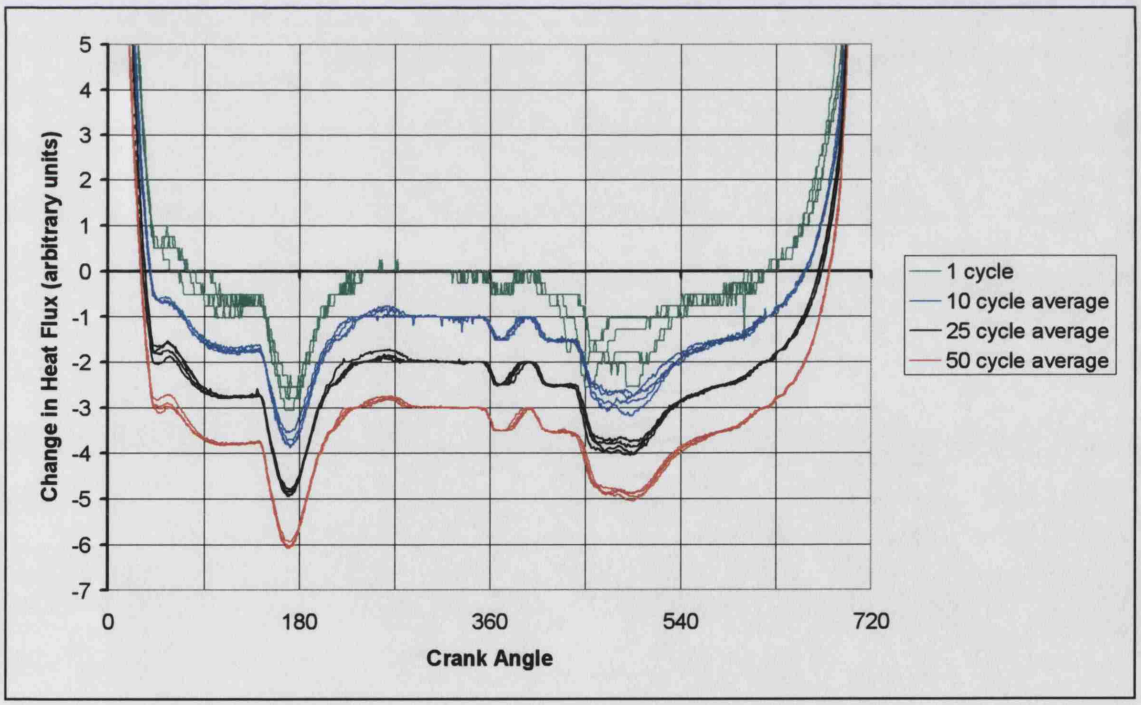

Figure 6.5 Motoring heat flux traces from location E1L when varying the number of OVI (390° CA) engine cycles logged (groups of traces are offset vertically by one increment to aid comparison)

6.3 FAILURE OF SENSORS AND SENSOR COATINGS

This section details how failures of the sensors and their coatings affected the programme and their results. The face of the sensors was covered with a black zynolyte coating and Vatell advised the author of this work that this coating was provided in order to improve the ability of the device to properly include heat transfer by radiation in the heat flux measurements. A non-coated sensor with a more reflective surface would be less capable of achieving this [Cengel (1994)]. Ioannou had experienced problems with the black coating on the sensor faces wearing away during firing tests and taking note of this information it was decided from the outset that where possible, standard motoring tests should be performed prior to firing tests, so as to increase the useful life of the sensors. Under motoring conditions the sensors operated as desired, but when some firing tests were attempted the sensors failed and in a different way to that expected. Due to the elevated pressures and temperatures, the failure would involve the inner thermocouple section of the sensor being pushed back within the nickel housing, loosening the rear electrical connection. During one test these parts were pulled back into the cylinder (presumably during the intake stroke) and were compressed between the piston and cylinder head, substantially damaging both engine components. While the sensors were being modified and repaired by the manufacturers, the CP cylinder head and piston crown were repaired simultaneously. Although the manufacturers were confident that this series of failures was due to a faulty batch, it was now decided that the possible risk to the engine and time plan of the work was sufficiently great that all the motoring tests should precede the more stressful firing tests. When the repaired sensors were returned to UCL, a second problem with the sensors occurred, where the black coating on the sensor face that was intended to improve heat transfer by radiation was being attacked and quickly removed by the gasoline, even during the motoring tests. The remainder of the tests had to be completed without the black coating because there was no time for the sensors to be re-coated by the manufacturers. This was not a concern because the amount of heat transfer due to radiation in the cylinder of a spark ignition engine is small in comparison to the convective heat transfer [Heywood (1988)]. In addition, the primary interest of this study was the intake and early compression portion of the cycle.

When testing recommenced with the black coating removed, it was immediately apparent that the response of the sensors to the convective heat transfer had changed. It was apparent that whilst making the sensors more receptive to heat transfer by radiation, the coating had been acting as an insulator which slowed the response of the devices to convective heat transfer. Since the initial motoring tests on the CP cylinder head with the coated sensors had indicated that the upper exhaust-side sensors experienced the most fuel wetting, a thorough injection sweep was performed with non-coated sensors at these 3 locations. When typical heat flux traces for coated and non-coated sensors are shown on the same plot (Figure 6.6), it is clear that the response and magnitude of the signals from the non-coated sensors were superior.

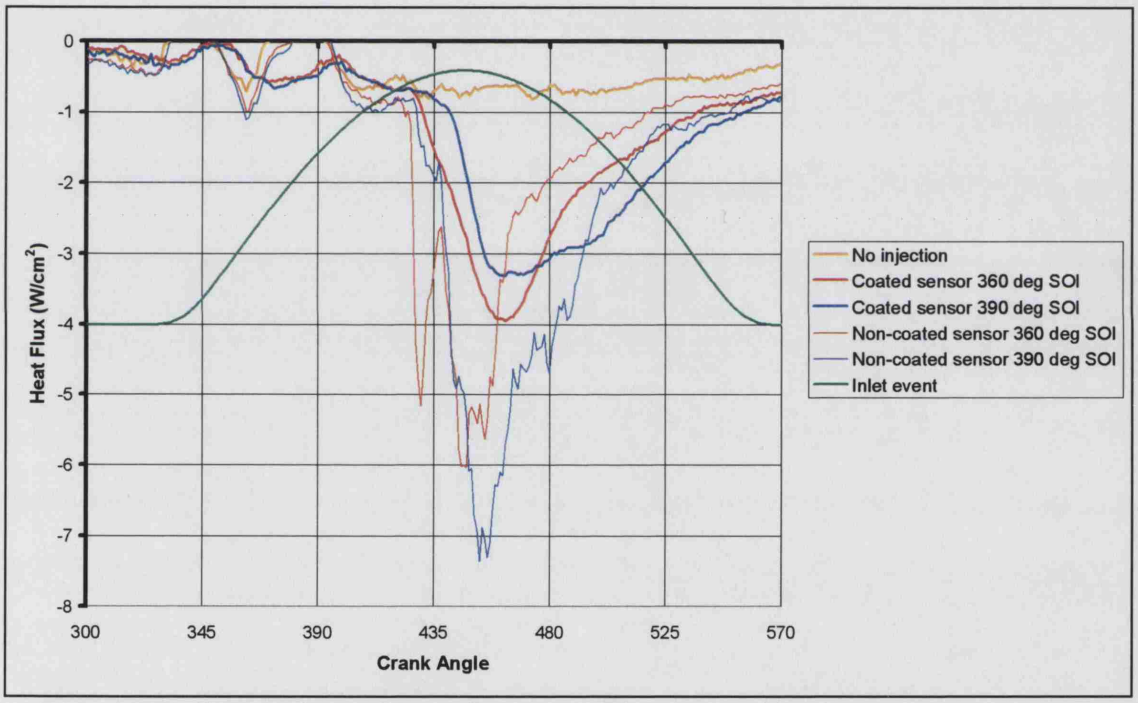

Figure 6.6 Comparison of heat flux traces from coated and non-coated sensors

There was a concern was that the steady state calibration of the sensors had changed with the coating removed. To ensure that the calibration was still valid, a simple steady-state calibration test was performed with the tips of the coated and non-coated sensors submerged in a water bath that was heated to 75°C while being stirred. The temperature and heat flux readings from both the coated and non-coated sensors were found to be identical, ensuring that the sensors were providing correct results and that the increased values from the non-coated sensors were only caused by the faster sensor response.

Figure 6.6 was used to measure the rate of increase in heat flux observed when using the coated and non-coated sensors. Both sensors detected the start of fuel impaction at approximately 420 °CA and both sensors generated heat flux traces that contained linear sections during this impaction period, but the slope of the non-coated heat flux trace was much steeper. The time taken for the heat flux to change by 3 W/cm^2 over this linear period was noted and the respective rates of change in heat flux are shown in Table 6.1.

Non-coated sensor (W/cm^2 per crank degree)	**Coated sensor** (W/cm^2 per crank degree)
0.8	0.1

Table 6.1 Gradient of heat flux traces during fuel impaction period

Possession of more responsive sensors was a huge advantage in the study of wall wetting as additional features could be observed in the heat flux traces, but a problem did arise in that many of the experiments had already been performed with the coated sensors. However, the traces from the coated sensors did reveal if wall wetting was occurring at a particular sensor location during a specific engine condition and it was decided that the most important tests should be repeated with the non-coated sensors. This not only allowed the collection of further wall wetting information for these important tests, but also permitted a sensor comparison to be performed that could be useful for the study of test results logged by coated sensors if needed at a later date.

6.4 QUANTIFICATION OF IMPACTED FUEL

6.4.1 Pulsewidth Variation Tests

The possibility of quantifying the amount of fuel that impacted the cylinder bore was first realised when performing the pulsewidth variation tests. In these motoring tests, the SOI timing was fixed for a series of test runs which used successively longer injection pulsewidths and a heat flux trace with no injection taking place was also logged for both cylinder heads to aid later analysis. The logged heat flux traces were then plotted on the same chart.

When a successively longer pulsewidth was used, an increasingly more negative heat flux value would be attained and the area enclosed between these successive 'wet' heat flux traces and the 'dry' no-injection heat flux trace would grow proportionately. The results of these tests formed the backbone of the quantitative fuel analysis in Excel as they confirmed that the area enclosed by these 'wet' and 'dry' heat flux traces was proportional to the amount of fuel injected. It was then intended that a numerical relationship between the area enclosed by the traces and wall wetting should be found.

The pulsewidth variation test performed on the CP cylinder head used a fixed 390° CA SOI timing and varied the injection duration from 2 to 20 ms. This value of SOI was used because it generated the strongest heat flux signals when performing the conventional motoring tests with an 8 ms pulsewidth. The pulsewidth variation test performed on the CP cylinder head used a coated sensor at location E1L and the resulting heat flux traces can be seen in Figure 6.7. The pulsewidth variation test performed on the AP cylinder head used 360° CA SOI timing and non-coated sensors at sensor location E1L. The AP tests also used injection durations of 2 to 20 ms and the resulting heat flux traces are shown in Figure 6.8.

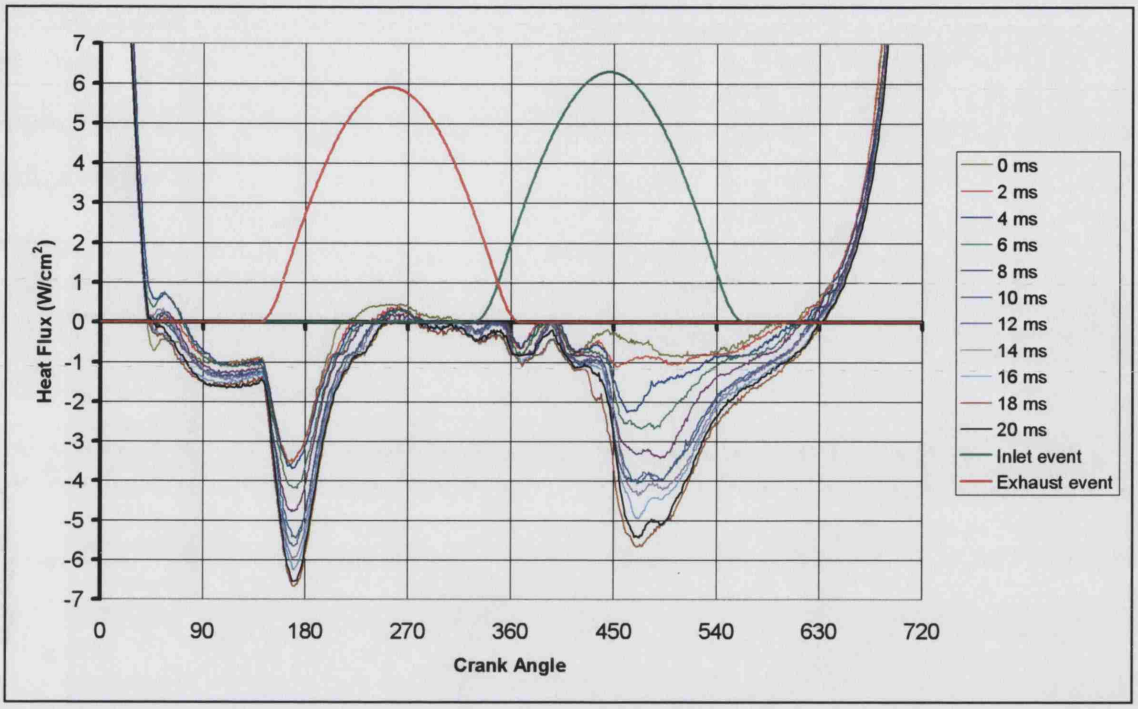

Figure 6.7 Pulsewidth variation test at E1L with fixed 390° CA injection timing (CP cylinder head, advanced inlet, motoring)

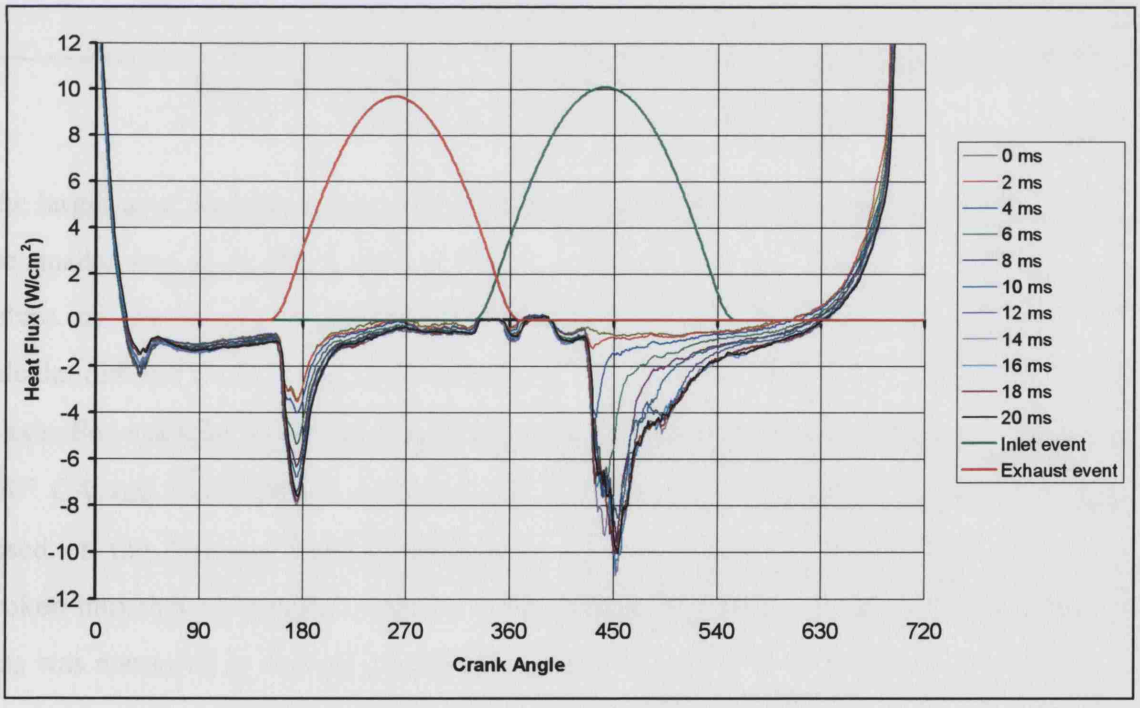

Figure 6.8 Pulsewidth variation test at E1L with fixed 360° CA injection timing (AP cylinder head, activated port, motoring)

Microsoft Excel was used to perform this quantification. The first task was to calculate the areas enclosed by the 'wet' and 'dry' heat flux traces that represented the evaporation of fuel from the sensor surface, where the two areas of interest are shaded black in Figure 6.9.

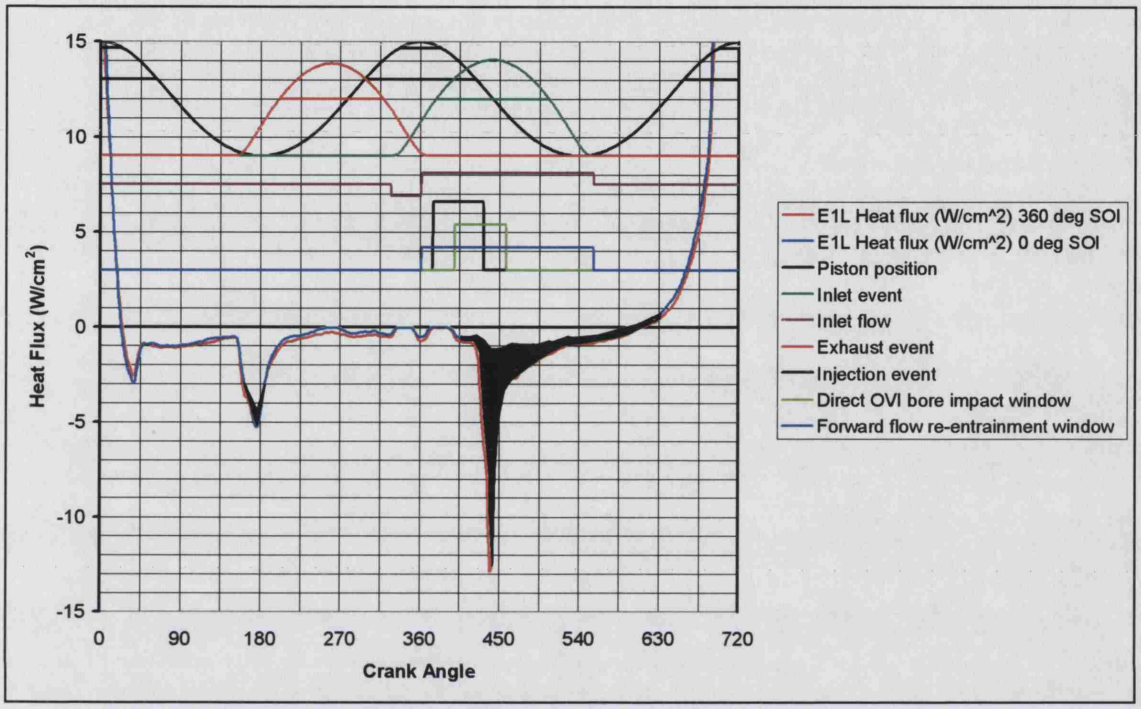

Figure 6.9 Area enclosed between wet and dry traces

The larger area was due to the main fuel impaction event which started at 420° CA and the smaller area soon after EVO was due to a period of reverse flow through the exhaust valves and forced convection during the exhaust event itself. To add flexibility to the calculations and focus on the areas of interest, two pairs of limits were introduced for the x-axis. For example, area calculations were restricted to the periods between 90° CA and 270° CA and 360° CA and 630° CA. The actual method of calculating the areas was based on the Simpson Rule of integration where the enclosed areas were effectively broken into thin rectangular strips to make calculation accurate and easy. Since the x-axis was measured in degrees crank angle which was readily converted into seconds and the y-axis was measured in W/cm^2, the area enclosed between the traces was in units of J/cm^2. By multiplying this enclosed area (A_E) by the circular area of the sensor tip (A_S), a value in joules could be calculated that represented the energy needed to evaporate the fuel from the sensor tip.

Dividing this value by the enthalpy of evaporation of gasoline of 310 J/g [Stone (1999)], a value for the mass of fuel evaporated (M_{fuel}) was found. This assumes no flow of fuel to or from the sensor except during injection and that there is no fuel accumulation.

$$M_{fuel} = \frac{A_E A_S}{310}$$

Although a study of inlet port fuel wetting with a CVI strategy by Burton (2004) concluded that the energy transfer from the port surface to the fuel caused both fuel warming and evaporation, only evaporation was considered here. This was for simplicity and due to the fact that high levels of forced convection experienced within the cylinder greatly assist fuel evaporation. The process of modelling fuel evaporation was also researched by Jackson (1996) and it was found that the extreme complexity of both the heat transfer process and the changing flow properties within the cylinder of the engine inhibit the ability to create an ideal theoretical model of this problem. This simplified approach provided a convenient value for fuel evaporated from the sensors that could be used to compare results from different cylinder heads or the motored rig work. The results from the pulsewidth variation tests were plotted with the mass of fuel injected on the x-axis and the mass of fuel evaporated from the sensor on the y-axis (Figure 6.10).

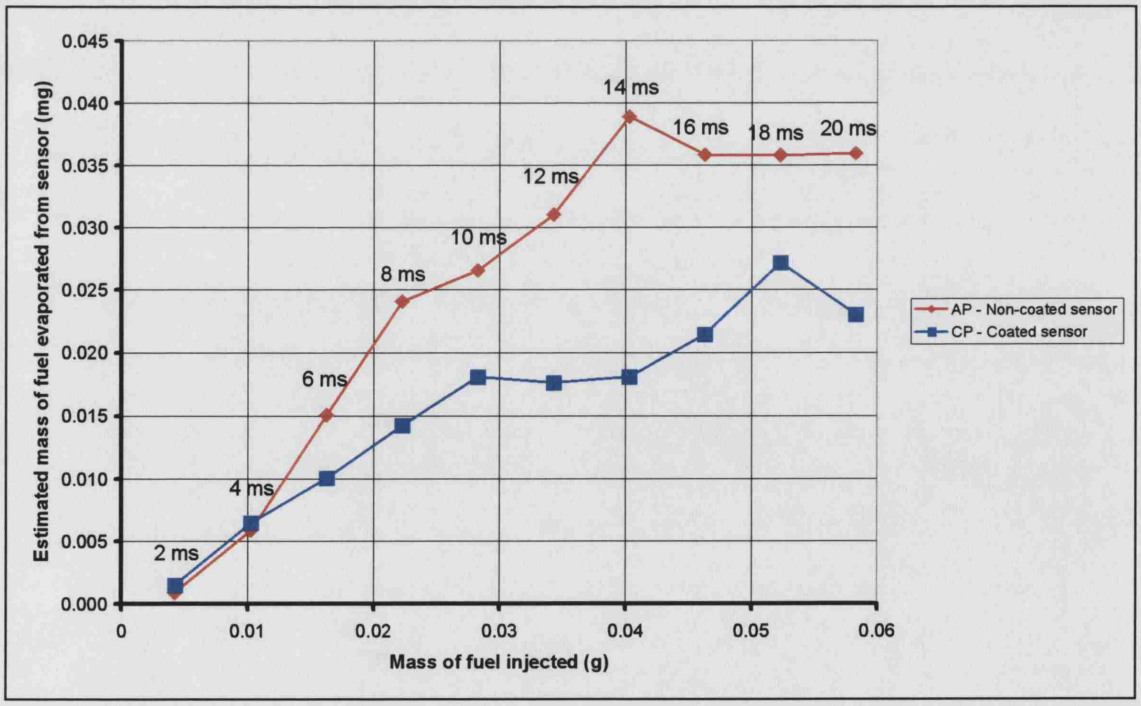

Figure 6.10 Injected and evaporated fuel masses during pulsewidth variation tests

6.4.2 Quantitative Comparison of Coated and Non-coated Sensors

It was clear from Figure 6.10 that the coated sensor trace from the CP head fell some way below that of the non-coated sensor trace from the AP head. It was appreciated that the different cylinder head designs would account for some of this difference, although the response of the sensors was felt to be the more likely cause due to the quite different heat flux response curves obtained for both sensors in Figure 6.6. In order to quantify the difference between the coated and non-coated sensors, a special set of tests was performed that used only the CP cylinder head, sensor location E1L and an injector sweep using standard injection pulsewidths of 8 ms. A test run with no injection occurring was also performed so as to allow the areas enclosed by the 'wet' and 'dry' heat flux traces from the different SOI timings to be compared. Calculation of these areas and estimation of impacted fuel was performed in the same way as in Section 6.4.1. Figure 6.11 shows the results of these tests where the estimated mass of fuel evaporated is plotted against the respective SOI timings. The injection timings that produced the most wall-wetting in this work were seen to be 360° CA and 390° CA. Since injection timings other than 360° CA and 390° CA were affected by the opening and closing of the inlet valves, only these two injection timings were considered any further.

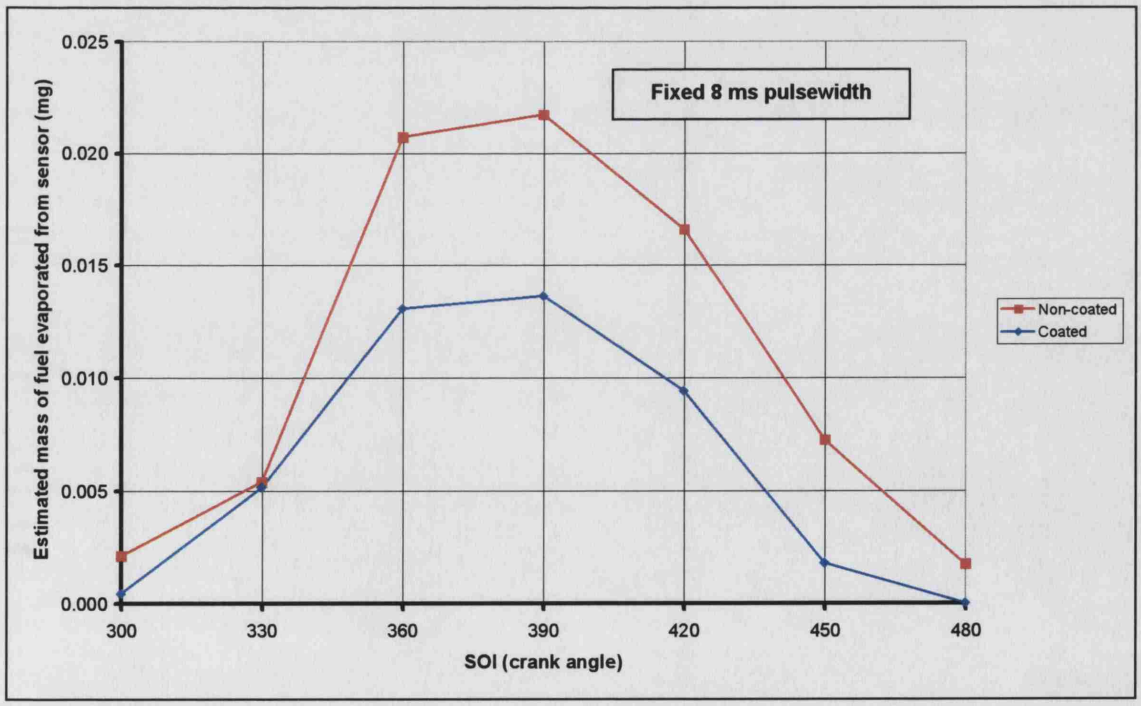

Figure 6.11 Comparison of evaporated fuel for coated and non-coated sensors

The relationship between the coated and non-coated sensors was simply expressed as a multiplication factor between the two different values obtained for the evaporated fuel. This value was conveniently found to be 1.6 for both injection timings. It was appreciated that a more thorough relationship between these sensors could be found, but since a majority of the tests used non-coated sensors and that any experiments of value were repeated with non-coated sensors, additional work on this problem was deemed unnecessary. Section 6.5 describes when each sensor was used.

6.4.3 Worksheet 'Quantity'

Figure 6.12 shows Worksheet 'Quantity' from the analysis program. This used the ideas and techniques already discussed in Section 6.4.1 for estimating the mass of fuel evaporated from a heat flux sensor. This worksheet also compares the amount of fuel detected by the heat flux work to that collected by the porous liner work.

	H	I
	EVO area	SOI area
Start CA:	90	360
Stop CA:	270	630

Crank Angle	Wet trace (W/cm²)	Dry trace (W/cm²)	Wet area (J/cm²)	Dry area (J/cm²)	EVO area (J/cm²)	SOI area (J/cm²)
0	16.39372	18.50993	0.0	0.0	0.00000	0.00000
1	15.79607	17.84133	0.002235	0.00252	0.00000	0.00000
2	15.15007	17.09382	0.002149	0.00243	0.00000	0.00000
3	14.45971	16.24711	0.002056	0.00232	0.00000	0.00000
4	13.74905	15.30154	0.001959	0.00219	0.00000	0.00000
5	12.99619	14.31753	0.001857	0.00206	0.00000	0.00000
6	12.22316	13.29517	0.001751	0.00192	0.00000	0.00000
7	11.43177	12.24255	0.001643	0.00177	0.00000	0.00000
8	10.62428	11.19998	0.001532	0.00163	0.00000	0.00000
9	9.79462	10.19001	0.001418	0.00149	0.00000	0.00000
10	8.95899	9.16785	0.001302	0.00134	0.00000	0.00000
11	8.10918	8.18590	0.001185	0.00121	0.00000	0.00000
12	7.26755	7.25852	0.001068	0.00107	0.00000	0.00000
13	6.45820	6.39784	0.000953	0.00095	0.00000	0.00000
14	5.69513	5.58752	0.000844	0.00083	0.00000	0.00000
15	4.96439	4.82769	0.00074	0.00072	0.00000	0.00000
16	4.28608	4.11437	0.000642	0.00062	0.00000	0.00000
17	3.63603	3.43135	0.00055	0.00052	0.00000	0.00000
18	3.01827	2.75642	0.000462	0.00043	0.00000	0.00000
19	2.42882	2.10774	0.000378	0.00034	0.00000	0.00000
20	1.88372	1.50149	0.000299	0.00025	0.00000	0.00000
21	1.37294	0.92959	0.000226	0.00017	0.00000	0.00000
22	0.92270	0.40013	0.000159	9.2E-05	0.00000	0.00000
23	0.48659	-0.07277	9.79E-05	2.3E-05	0.00000	0.00000
24	0.07268	-0.49513	3.88E-05	-3.9E-05	0.00000	0.00000
25	-0.30894	-0.87304	-1.6E-05	-9.5E-05	0.00000	0.00000

Area enclosed between wet and dry traces (J/cm²)	0.042
Coated sensor (1.6) or uncoated sensor (1.0)	1.0
Energy needed to evaporate fuel from sensor area (J)	0.0083
Estimated mass of fuel detected by heat flux sensor (g)	0.00003
Injection pulsewidth used in heat flux work (ms)	8
Mass of fuel per injection (g)	0.0223
Percentage of fuel injected detected by sensor (%)	0.120
Equivalent percentage over porous pocket area (%)	**7.645**
Mass of fuel collected in pocket (g)	0.1652
Injection pulsewidth used in porous work (ms)	4.5
Mass of fuel per injection (g)	0.0118
Percentage of fuel injected collected in pocket (%)	**14**
Fuel detected by heat flux as percentage of porous (%)	**54.61**

Lifts / Tests / Data / Main / Plotting / Quantify / Chart /

Figure 6.12 Calculations on 'Quantity' worksheet

The heat flux data sets for the 'wet' and 'dry' traces were originally chosen by the user in worksheet 'Data' and presented in columns B and C here. The areas enclosed between the x-axis and both the 'wet' and 'dry' traces throughout the entire engine cycle were calculated in columns E and F respectively.

The user then entered four desired values of crank angle into the cells at the top of columns H and I that imposed the limits on the area calculation. Of the incremental areas calculated in columns E and F, only those that fell within the desired limits were included. The total desired net area enclosed between the 'wet' and 'dry' traces was then presented in cell L7. Cell L8 contained a logic statement which established if the data being read from file was for a non-coated or coated sensor, where a 1.0 or 1.6 was presented respectively. Cells L9 and L10 used the area of the sensing tip and the enthalpy of evaporation of gasoline to determine an estimate for how much fuel had been evaporated from the sensor surface. Cell L12 calculated how much fuel was injected into the firing engine and cell L13 expressed as a percentage how much fuel was detected by the sensor as a percentage of the amount of fuel injected. In order to compare this heat flux value with the equivalent value from the motored rig work, cell L14 multiplied the amount of fuel detected by the heat flux sensor by a specific number. This number had a value of approximately 64 and accounted for the ratio of the areas of the heat flux sensor's small tip to the area of the larger collection pocket of the porous liner. Finally, this equivalent value for the heat flux sensor technique was expressed as a percentage of that obtained from the motored rig work in cell L21. The most comparable test condition for the porous liner work and heat flux work was when the AP cylinder head was motored with open valve injection taking place and is the example shown in Figure 6.12. The amount of fuel impaction implied by the results from the heat flux sensors in the firing engine was approximately 55% of the amount of fuel collected by the porous liner technique. It was expected that the heat flux value for the amount of evaporated fuel would be smaller than the value of fuel collected by the motored rig due to several reasons. Firstly, the heat flux engine was warmed by warm water, which would evaporate some fuel prior to detection by the heat flux sensor. Secondly, the large collection pocket of the motored rig, unlike the relatively small tip of the heat flux sensor would ensure that most of the fuel that impacted the bore directly during injection would be detected or collected. The pulsewidth variation test proved that the impact zone does not remain at exactly the same location and emphasised this problem. However, it should not be forgotten that heat flux sensors at other locations were detecting fuel and these could be added to form a revised value for evaporated mass of fuel. The piston motion and air flows also account for some of the differences.

6.4.4 Additional Information from the Pulsewidth Variation Tests

It was noticed from the AP cylinder head curve in Figure 6.10 that the initial 2 ms injection resulted in almost no wall-wetting, indicating that the fuel was not reaching the cylinder wall even though the valve was almost fully open. The 4 ms injection also only added a limited amount of fuel to the cylinder wall. The longer injections of 16, 18 and 20 ms resulted in heat flux readings not much different than that for the 14 ms injection, which indicated that no further fuel had been added to the sensor even though these injections were longer. Figure 6.10 showed the wall wetting was quite similar for injections of 6 ms and 8 ms, but the 10 ms injection did not have the same proportionate increase in wetting, indicating that the fuel droplets were being directed away from the sensor. However, the rate of fuel application seen with the 6 and 8 ms injections returned for the 14 ms injection. Although the equivalent pulsewidth variation plot for the CP head would be expected to be different due to its different design and the use of a less responsive coated sensor, the general shape of the two graph lines for the two traces was very similar.

In an attempt to understand this, focus was placed on the results of the AP head because they were logged with the non-coated sensors. Special emphasis was also placed on the calculation of the times of flight of the fuel droplets to the inlet valves and cylinder wall. The SOI timing set in the injector controller was known to be 360° CA and the time taken for fuel to emerge from the injector was found to be almost 2 ms or approximately 14° CA. This timing was confirmed by Romunde (2004) and the method by which it was found is described in Appendix V. The times of flight for the fuel from the injector to the inlet valve and inlet valve to cylinder wall were 25° CA and 10° CA respectively.

Figure 6.13 plots inlet valve lift and representations of the 2 to 20 ms injections of the pulsewidth variation test for the AP head against crank angle. The different injection pulsewidths are shown twice in such a way that they represent both when the injected fuel would have passed the inlet valves and then when it would have impacted on the cylinder wall, where the bars on the plot represent the final 2 ms of each 360° SOI injection. The wall impaction section (shown in red in Figure 6.13) was included to give a basic indication of when the wall impactions were expected.

The valve passing section (shown in blue in Figure 6.13) describes two vital pieces of information. Firstly it indicates when the injection pulsewidths were scheduled to pass the inlet valves. Secondly the magnitude of these bars represents the area enclosed by the 'wet' and 'dry' heat flux traces by the individual injections. These area values were used because they were deemed as more trustworthy than quoting estimates of mass of fuel which were based on many assumptions.

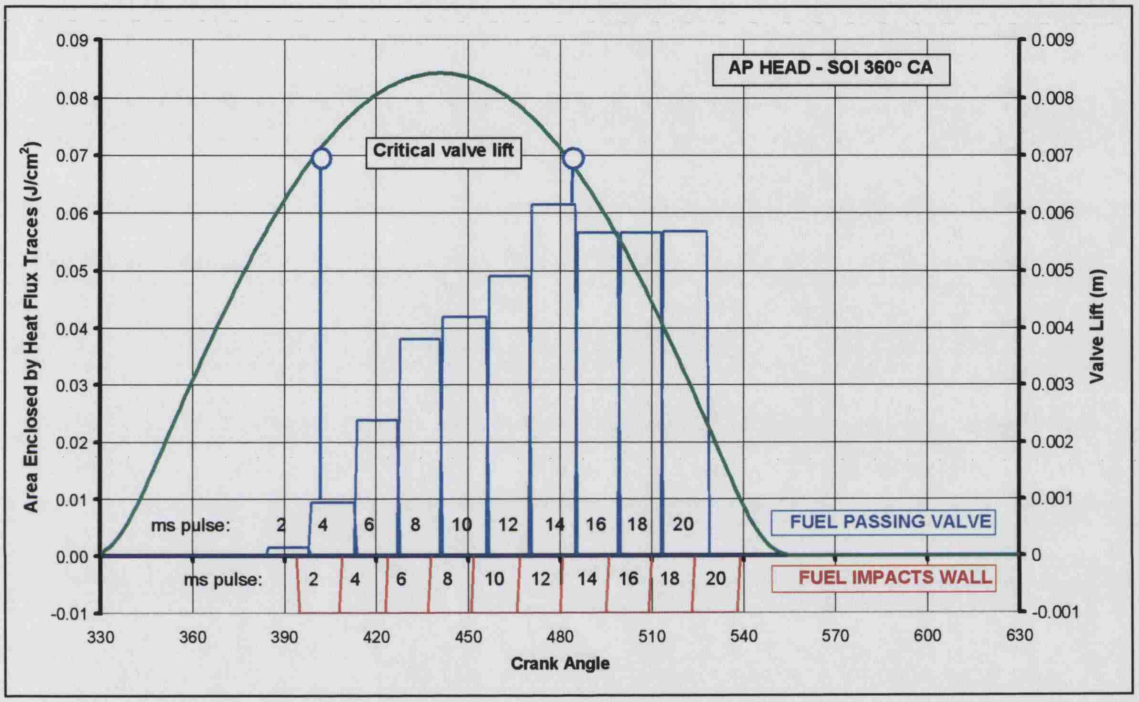

Figure 6.13 Pulsewidth variation test impaction times and wetting events (each bar shows the last 2 ms of a 360° CA injection event)

The heat flux traces in Figure 6.6 showed that the earliest fuel could have impacted the cylinder wall was approximately 420° CA. This was compared with the information in Figure 6.13 where it can be seen that all of the 2 ms injection and a portion of the 4 ms injection were scheduled to impact the cylinder wall before this threshold value of 420 ° CA. The valve passing section of Figure 6.13 shows that if only the tail-end of the 4 ms injection could wet the cylinder wall, it must follow that a valve lift of less than 0.007 m was preventing the fuel droplets from impacting this sensor location. Figure 6.10 also showed that the last three injections of 16, 18 and 20 ms failed to wet the cylinder wall any more than the 14 ms injection. Observation of the valve impact section on Figure 6.13 can reveal that for this truncation of longer injections to occur during the valve

closing period, a valve lift of 0.007 m or less must have been preventing the fuel from impacting the cylinder wall. This indicated that the wetting of this sensor location could only have occurred at a valve lift above 0.007 m. Figure 6.13 also showed that the bar representing the tail-end of the 10 ms injection was not much bigger than that for the 8 ms injection, with the increase being only one third of that expected. This indicated that the wetting was lower than expected and was a trend supported by the CP plot. Since this last section of the 10 ms injection coincided with the point of maximum lift of the inlet valve, it could only be assumed that this reduction in wetting was due to the maximum lift of the valve directing the droplets away from the heat flux sensor.

It was not only the pulsewidth variation tests that showed signs of this fuel droplet deflection. Heat flux traces from any sensor location that detected fuel impaction indicated this effect. When an injection sweep was performed on the CP cylinder head with a non-coated heat flux sensor at location E1L, it was clear than fuel droplets were being directed away from the sensor. Figure 6.14 shows the heat flux traces obtained from this sensor location in addition to theoretical cylinder wall impaction times.

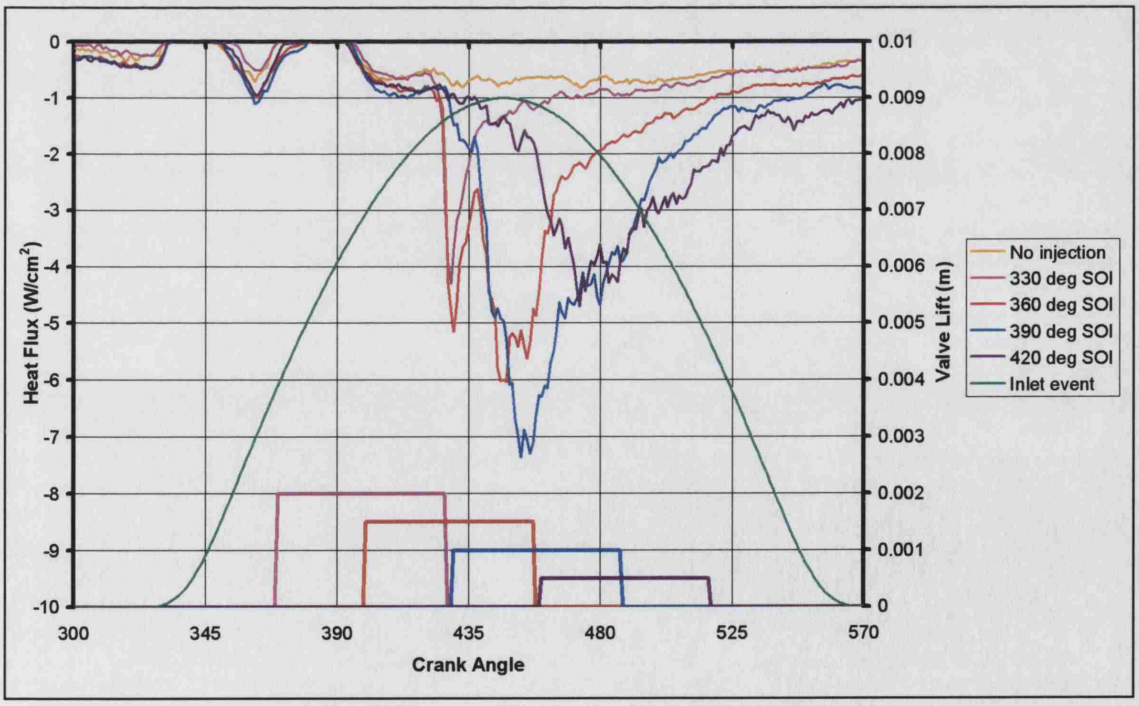

Figure 6.14 Heat flux traces and predicted cylinder wall impactions during an injection sweep at E1L on CP head

The threshold value of 420° CA for the start of impaction was again visible in that it allowed only the tail-end of the 330° CA injection to impact the cylinder wall, where a heat flux of -5 W/cm^2 was observed before the trace returned towards zero. The initial portion of the 360° CA injection was also heavily truncated until the 420° CA threshold value after which the heat flux reached a value -5 W/cm^2 before returning towards zero as with the 330° CA injection. The large spikes at 435° CA were thought to be due to air motion near to the sensor and are discussed in more detail in Section 6.6.1. The heat flux for the 360° CA injection then reached -6 W/cm^2 and became no more negative after approximately 460° CA even though impaction was still scheduled, indicating that these droplets were being directed away from the sensor. Fuel impaction due to the 390° CA injection occurred as expected from 420° CA and reached a heat flux of -7.5 W/cm^2, but stopped at approximately 460° CA which was much earlier than predicted and implied that these droplets were also being directed away from the sensor location. The 420° CA injection started to wet the cylinder wall as expected, but the application of fuel stopped early at approximately 480° CA and the heat flux returned towards zero. Using this 480° CA value and the time of flight from inlet valve to cylinder wall, it was found that an inlet valve lift of less than 0.008 m prevented the fuel droplets from impacting on the sensor surface. This was a higher lift value than the equivalent 0.007 m value found for the AP cylinder head and can be attributed to the different cylinder head design generating different airflows within the cylinder. This flow vectoring effect caused by the inlet valves was observed on several occasions, as is discussed in the main results section.

6.5 ORDER OF PRESENTATION OF REMAINING RESULTS

In summary, a wide range of various tests was performed. Initial calibration tests deduced the optimal number of engine cycles that should be logged and experiments with different engine temperatures set benchmarks for the bulk of the experiments. In the main experiments, the CP cylinder head was tested with different inlet valve timing, while the AP cylinder head was tested with and without port deactivation. Both cylinder heads were tested under motoring and firing conditions with a range of SOI timings and for each of these experimental combinations, the heat flux sensors were positioned in different places on the cylinder bore or piston. Additionally, pulsewidth variation tests

were performed on both cylinder heads. The problems with the sensors complicated the planned test matrix enormously and required some tests to be repeated and the additional coating comparison tests to be performed. The order in which the tests were actually performed is shown in Table 6.2. For simplicity, the results are discussed in the order described in Table 6.3.

Batch	Head	Valve or port	Condition	Sensor	Batch type
1	CP	Advanced inlet	Motoring	Coated	Calibrations
2	CP	Advanced inlet	Motoring	Coated	Standard
3	*CP*	*Advanced inlet*	*Motoring*	*Coated*	*Pulsewidth variation*
4	CP	Advanced inlet	Firing	Coated	Standard
5	*CP*	*Advanced inlet*	*Motoring*	Coated and Non-coated	*Coating comparison*
6	AP	Deactivated port	Motoring	Non-coated	Standard
7	AP	Activated port	Motoring	Non-coated	Standard
8	*AP*	*Activated port*	*Motoring*	*Non-coated*	*Pulsewidth variation*
9	CP	Retarded inlet	Motoring	Non-coated	Standard
10	CP	Retarded inlet	Firing	Non-coated	Standard
11	AP	Deactivated port	Firing	Non-coated	Standard
12	AP	Activated port	Firing	Non-coated	Standard

Table 6.2 Sequence in which the tests were performed

Order	Cylinder head	Valve or port	Condition
1	CP	Advanced inlet	Motoring
2			Firing
3		Retarded inlet	Motoring
4			Firing
5	AP	Deactivated port	Motoring
6			Firing
7		Activated port	Motoring
8			Firing

Table 6.3 Order of results presentation

6.6 RESULTS AND DISCUSSION - CP CYLINDER HEAD

6.6.1 Advanced Inlet, Motoring

Most of the results in this section were generated by coated sensors, although the tests that gave the most interesting results were repeated using non-coated sensors. Traces from coated sensors at locations E1-LCR were included here simply to aid comparison with the equivalent CP firing tests which only used coated sensors.

Sensor locations E1-LCR

The most wall wetting was always observed on the exhaust side of the bore by the upper row of sensors, where these sensor locations E1L, E1C and E1R were collectively designated E1-LCR. This was no surprise because the previous porous liner work predicted that this exhaust side would experience the greater amount of fuel impaction.

Figure 6.18 in the result plot section shows the motored heat flux traces for both 0° CA SOI (CVI) and no injection for when using coated sensors. Since there was no apparent difference between the CVI and no injection heat flux traces during the inlet event, it was concluded that there were no significant fuel droplet populations impacting the sensors during the CVI tests. It is also important to note that the strong correlation between the left, centre and right traces suggests that the airflow over the three sensor locations must be similar. Another feature was how the heat flux dipped to –2.5 W/cm^2 when the sensors were cooled by both a brief period of reverse flow through the exhaust valves at EVO and forced convection during the forward flow that followed. However, when an OVI strategy was employed, fuel impaction on sensors E1L and E1C was readily observed as shown in Figure 6.19, although sensor E1R appeared to have experienced no significant wetting. The fuel impingement first occurred at approximately 425° CA at E1L, then a short time later at E1C with heat flux values of -2.5 and -2.0 W/cm^2 respectively. By 470° CA, the heat flux in both cases started to return to that of the no-injection condition, implying that the majority of the remaining fuel had evaporated. Although it was possible that the fuel had simply 'flowed' away from the sensors, this was thought unlikely as correlation with results from surrounding sensors showed that the fuel did not reappear at another sensor location.

A decrease in wetting from sensor location E1L to location E1R on the exhaust side of the cylinder was in fact a key feature observed throughout the CP and AP results. This was due to the cylinder head designs, where in both cases it was possible to observe sensor location E1L through the right hand swirl port when the inlet valves were fully open. Figure 6.15 shows this effect with the sensor at E1L withdrawn and replaced by a beam of light directed into the empty sensor location. This shows a view of the sensor locations through the AP head rather than the CP head, where despite the physical differences between the CP and AP inlet ports, the area of cylinder bore visible through the opened inlet valves was very similar. When the camera was positioned at different locations in front of the ports, it was possible to observe all of the sensor face at location E1L and a portion of sensor face at location E1C through the right hand swirl port. It was also possible to see a portion of the sensor face at location E1C through the left hand dump port. Location E1R could not be seen through either port. The injector did not however have a clear line of sight of any part of the cylinder bore, but it was conceivable that the injected droplets could be entrained in the airflow and impact on the sensors. Some of the fuel droplets may even have impacted on the inlet valves and then been quickly re-entrained into the flow. Some of the droplets were probably vaporised on the back of the inlet valves as was confirmed by the initial cylinder head water temperature calibration test when a warmer coolant temperature reduced cylinder wall wetting even for an OVI strategy.

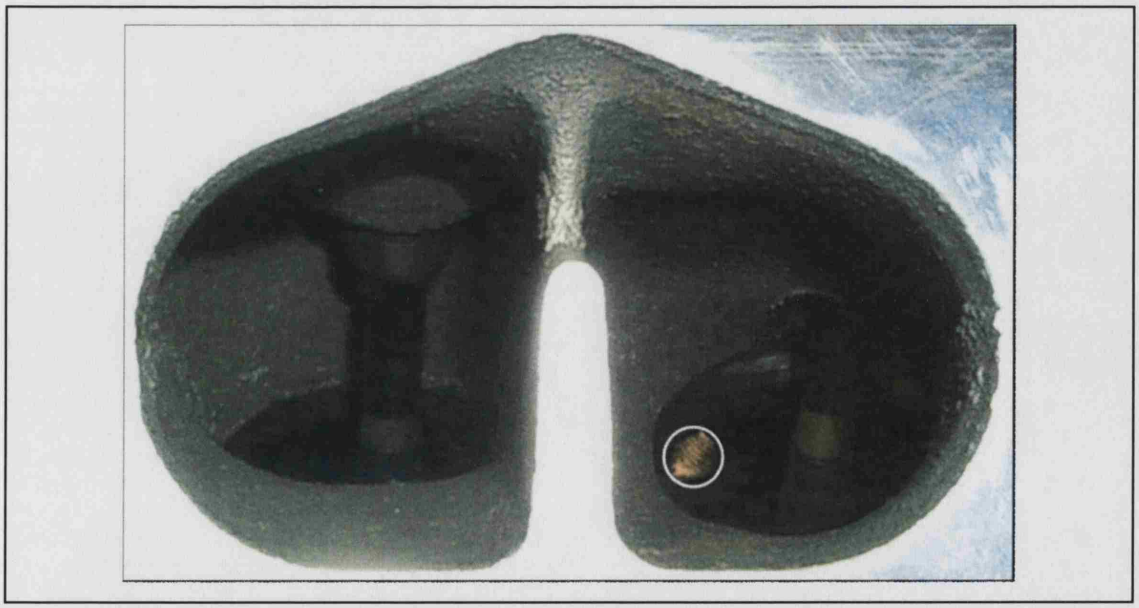

Figure 6.15 Sensor E1L (circled) visible through open inlet valve in swirl port

A rapid decrease and increase in heat flux at approximately 435° CA was visible on the heat flux trace from sensor location E1L. This event fell within the wetting window described by the pulsewidth variation tests and Figure 6.13, but occurred too early for it to be due to the small reduction in wetting at MOP that was observed in the pulsewidth variation tests. Figure 6.16 shows the location of the sensors relative to the features within the cylinder. It was believed these spikes in heat flux were due to air flow effects generated by swirl (clockwise in Figure 6.16) interacting with the edge of the exhaust shrouding and momentarily directing the entrained droplets away from the sensor.

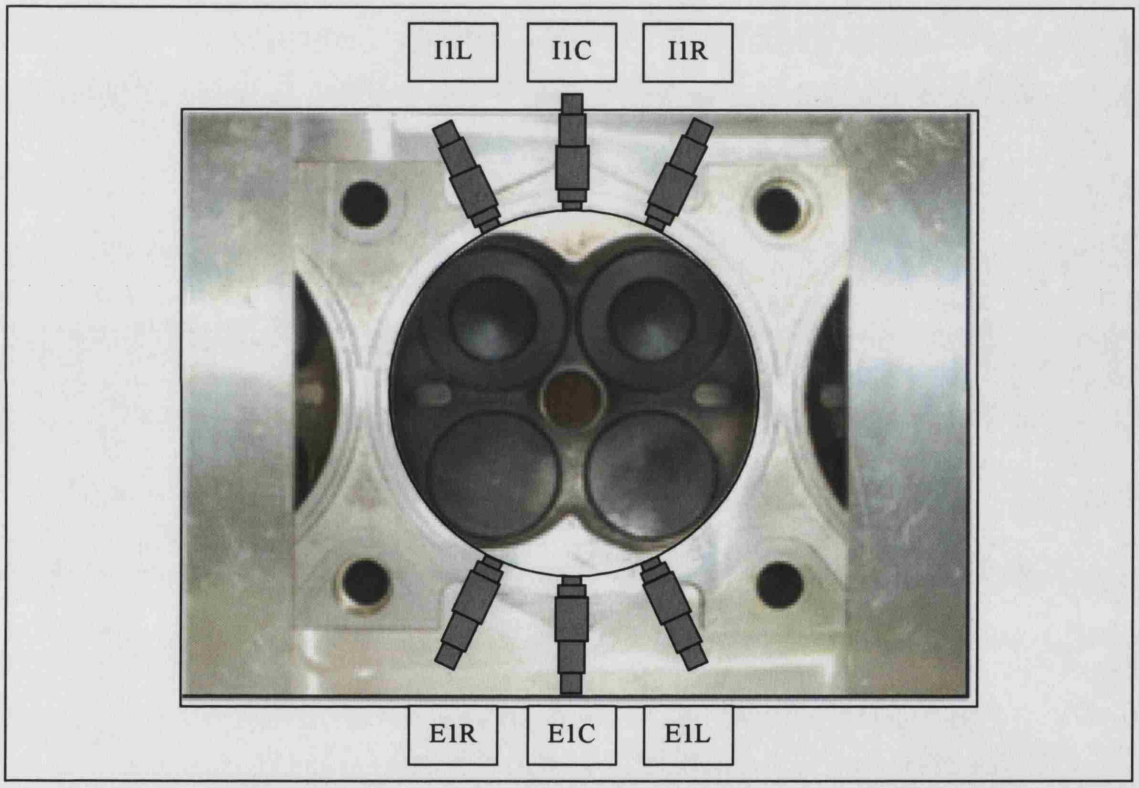

Figure 6.16 AJ33 CP pent roof design with heat flux sensor locations superimposed. Note blanking plate that covers water and oil passages

Figure 6.16 also shows that the valve shrouds in this head design were slightly different to those of the AP design shown in Figure 2.2 and it was believed that this would slightly reduce the wall wetting experienced by the CP cylinder head design. In the CP head, the edges of the shrouding nearest the valves contained a large chamfer and did not possess a sharp edge as in the AP design. This would mean that the incoming charge would be free to escape to the inlet side of the cylinder earlier than in the AP head and the flow would

not direct the fuel droplets towards the exhaust side of the bore with such force. A further visible difference from the AP head design was that the floor of the swirl port had been raised slightly, to achieve a staggered port effect so as to improve airflow into the cylinder. This would not only increase volumetric efficiency, but also tend to direct the flow down the axis of the cylinder rather than across it to cause wall wetting. Figure 6.17 shows the newer CP inlet port design.

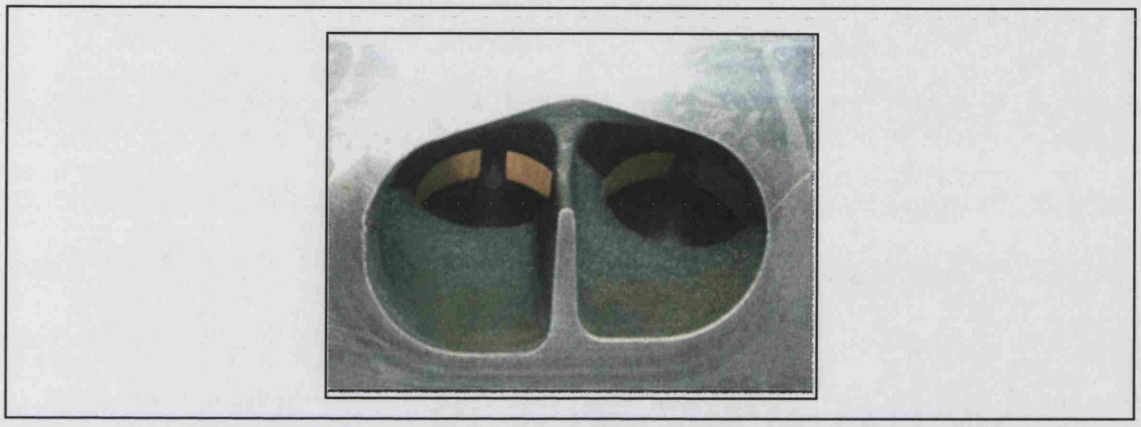

Figure 6.17 AJ33 CP inlet port design. Note raised floor of right hand swirl port

Figure 6.20 in the result plot section is effectively a repeat of the heat flux traces in Figure 6.14, but was included again to aid comparison with Figure 6.21 on the same page which contains the heat flux traces for sensor location E1C.

Figure 6.21 in the result plot section shows the heat flux traces generated with a non-coated sensor at sensor location E1C for the same injection timings presented in Figure 6.20, where the general trends were very similar to that of location E1L. The most interesting aspect of this figure is that the initial -5 W/cm^2 spikes at 430° CA that were observed for 330 and 360° CA SOI timings at location E1L were not present at this central location, but instead the heat flux continued directly to its most negative value of -8 W/cm^2. This indicated that the flow through the inlet valves was not momentarily directed away from the central sensor as it was with the left sensor. It is likely that the extra width of the overhanging exhaust valve shrouding (as shown in Figure 6.16) made this location less sensitive to the changing airflows than location E1L and allowed the impaction of fuel droplets to continue uninterrupted throughout the same period.

The heat flux trace from location E1C for the 420° CA injection timing was quite similar to that from the left sensor location E1L. The only difference was that it occurred approximately 10° CA later, illustrating that the swirl motion within the cylinder affected droplet impaction times around the cylinder bore.

Sensor locations I1-LCR

Figure 6.22 shows the heat flux traces obtained at the upper sensor locations on the inlet side of the block I1L, I1C and I1R, which were collectively designated I1-LCR. Only coated sensor tests were performed here and since the heat flux traces generated for no injection, CVI and OVI were identical, it was decided that no significant amount of fuel had impacted these sensor locations. The negative heat flux value of -1 W/cm^2 that occurred during the induction stroke could be attributed to the flow of cool air passing the sensors. A minute dip in the heat flux traces highlighted that EVO could still be detected even on the inlet side of the cylinder, although no equivalent feature was observed for IVO from the exhaust side because the piston covered the sensors at this time.

Sensor locations E2-LCR and I2-LCR

Only coated sensor tests were performed at these lower sensor locations, where these locations generally provided less information than the upper locations. The main reason for this was that they were covered by the piston for approximately 38% of the engine cycle instead of just 12% for the upper sensors. This explained why the peak positive heat flux observed during the compression stroke is typically about one fifth of that recorded by the upper sensors. However, only the early part of the inlet event suffered from this covering effect, allowing the lower sensors to detect fuel impaction if it occurred during the remainder of the induction event. Figure 6.23 shows the heat flux traces recorded at locations E2-LCR for OVI which indicated an extremely small level of wetting. The wetting was so small that that these heat flux traces were almost indistinguishable from those for no injection and there was no sign of wetting caused by a fuel film flowing down from the upper sensors. It was clear even from this small level of wetting that the wall wetting reduced from sensor E2L to E2R in the same trend as

observed with the upper sensor locations. The OVI heat flux trace from sensor E2R was in fact very similar to the traces obtained when the motoring test was performed with no injection occurring. The heat flux traces recorded at sensor locations I2-LCR showed no indication of fuel impaction.

Sensor locations on the piston

The heat flux traces recorded on the piston were expected to be different from those recorded on the cylinder wall because the piston-based heat flux sensors were at no point shielded from the cylinder gases by the piston. It should be noted that none of the piston-based heat flux results charts shown in this work contain any information indicating potential fuel impaction time windows as this information was deemed too complex to calculate with confidence due to the nature of the in-cylinder motion. Figure 6.24 shows the heat flux traces recorded at locations PIL2, PC and PEL2 for CVI and no injection. The injection and no injection traces were similar for each location throughout the duration of the engine cycle, indicating that there were no specific liquid fuel impaction periods. In fact, this implies that there was little or no fuel on the piston during this injection strategy. The dip in the trace to -1.5 W/cm^2 at 360° CA at location PC was caused by the flow of gas from the inlet valves passing and cooling the sensor. This feature was more evident on the traces obtained from sensors at the centre of the piston than at the more sheltered sensor locations at the edge of the piston. It is possible that this strong air flow helped generate the unusual features observed in the heat flux traces at location E1L and E1C during OVI conditions. The heat flux traces from the piston-based sensors also showed evidence of the EVO event, with a small peak appearing on the traces at about 180° CA. The reason for a peak and not a dip as found on the cylinder based traces was that the piston was not heated to 60°C like the cylinder bore and the convective heat transfer from the gas as it flowed through the exhaust valve effectively heated the cooler piston based sensors for a brief period. This peak was quite small because the piston was still quite far from the valves after having just passed BDC. This peak also occurred later in the heat flux trace due to this increase distance of valve to piston.

Figure 6.25 contains the heat flux traces recorded for OVI conditions at the same sensor locations. The heat flux trace recorded at location PIL2 was quite similar to that recorded during the tests with no injection occurring, indicating that the upper portion of the piston was not wetted by fuel. The heat flux trace observed at the central sensor location PC contained no visible evidence of fuel impaction, but again dipped to -1.5 W/cm^2 at 360° CA. It was believed that the piston surface was covered by a thin fuel film and the reverse flow of gas from the exhaust valves to the inlet valves helped evaporate this film, causing this dip in heat flux.

The heat flux trace obtained at sensor location PEL2 was different to that recorded at any other sensor location, with the exception of location PER2 which was quite similar to PEL2. When an OVI test was performed, the peak heat flux recorded at these locations during compression was reduced drastically, sometimes to a quarter of that recorded during a CVI test. Additionally, the heat flux remained positive throughout the exhaust stroke and the characteristic dip in heat flux at 360° CA was not present. It is believed that this was because the lower sensors PEL2 and PER2 were covered by a thick film of fuel which persisted throughout the cycle. These sensors were effectively insulated from the cylinder gases by this fuel layer. The heat flux traces did not indicate when the fuel was impacting these piston sensors due to lack of sensitivity to additional fuel adding to an existing wet surface. This could potentially be avoided by operating the engine in a fired (rather than motoring) condition, or pre-heating the piston crown. Wetting on this portion of the piston crown would also coincide with what was seen on the motored rig, with wetting on this side of the cylinder below the porous liner.

A visual examination was made of this area by removing the spark plug after a prolonged period of motored engine operation and inserting an endoscope. This confirmed that the exhaust side of the piston was covered by a puddle of fuel, mostly over sensors PEL2 and PER2.

6.6.2 Advanced Inlet, Firing

These tests also used the coated sensors, but were not repeated using non-coated sensors due to two reasons. Firstly, the motoring and firing heat flux traces generated by the coated sensors during the induction period were almost identical, therefore, it was deemed a fair assumption that repeating the firing tests with non-coated sensors would again generate results similar to the motoring tests. Secondly, a majority of the experiments were yet to be completed at this point and it was decided that these other tests should be performed in preference to repeating firing tests that could potentially damage the sensors again.

Sensor locations E1-LCR

Figure 6.26 shows the heat flux traces recorded with CVI, where the left and central sensor locations had a slightly more negative heat flux value than the right sensor location during the induction period. Initially this appeared to be due to fuel impaction on these two sensors, but careful inspection of the traces showed that this was due to swirl motion within the cylinder cooling these sensors more than the right hand sensor. Figure 6.27 shows the heat flux traces for OVI, where the heat flux traces from the left and central sensors showed characteristic wetting by producing reduced heat fluxes of -2 W/cm^2 and -3 W/cm^2 respectively at 500° CA. This further reduction also coincided very well with the fuel impaction time predicted by the analysis software. Also, the heat flux trace from the central sensor location was different to the left and right sensors at EVO where it experienced a brief period of re-heating. This effect was also seen for the OVI test and it was believed to be due to the valve shrouding directing the hot gas flow towards the central sensor location.

Sensor locations I1-LCR

The heat flux traces for CVI and OVI were identical and did not indicate any fuel impaction. Figure 6.28 shows that a slightly negative heat flux of -1.5 W/cm^2 was recorded during the induction period for sensors I1-LCR during OVI tests and was attributed to the cool air flowing in through the adjacent inlet valves.

Sensor locations E2-LCR and I2-LCR

When using CVI, there was no indication of fuel impaction from the heat flux traces at any of the lower six sensor locations. Figure 6.29 shows the heat flux traces recorded for OVI, where there was a small amount of wetting at locations E2L and E2C of similar magnitude to that observed in the equivalent motoring test. The heat flux trace obtained from location E2R was similar to that obtained from when no injection was occurring, which indicated that no fuel impaction had occurred. During the combustion period there was a period of sensor heating with a heat flux reading of 15 W/cm^2 being reached even though the sensors were shielded by the piston. The heat flux dropped rapidly towards zero at 60° CA before rapidly rising once again to 10 W/cm^2 when the retreating motion of the piston exposed the lower sensors to the bulk of the hot cylinder gases.

Sensor locations on the piston

Figures 6.30 and 6.31 show the heat flux traces recorded from the piston for OVI and did not indicate any specific fuel impaction periods. However, these piston-based heat flux readings remained negative for longer throughout the induction event than those observed on the cylinder bore. This was probably due to the hotter piston being cooled more by the incoming cool air, where the heat flux sensors indicated that the piston crown could get up to 50° C warmer than the cylinder wall during combustion. Figure 6.30 shows that the peak heat flux values obtained from these piston-based sensors were approximately 150 W/cm^2. It was also likely that the piston was being cooled by fuel impactions which were more random in both time and location than those found on the bore due to the piston being further away and near BDC. It was believed that the thick insulating fuel puddle observed in the motoring tests could not form on the piston crown due to the increased temperatures and the distinctive heat flux traces observed on the piston during motoring tests were not repeated. It was confirmed though that some fuel could remain on these sensors throughout a firing test when it was observed that the sensor tips were slightly wet with fuel when they were removed at the end of the firing test. Another difference with the firing tests in comparison to the motoring tests was that at 360° CA there was a positive peak in the heat flux traces of up to 8 W/cm^2 instead of a dip. This was probably a combination of two effects, firstly due to the hot exhaust

gases that had flowed back into the inlet ports at IVO returning once again into the cylinder and secondly that hot gases remaining in the cylinder were re-directed towards the sensors.

6.6.3 Retarded Inlet, Motoring

Sensor locations E1-LCR

Figure 6.32 shows the heat flux traces recorded at locations E1-LCR for no injection and CVI, where the negative heat flux of -1 W/cm^2 obtained at 400° CA indicated fresh cool air entered the cylinder and cooled the sensors. By comparing the heat flux traces for advanced (Figure 6.20) and retarded motoring, it was clear that the first flow of air into the cylinder was much more abrupt for the retarded case, reaching the heat flux value of -1 W/cm^2 very rapidly. Initially, it was thought that this was due to the use of non-coated sensors, but the following OVI results proved that the flow was quite different for this retarded inlet condition. Unlike in the advanced inlet valve tests, the heat flux traces from sensor location E1L no longer possess the spikes at 435° CA, probably due to the stronger air flow through the inlet valves.

Despite the more rapid inlet flow, no fuel impaction was evident for the CVI case. The heat flux traces for the OVI tests are shown in Figure 6.33 where the traces clearly indicated fuel impaction on the three sensors. A very interesting feature of these traces was that the central sensor location now experienced the greatest fuel wetting with a heat flux value of -8 W/cm^2 at 470° CA. It was believed that this stronger flow of incoming air amplified the swirl motion within the cylinder and allowed the fuel droplets to reach further around the cylinder bore. The left hand sensor location reached a heat flux reading of approximately half this, while the most negative right hand heat flux value was approximately -2 W/cm^2. The value of heat flux recorded at 400° CA in the OVI and CVI cases were -2 W/cm^2 and -1 W/cm^2 respectively, where the main fuel impaction event did not begin until 440° CA. It was thought that this difference was due to the sensors being slightly wet with fuel from the previous cycle and being cooled by the incoming cool air from the inlet valves. Interestingly, the wall wetting window that was governed by valve lift and seen in the advance inlet valve traces can again be observed in

these retarded inlet heat flux traces. It can be seen that this wetting window has been retarded by approximately the same amount as the inlet valves. Both the CVI and OVI heat flux traces showed the effects of EVO where the reverse flow followed by enhanced convection cooled the sensors. The OVI case was approximately 3 W/cm^2 more negative than the CVI case at 160° CA, which again indicated that the sensors were already slightly wet from the previous cycle.

Sensor locations I1-LCR

Figure 6.34 shows the heat flux traces obtained for no injection and CVI while Figure 6.35 shows the traces obtained for OVI. Since sensors I1-LCR were closer to the inlet valves than sensors E1-LCR, they experienced the cooling effect from the incoming air earlier, at approximately 390° CA. Comparing the CVI and OVI cases it was concluded that wetting had occurred under OVI conditions at sensor locations I1-LCR because of the rapid decrease in heat flux at approximately 430° CA. As with the initial cooling effect, this fuel impaction was also approximately 10° CA earlier than that experienced by sensors E1-LCR. It was the central sensor location that was wetted the least, while the left and right locations were impacted by a similar amount of fuel, recording a heat flux of -3 W/cm^2. It was believed that the prominent valve shrouding between the inlet valves restricted flow towards the central sensor location, whereas the left and right hand sensors were positioned at the ends of the shrouding and could be reached more easily. It should be remembered that wetting of sensors I1-LCR did not occur when the inlet timing was fully advanced by the maximum 48° CA.

Sensor locations on the piston

Figures 6.36 and 6.37 show the heat flux traces recorded from the piston-based sensors for CVI, no injection and OVI. No obvious fuel impactions were detected in the traces, as when advanced inlet timing was used. The dip in heat flux that occurred just after 400° CA was due to the flow of air from the inlet valves cooling the sensors and as with the advanced inlet condition, sensor location PC is cooled the most.

6.6.4 Retarded Inlet, Firing

Sensor locations E1-LCR

The CVI heat flux traces shown in Figure 6.38 did not indicate any fuel impaction on the sensors. However, the OVI heat flux traces shown in Figure 6.39 clearly indicated fuel impaction had occurred, where it was found that 360° CA injection timing wetted the bore more than 390° CA injection timing. During the induction stroke, the OVI traces reflected those obtained from the motored tests in both shape and magnitude, with the heat flux at sensor E1C reaching a heat flux of -9 W/cm^2.

Sensor locations I1-LCR

The heat flux traces for both CVI and OVI firing tests as shown in Figures 6.40 and 6.41 were extremely similar to those of the equivalent motoring tests during the induction period. In the OVI test, the central sensor location experienced the least fuel-wetting, while the left sensor location reached a heat flux of -5 W/cm^2 at 450° CA.

Sensor locations on the piston

There were no fuel droplet impactions detected by any of the piston-based sensors under these test conditions. The heat flux traces resembled those recorded for the advanced inlet valve tests and the only difference was the reduced size of the characteristic peak in heat flux at 360° CA due to hot gases being redirected towards the sensors.

6.7 RESULTS AND DISCUSSION - AP CYLINDER HEAD

6.7.1 Deactivated Port, Motoring

Sensor locations E1-LCR

Initially the engine was motored with CVI and no injection occurring and the respective heat flux traces showed no indication of fuel impaction. When the engine was again motored but with fuel injection taking place at 360° CA there was a clear indication that fuel impaction had occurred at approximately 400° CA, as shown in Figure 6.42. It was

expected that the use of these non-coated sensors would generate a large negative heat flux at the time of fuel impaction, but the addition of port deactivation resulted in a very negative heat flux reading of -13 W/cm^2 at sensor locations E1L and E1C. It is believed that the increased gas velocities through the active port enhanced convective heat transfer. The dip in heat flux experienced with the CP cylinder head due to EVO was again visible with the AP cylinder head. Interestingly, this very negative heat flux reading of -13 W/cm^2 occurred approximately 15° CA earlier than that of the activated port condition, where the activated condition did not achieve such a negative heat flux reading. This indicated that in this deactivated condition, fuel impaction on the cylinder wall must still have been occurring, although not at this sensor location. The small kink in the linear section of the heat flux trace at 435° CA was assumed to be due to the same valve shrouding effect as observed in the CP head at location E1L.

An injection sweep was performed at sensor location E1L and the heat flux traces generated are shown in Figure 6.43. The traces show that no wall wetting occurred before 425° CA, due to the flow vectoring effect of the inlet valves. As with all of the tests performed with the AP cylinder head, it was found that a 360° CA injection timing generated the most negative heat flux reading, but these were reached in only 20° CA, which was earlier than when fuel impaction was due to finish. It was believed that the opening inlet valve then directed the remainder of the fuel from this injection away from the sensor. A very interesting feature is observed with the 390° CA injection where initially the heat flux trace resembles that of the 360° CA injection, but because this injection started later, the tail end was caught by the valve closure event which directed the fuel droplets back onto the sensor again. This gives the trace a distinctive 'hook' shape. The final 420° CA injection shows this effect even more clearly, with the heat flux trace resembling a 'w' during the induction period. This was because the fuel droplets from this one injection were passing the inlet valve throughout the critical period near the maximum lift of the inlet valve when it could divert the droplets away from the sensor. It can be confirmed that it was droplet impaction and not airflow evaporating a fuel puddle from the sensor that caused this second dip in heat flux because during the 360° CA injection test, the sensor would recently have been wetted by droplet impaction to cause the main dip in heat flux, but no second dip was present.

Sensor locations I1-LCR

When the engine was motored with no injection occurring, there was a larger cooling effect on sensor I1R than the sensors I1C and I1L. This was due to the port deactivation increasing the flow through this right hand inlet valve and eliminating the flow through the inlet valve nearest to sensor location I1L. Figure 6.44 shows the heat flux traces for the OVI condition, which were identical to those of no injection, indicating that no wall wetting occurred. The most negative heat flux recorded was -2 W/cm^2 and occurred at approximately 400° CA.

Sensor locations E2-LCR

The heat flux traces recorded at locations E2-LCR for when using an OVI timing of 360° CA are shown in Figure 6.45. It was immediately apparent that fuel impaction had started to occur at sensor E2L at approximately 400° CA, with a heat flux reading of -5 W/cm^2. Sensor E2C had also experienced some fuel impaction at a similar timing, but to a lesser extent with a heat flux reading of -2 W/cm^2. Sensor location E2L produced a hook shaped curve which indicated that the fuel impaction was being directed away from the sensor. The heat flux reading from location E2C became more negative at the same time that the reading from location E2L became less negative, which meant that fuel impaction was beginning at E2C when fuel impaction was stopping at E2L. This could indicate that the flow vectoring effect of the inlet valve had moved the droplet impaction zone from sensor location E2L to sensor location E2C. When using CVI, no indication of fuel impaction was observed on the heat flux traces.

Sensor locations on the piston

Figures 6.46 and 6.47 show the heat flux traces recorded from the piston-based sensors for CVI, no injection and OVI. The no injection condition indicated a small dip in heat flux which peaked at approximately 440° CA for sensor locations PEL1 and PEL2, which could be attributed to the incoming flow through the inlet valves cooling the sensors. This was the only time such specific piston cooling would be detected in this work. However, The CVI and OVI conditions also indicated the small dip in heat flux at

this point, but no indication of fuel impaction was given at these sensor locations. This small dip was slightly larger for the OVI case, probably because the sensors were wet with fuel from fuel impactions which were undetectable as individual events and spread over a greater area than those found on the bore sensors due to the greater distances from the inlet valves.

6.7.2 Deactivated Port, Firing

Sensor locations E1-LCR

When CVI and OVI were used in the firing tests, the heat flux traces recorded during the induction period were again very similar to those obtained during the equivalent motoring tests. Figure 6.48 shows that the most negative heat flux readings at sensor locations E1L and E1C for OVI conditions were -14 W/cm^2 and -10 W/cm^2 respectively, both occurring at 400° CA. The heat flux traces from location E1L exhibited a clear 'hook' shape that was typical of inlet valve flow vectoring effect. The point of interest here was that this hook shape proved that the inlet valve vectoring effect could still occur during firing conditions. This heat flux reading of -14 W/cm^2 was one of the most negative values recorded in this work, while sensor location E1R did not appear to experience any fuel impaction.

Sensor locations I1-LCR

The heat flux traces recorded at sensor locations I1-LCR for when using CVI are shown in Figure 6.49. The trace for sensor location I1R contained an extended period of negative heat flux with a heat flux value of approximately -3 W/cm^2 during the induction period. This effect was very similar to that observed for the equivalent motoring test with no injection occurring when a heat flux of -2 W/cm^2 was achieved. It was believed that the heat flux was more negative in this firing test because the sensor was relatively warm due to combustion, allowing for a greater amount of convective heat transfer and sensor cooling. Sensor locations I1L and I1C were not exposed to the incoming cool flow through the sole active port, so their heat flux traces do not exhibit such a feature. The heat flux traces obtained with OVI were identical to those of CVI traces.

6.7.3 Activated Port, Motoring

Sensor locations E1-LCR

The heat flux traces for OVI are shown in Figure 6.50. It was apparent that the use of CVI timing did not result in fuel impaction on the sensors, while OVI did indicate fuel impaction with heat flux readings of -9 W/cm^2 and -4 W/cm^2 being recorded at sensor locations E1L and E1C respectively. These values occurred at approximately 450° CA, which was later than in the deactivated port condition. It was concluded that this delay was due to the reduced gas velocities achieved by activating the port. The reduced gas velocity also seemed to make the inlet valve flow vectoring effect less powerful because these heat flux traces possessed no hook shape, unlike those of the deactivated tests.

Sensor locations I1-LCR

Figure 6.51 shows the heat flux traces obtained at sensor locations I1-LCR for the OVI case, where no indication of fuel impaction was detected for either the CVI or OVI conditions at these three sensor locations.

6.7.4 Activated Port, Firing

Sensor locations E1-LCR

The heat flux traces for OVI are shown in Figure 6.52. The traces for sensor locations E1C ad E1R are similar to those recorded for motoring conditions, although the heat flux values are smaller in magnitude. The heat flux trace from sensor location E1L reached a heat flux of -5 W/cm^2 at 450° CA.

Sensor locations I1-LCR

The heat flux traces for the OVI tests are shown in Figure 6.53. There were no obvious differences between the CVI and OVI heat flux traces, indicating there was no fuel impaction for the OVI condition. A heat flux of -2.5 W/cm^2 was recorded at 450° CA due to the flow of cool air from the near by inlet valves passing the sensors.

6.8 ADDITIONAL FINDINGS FROM THE HEAT FLUX RESULTS

Figures 6.54 and 6.55 show the heat flux traces recorded at locations E1-LCR and I1-LCR, but include the peak heat flux section observed during combustion. Although not directly related to wall wetting, it was interesting that the peak heat flux recorded from locations I1-LCR during firing conditions was only 50 W/cm^2 whereas a peak of 130 W/cm^2 was recorded from E1-LCR. This effect was observed for both the CP and AP cylinder heads, regardless of inlet valve timing or port deactivation. It was believed that the cooler crevice volume on the inlet side of the cylinder quenched the flame, leaving a cooler pocket of air in the crevice volume. The heat flux would then rise as the piston uncovered the sensors at approximately 40° CA and exposed them to the bulk of the hot gases in the cylinder. However, the hotter exhaust side of the cylinder did not quench the flame within the crevice volume and permitted combustion to continue. This generated the larger values of heat flux and traces that were not affected by piston covering the sensors.

6.9 CONCLUSIONS OF HEAT FLUX RESULTS

The heat flux technique has proven itself to be an excellent means of gaining information on cylinder wall and piston wetting in a 4-valve engine that was operating at 1200 rpm, under motoring or part load firing conditions.

Motoring tests were performed with the CP and AP cylinder heads using both CVI and OVI strategies and it was found that only the OVI strategy resulted in any wetting, with the CVI strategy failing to wet the cylinder wall or piston at any time. The results for both cylinder heads indicated that during motoring or firing conditions, impaction of fuel mainly occurred at sensor locations on the exhaust side of the cylinder bore during induction. It was found that the injector almost had a clear line of sight of these sensor locations when the inlet valves were open which allowed the fuel droplets entrained in the airflow to pass across the cylinder and impact on these sensors. The swirl motion was apparent by the time delay in impaction of droplets around the cylinder bore, with the sensors opposite the swirl inlet port experiencing droplet impacts first. Impaction of

droplets at sensor locations on the inlet side of the cylinder bore was extremely rare, where sensor locations E2-LCR generally experienced more wall wetting on the AP cylinder head, especially due to port deactivation. The piston appeared to experience a surprisingly small amount of wetting, with no obvious fuel droplet impactions being detected from the heat flux traces. Any wetting that did occur was limited to the exhaust side of the piston.

During the firing tests attention was focused on sensor locations E1-LCR on the exhaust side of the cylinder bore since the earlier motoring tests revealed that this area suffered from wall wetting more than anywhere else in the cylinder. Firing tests were performed on the CP cylinder head with both advanced and retarded inlet valve timing and on the AP cylinder head with both an activated or deactivated dump port. These firing tests generated heat flux traces that were almost identical to those of the equivalent motoring tests during the induction period, with some firing traces showing only slightly smaller heat flux values during the droplet impaction period. This is important because it confirms that the wall wetting occurs via airborne droplets and not wall film. It is also important to note that the higher engine surface temperatures from combustion did not eliminate the presence of the airborne droplets, indicating that they must have remained airborne from injection to impaction on the heat flux sensor.

Retarding the inlet valve timing of the CP cylinder head during motoring or firing conditions by 48° CA caused the fuel impaction event at sensor location E1-LCR on the exhaust side of the cylinder bore to become retarded by an equal amount, although the magnitude and duration of the droplet impactions remained unchanged. However, this retarded inlet valve condition was the only condition used during this study that caused sensor locations I1-LCR on the inlet side of the cylinder bore to detect any fuel droplet impaction. This was due to the late IVO causing the velocity of the gas entering the cylinder to be higher than usual and force the fuel droplets to this area.

The pulsewidth variation tests proved to be extremely useful as they initially indicated that the amount of wetting was proportional to the amount of fuel injected. The results of the pulsewidth variation tests also revealed that fuel impaction at a given location was

directly related to inlet valve lift, which then helped explain the shape of the heat flux traces during the droplet impaction period. It was clear from the CP and AP results from the exhaust side of the bore that fuel droplet impaction on a sensor often stopped earlier than expected due to the opening inlet valves directing the fuel droplets away from the sensor. Some heat flux traces for injections with a later SOI contained clear evidence that closure of the inlet valve allowed wetting to begin once again. This was mostly experienced with the AP cylinder head when using a deactivated port. In fact, port deactivation was seen to drastically increase the level of wall wetting and the most negative values of heat flux experienced in this study were found during this condition. It was believed that the higher gas velocity would carry the fuel droplets across the cylinder to impact on the sensors. These very negative heat flux readings were also attained within a much shorter period after SOI than in any other condition and stopped becoming even more negative accordingly abruptly as the droplets were directed away from the sensor. This indicates that the higher gas velocities created a more concentrated impaction zone and that these faster flows were more sensitive to the lift of the inlet valve. The higher gas velocity would also have assisted in creating such negative heat flux values by enhancing heat transfer by convection, but the actual proportion cannot be determined.

Although the heat flux technique is excellent at providing time-based information on fuel impaction, attempts to quantify the amounts of fuel detected should be approached with care. Firstly, the pulsewidth variation tests proved that not all of the fuel that impacted the cylinder bore was detected by the heat flux sensors. Secondly, the very nature of gasoline evaporation from warm engine surfaces is extremely complex due to the heat transfer mechanisms and local gas flows within the engine.

The results presented indicate that the newer CP cylinder head is generally less prone to wall-wetting than the AP cylinder head and this can be directly attributed to modifications in the design. The removal of the port deactivation facility was by far the greatest factor in this reduction, although the raising of the swirl port and revised valve shrouding were also believed to be responsible for a small reduction in wall wetting. Their combined effect was to introduce a flow into the cylinder that travelled more down the axis of the cylinder, rather than across the cylinder to wet the exhaust side of the

bore. Measurement of how much each of these reduces wall wetting would be extremely difficult.

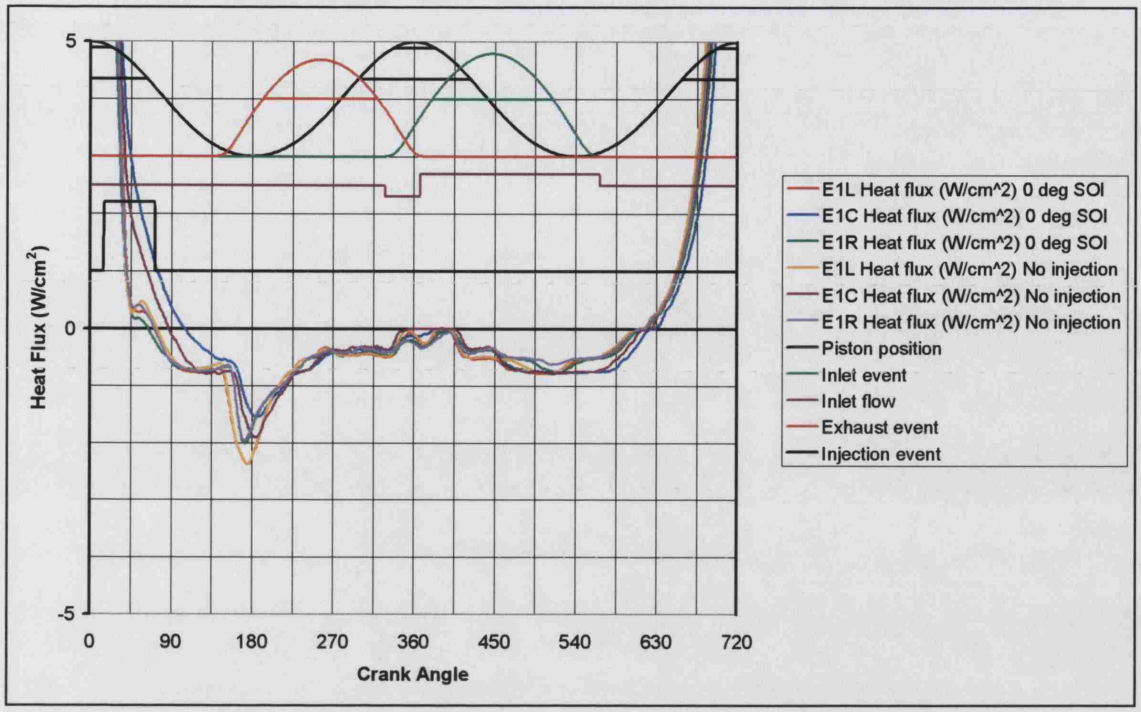

Figure 6.18 Locations E1-LCR with 0° CA injection timing and no injection (CP cylinder head, advanced inlet, motoring)

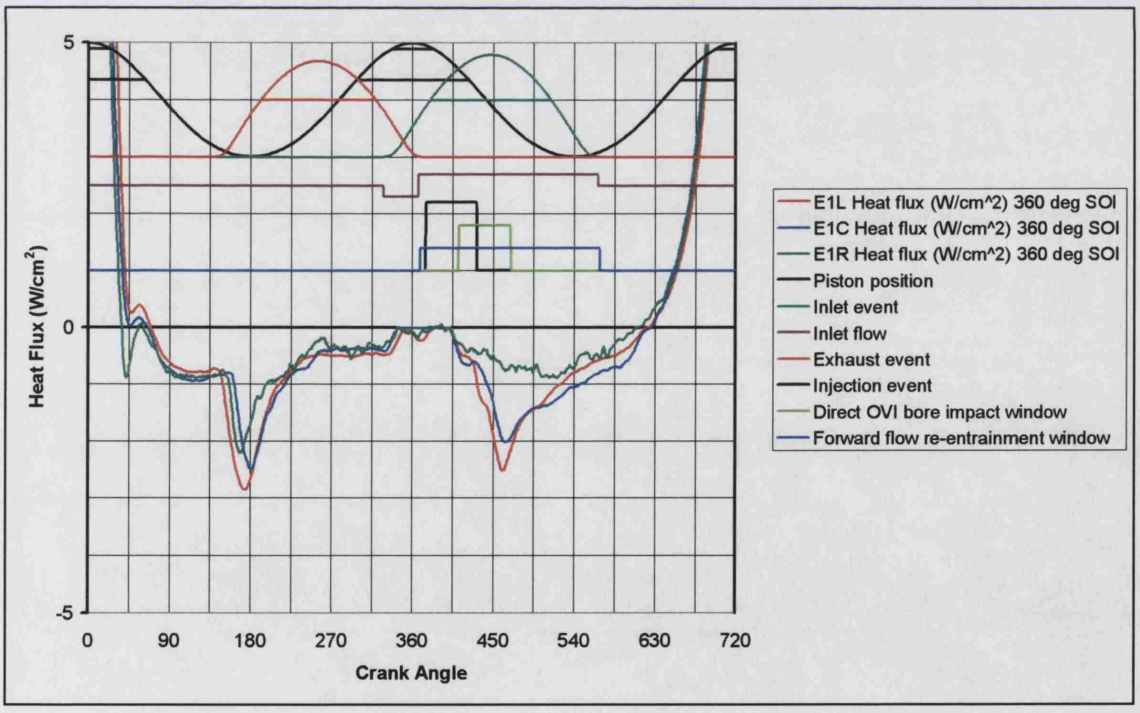

Figure 6.19 Locations E1-LCR with 360° CA injection timing (CP cylinder head, advanced inlet, motoring)

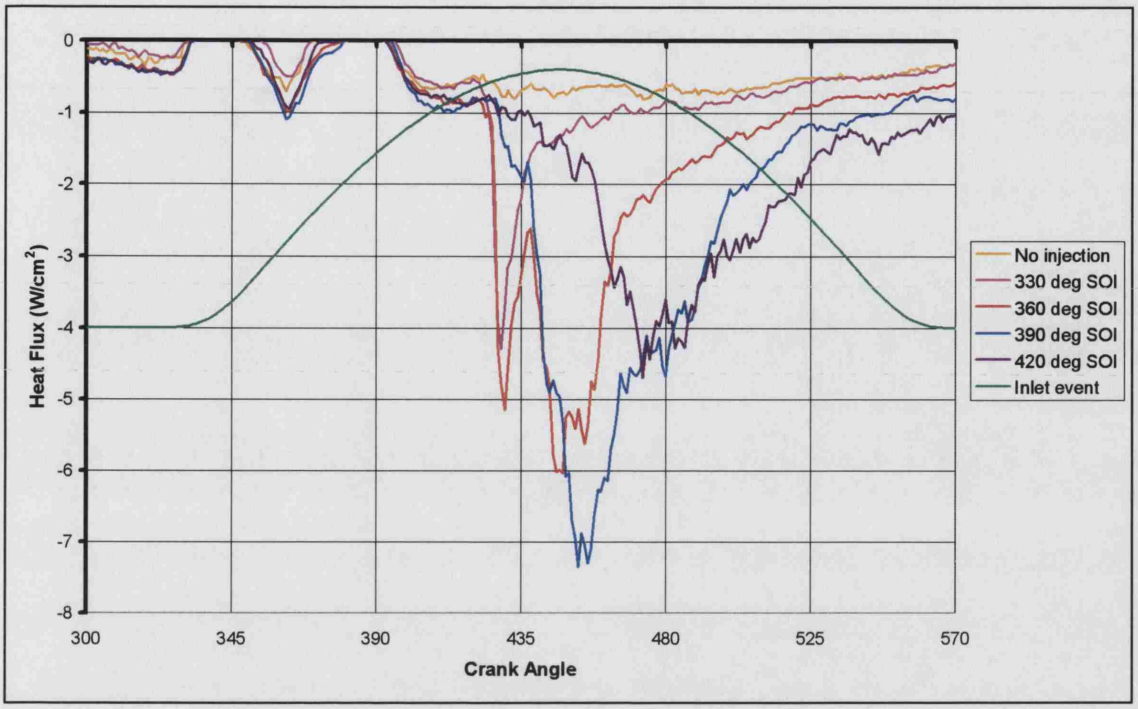

Figure 6.20 Injection sweep at location E1L with a non-coated sensor (CP cylinder head, advanced inlet, motoring)

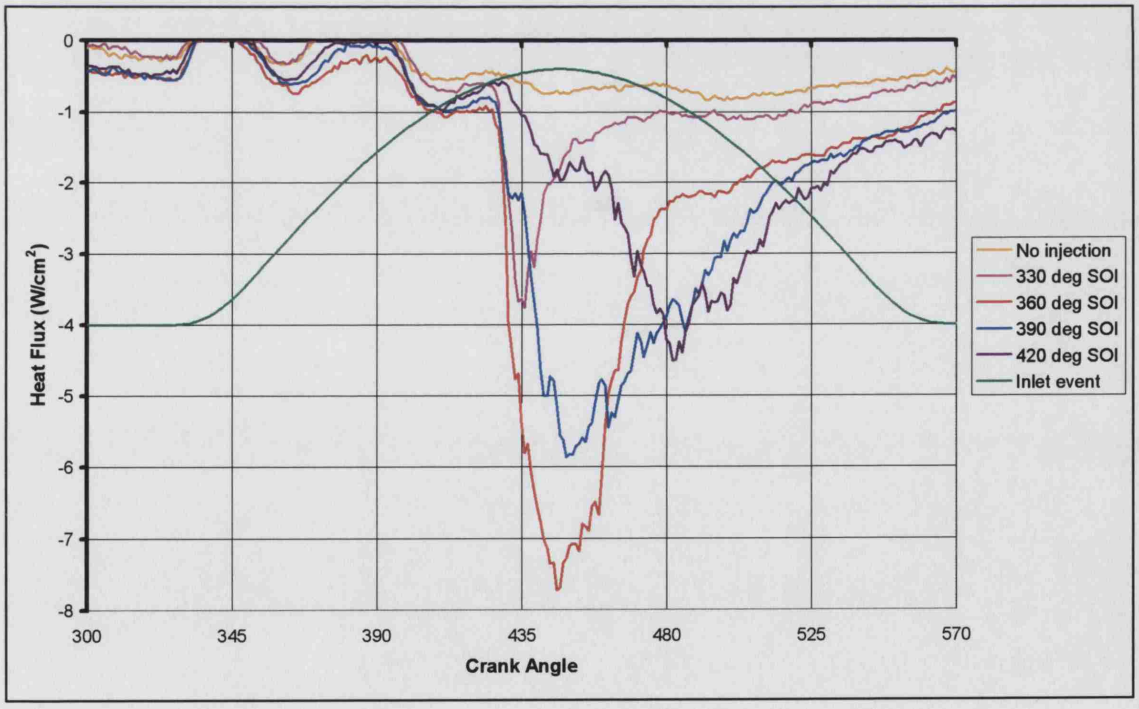

Figure 6.21 Injection sweep at location E1C with a non-coated sensor (CP cylinder head, advanced inlet, motoring)

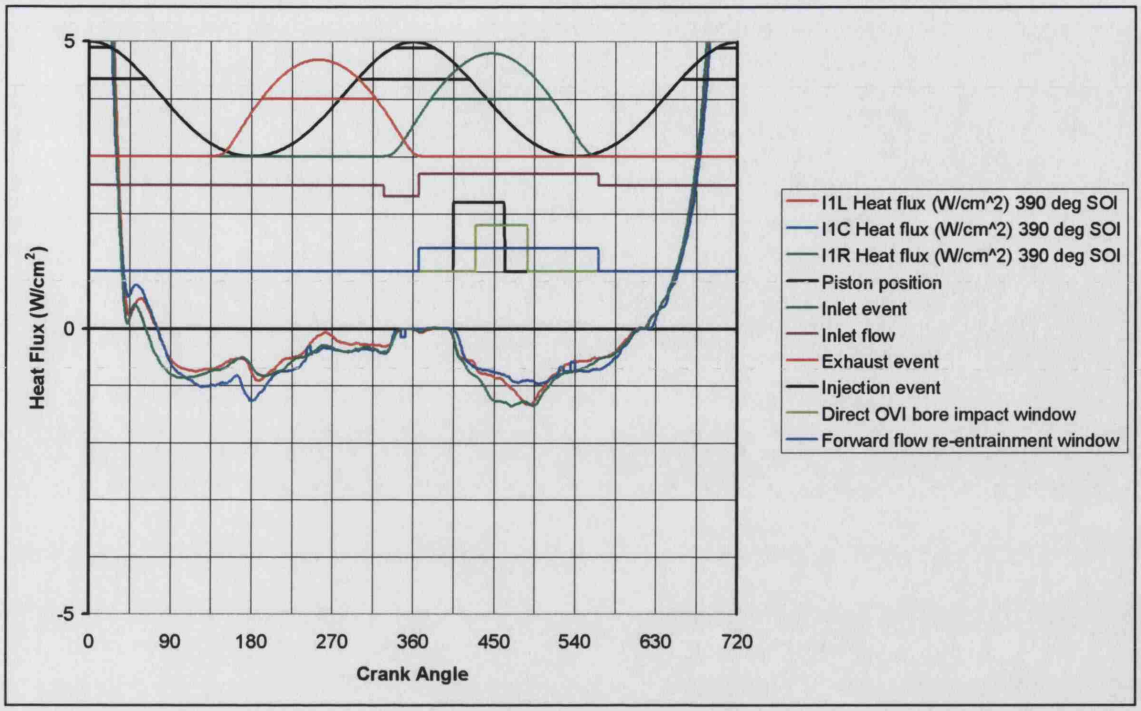

Figure 6.22 Locations I1-LCR with 390° CA injection timing

(CP cylinder head, advanced inlet, motoring)

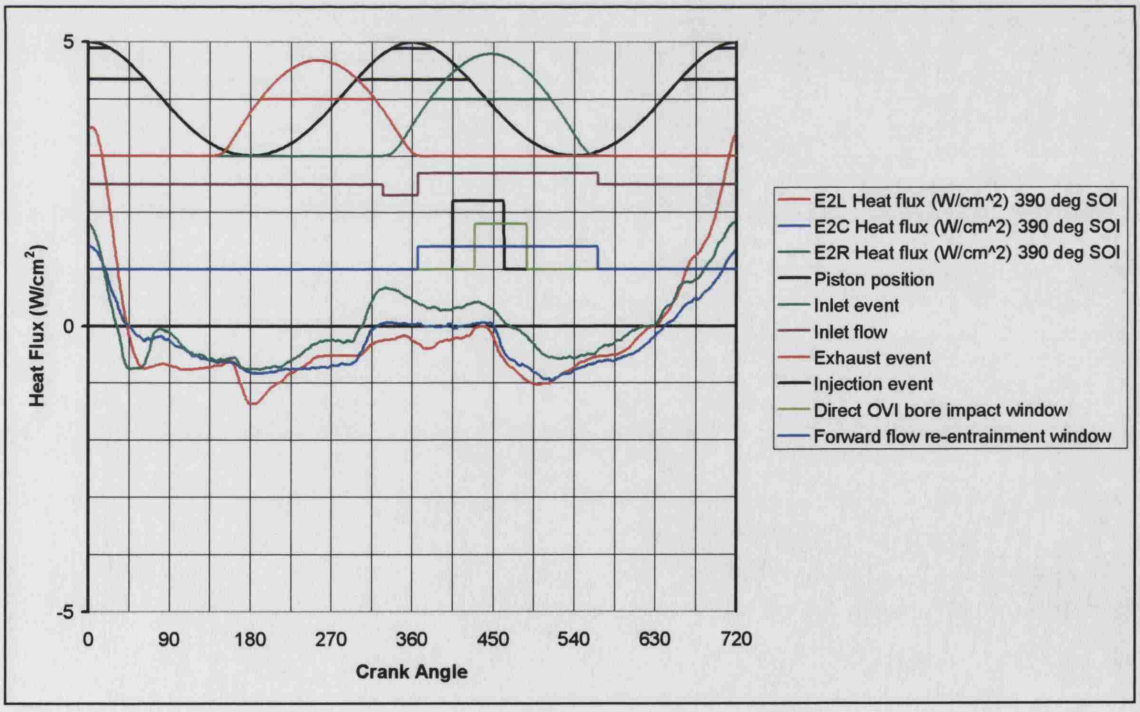

Figure 6.23 Locations E2-LCR with 390° CA injection timing

(CP cylinder head, advanced inlet, motoring)

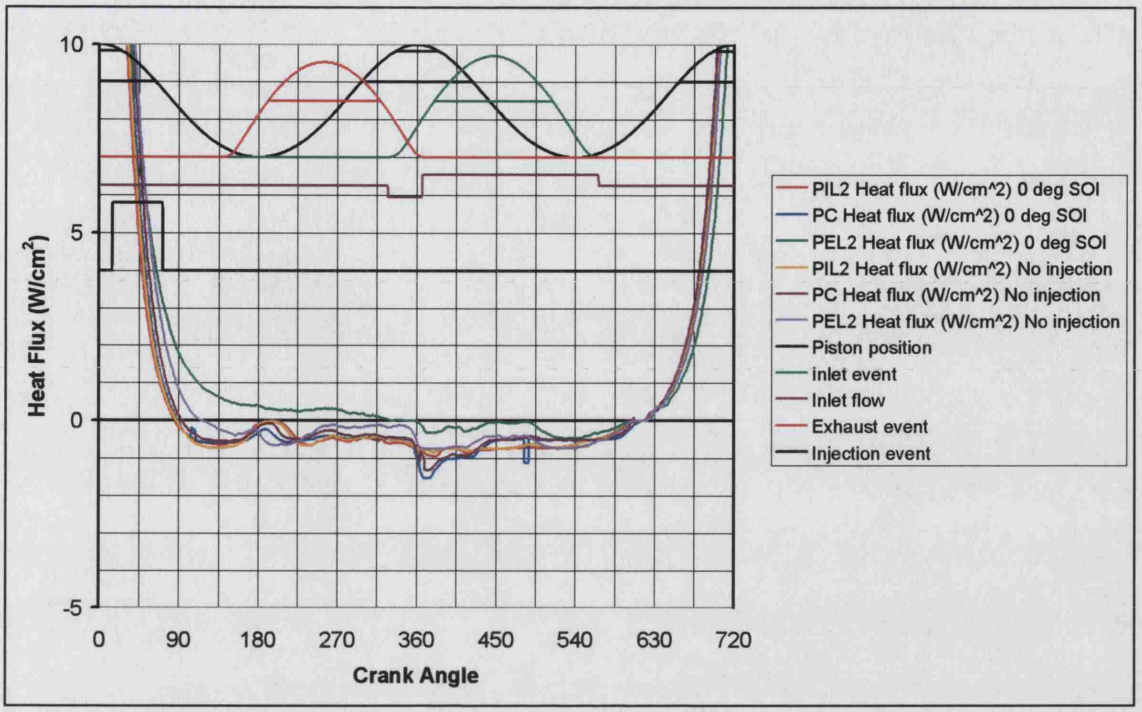

Figure 6.24 Locations PIL2, PC, PEL2 with 0° CA injection and no injection (CP cylinder head, advanced inlet, motoring)

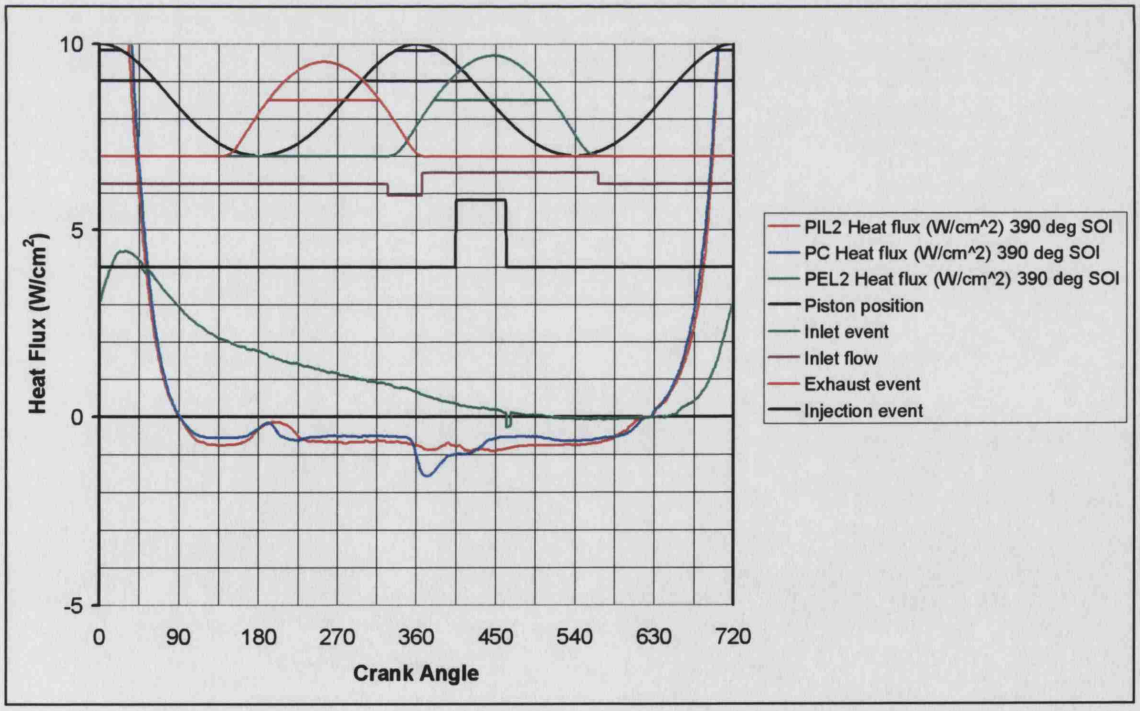

Figure 6.25 Locations PIL2, PC, PEL2 with 390° CA injection (CP cylinder head, advanced inlet, motoring)

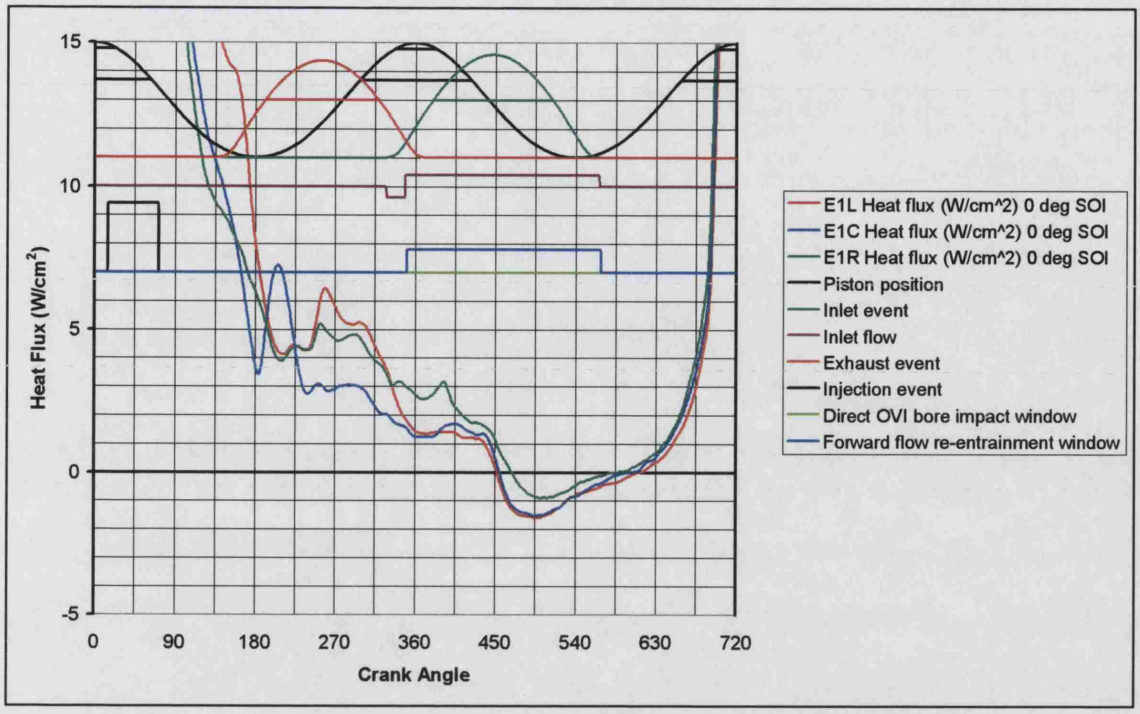

Figure 6.26 Locations E1-LCR with 0° CA injection

(CP cylinder head, advanced inlet, firing)

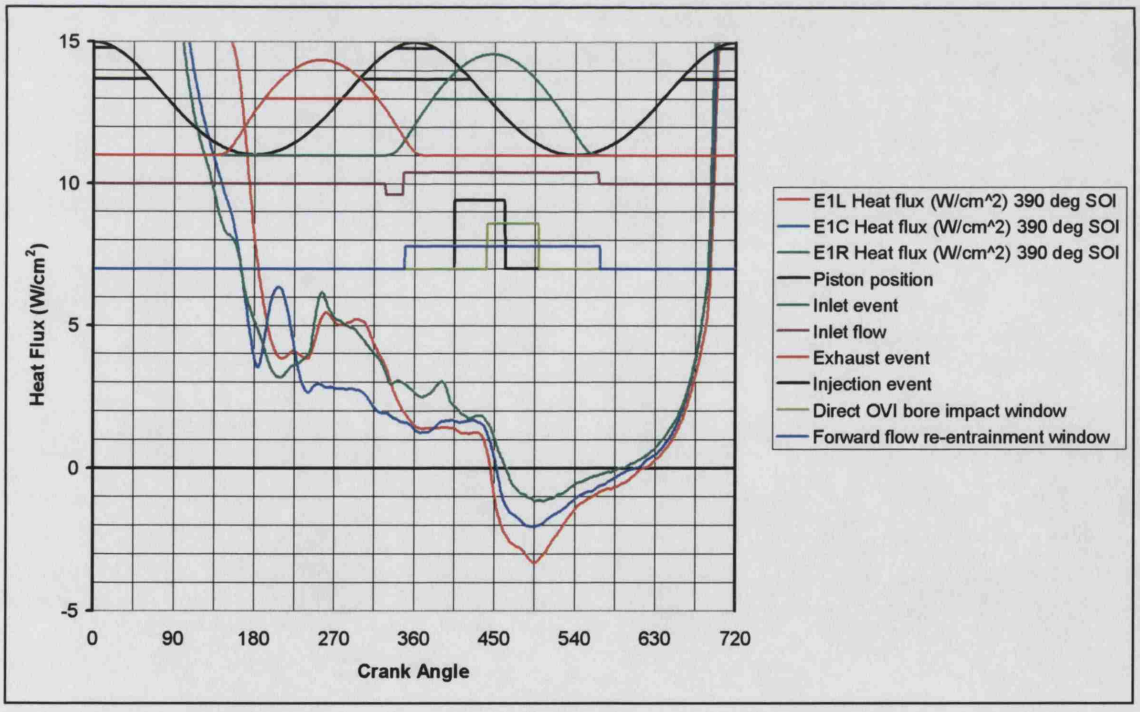

Figure 6.27 Locations E1-LCR with 390° CA injection

(CP cylinder head, advanced inlet, firing)

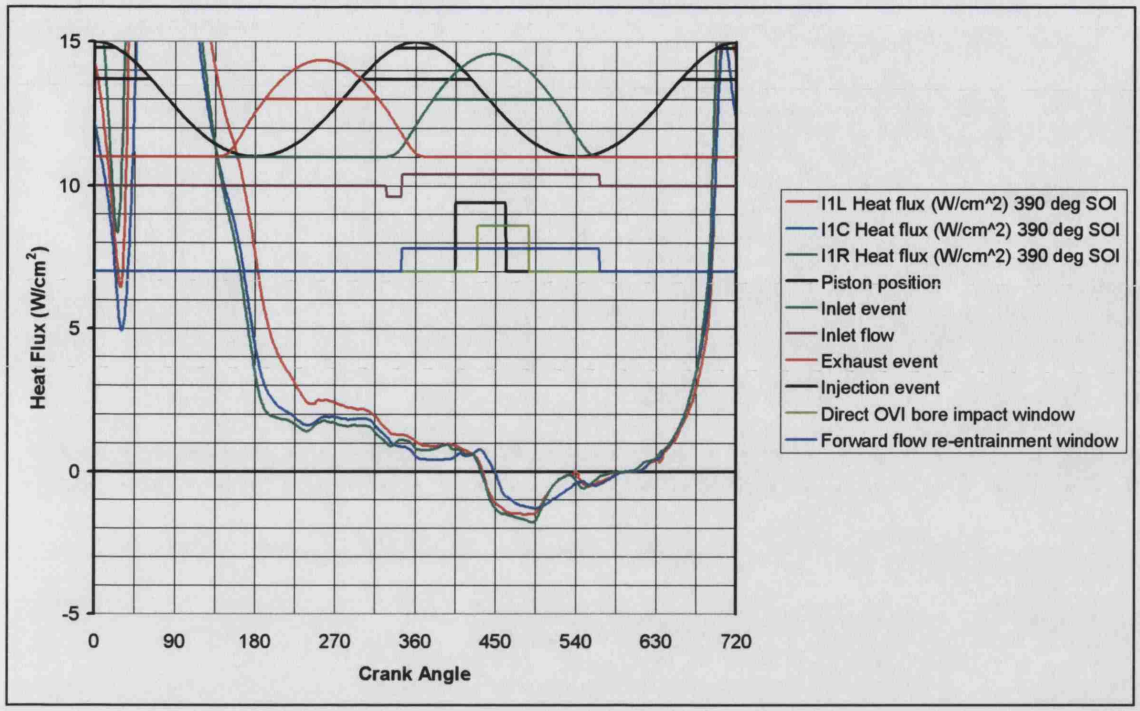

Figure 6.28 Locations I1-LCR with 390° CA injection

(CP cylinder head, advanced inlet, firing)

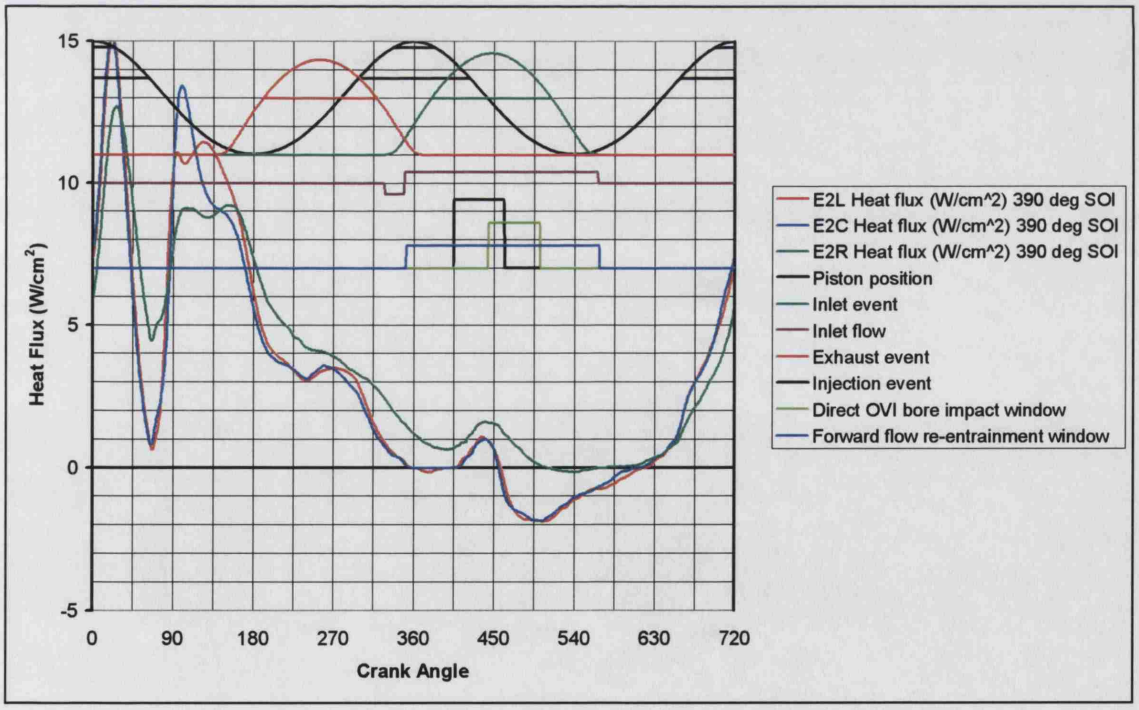

Figure 6.29 Locations E2-LCR with 390° CA injection

(CP cylinder head, advanced inlet, firing)

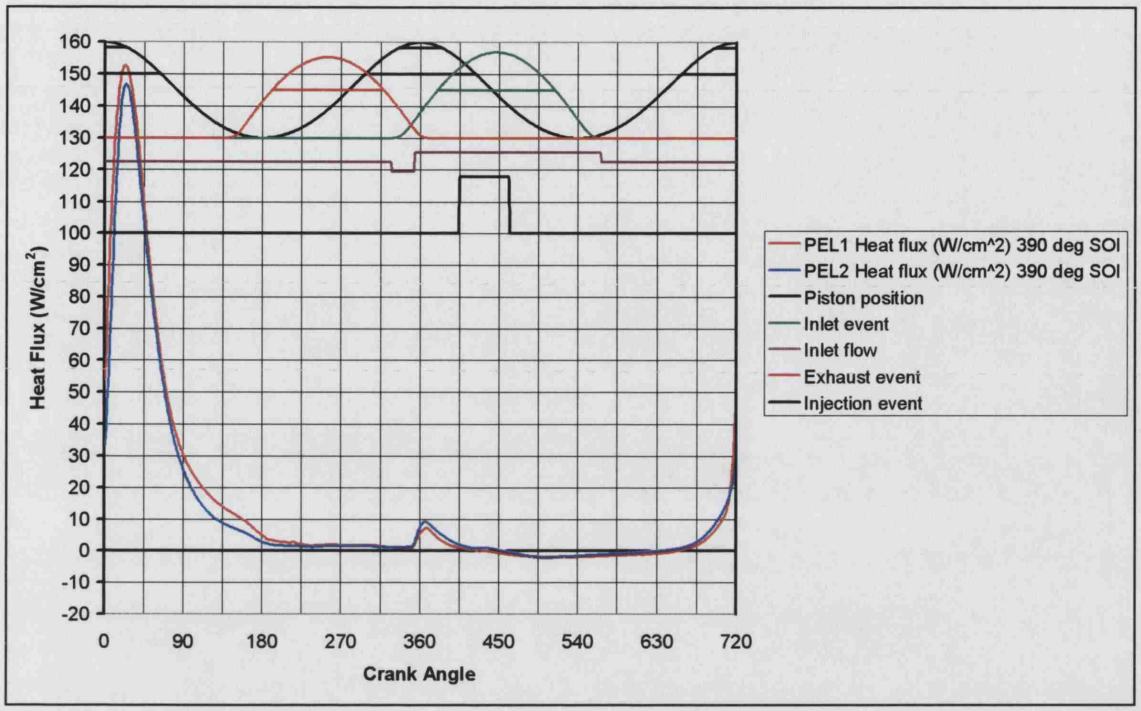

Figure 6.30 Locations PEL1 and PEL2 with 390° CA injection

(CP cylinder head, advanced inlet, firing)

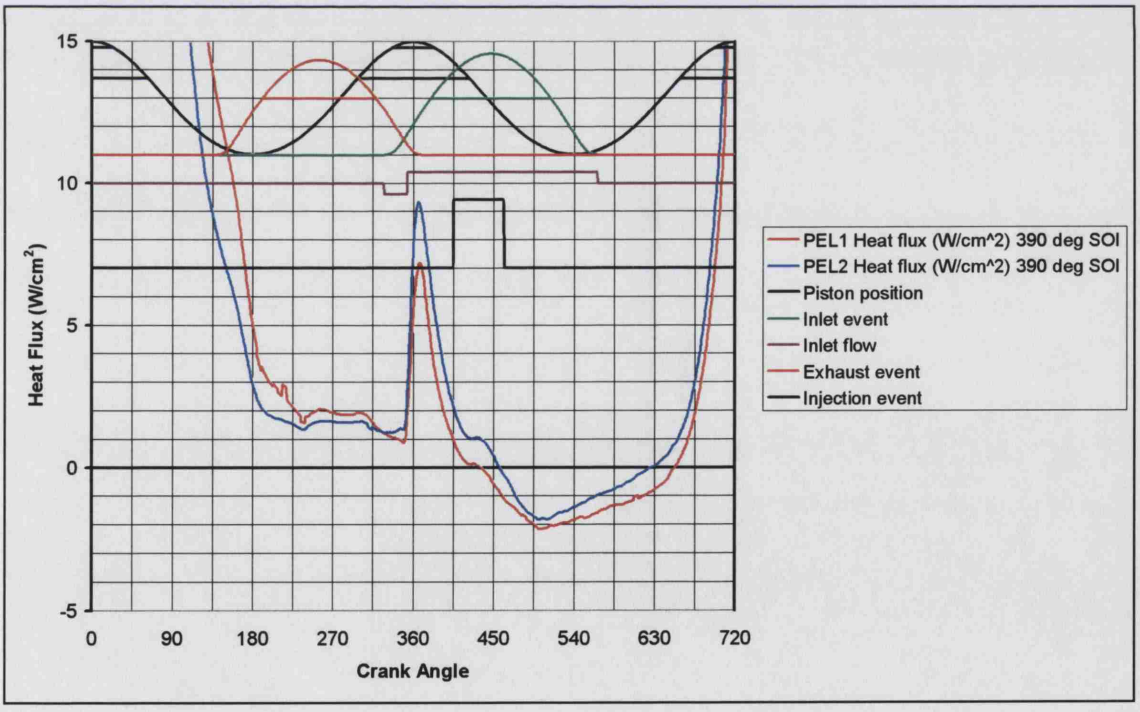

Figure 6.31 Locations PEL1 and PEL2 with 390° CA injection

(CP cylinder head, advanced inlet, firing)

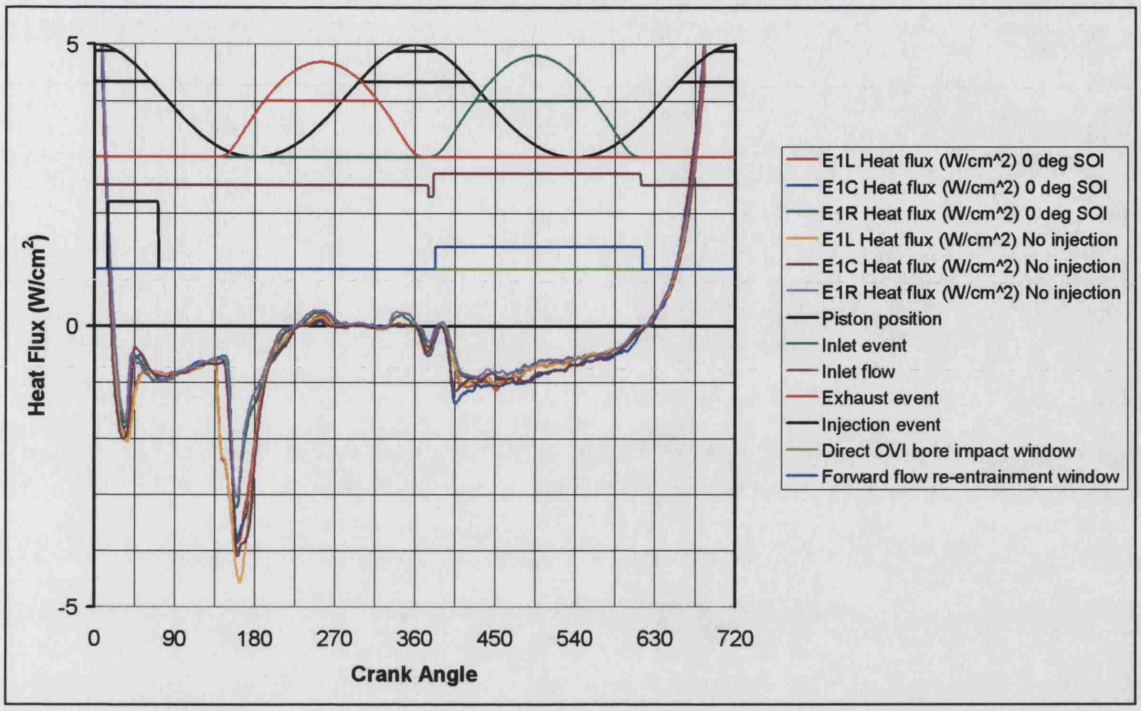

Figure 6.32 Locations E1-LCR with 0° CA injection and no injection

(CP cylinder head, retarded inlet, motoring)

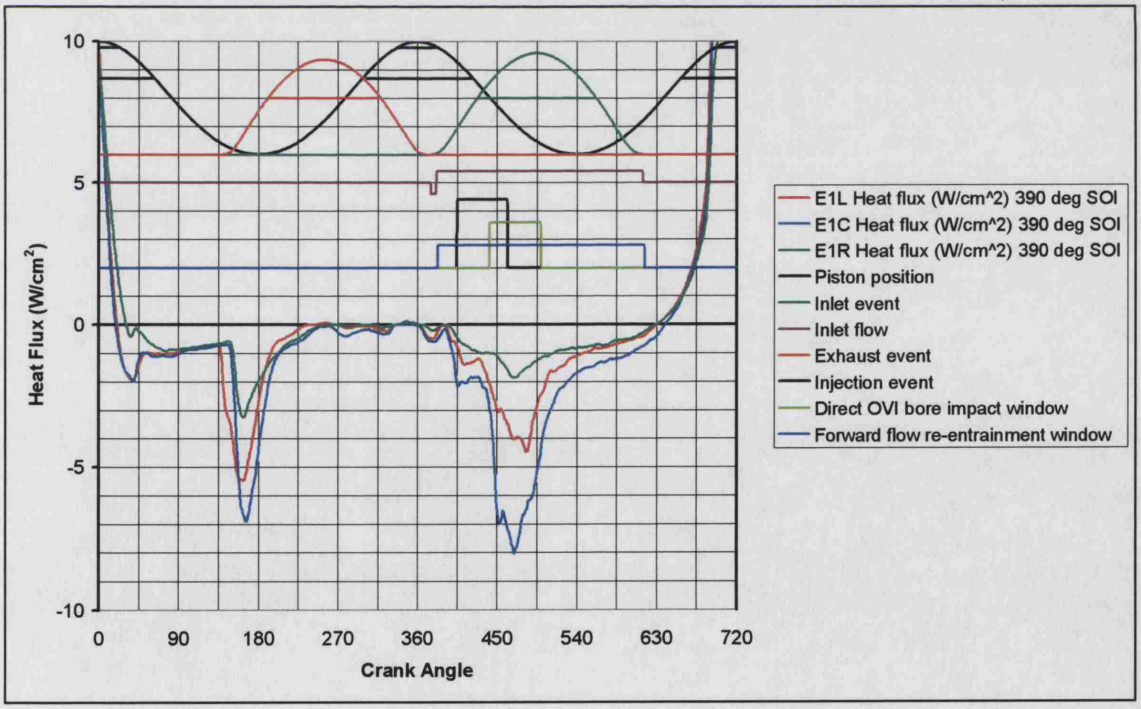

Figure 6.33 Locations E1-LCR with 390° CA injection

(CP cylinder head, retarded inlet, motoring)

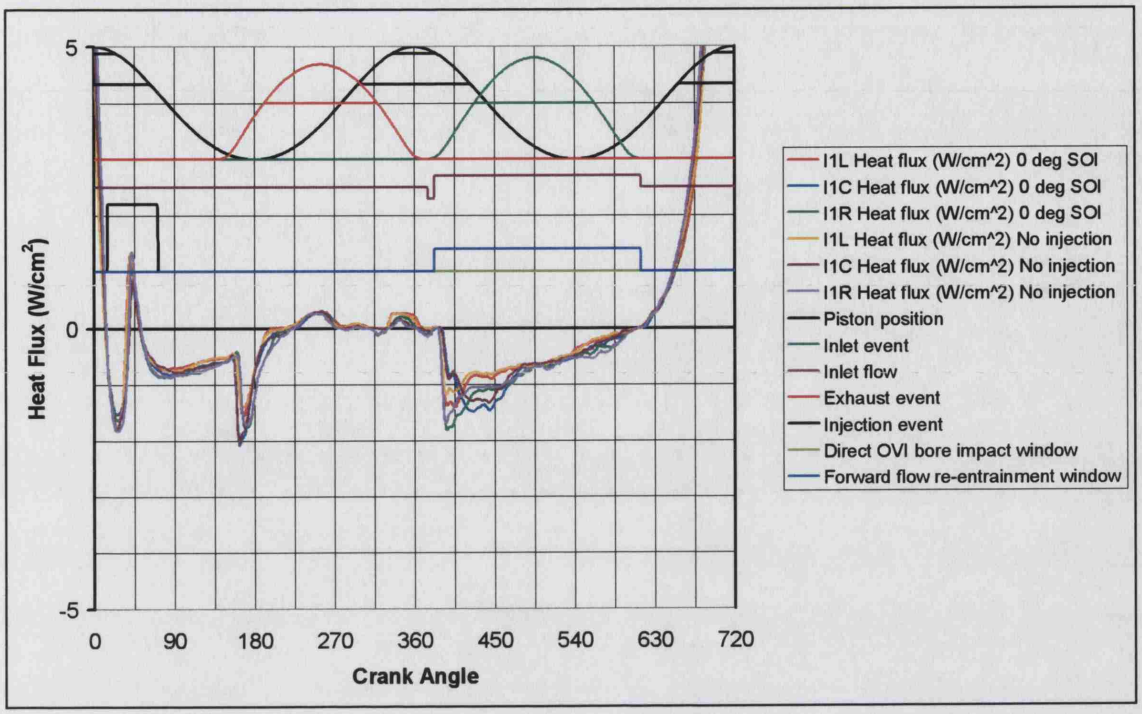

Figure 6.34 Locations I1-LCR with 0° CA injection and no injection

(CP cylinder head, retarded inlet, motoring)

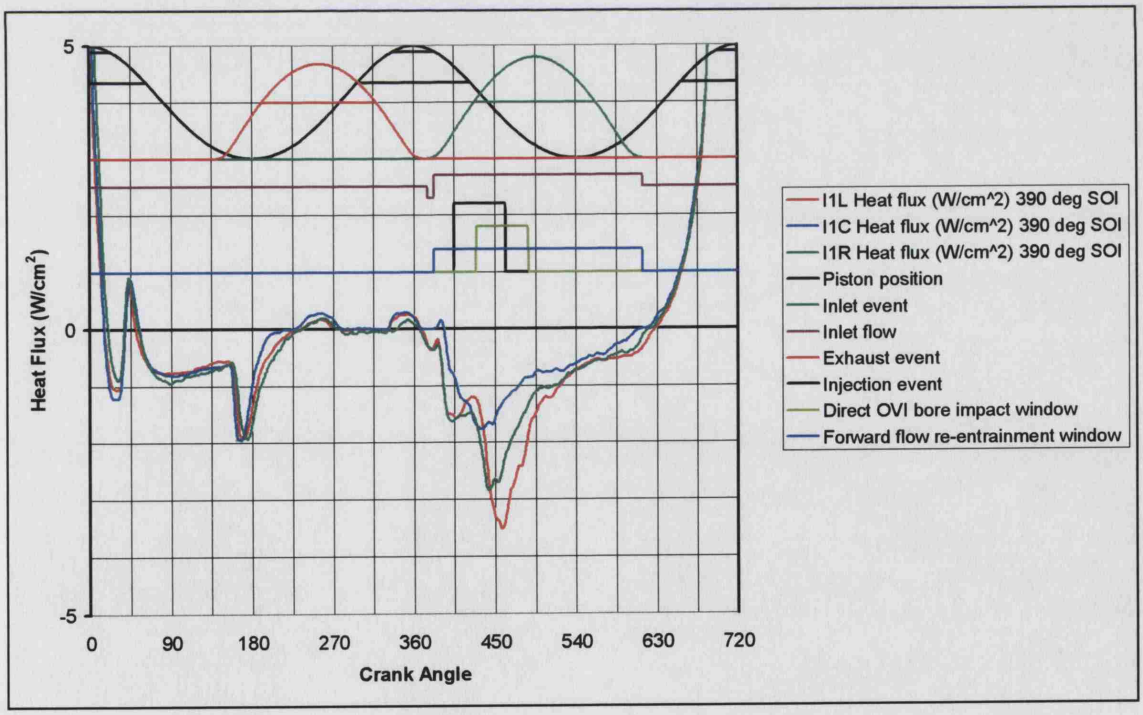

Figure 6.35 Locations I1-LCR with 390° CA injection

(CP cylinder head, retarded inlet, motoring)

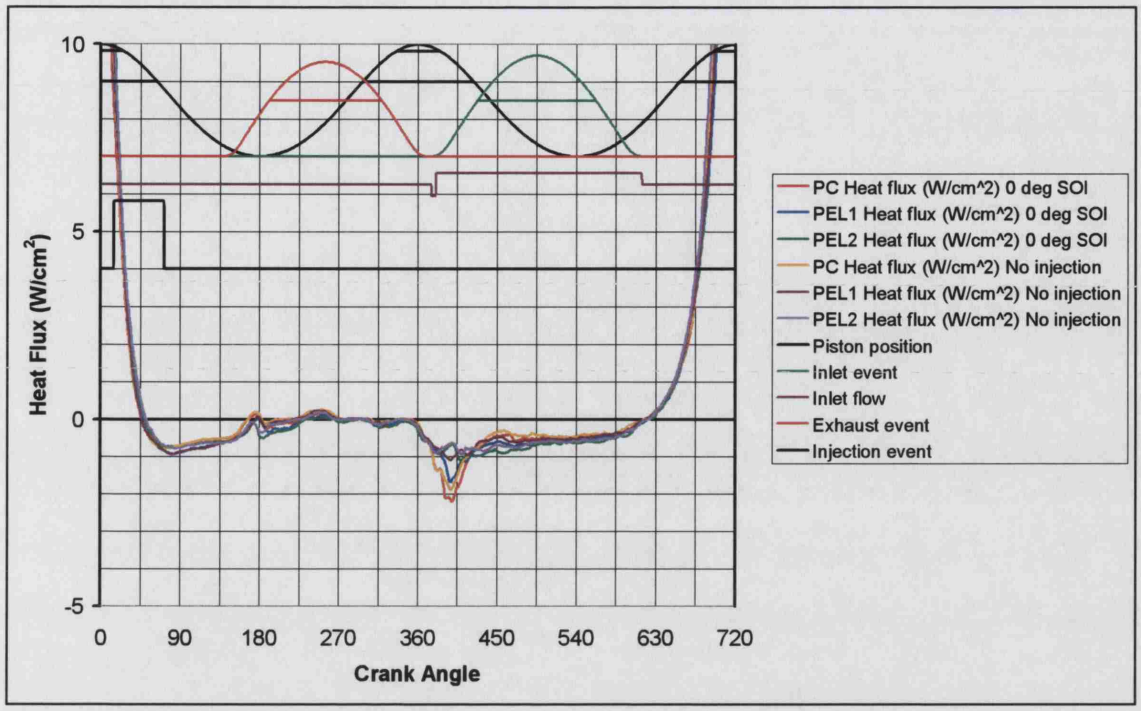

Figure 6.36 Locations PC, PEL1 and PEL2 with 0° CA injection and no injection (CP cylinder head, retarded inlet, motoring)

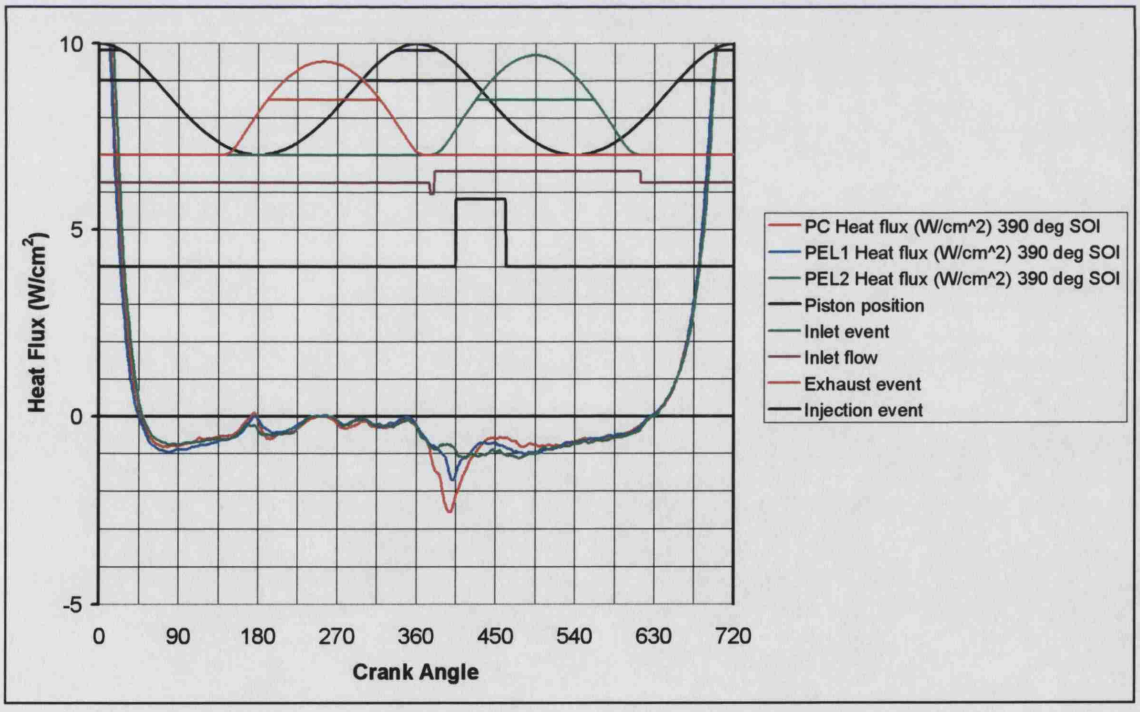

Figure 6.37 Locations PC, PEL1 and PEL2 with 390° CA injection (CP cylinder head, retarded inlet, motoring)

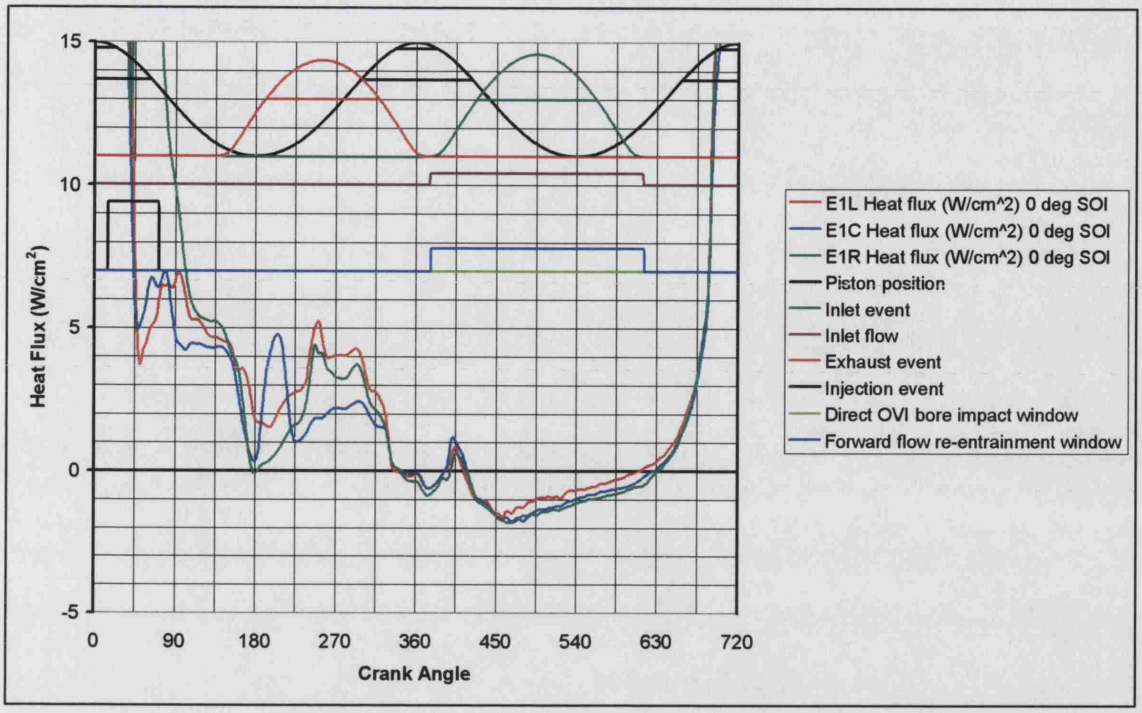

Figure 6.38 Locations E1-LCR with 0° CA injection

(CP cylinder head, retarded inlet, firing)

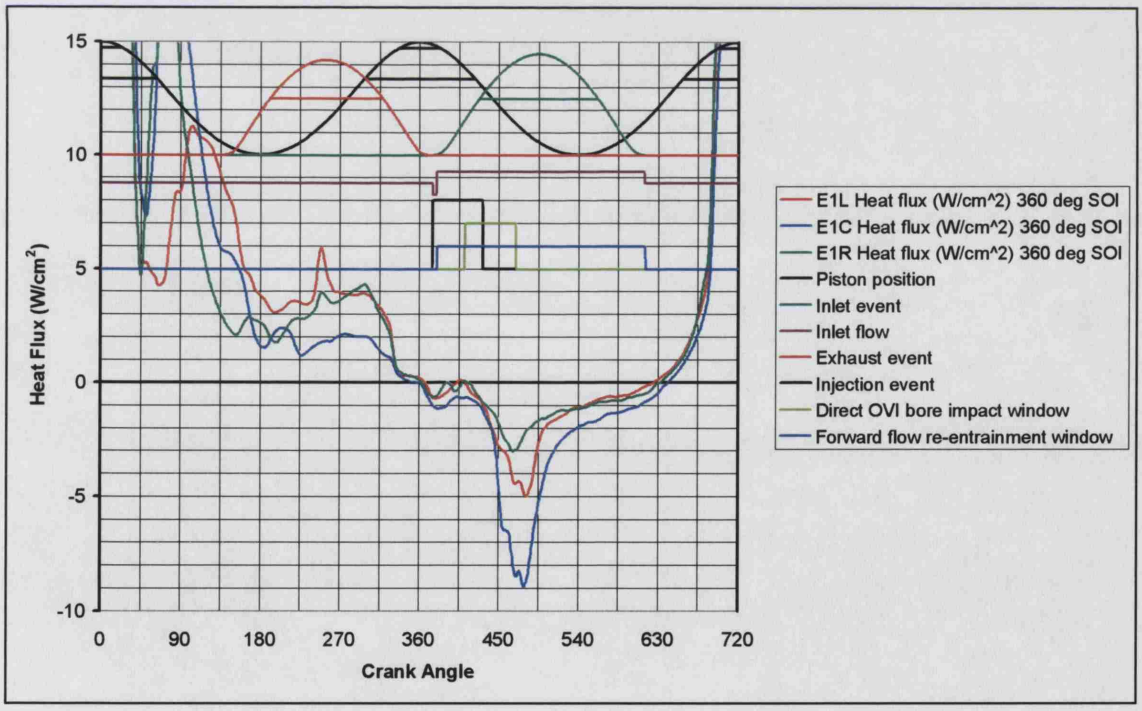

Figure 6.39 Locations E1-LCR with 360° CA injection

(CP cylinder head, retarded inlet, firing)

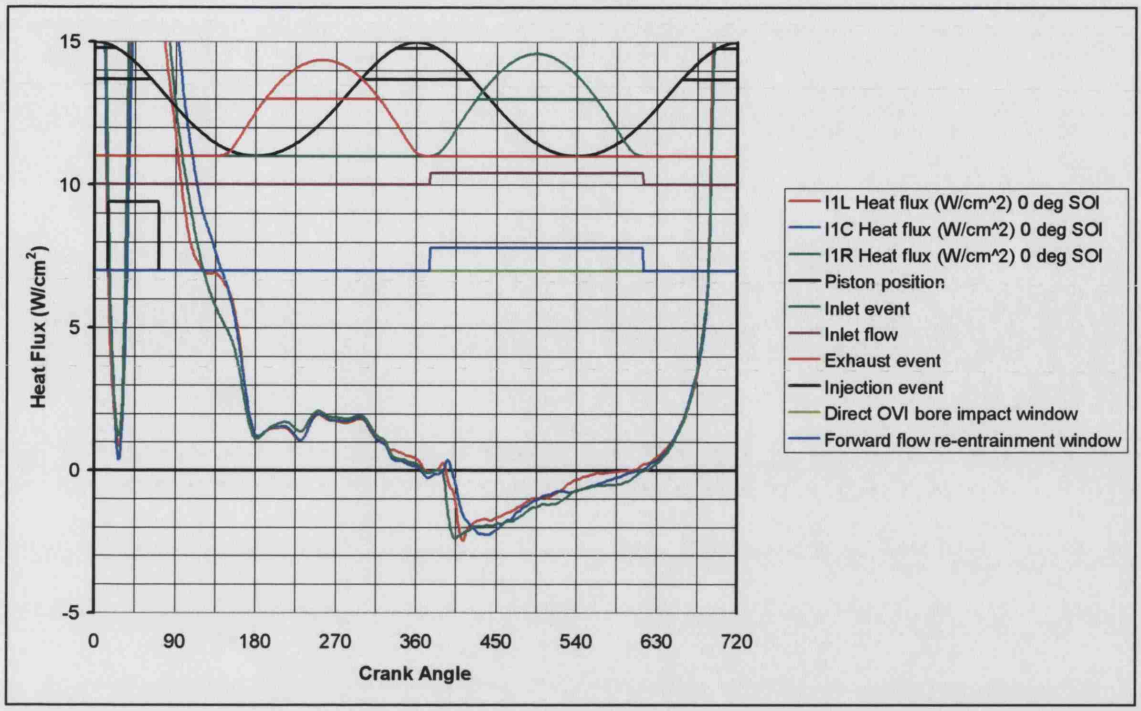

Figure 6.40 Locations I1-LCR with 0° CA injection

(CP cylinder head, retarded inlet, firing)

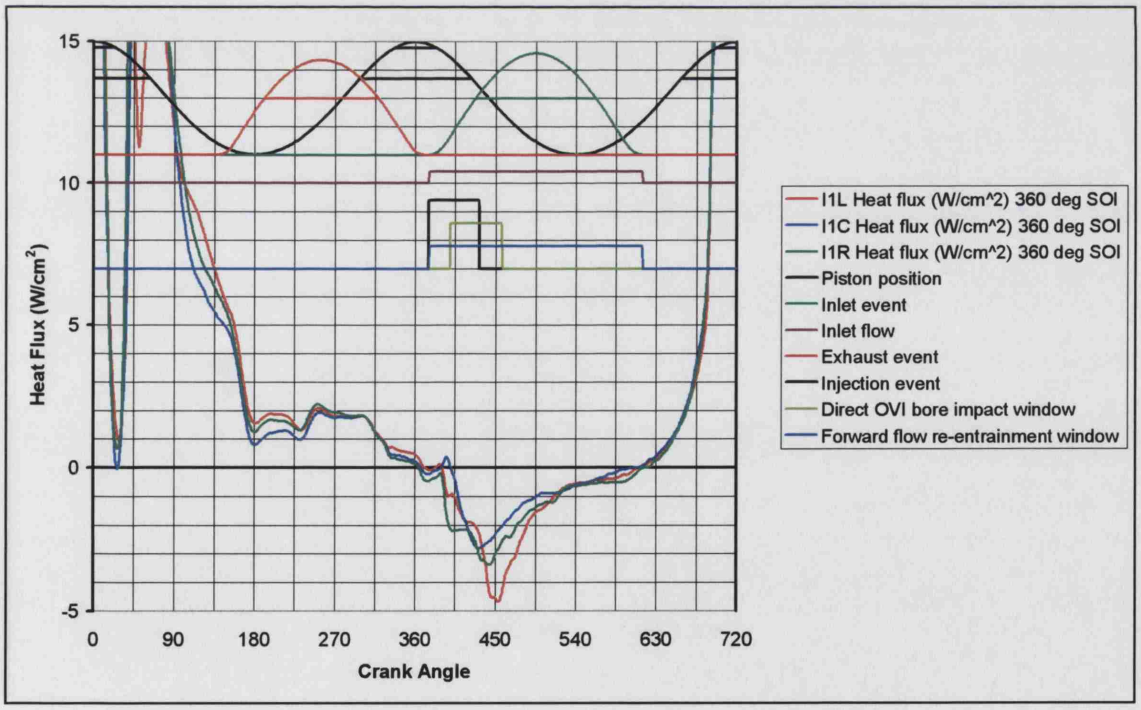

Figure 6.41 Locations I1-LCR with 360° CA injection

(CP cylinder head, retarded inlet, firing)

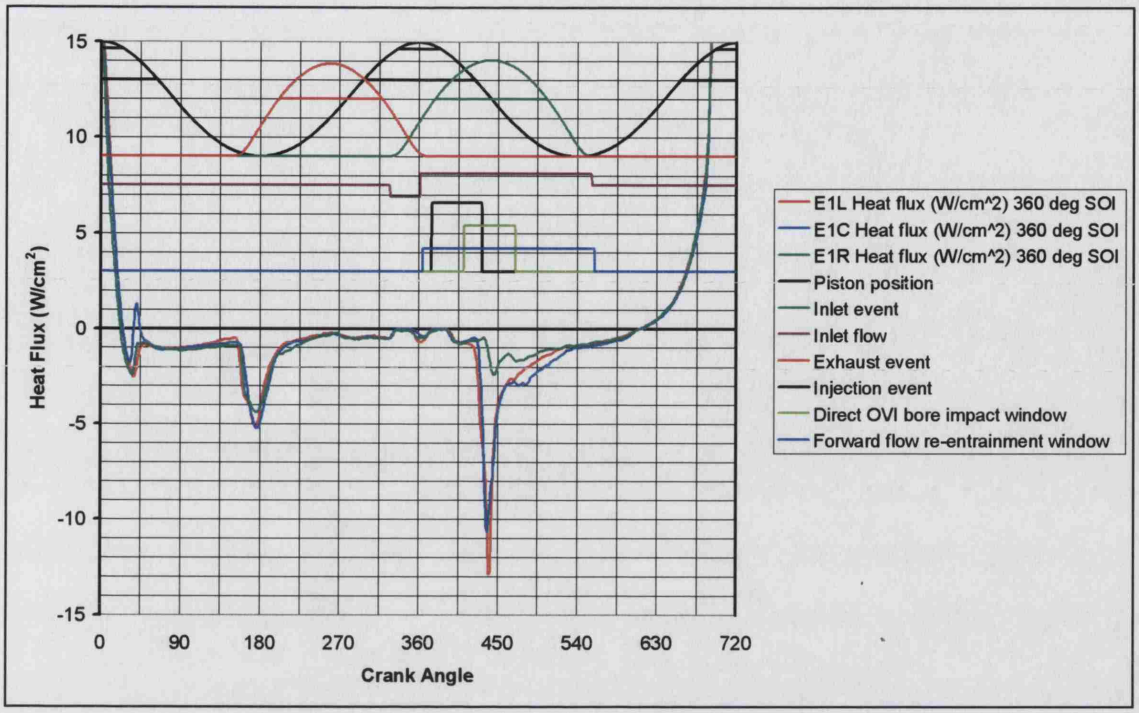

Figure 6.42 Locations E1-LCR with 360° CA injection timing

(AP cylinder head, deactivated port, motoring)

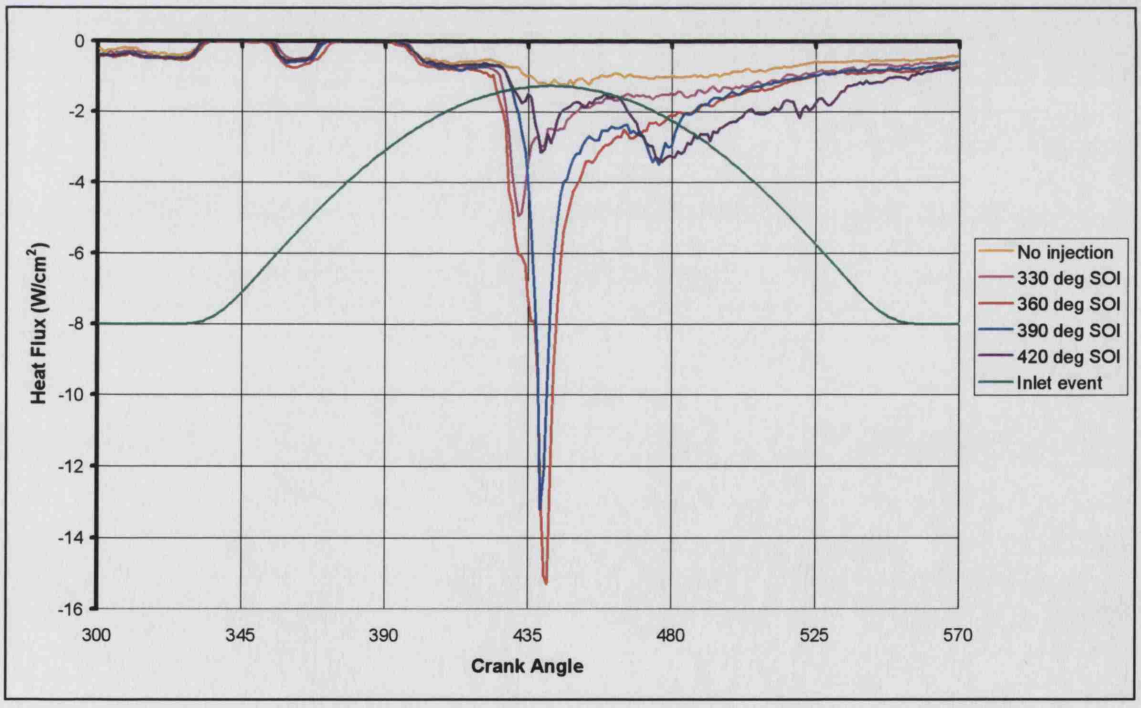

Figure 6.43 Injection sweep at location E1L with a non-coated sensor

(AP cylinder head, deactivated port, motoring)

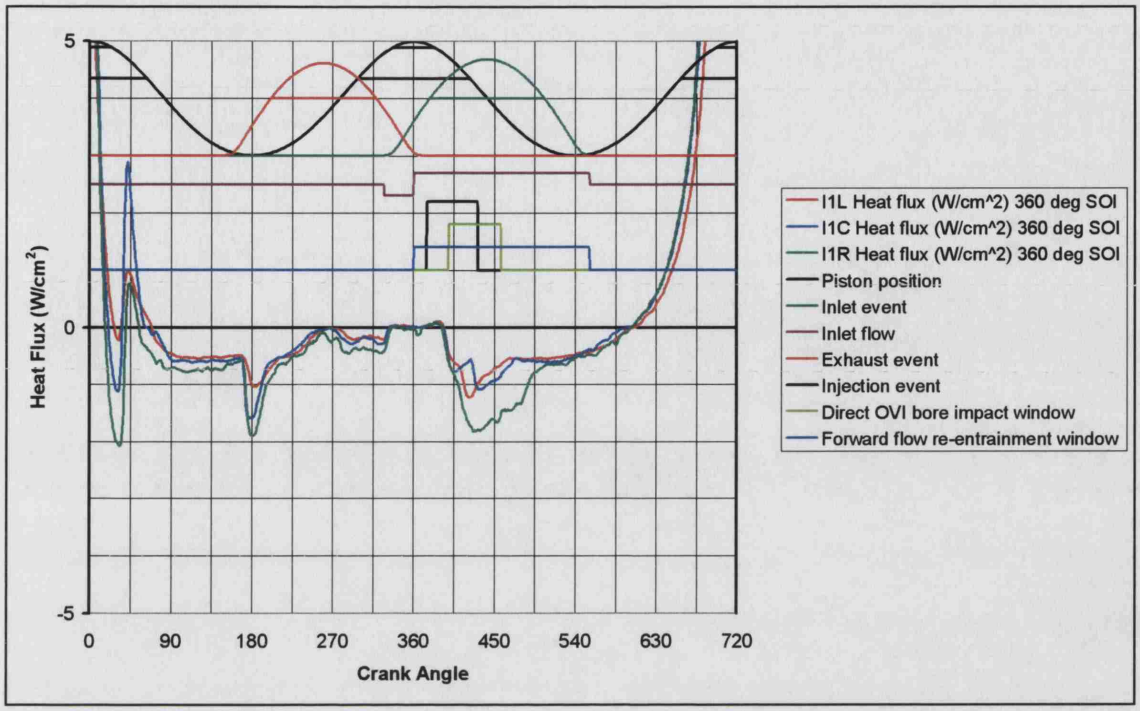

Figure 6.44 Locations I1-LCR with 360° CA injection timing

(AP cylinder head, deactivated port, motoring)

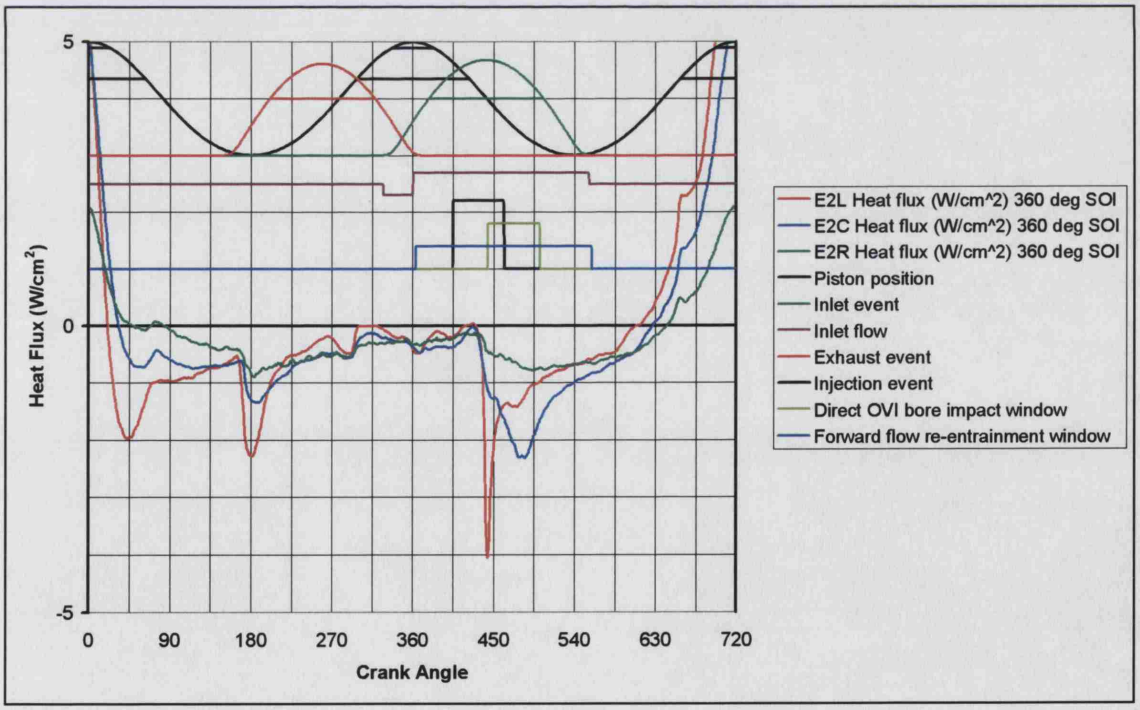

Figure 6.45 Locations E2-LCR with 360° CA injection timing

(AP cylinder head, deactivated port, motoring)

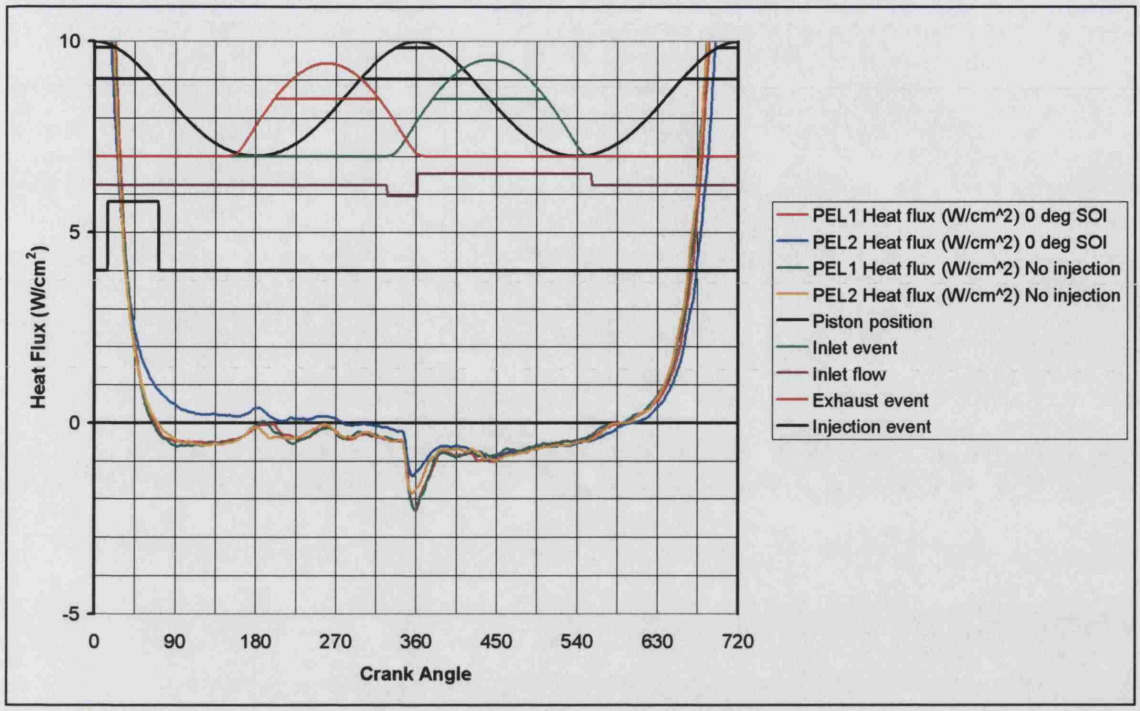

Figure 6.46 Locations PEL1, PEL2 with 0° CA injection timing and no injection (AP cylinder head, deactivated port, motoring)

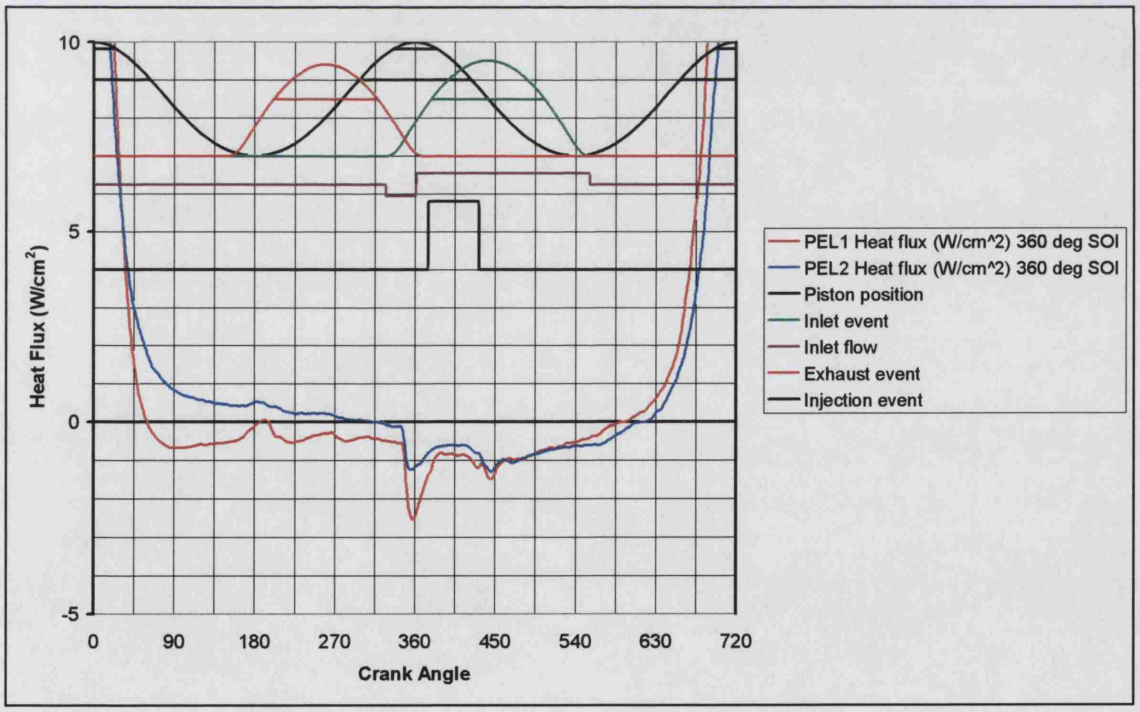

Figure 6.47 Locations PEL1 and PEL2 with 360° CA injection timing (AP cylinder head, deactivated port, motoring)

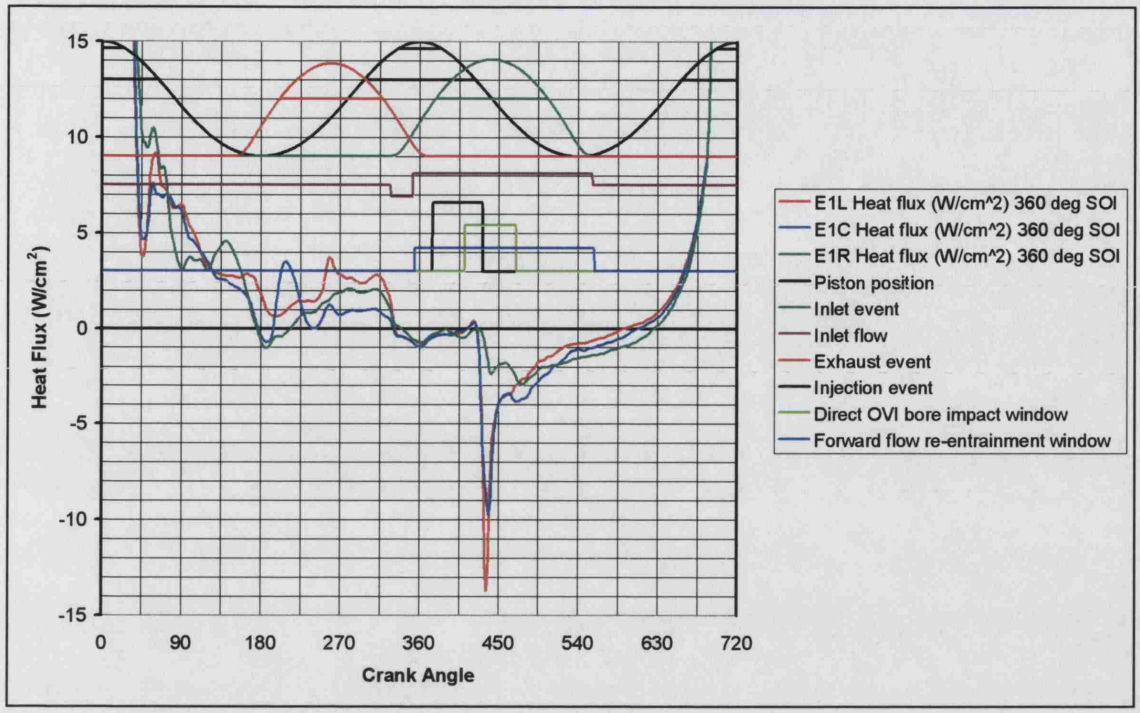

Figure 6.48 Locations E1-LCR with 360° CA injection timing

(AP cylinder head, deactivated port, firing)

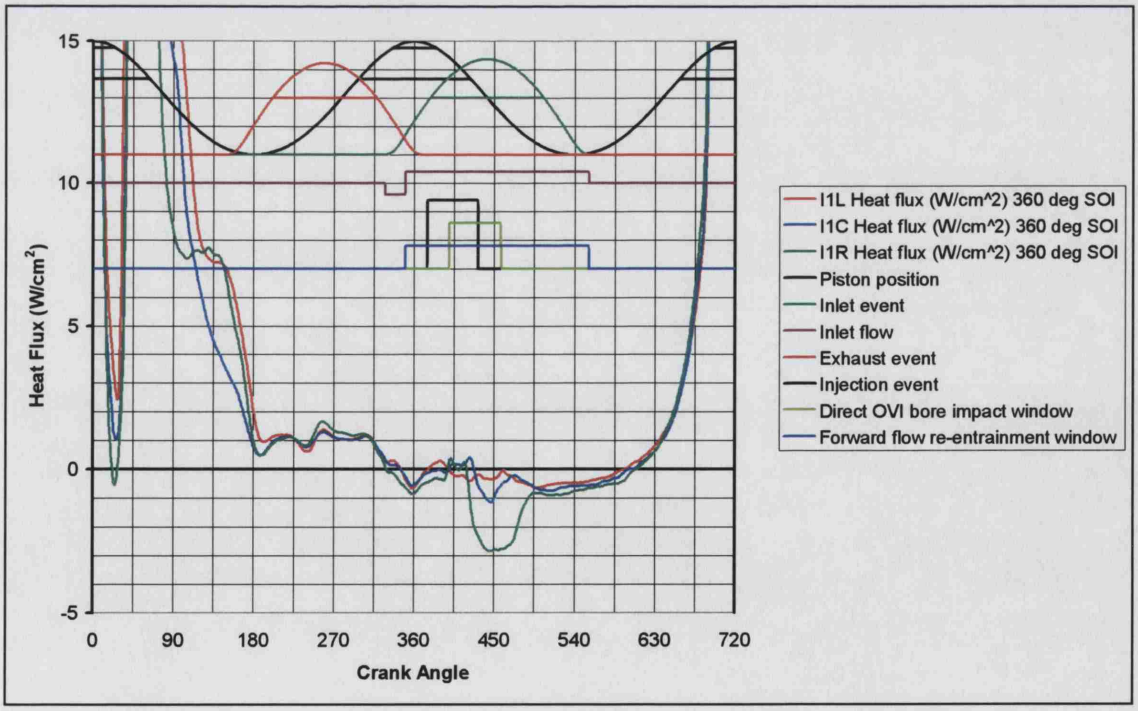

Figure 6.49 Locations I1-LCR with 360° CA injection timing

(AP cylinder head, deactivated port, firing)

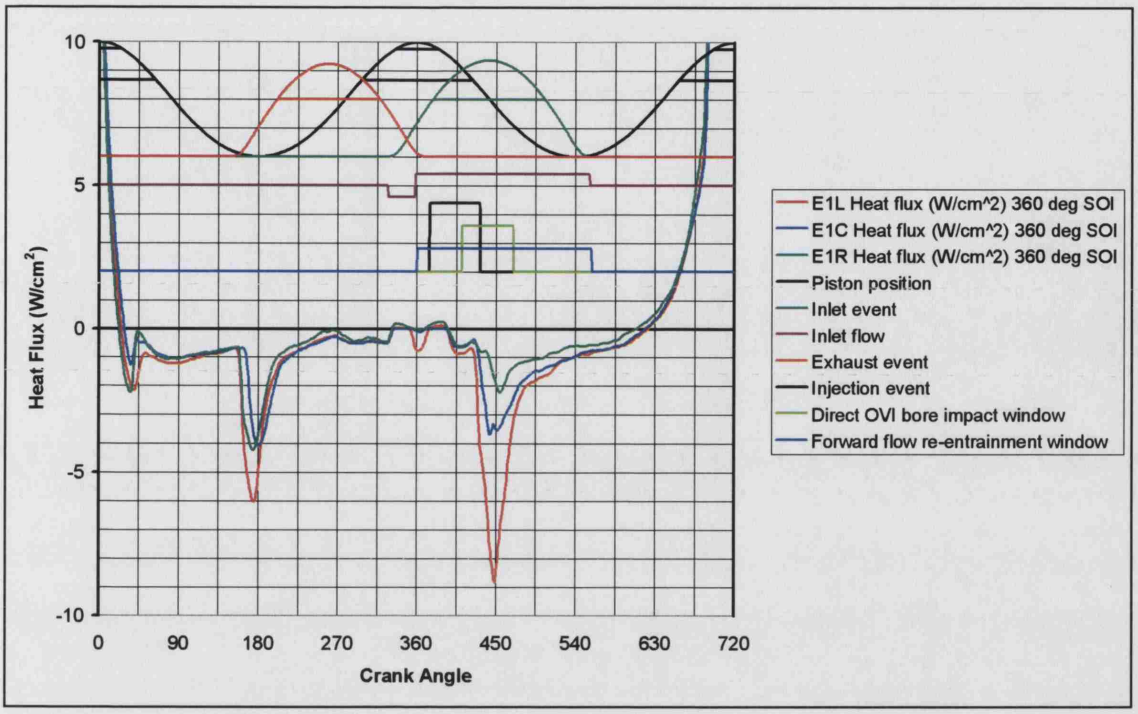

Figure 6.50 Locations E1-LCR with 360° CA injection timing

(AP cylinder head, activated port, motoring)

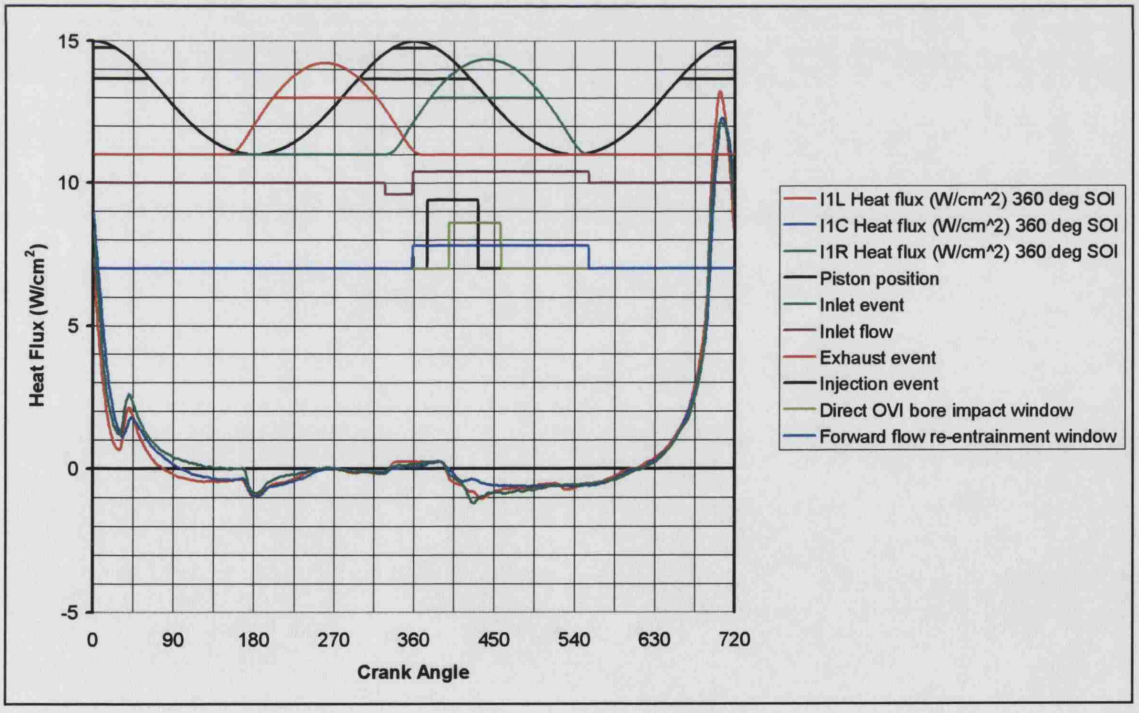

Figure 6.51 Locations I1-LCR with 360° CA injection timing

(AP cylinder head, activated port, motoring)

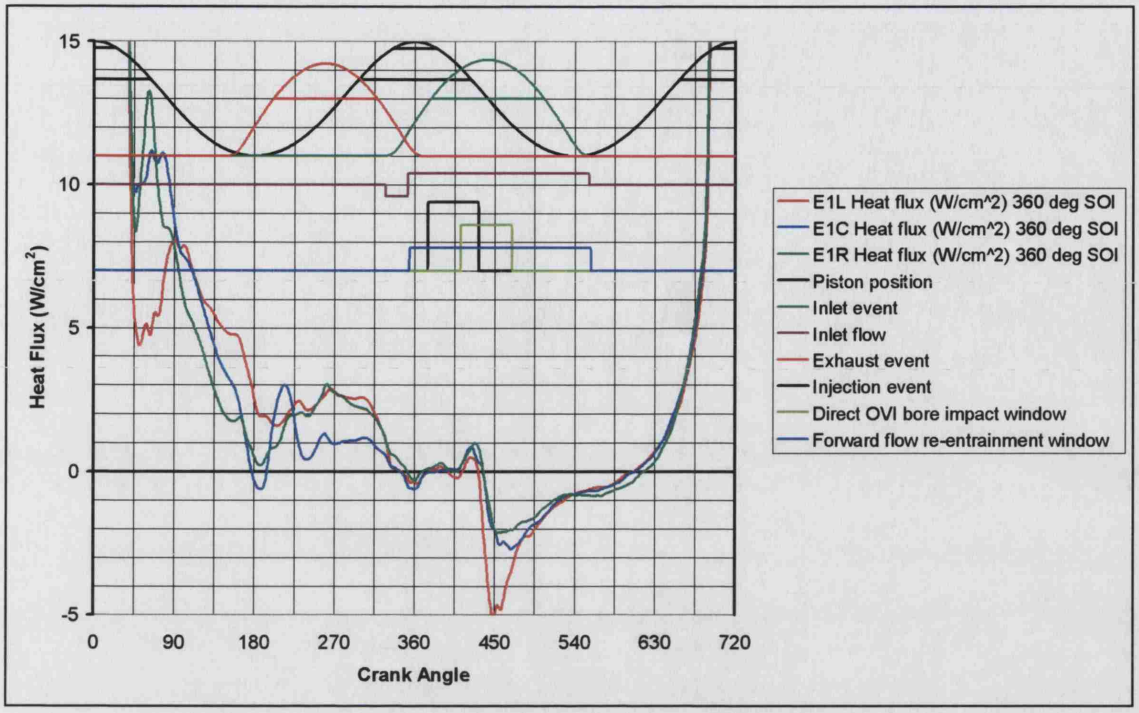

Figure 6.52 Locations E1-LCR with 360° CA injection timing

(AP cylinder head, activated port, firing)

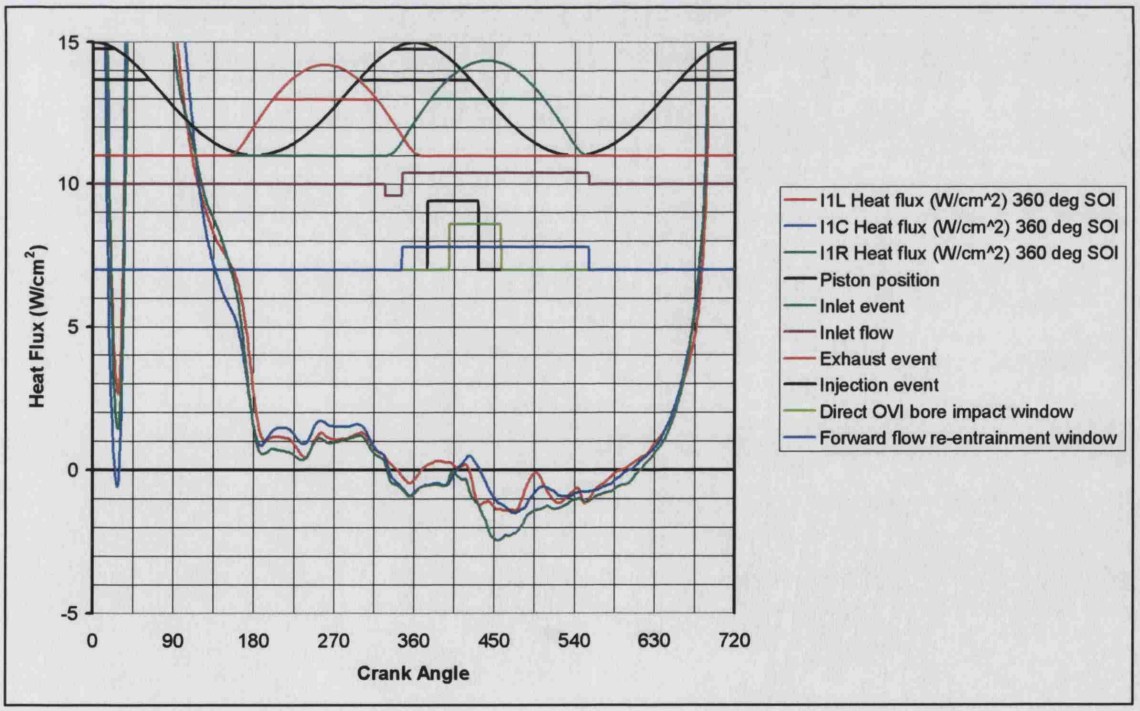

Figure 6.53 Locations I1-LCR with 360° CA injection timing

(AP cylinder head, activated port, firing)

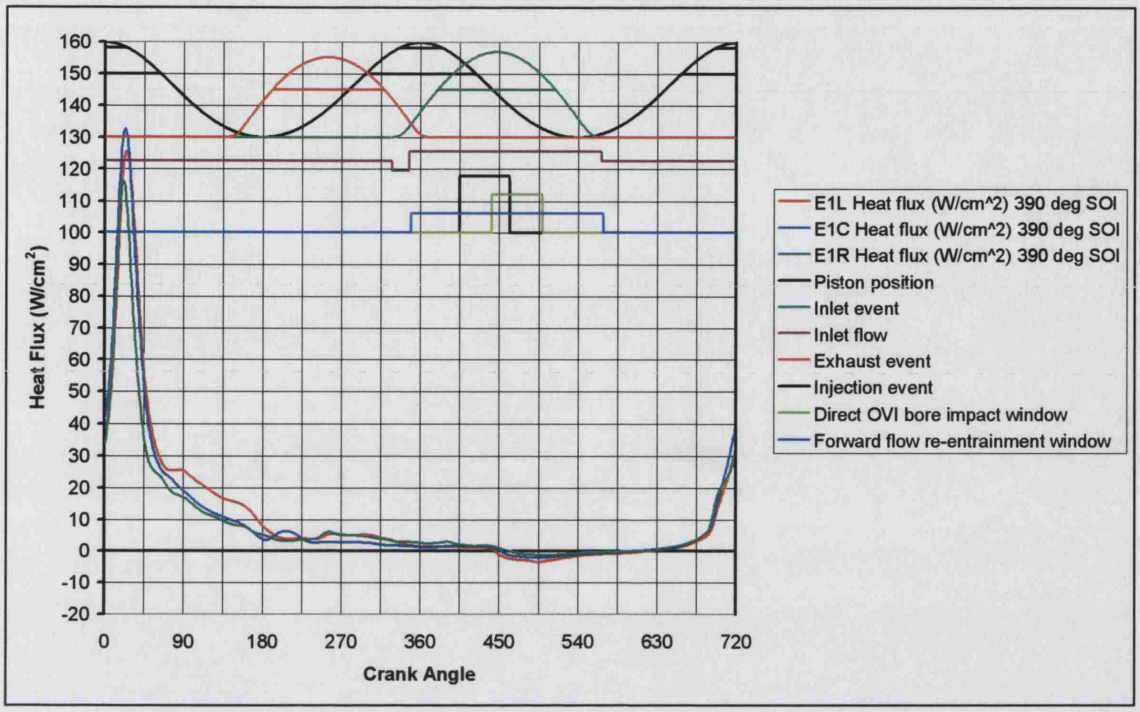

Figure 6.54 Locations E1-LCR with 390° CA injection

(CP cylinder head, advanced inlet, firing)

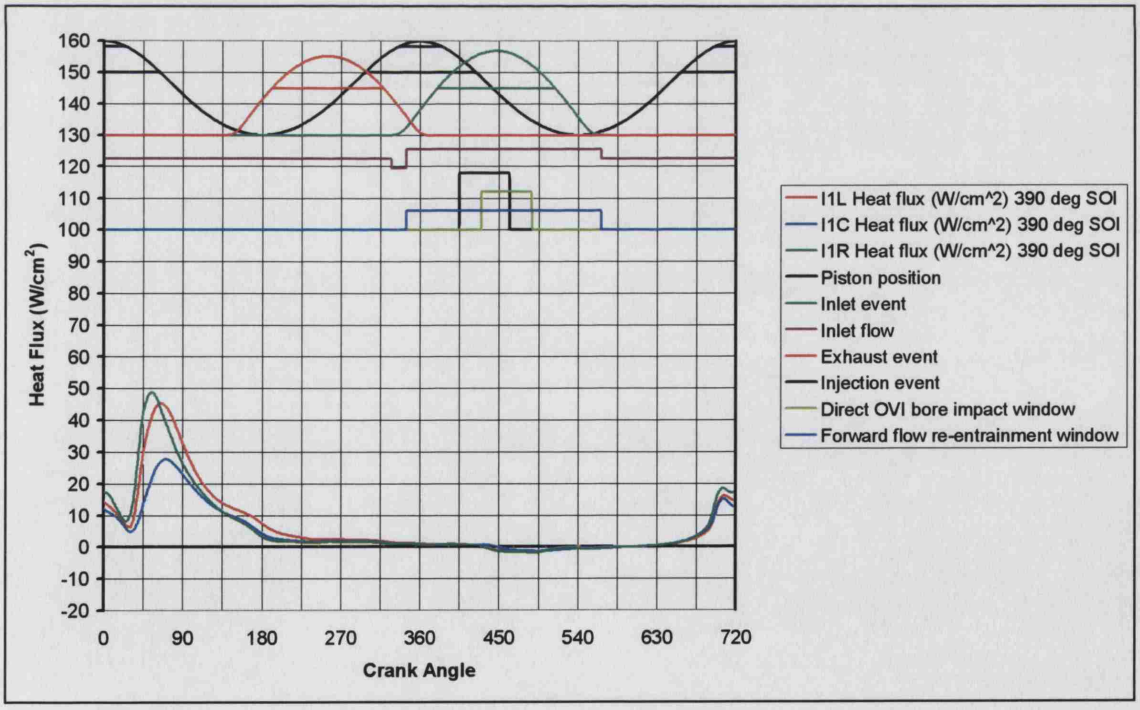

Figure 6.55 Locations I1-LCR with 390° CA injection

(CP cylinder head, advanced inlet, firing)

CHAPTER 7

CONCLUSIONS

7.1 CONCLUSIONS

7.1.1 Porous Liner Technique

The study by Ioannou showed that for a Ford Modular V8 4-valve cylinder head operating at a simulated 1500 rpm on a room temperature motored rig, 60% of the injected fuel was collected on the cylinder bore for both CVI and OVI conditions. The AJ26 and AJ33 AP cylinder heads compared in this porous liner work caused much less wall wetting and generated equivalent CVI wall wetting figures of only 33% and 4 % respectively. The AJ33 AP cylinder head produced a wall wetting value of only 14% for OVI conditions. These are all worst-case values which would be higher than those experienced by a running engine. The difference between the AJ26 and AJ33 AP cylinder heads was attributed to a combination of intake geometry, port deactivation and injector performance. The endoscope observations confirmed the belief that the core swirl design of the AJ33 AP cylinder head was chiefly responsible for the difference in results as the fuel impactions observed for this cylinder head were further down the cylinder and further around the circumference of the cylinder in a spiral pattern. Port deactivation in the AJ33 AP head was seen to increase wall wetting, but not to the levels of the AJ26 cylinder head. Insertion of the advanced Denso 12-hole injector from the AJ33 head into the AJ26 head during CVI tests resulted in a reduction in wall wetting, indicating that this injector was superior to the one used in the AJ26 cylinder head.

When the speed was increased to replicate 2500 rpm with a wide open throttle, the amount of wall wetting increased as expected. CVI caused the AJ26 head to wet the cylinder wall twice as much as the AJ33 AP head, while the OVI timings returned similar levels of wall wetting for the AP head due to the presence of both liquid wall film and airborne droplets. Opening the deactivation flap of the AJ33 AP at this speed again caused a drop in wall wetting, as did using the 12-hole injector in the AJ26 cylinder head. The effect of the 12-hole injector was also more noticeable at this speed.

The porous liner did have several disadvantages in the study of wall wetting, although this technique generally presented a worst case scenario. Additionally, this test rig revealed the approximate location of droplet impaction on the cylinder bore which helped in the design of the heat flux engine.

7.1.2 Heat Flux Technique

This technique had several advantages over the porous liner technique, mainly that the engine could be fired as well as motored to explore wall wetting. Similarly, the ability to control the cylinder block and cylinder head water temperatures indicated what promoted or reduced wall wetting and allowed an optimum setting to be used which helped the sensors detect the fuel.

The AJ33 CP cylinder head was the main focus of this work, but the AJ33 AP head was again used to bridge the gap between the porous liner and heat flux results. The heat flux results proved conclusively for both cylinder heads that OVI wetted the cylinder bore with airborne fuel droplets and that CVI caused no wall wetting in any condition. This was known because the wall wetting detected on the heat flux traces coincided with the predicted times of flight of fuel passing directly from the injector through the open inlet valves and impacting on the cylinder wall. Up until this impact point the heat flux trace would resemble that of a motored trace with no injection occurring. There was also no evidence that wall films were transporting the fuel to the sensors, even under CVI conditions. This was quite different to the results established by Ioannou when investigating the Ford 4.6 Litre modular V8 engines who found that a combination of fuel wall films and airborne droplets were responsible for the wall wetting. In all of the results for both the AP and CP cylinder heads, the sensors high on the exhaust side of the bore experienced the most wall wetting. This was because the fuel injector almost had a direct line of sight of the sensors and the view was only blocked by the edge of the valve seat near to the spark plug. It was clear that the injected droplets could pass through the open inlet valves and across the cylinder to impact on the exhaust side of the cylinder wall. The high performance of the Denso 12-hole injector was also responsible for the reduction in wall wetting because it generated a relatively high proportion of very small fuel droplets that remained entrained in the airflow.

Since only OVI was seen to cause wall wetting, further investigations into this injection strategy were performed. The pulsewidth variation test was extremely important in this work as it proved that the amount of wall wetting was proportional to the amount of fuel injected and that there was a direct relationship between inlet valve lift and the location of the wall wetting. Low valve lifts resulted in no wall wetting being detected, while

maximum lift resulted in a reduction in wall wetting as the impaction area momentarily moved away from the sensor. Similarly, showing several OVI heat flux traces on one chart was also quite revealing as it indicated the relevant impaction magnitudes and helped distinguish the features unique to the different injection timings. This flow vectoring effect of the inlet valve could occur in any port fuel injected engine and should be considered by engine designers if an OVI strategy is to be employed successfully and avoid the detrimental effects of wall wetting. The main physical differences between the AP and CP cylinder heads accounted for the reduction in wall wetting under OVI test conditions.

Port deactivation of the AP cylinder head was found to create higher levels of wall wetting due to the higher gas velocities carrying fuel droplets across to the exhaust sensors. Even the lower exhaust side sensors were exposed to noticeable levels of wetting during this condition, illustrating how the higher flows dictate where fuel impaction occurs. However, the CP cylinder head had less wetting than the AP head even when the deactivation flap was open because the right hand swirl port of the CP head had a steeper entry angle and helped the airborne droplets avoid impacting the sensors. This was complemented by less aggressive inlet valve shrouding that did not force the flow towards the exhaust side of the cylinder as much as in the AP head. These small changes in cylinder head design highlight the fact that wall wetting is generally quite sensitive to engine geometry and this should be remembered in the design of all port fuel injected engines.

Retarding the inlet valve of the CP cylinder head did not affect the levels of wall wetting, but simply retarded the wetting by an equal amount. Due to the larger inlet flow, this was the only time in the heat flux work that the upper inlet side sensors detected any fuel droplet impactions.

The piston experienced no specific fuel impactions as seen on the cylinder wall, although the piston was found to possess a fuel film on the exhaust side during some OVI motoring tests. It was believed that since the piston was further away from the injector, any possible impaction covered a relatively large area.

The LabVIEW software proved to be an excellent tool for logging the heat flux data and storing it in and Excel format. The analysis program helped in the understanding of the complex heat flux traces in a number of ways, whether by comparing traces to one another or to other relevant data. A prime reason for using Excel was that the values in the spreadsheet were easily accessible, and this proved extremely useful throughout the development and deployment of the program.

The problems with the heat flux sensors caused much frustration and wasted much valuable experimentation time, but these events led to the chance discovery that removal of the zynolyte coating from the sensors made them more responsive. This added response was then what permitted so much extra detail to be revealed about the fuel droplet impactions.

It has been mentioned that wall wetting can be quite detrimental to internal combustion engines because it causes bore washing, the formation of acidic chemicals and results in both increased fuel consumption and high HC emissions. A further negative affect is on engine transients when either a hold up of fuel or addition of extra fuel will briefly result in a lean or rich mixture that will reduce torque [Baker (1995)]. Due to the nature of the heat flux results indicating that only airborne droplets impacted the cylinder bore, it was thought that this type of wall wetting will not have a noticeable affect on transient behaviour of the engine. It should be noted that whilst it was possible to identify the mechanisms affecting the flight of the droplets to the cylinder wall during OVI, the level of wetting that the liner received was reassuringly small compared to previously tested configurations [Ioannou (2000)]. This fact, coupled with the lack of measurable fuel impacting during CVI, suggests that a production engine based upon the engine geometries tested in this work should not suffer from any durability concerns related to bore wetting.

7.2 ORIGINAL ASPECTS OF THIS STUDY

This was the first time that heat flux sensors had been used to detect liquid fuel on the piston of a fired or motored engine. The results were then automatically logged by LabVIEW and analyzed in the extensive Excel computational program which is also a new step for wall wetting research. Ioannou had made the most thorough study of wall wetting thus far and was only capable of studying the heat flux traces obtained from the cylinder bore and the results were manually handled prior to a visual interpretation.

The most important mechanical feature of this work was the integrated design of the piston, cylinder block and arm mechanism that successfully and reliably carried the heat flux sensor wires from the moving piston.

Once the LabVIEW software had logged the data, the Excel analysis provided comprehensive assistance in the understanding of the complex and unique heat flux traces. This initially included geometric engine information such as piston position and valve events, but then also considered flow information calculated from experimental data and carefully calculated predictions on when fuel droplets may impact engine surfaces. Ioannou postulated that it was possible to determine the quantity of fuel impacting the sensor by comparing both wet and dry heat flux traces and this was fully explored in this work in a very flexible format. The pulsewidth variation test technique was also developed to aid in both the quantification and understanding of the wall wetting experienced.

The results themselves are quite unique as no other evidence has been found in the literature of a similar in-cylinder wall wetting investigation. The influence of cylinder head design, injection timing, valve timing and port deactivation on wall wetting has been studied in depth. Open valve injection and port deactivation in particular were found to generate large amounts of wall wetting, while retarding the inlet event simply acted to retard the wall wetting event by an equal amount. A key discovery was the close link between inlet valve lift and location of wall wetting on the exhaust side of the cylinder bore. These findings can be used to further develop both the V8 and V6 engines with a greater insight into what promotes or reduces cylinder wall wetting.

7.3 RECOMMENDATIONS FOR FURTHER WORK

There are a few possible improvements that could be made to the porous liner technique. Small electric heaters could be introduced into the cylinder head to explore what effects fuel evaporation within the inlet port has on wall wetting and liquid fuel formation. Knowledge gained from the heat flux work suggests that heated water may instead be passed through the cylinder head to achieve warmer port surfaces. The amount of fuel collected under heated or cool conditions would then provide more information about the wetting characteristics. A porous collection point could be introduced just below the dummy cylinder to try and account for some of the fuel that may other wise go uncollected and would hit the piston in the real engine.

The most important suggestion for further work is aimed primarily at recording heat flux traces from the piston. It was clear from this work that the piston was being impacted by a small amount of fuel droplets, but it was impossible to tell the exact point in the cycle when the impactions were occurring. Synchronization between the fuel injector and logging equipment would be required so that only one injection occurs and only the engine cycle in which it occurs gets logged. The extreme time restrictions imposed upon this work eliminated any chances of this being performed. Since most research in the near future will be on direct injection engines, this would be of increased importance.

If work is to continue with heat flux sensors, it is highly recommended that the sensors are used without the black coating on their sensing face so as to provide signals with a faster response and an increased amount of information. The pulsewidth variation tests indicated that the fuel spray was being directed away from the sensor by the inlet valve and this should be considered in the placement of heat flux sensors in future. Since the droplet impact zone did not move very far, placing the sensor locations closer together would provide more information on which direction the droplet impaction zone moves in. This may require additional sensor locations though, because all the sensor locations used here provided useful information. Similarly, the quantification of fuel detected by several sensors should be considered and methods for accounting for the fuel that might possibly impact between sensors should be also devised.

REFERENCES

Amann,C. *'Cylinder-Pressure Measurement and its Use in Engine Research'*, SAE paper 852067, **1985**

Autocar. *'Fuel Blamed for BMW Engine Damage'*, Autocar Magazine article, Publisher: Haymarket, February 18th, **1998**

Baker,T. *'Port Throttles Applied to a High-Performance 4-Valve S.I. Engine'*, Ph.D. Thesis, Department of Mechanical Engineering, University College London, **1995**

Ball,J. *'Emission Rates and Elemental Composition of Particles Collected from 1995 Ford Vehicles Using the Urban Dynamometer Driving Schedule, the Highway Fuel Economy Test and the US06 Driving Cycle'*, SAE paper 972914, **1997**

Basaki,M. Saito,K. and Nakashima,T. *'Analysis of Oil Consumption at High Engine Speed by Visualization of the Piston Ring Behaviors'*, SAE paper 012877, **2000**

Bauer,W. Balun,P. Heywood,J. *'Heat Transfer and Mixture Vaporization in Intake Port of Spark-Ignition Engine'*, SAE paper 972983, **1997**

Bendat,J. Piersol,A. *'Random Data Analysis and Measurement Procedures'*, 3rd edition, Publisher: Wiley, **2000**

Benson,R. Whitehouse,N. *'Internal Combustion Engines – A detailed introduction to the thermodynamics of spark and compression ignition engines, their design and development'*, Volume 1, Publisher: Pergamon, **1979**

Birch,S. *'Combustion and Expansion at Saab'*, Automotive Engineering International Magazine, article March, **2001**

Boehm,G. Harrer,J. *'Nickel Coated Pistons for Improved Durability in Knock Control Engines'*, SAE paper 900453, **1990**

Bourke,M Evers,L. *'Fuel Film Dynamics in the Intake Port of a Fuel Injected Engine'*, SAE paper 940446, **1994**

Brogan,M. Swallow,D Brisley,R. *'A New Approach to Meeting Future European Emission Standards with the Orbital Direct Injection Gasoline Engine'*, SAE paper 2000-01-2913, **2000**

Burton,J. *'Processes Affecting the State and Behaviour of Fuel in the Intake Port of a Spark Ignition Engine'*, Ph.D. Thesis, University of Nottingham, **2004**

Cadle,S. *'Exhaust Particulate Matter Emissions from In-Use Passenger Vehicles Recruited in Three Locations – CRC Project E-24'*, SAE paper 1999-01-1545, **1999**

Caines,A. Haycock,R. *'Automotive Lubricant Reference Book'*, Publisher: Society of Automotive Engineers, **1996**

Castaing,B. Cowart,J. Cheng,W. *'Fuel Metering Effects on Hydrocarbon Emissions and Engine Stability During Cranking and Start-up in a Port Fuel Injected Spark Ignition Engine'*, SAE paper 2000-01-2836, **2000**

Cengel,Y. Boles,M. *'Thermodynamics – An Engineering Approach'*, Publisher: McGraw-Hill, 2nd edition, **1994**

Crosse,J. *'Throw out the Throttle'*, Autocar Magazine, article February 21st, **2001**

Curtis,E. Russ,S. Aquino,C. Lavoie,G. Trigui,N. *'The Effects of Injector Targeting and Fuel Volatility on Fuel Dynamics in a PFI Engine During Warm-Up: Part II-Modelling Results'*, SAE paper 982519, **1998**

Dawson,M. Hochgreb,S. *'Liquid Fuel Visualization Using Laser-Induced Fluorescence During Cold Start'*, SAE paper 982466, **1998**

Department of Energy – U.S. 'US06 Aggressive Driving Cycle', Website address: http://www.ott.doe.gov/otu/field_ops/emis_tour/us06.html, (Visited on 2/4/01), **2001**

Dieselnet.com 'Emission Test Cycles', Website address: http://www.dieselnet.com/, (Visited on 2/4/01), **2001**

Egermann,J. Leipertz,A. *'Influence of Fuel Properties on Mixture Formation: An Experimental Analysis for High Pressure Swirl Injectors'*, SAE paper 2000-01-2863, **2000**

Endres,H. *'Combustion Systems Trends for Multi-Valve Gasoline Engines'*, SAE paper 900652, **1990**

Environmental Protection Agency. 'Dynamometer Driving Schedules', Website address: http://www.epa.gov/otaq/labmthod.htm, (Visited on 2/4/01), **2001**

Ferguson,C. *'Internal Combustion Engines – Applied Thermosciences'*, Publisher: Wiley and Sons, **1986**

Flierl,R. Klüting,M. *'The Third Generation of Valvetrains – New Fully Variable Valvetrains for Throttle-Free Load Control'*, SAE paper 011227, **2000**

Froelund,K. *'Real-Time Steady-State Measurement of PCV-Contribution to Oil Consumption on Ford 4.6L SI-Engine'*, SAE paper 2000-01-2876, **2000**

Fry,M. *'Optimisation of Mixture Preparation in a S.I. Engine'*, Ph.D. Thesis, Department of Mechanical Engineering, University College London, **1999**

Fry,M. Nightingale,C. Richardson,S. *'High Speed Photography and Image Analysis Techniques Applied to Study Droplet Motion Within the Porting and Cylinder of a 4-valve SI Engine'*, SAE paper 952525, **1995**

Funatani,K. Kurosawa,K. *'Improved Engine Performance Via Use of Nickel Ceramic Coatings (NCC Coat)'*, SAE paper 940852, **1994**

Grimm,B. *'Review of Simple Heat Release Computations'*, SAE paper 900445, **1990**

Guezennec,Y. Hamama,W. *'Two-Zone Heat Release Analysis of Combustion Data and Calibration of Heat Transfer Correlation in an IC Engine'*, SAE paper 1999-01-0218, **1999**

Hall,D. *'Measurement of the Number of Emitted Gasoline Particles: Genuine or Artefact'*, SAE paper 2000-01-2957, **2000**

Hara,S. Hidaka,A. Tomisawa,N. Nakamura,M. Todo,T. *'Application of a Variable Valve Event and Timing System to Automotive Engines'*, SAE paper 2000-01-1224, **2000**

Hartfield-Wünsch,S. Tung,S. Rivard,C. *'Development of a Bench Wear Test for the Evaluation of Engine Cylinder Components and the Correlation with Engine Test Results'*, SAE paper 932693, **1993**

Heisler,H *'Advanced Engine Technology'*, Publisher: Arnold, **1998**

Hentschel,W. Grote,A. Langer,O. *'Measurement of Wall Film Thickness in the Intake Manifold of a Standard Production SI Engine by a Spectroscopic Technique'*, SAE paper 972832, **1997**

Heywood,J.B. *'Internal Combustion Engine Fundamentals'*, Publisher: McGraw Hill Book Co., **1988**

Hoel,P. *'Introduction to Mathematical Statistics'*, Publisher: Wiley and Sons. 5th Edition **1984**

Horie,K. Nishizawa,K. Ogawa,T. Akazaki,S. Miura,K. *'The Development of a High Fuel Economy and High-Performance Four-Valve Lean Burn Engine'*, SAE paper 920445, **1992**

Huang,Y. Matthews,R. Ellzey,J. *'Effects of Fuel Volatility, Load and Speed on HC Emissions Due to Piston Wetting'*, SAE paper 2001-01-2024, **2001**

Ifeachor,E Jervis,B. *'Digital Signal Processing – A Practical Approach'*, Publisher: Addison-Wesley, **1995**

Ioannou,M. *'An Investigation of the Liquid Fuel Films within the Cylinder of a Spark Ignition Engine'*, Ph.D. Thesis, Department of Mechanical Engineering, University College London, **2000**

Ioannou,M. Nightingale,C. *'Application of Heat Flux Sensors to Detect Liquid Fuel Films within the Cylinder of a Firing SI Engine'*, SAE paper 2000-01-2841, **2000**

I.R.Telemetrics. *'Wireless Measurement Systems'*, Website address: http://www.irtelemetrics.com/, (Visited on 2/2/2001), **2001**

Jackson,S. *'Mixture Preparation Process in SI Engines with Particular Reference to an Air-Assisted Fuel Vaporiser'*, Ph.D. Thesis, Department of Mechanical Engineering, University College London, **1996**

Jensen,T. Schramm,J. *'A Three-Zone Heat Release Model for Combustion Analysis in a Natural Gas SI Engine – Effects of Crevices and Cyclic Variations on UHC Emissions'*, SAE paper 2000-01-2802, **2000**

Jobson,E. Salomonsson,P. *'Research Results and Progress in LeaNOx II - A Co-operation for Lean NOx Abatement'*, SAE paper 2000-01-2909, **2000**

Kamo,R. *'Thin Thermal Barrier Coatings for Engines'*, SAE paper 890143, **1989**

Kim,G. Choi,M. Bae,S. *'Gas Flows Through the Inter-Ring Crevice and Their Influence on UHC Emissions'*, SAE paper 1999-01-1533, **1999**

Koch,F. Geiger,U. Hermsen,F. *'PIFFO – Piston Friction Force Measurements During Engine Operation'*, SAE paper 960306, **1996**

Koederitz,K. Drallmeier,J. *'Film Atomization From Valve Surfaces During Cold Start'*, SAE paper 1999-01-0566, **1999**

Kume,T. Iwamoto,Y, Iida,K. Murakami,M. Akishino,K. Ando,H. *'Combustion Control Technologies for Direct Injection SI Engines'*, SAE paper 960600, **1996**

Lancaster,D. *'Measurement and Analysis of Engine Pressure Data'*, SAE paper 750026, **1975**

Laurent 'INDIRECT.EXT.3.1', Website address: http://longre.free.fr/english/, (Visited on 2/4/03), **2003**

Lindgren,R. Denbratt,I. *'Modelling Gasoline Spray-Wall Interaction – A Review of Current Models'*, SAE paper 2000-01-2808, **2000**

Lumley,J. *'Engines, An Introduction'*, Publisher: Cambridge University Press, **1999**

Lynn,P. Fuerst,W. *'Introductory Digital Signal Processing with Computer Applications'*, Publisher: Wiley and Sons, **1994**

Maassen,F. Kock,F. Schwaderlapp,M. *'Analytical and Empirical Methods for Optimization of Cylinder Liner Bore Distortion'*, SAE paper 2001-01-0569, **2001**

Malaczynski,G. Xiaohong,Q. Hamdi,A. Elmoursi,A. *'Bench Test for Scuff Evaluation of Surface Modified Piston and Bore Materials'*, SAE paper 960013, **1996**

McCullough,J. *'Engine Cylinder Pressure Measurements'*, SAE paper presented at the SAE Annual Meeting in Detroit , **1953**

McGee,J. Curtis,E. Russ,S. Lavoie,G. *'The Effects of Port Fuel Injection Timing and Targeting on Fuel Preparation Relative to a Pre-Vaporized System'*, SAE paper 2001-01-2834, **2000**

Meyer,R. Yilmaz,E. Heywood,J. *'Liquid Fuel Flow in the Vicinity of the Intake Valve of a Port-Injected Engine'*, SAE paper 982471, **1998**

Meyer,R. Heywood,J. *'Effect of Engine and Fuel Variables on Liquid Fuel Transport into the Cylinder in Port-Injected SI Engines'*, SAE paper 1999-01-0563, **1999a**

Meyer,R. Heywood,J. *'Evaporation of In-Cylinder Liquid Fuel Droplets in an SI Engine: A Diagnostic-Based Modeling Study'*, SAE paper 1999-01-0567, **1999b**

Miller,M. *'Mixture Preparation in Automotive Spark-Ignition Engines'*, Ph.D. Thesis, Department of Mechanical Engineering, University College London, **1992**

Miorali,M. Pedicillo,A. *'Measurement of the Fuel Stored on the Wall of a Port Fuel Injected Engine Equipped with a Double Fuel Injection System'*, SAE paper 982472, **1998**

Müller,H. *'Comparative Experiments with Piezoelectric Pressure Transducers to Determine their Suitability of Use in Combustion Engines'*, Translated from 'MTZ Motortechnische Zeitschrift', Kistler Instruments Ltd. paper 1986, **1986**

Mure,C. Rhee,K. *'Instantaneous Heat Transfer over the Piston of a Motored Direct Injection-Type Diesel Engine'*, SAE paper 890469, **1989**

Nakayama,K. Yasutake,Y. Takiguti,M. Furuhama,S. *'Effect of Piston Motion on Piston Skirt Friction of a Gasoline Engine'*, SAE paper 970839, **1997**

National Instruments 'PCI-MIO-16E-4 board', Website address: http://www.ni.com/, (Visited on 5/1/02), **2002**

Offner,G. Herbst,H. Priebsch,H. *'A Methodology to Simulate Piston Secondary Movement under Lubricated Contact Conditions'*, SAE paper 2001-01-0565, **2001**

Ogawa,H. Kimura,S. Koike,M. *'A Study of Heat Rejection and Combustion Characteristics of a Low-temperature and Pre-mixed Combustion Concept Based on Measurement of Instantaneous Heat Flux in a Direct-Injection Diesel Engine'*, SAE paper 2001-01-2792, **2000**

Oliveira,I. Hochgreb,S. *'Detailed Calculation of Heating, Evaporation and Reaction Processes of a Thin Liquid Layer of Hydrocarbon Fuel'*, SAE paper 2000-01-0959, **2000**

O'Rouke,P. Amsden,A. *'A Spray/Wall Interaction Submodel for the KIVA-3 Wall Film Model'*, SAE paper 2000-01-0271, **2000**

Ostermann,A. *'Experiences with Nickel-Silicon-Carbide Coatings in Cylinder Bores of Small Aluminium Engines'*, SAE paper 790843, **1979**

Owen,K. Coley,T. *'Automotive Fuels Reference Book'*, Second Edition, Publisher: Society of Automotive Engineers, **1995**

Pearson,R. *'The Use of Multiple Poppet Valves in Reciprocating Internal Combustion Engines'*, Institution of Mechanical Engineers, Fluid Mechanics & Dynamics of Multi-Valve Engines papers, 9th June, **1999**

Pierik,R. Burkhard,J. *'Design and Development of a Mechanical Variable Actuation System'*, SAE paper 2000-01-1221, **2000**

Pierson,S. *'The Application of Commercial CFD to Improve Gasoline Port Fuel Injector Design and Targeting'*, Ph.D. Thesis, Cranfield University, **2002**

Pietrobello,G. Cocchi,M. Bolletta,A. *'Piston and Piston Ring Design and Development for the Formula 1 Engine'*, SAE paper 942518, **1994**

Queenan,K.B. *'Observation and Measurement of Fuel Distribution Within a Spark-Ignition Engine'*, Ph.D. Thesis, Department of Mechanical Engineering, University College London, **1998**

Radil,K. *'Test Method to Evaluate Cylinder Liner-Piston Ring Coatings for Advanced Heat Engines'*, U.S. Army Research Laboratory paper ARL-MR-362, NASA/TM paper 1996-107526, **1996**

Radil,K. *'The Influence of Honing on the Wear of Ceramic Coated Piston Rings and Cylinder Liners'*, U.S. Army Research Laboratory paper ARL-TR-2089, NASA/TM paper 2000-209794, **2000**

Rao,V. Kabat,D. Yeager,D. Lizotte,B *'Engine Studies of Solid Film Lubricant Coated Pistons'*, SAE paper 97009, **1997a**

Rao,V. Kabat,D. Cikanek,H. Fucinari,C. *'Material Systems for Cylinder Bore Applications – Plasma Spray Technology'*, SAE paper 970023, **1997b**

Rogers,G. Mayhew,Y. 'Engineering Thermodynamics Work and Heat Transfer', Publisher: Longman GroupLtd, 4th Edition,**1992**

Rowe,M. *'Get Piston-Ring Data from Within an Engine'*, Test and Measurement World Magazine, article February 15th, **1998**

Russ,S. Stephens,J. Aquino,C. Curtis,E. Fry,J. *'The Effects of Injector Targeting and Fuel Volatility on Fuel Dynamics in a PFI Engine During Warm-Up: Part I-Experimental Results'*, SAE paper 982519, **1998**

Scarlett,M. *'The Truth About BMW Cylinder Wear'*, Autocar Magazine Article, 18th March, **1998**

Schorr,H. *'Tribology and Wear'*, Bosch Automotive Handbook, Publisher: Robert Bosch, 4th edition, **1996**

Senda,J. Ohnishi,M. Takahashi,T. Fujimoto,H. *'Measurement and Modeling on Wall Wetted Fuel Film Profile and Mixture Preparation in Intake Port of SI Engine'*, SAE paper 1999-01-0798, **1999**

Senda,J. Hojyo,Y. Fujimoto,H. *'Modelling of tomization Process in Flash Boiling Spray'*, SAE paper 941925, **1994**

Senda,J. Higaki,T. Sagane,Y. Fujimoto,H. *'Modeling and Measurement on Evaporation Process of Multicomponent Fuels'*, SAE paper 2000-01-0280, **2000**

Shayler,P. Colechin,M. *'Fuel Film Evaporation and Heat Transfer in the Intake Port of an SI Engine'*, SAE paper 961120, **1996a**

Shayler,P. Colechin,M. *'Heat Transfer Measurements in the Intake Port of a Spark Ignition Engine'*, SAE paper 960273, **1996b**

Shayler,P. Davies,M. Colechin,M. *'Intake Port Fuel Transport and Emissions: The Influence of Injector Type and Fuel Composition'*, SAE paper 961996, **1996c**

Shayler,P. Davies,M. *'Audit of Fuel Utilisation During the Warm-Up of SI Engines'*, SAE paper 971656, **1997**

Shayler,P. Winborn,L. *'The Build-Up of Oil Dilution by Gasoline and the Influence of Vehicle Usage Patterns'*, SAE paper 012838, **2000a**

Shayler,P. Winborn,L. *'Fuel Transport to the Crankcase, Oil Dilution and HC Return with Breather Flow During the Cold Operation of a SI Engine'*, SAE paper 011235, **2000b**

Shuster,M. Mahler,F. Macy,D. Frame,R. Deis,M. *'Piston Ring Microwelding Phenomenon and Methods of Prevention'*, SAE paper 960745, **1996**

Skippon,S. Norton,D. *'The effects of Gasoline Volatility on Mass and Composition of the Inlet Port Wall Film in Port Injected Engines'*, SAE paper 982517, **1998**

Stanlmaier,R. Roberts,C. Ezekoye,O. Matthews,R. *'Condensation of Fuel on Combustion Chamber Surfaces as a Mechanism for Increased HC Emissions from SI Engines During Cold Start'*, SAE paper 972884, **1997**

Stanton,D. Rutland,C. *'Multi-Dimensional Modeling of Heat and Mass Transfer of Fuel Films Resulting from Impinging Sprays'*, SAE paper 980132, **1998**

Steeper,R. Stevens,E. *'Characterization of Combustion, Piston Temperatures, Fuel Sprays and Fuel-Air Mixing in a DISI Optical Engine'*, SAE paper 2000-01-2900, **2000**

Stone,C. Lim,E. Ewart,P. Lloyd,G. Williams,R. *'Temperature and Heat Flux Measurements in a Spark Ignition Engine'*, SAE paper 2000-01-1214, **2000**

Stone,R. *'Introduction to Internal Combustion Engines'*, Publisher: Macmillan Press Ltd, 3rd edition, **1999**

Suhara,T. Ato,S. Takiguchi,M. Furuhama,S. *'Friction and Lubrication Characteristics of Piston Pin Boss Bearings of an Automotive Engine'*, SAE paper 970840, **1997**

Tanner,J. *'Silicon Carbide Reduces Bore Wear'*, SAE paper 830069, February 28 – March 4, **1983**

Taylor,C.F. *'The Internal Combustion Engine in Theory and Practice, Volume II: Combustion, Fuels, Materials, Design'*, M.I.T press, **1986**

Teraguchi,S. Suzuki,W. Takiguchi,M. *'Effects of Lubricating Oil Supply on Reductions of Piston Slap Vibration and Piston Friction'*, SAE paper 2001-01-0566, **2001**

Ting,L. *'Development of a Reciprocating test Rig for Tribological Studies of Piston Engine Moving Components - Part I: Rig Design and Piston Ring Friction Coefficients Measuring Method'*, SAE paper 930685, **1993a**

Ting,L. *'Development of a Reciprocating test Rig for Tribological Studies of Piston Engine Moving Components - Part II: Measurements of Piston Ring Friction Coefficients and Rig Test Confirmation'*, SAE paper 930686, **1993b**

Tomanik,E. *'Piston Ring Pack and Cylinder Wear Modeling'*, SAE paper 2001-01-0572, **2001**

Vatell 'Heat Flux Sensors', Website address: http://www.vatell.com/, (Visited on 2/4/01), **2001**

Wilks,N. *'A Hard Act to Follow'*, Professional Engineering Magazine article, November 15th, **2000**

Williams,P.A. *'Characterization of Fuel Sprays in Spark Ignition Engines – Volume 1'*, Ph.D. Thesis, Department of Mechanical Engineering, University College London, **1994**

Wilson,T. Bryanston-Cross,P. Chana,K. Dunkley,P. *'High Bandwidth Heat Transfer and Optical Measurements in an Instrumented Spark Ignition Internal Combustion Engine'*, SAE paper 2002-01-0747, **2002**

Wimmer,A. Pivec,R. *'Heat Transfer to the Combustion Chamber and Port Walls of IC Engines – Measurement and Prediction'*, SAE paper 2000-01-0568, **2000**

Witze,P. Greeen,R. *'LIF and Flame-Emission Imaging of Liquid Fuel Films and Pool Fires in an SI Engine During a Simulated Cold Start'*, SAE paper 970866, **1997**

Xiaohong,Q. Elmoursi,A. Malaczynski,G. Hamdi,A. *'A Diamond-Like Carbon Coating for Aluminium Alloy Piston/Bore Application'*, SAE paper 960014, **1996**

Yoshida,H. Sugihara,H. Kusama,K. *'Practical Use of Two Piston Ring Set for Gasoline Engine'*, SAE paper 950817, **1995**

Zhao,F. *'Automotive Gasoline Direct-Injection Engines'*, ISBN 0-7680-0882-4, Publisher: SAE, **2002**

APPENDIX I

POROUS LINER TECHNIQUE TABULATED DATA

I-1 AJ26 and AJ33 Tabulated Results

The layout of the results is as follows:

Test number	Cylinder head	Injector	Crank (rpm)	Injection Type	Dump port	Insert
1	AJ26	Side-fed twin spray	1100	CVI	n/a	37mm
2	AJ26	Side-fed twin spray	1100	CVI	n/a	10mm
3	AJ26	Side-fed twin spray	1500	CVI	n/a	37mm
4	AJ26	Side-fed twin spray	1500	CVI	n/a	10mm
5	AJ26	Side-fed twin spray	2500	CVI	n/a	37mm
6	AJ26	Side-fed twin spray	2500	CVI	n/a	10mm
7 – 13	AJ33	12-hole cone spray	1200	Sweep	Deact	37mm
14 – 20	AJ33	12-hole cone spray	1200	Sweep	Deact	10mm
21	AJ33	12-hole cone spray	1200	OVI	Active	37mm
22 – 28	AJ33	12-hole cone spray	1500	Sweep	Deact	37mm
29 – 35	AJ33	12-hole cone spray	1500	Sweep	Deact	10mm
36	AJ33	12-hole cone spray	1500	OVI	Active	37mm
37 – 39	AJ33	12-hole cone spray	2500	Sweep	Deact	37mm
40 – 42	AJ33	12-hole cone spray	2500	Sweep	Deact	10mm
43 – 45	AJ33	12-hole cone spray	2500	Sweep	Active	37mm
46 – 48	AJ33	12-hole cone spray	2500	Sweep	Active	10mm
49	AJ26	12-hole cone spray	1200	CVI	n/a	37mm
50	AJ26	12-hole cone spray	1200	CVI	n/a	10mm
51	AJ26	12-hole cone spray	1500	CVI	n/a	37mm
52	AJ26	12-hole cone spray	1500	CVI	n/a	10mm
53	AJ26	12-hole cone spray	2500	CVI	n/a	37mm
54	AJ26	12-hole cone spray	2500	CVI	n/a	10mm

Table I-1 Results table layout

AJ26 Results

These results are for CVI only. OVI was not explored with the test rig since this was not employed in the calibration used in the production engine.

AJ26 1100rpm Fast Cold Idle

Cylinder head	AJ26
Equivalent crank speed	1100 rpm
Inlet manifold depression	420mmHg
Test duration	15 minutes
Pulsewidth	8.2ms
Mass per 8.2ms injection	0.021g

Collection test: 1	Insert: 37mm					SOI (Cam angle wrt MOP): 90				
	Exhaust					Inlet				
	E1	E2	E3	E4		I1	I2	I3	I4	
% of gasoline injected		7.067	31.7							
Total %:					38.76					0
Overall Total %:										38.76

Collection test: 2	Insert: 10mm					SOI (Cam angle wrt MOP): 90				
	Exhaust					Inlet				
	E1	E2	E3	E4		I1	I2	I3	I4	
% of gasoline injected		9.213	15.14							
Total %:					24.35					0
Overall Total %:										24.35

AJ26 1500rpm World Wide Mapping Point 2.62 bar

Cylinder head	AJ26
Equivalent crank speed	1500 rpm
Inlet manifold depression	410mmHg
Test duration	15 minutes
Pulsewidth	5ms
Mass per 5ms injection	0.012g

Collection test: 3	Insert: 37mm					SOI (Cam angle wrt MOP): 90				
	Exhaust					Inlet				
	E1	E2	E3	E4		I1	I2	I3	I4	
% of gasoline injected		5.117	28.18							
Total %:					33.3					0
Overall Total %:										33.3

Collection test: 4	Insert: 10mm					SOI (Cam angle wrt MOP): 90				
	Exhaust					Inlet				
	E1	E2	E3	E4		I1	I2	I3	I4	
% of gasoline injected		2.358	13.05							
Total %:					15.41					0
Overall Total %:										15.41

AJ26 2500rpm Wide Open Throttle

Cylinder head	AJ26
Equivalent crank speed	2500 rpm
Inlet manifold depression	5mmHg
Test duration	7 minutes
Pulsewidth	15ms
Mass per 15ms injection	0.039g

Collection test: 5	Insert: 37mm					SOI (Cam angle wrt MOP): 90				
	Exhaust					Inlet				
	E1	E2	E3	E4		I1	I2	I3	I4	
% of gasoline injected		26.01	18.62	1.45		2.137	6.3	5.035		
Total %:					46.13					13.47
Overall Total %:										59.59

Collection test: 6	Insert: 10mm					SOI (Cam angle wrt MOP): 90				
	Exhaust					Inlet				
	E1	E2	E3	E4		I1	I2	I3	I4	
% of gasoline injected		16.16	12.83				4.756	4.062		
Total %:					28.99					8.818
Overall Total %:										37.81

AJ33 Results - 1200rpm Fast Cold Idle

Cylinder head	AJ33
Equivalent crank speed	1200 rpm
Inlet manifold depression	362mmHg
Test duration	15 minutes
Pulsewidth	4.5ms
Mass per 4.5ms injection	0.012g

Collection test: 7	Insert: 37mm					SOI (Cam angle wrt MOP): 0				
	Exhaust					Inlet				
	E1	E2	E3	E4		I1	I2	I3	I4	
% of gasoline injected		11.71								
Total %:					11.71					0
Overall Total %:										11.71

Collection test: 8	Insert: 37mm					SOI (Cam angle wrt MOP): 22.5				
	Exhaust					Inlet				
	E1	E2	E3	E4		I1	I2	I3	I4	
% of gasoline injected		5.411								
Total %:					5.411					0
Overall Total %:										5.411

Collection test: 9	Insert: 37mm					SOI (Cam angle wrt MOP): 90				
	Exhaust					Inlet				
	E1	E2	E3	E4		I1	I2	I3	I4	
% of gasoline injected		2.016								
Total %:					2.016					0
Overall Total %:										2.016

Collection test: 10	Insert: 37mm					SOI (Cam angle wrt MOP): 180				
	Exhaust					Inlet				
	E1	E2	E3	E4		I1	I2	I3	I4	
% of gasoline injected		2.016								
Total %:					2.016					0
Overall Total %:										2.016

Collection test: 11	Insert: 37mm					SOI (Cam angle wrt MOP): -90				
	Exhaust					Inlet				
	E1	E2	E3	E4		I1	I2	I3	I4	
% of gasoline injected		2.837								
Total %:					2.837					0
Overall Total %:										2.837

Collection test: 12	Insert: 37mm					SOI (Cam angle wrt MOP): -45				
	Exhaust					Inlet				
	E1	E2	E3	E4		I1	I2	I3	I4	
% of gasoline injected		4.85								
Total %:					4.85					0
Overall Total %:										4.85

Collection test: 13	Insert: 37mm					SOI (Cam angle wrt MOP): -22.5				
	Exhaust					Inlet				
	E1	E2	E3	E4		I1	I2	I3	I4	
% of gasoline injected		7.159								
Total %:					7.159					0
Overall Total %:										7.159

Collection test: 14	Insert: 10mm					SOI (Cam angle wrt MOP): 0				
	Exhaust					Inlet				
	E1	E2	E3	E4		I1	I2	I3	I4	
% of gasoline injected		12.96								
Total %:					12.96					0
Overall Total %:										12.96

Collection test: 15	Insert: 10mm					SOI (Cam angle wrt MOP): 22.5				
	Exhaust					Inlet				
	E1	E2	E3	E4		I1	I2	I3	I4	
% of gasoline injected		10.82								
Total %:					10.82					0
Overall Total %:										10.82

Collection test: 16	Insert: 10mm					SOI (Cam angle wrt MOP): 90				
	Exhaust					Inlet				
	E1	E2	E3	E4		I1	I2	I3	I4	
% of gasoline injected		6.196								
Total %:					6.196					0
Overall Total %:										6.196

Collection test: 17	Insert: 10mm					SOI (Cam angle wrt MOP): 180				
	Exhaust					Inlet				
	E1	E2	E3	E4		I1	I2	I3	I4	
% of gasoline injected		6.065								
Total %:					6.065					0
Overall Total %:										6.065

Collection test: 18	Insert: 10mm					SOI (Cam angle wrt MOP): -90				
	Exhaust					Inlet				
	E1	E2	E3	E4		I1	I2	I3	I4	
% of gasoline injected		4.625								
Total %:					4.625					0
Overall Total %:										4.625

Collection test: 19	Insert: 10mm					SOI (Cam angle wrt MOP): -45				
	Exhaust					Inlet				
	E1	E2	E3	E4		I1	I2	I3	I4	
% of gasoline injected		6.371								
Total %:					6.371					0
Overall Total %:										6.371

Collection test: 20	Insert: 10mm					SOI (Cam angle wrt MOP): -22.5				
	Exhaust					Inlet				
	E1	E2	E3	E4		I1	I2	I3	I4	
% of gasoline injected		12.26								
Total %:					12.26					0
Overall Total %:										12.26

AJ33 1200rpm Fast Cold Idle with Activated Dump Port

Collection test: 21	Insert: 37mm					SOI (Cam angle wrt MOP): 0				
	Exhaust					Inlet				
	E1	E2	E3	E4		I1	I2	I3	I4	
% of gasoline injected		9.47								
Total %:					9.47					0
Overall Total %:										9.47

AJ33 1500rpm World Wide Mapping Point 2.62 bar

Cylinder head	AJ33
Equivalent crank speed	1500 rpm
Inlet manifold depression	420mmHg
Test duration	15 minutes
Pulsewidth	4.6ms
Mass per 4.6ms injection	0.013g

Collection test: 22	Insert: 37mm					SOI (Cam angle wrt MOP): 0				
	Exhaust					Inlet				
	E1	E2	E3	E4		I1	I2	I3	I4	
% of gasoline injected		13.43								
Total %:					13.43					0
Overall Total %:										13.43

Collection test: 23	Insert: 37mm					SOI (Cam angle wrt MOP): 22.5				
	Exhaust					Inlet				
	E1	E2	E3	E4		I1	I2	I3	I4	
% of gasoline injected		12.07								
Total %:					12.07					0
Overall Total %:										12.07

Collection test: 24	Insert: 37mm					SOI (Cam angle wrt MOP): 90				
	Exhaust					Inlet				
	E1	E2	E3	E4		I1	I2	I3	I4	
% of gasoline injected		2.001								
Total %:					2.001					0
Overall Total %:										2.001

Collection test: 25	Insert: 37mm					SOI (Cam angle wrt MOP): 180				
	Exhaust					Inlet				
	E1	E2	E3	E4		I1	I2	I3	I4	
% of gasoline injected		3.876								
Total %:					3.876					0
Overall Total %:										3.876

Collection test: 26	Insert: 37mm					SOI (Cam angle wrt MOP): -90				
	Exhaust					Inlet				
	E1	E2	E3	E4		I1	I2	I3	I4	
% of gasoline injected		5.51								
Total %:					5.51					0
Overall Total %:										5.51

Collection test: 27	Insert: 37mm					SOI (Cam angle wrt MOP): -45				
	Exhaust					Inlet				
	E1	E2	E3	E4		I1	I2	I3	I4	
% of gasoline injected		5.65								
Total %:					5.65					0
Overall Total %:										5.65

Collection test: 28	Insert: 37mm					SOI (Cam angle wrt MOP): -22.5				
	Exhaust					Inlet				
	E1	E2	E3	E4		I1	I2	I3	I4	
% of gasoline injected		14.34								
Total %:					14.34					0
Overall Total %:										14.34

Collection test: 29	Insert: 10mm					SOI (Cam angle wrt MOP): 0				
	Exhaust					Inlet				
	E1	E2	E3	E4		I1	I2	I3	I4	
% of gasoline injected		14.2								
Total %:					14.2					0
Overall Total %:										14.2

Collection test: 30	Insert: 10mm					SOI (Cam angle wrt MOP): 22.5				
	Exhaust					Inlet				
	E1	E2	E3	E4		I1	I2	I3	I4	
% of gasoline injected		12.29								
Total %:					12.29					0
Overall Total %:										12.29

Collection test: 31	Insert: 10mm					SOI (Cam angle wrt MOP): 90				
	Exhaust					Inlet				
	E1	E2	E3	E4		I1	I2	I3	I4	
% of gasoline injected		5.62								
Total %:					5.62					0
Overall Total %:										5.62

Collection test: 32	Insert: 10mm					SOI (Cam angle wrt MOP): 180				
	Exhaust					Inlet				
	E1	E2	E3	E4		I1	I2	I3	I4	
% of gasoline injected		5.497								
Total %:					5.497					0
Overall Total %:										5.497

Collection test: 33	Insert: 10mm					SOI (Cam angle wrt MOP): -90				
	Exhaust					Inlet				
	E1	E2	E3	E4		I1	I2	I3	I4	
% of gasoline injected		3.428								
Total %:					3.428					0
Overall Total %:										3.428

Collection test: 34	Insert: 10mm					SOI (Cam angle wrt MOP): -45				
	Exhaust					Inlet				
	E1	E2	E3	E4		I1	I2	I3	I4	
% of gasoline injected		6.022								
Total %:					6.022					0
Overall Total %:										6.022

Collection test: 35	Insert: 10mm					SOI (Cam angle wrt MOP): -22.5				
	Exhaust					Inlet				
	E1	E2	E3	E4		I1	I2	I3	I4	
% of gasoline injected		8.96								
Total %:					8.955					0
Overall Total %:										8.955

AJ33 1500rpm World Wide Mapping Point 2.62 bar with Activated Dump Port

Collection test: 36	Insert: 37mm					SOI (Cam angle wrt MOP): 0				
	Exhaust					Inlet				
	E1	E2	E3	E4		I1	I2	I3	I4	
% of gasoline injected		10.81								
Total %:					10.81					0
Overall Total %:										10.81

AJ33 Deactivated 2500rpm Wide Open Throttle

Cylinder head	AJ33
Equivalent crank speed	2500 rpm
Inlet manifold depression	5mmHg
Test duration	7 minutes
Pulsewidth	13.9ms
Mass per 13.9ms injection	0.04g

Collection test: 37	Insert: 37mm					SOI (Cam angle wrt MOP): 90				
	Exhaust					Inlet				
	E1	E2	E3	E4		I1	I2	I3	I4	
% of gasoline injected	14.77	7.014		1.177			9.837	0.873	1.758	
Total %:					22.96					12.47
Overall Total %:										35.43

Collection test: 38	Insert: 37mm					SOI (Cam angle wrt MOP): -90				
	Exhaust					Inlet				
	E1	E2	E3	E4		I1	I2	I3	I4	
% of gasoline injected	9.594	1.194				0.315	0.231			
Total %:					10.79					0.546
Overall Total %:										11.34

Collection test: 39	Insert: 37mm					SOI (Cam angle wrt MOP): -45				
	Exhaust					Inlet				
	E1	E2	E3	E4		I1	I2	I3	I4	
% of gasoline injected	9.899	0.27				5.532	9.837			
Total %:					10.17					15.37
Overall Total %:										25.54

Collection test: 40	Insert: 10mm					SOI (Cam angle wrt MOP): 90				
	Exhaust					Inlet				
	E1	E2	E3	E4		I1	I2	I3	I4	
% of gasoline injected	11.79	3.685		1.02		1.183	1.6		0.53	
Total %:					16.5					3.313
Overall Total %:										19.81

Collection test: 41		Insert: 10mm						SOI (Cam angle wrt MOP): -90				
		Exhaust						Inlet				
		E1	E2	E3	E4			I1	I2	I3	I4	
% of gasoline injected		4.417	0.513					1.628				
Total %:						4.93						1.628
Overall Total %:												6.558

Collection test: 42		Insert: 10mm						SOI (Cam angle wrt MOP): -45				
		Exhaust						Inlet				
		E1	E2	E3	E4			I1	I2	I3	I4	
% of gasoline injected		5.521	0.766					4.851				
Total %:						6.287						4.851
Overall Total %:												11.14

AJ33 Activated 2500rpm Wide Open Throttle

Collection test: 43	Insert: 37mm					SOI (Cam angle wrt MOP): 90				
	Exhaust					Inlet				
	E1	E2	E3	E4		I1	I2	I3	I4	
% of gasoline injected	2.659	7.121	0.434	0.896			10.97	3.194	5.262	
Total %:					11.11					19.43
Overall Total %:										30.54

Collection test: 44	Insert: 37mm					SOI (Cam angle wrt MOP): -90				
	Exhaust					Inlet				
	E1	E2	E3	E4		I1	I2	I3	I4	
% of gasoline injected		0.885	4.592							
Total %:					5.476					0
Overall Total %:										5.476

Collection test: 45	Insert: 37mm					SOI (Cam angle wrt MOP): -45				
	Exhaust					Inlet				
	E1	E2	E3	E4		I1	I2	I3	I4	
% of gasoline injected		1.634	4.721							
Total %:					6.355					0
Overall Total %:										6.355

Collection test: 46	Insert: 10mm					SOI (Cam angle wrt MOP): 90				
	Exhaust					Inlet				
	E1	E2	E3	E4		I1	I2	I3	I4	
% of gasoline injected	1.47	3.606	1.099	1.73			6.006	1.341	1.014	
Total %:					7.904					8.361
Overall Total %:										16.26

Collection test: 47	Insert: 10mm					SOI (Cam angle wrt MOP): -90				
	Exhaust					Inlet				
	E1	E2	E3	E4		I1	I2	I3	I4	
% of gasoline injected		0.479	1.008	0.451						
Total %:					1.938					0
Overall Total %:										1.938

Collection test: 48	Insert: 10mm					SOI (Cam angle wrt MOP): -45				
	Exhaust					Inlet				
	E1	E2	E3	E4		I1	I2	I3	I4	
% of gasoline injected		0.423	1.51							
Total %:					1.932					0
Overall Total %:										1.932

AJ26 and Denso 12-Hole Injector

1200rpm Fast Cold Idle

Cylinder head	AJ26
Equivalent crank speed	1200 rpm
Inlet manifold depression	420mmHg
Test duration	15 minutes
Pulsewidth	6.83ms
Mass per 6.83ms injection	0.019g

Collection test: 49	Insert: 37mm					SOI (Cam angle wrt MOP): 90				
	Exhaust					Inlet				
	E1	E2	E3	E4		I1	I2	I3	I4	
% of gasoline injected		30.72	5.348							
Total %:					36.06					0
Overall Total %:										36.06

Collection test: 50	Insert: 10mm					SOI (Cam angle wrt MOP): 90				
	Exhaust					Inlet				
	E1	E2	E3	E4		I1	I2	I3	I4	
% of gasoline injected		9.182	15.05							
Total %:					24.24					0
Overall Total %:										24.24

AJ26 1500rpm World.Wide Mapping Point 2.62 bar

Cylinder head	AJ26
Equivalent crank speed	1500 rpm
Inlet manifold depression	410mmHg
Test duration	15 minutes
Pulsewidth	4.7ms
Mass per 4.7ms injection	0.012g

Collection test: 51	Insert: 37mm					SOI (Cam angle wrt MOP): 90				
	Exhaust					Inlet				
	E1	E2	E3	E4		I1	I2	I3	I4	
% of gasoline injected		23.89	8.494							
Total %:					32.38					0
Overall Total %:										32.38

Collection test: 52	Insert: 10mm					SOI (Cam angle wrt MOP): 90				
	Exhaust					Inlet				
	E1	E2	E3	E4		I1	I2	I3	I4	
% of gasoline injected		3.755	8.547							
Total %:					12.3					0
Overall Total %:										12.3

AJ26 2500rpm Wide Open Throttle

Cylinder head	AJ26
Equivalent crank speed	2500 rpm
Inlet manifold depression	5mmHg
Test duration	7 minutes
Pulsewidth	13.9ms
Mass per 13.9ms injection	0.04g

Collection test: 53	Insert: 37mm					SOI (Cam angle wrt MOP): 90				
	Exhaust					Inlet				
	E1	E2	E3	E4		I1	I2	I3	I4	
% of gasoline injected	1.33	17.05	17.94			4.079	1.583			
Total %:					36.32					5.662
Overall Total %:										41.98

Collection test: 54	Insert: 10mm					SOI (Cam angle wrt MOP): 90				
	Exhaust					Inlet				
	E1	E2	E3	E4		I1	I2	I3	I4	
% of gasoline injected		10.92	8.828	1.025			4.772	3.594		
Total %:					20.77					8.366
Overall Total %:										29.14

APPENDIX II

ENGINE TECHNICAL DRAWINGS

II-1 Heat Flux Engine Technical Drawings:

1. Cylinder Block
2. Piston Body
3. Piston Lug Ring
4. Piston Crown
5. Piston Top Ring
6. Arm Mount
7. Arm
8. Wire Clip
9. Engine Assembly

Note that the drawings were originally produced in I-DEAS before transfer into this thesis. Not all dimensions are shown as the 3D computer representations were used directly by the UCL technical staff in order to generate the CNC machine tool paths.

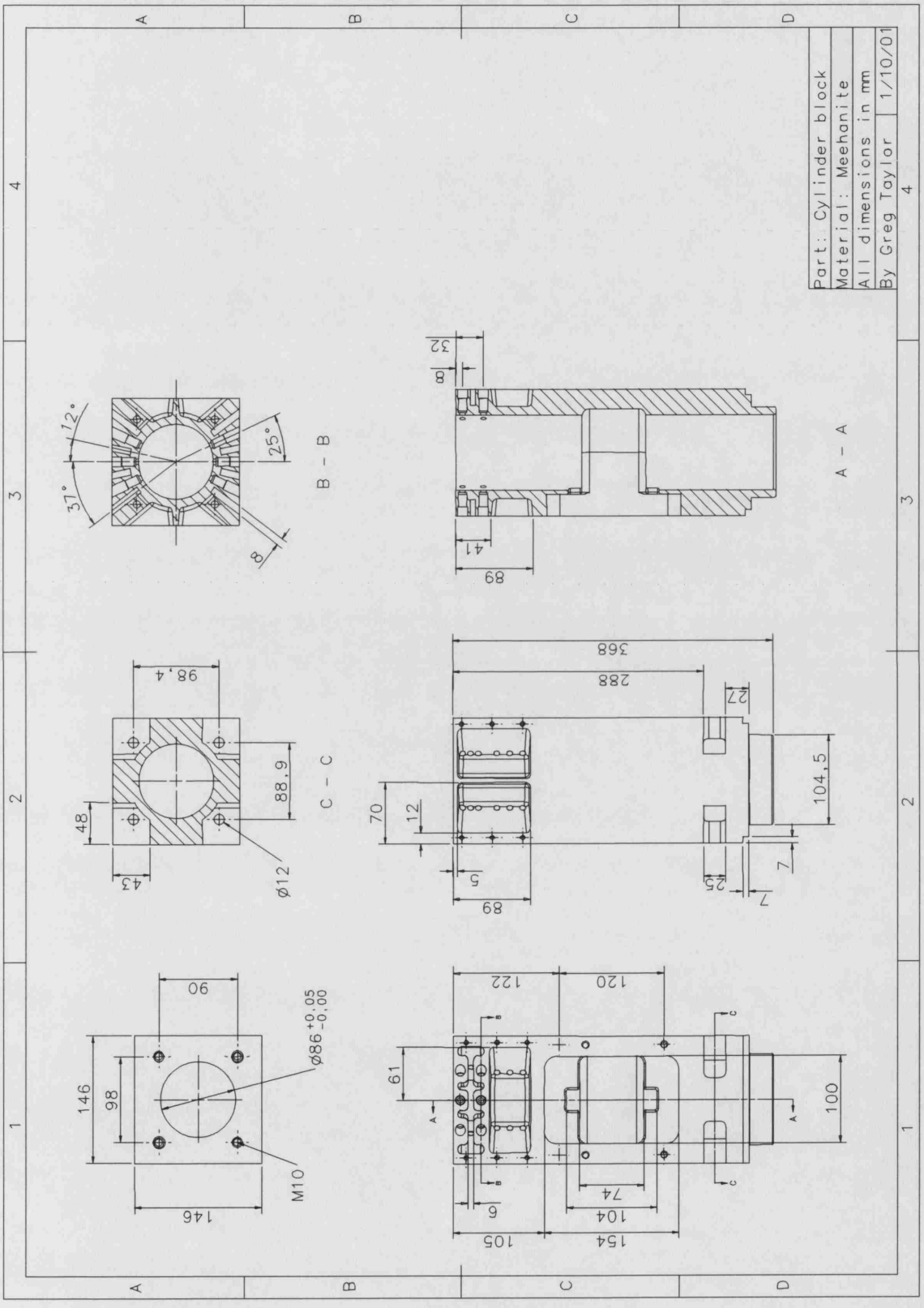
Part: Cylinder block
Material: Meehanite
All dimensions in mm
By Greg Taylor 1/10/01
A - A
B - B
C - C
37°
12°
25°
8
32
8
41
89
368
288
27
104,5
70
12
5
89
25
7
7
98,4
88,9
48
43
ø12
90
ø86 +0,05 -0,00
146
98
M10
146
122
120
61
100
74
104
6
105
154

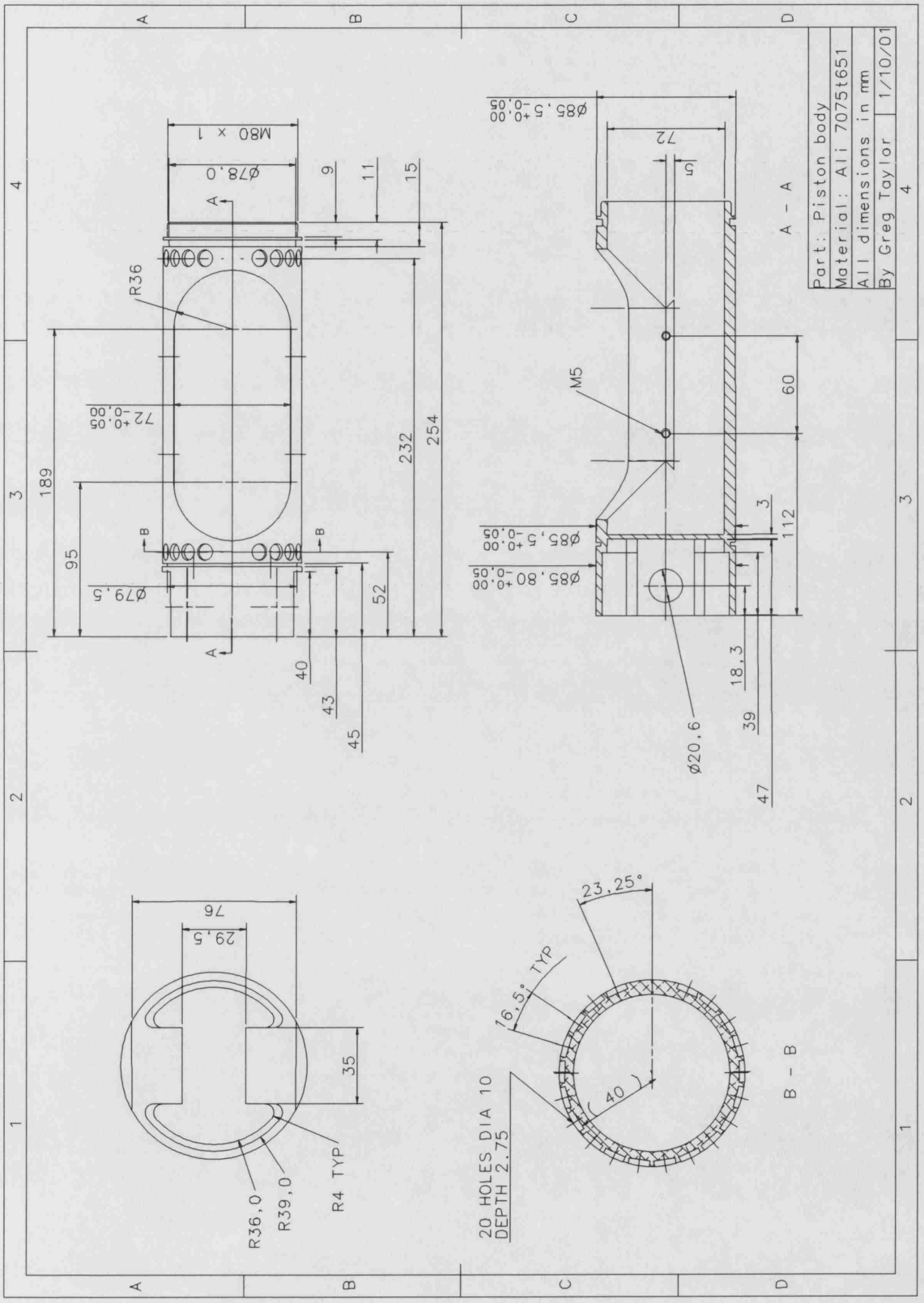
Part: Piston body
Material: Al 7075t651
All dimensions in mm
By Greg Taylor 1/10/01
A - A
B - B
M80 x 1
Ø78,0
R36
72 +0 -0,05
Ø79,5
189
95
232
254
52
40
43
45
6
11
15
Ø85,5 +0 -0,05
72
5
M5
60
3
112
Ø85,5 +0 -0,05
Ø85,80 +0 -0,05
Ø20,6
18,3
39
47
76
29,5
35
R36,0
R39,0
R4 TYP
20 HOLES DIA 10
DEPTH 2.75
23,25°
16,5° TYP
40

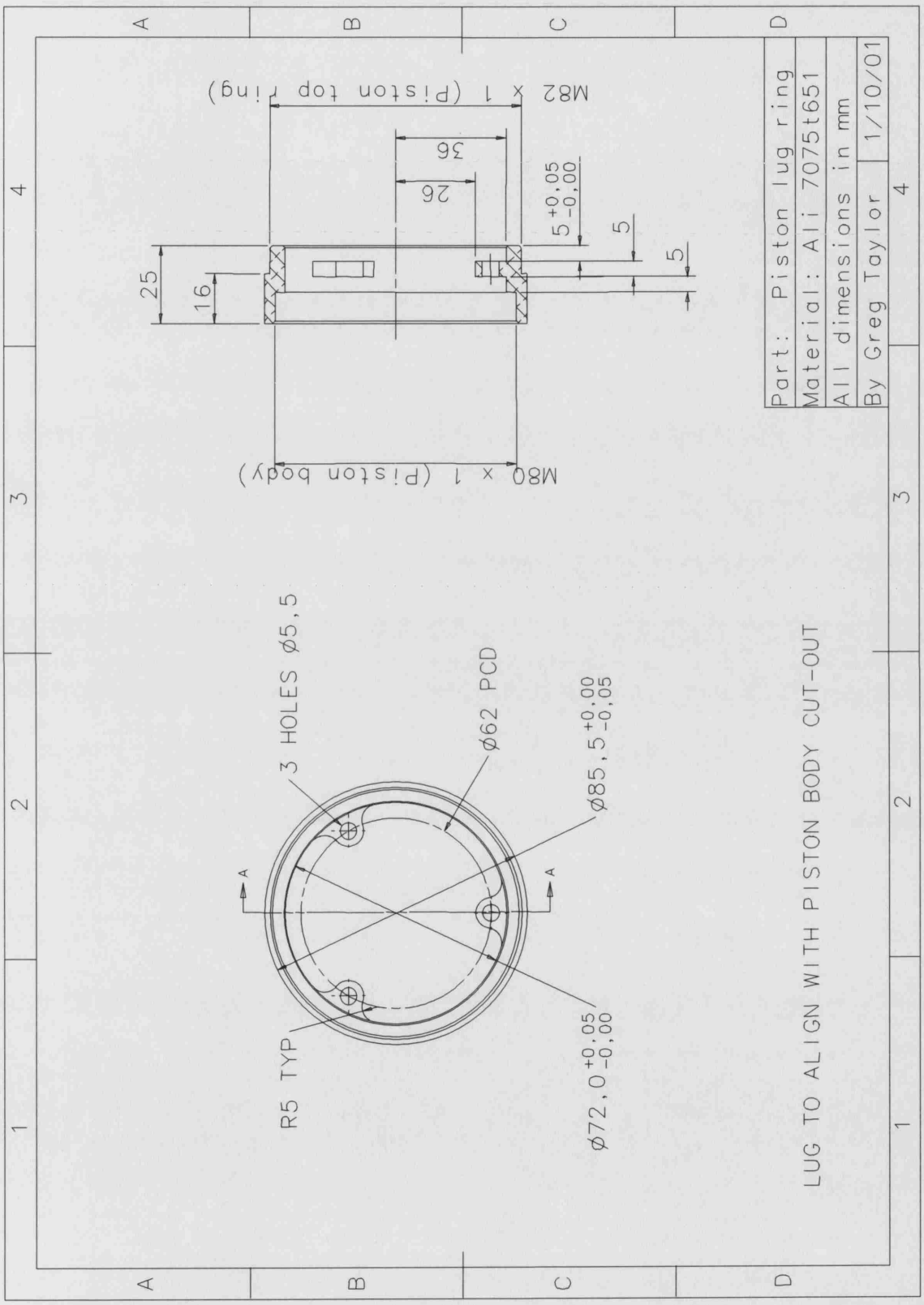
M82 x 1 (Piston top ring)
36
26
5 +0,05 -0,00
5
5
25
16
M80 x 1 (Piston body)
3 HOLES ø5,5
ø62 PCD
ø85,5 +0,00 -0,05
R5 TYP
ø72,0 +0,05 -0,00
A
A
LUG TO ALIGN WITH PISTON BODY CUT-OUT
Part: Piston lug ring
Material: Ali 7075t651
All dimensions in mm
By Greg Taylor 1/10/01
A
B
C
D
1
2
3
4

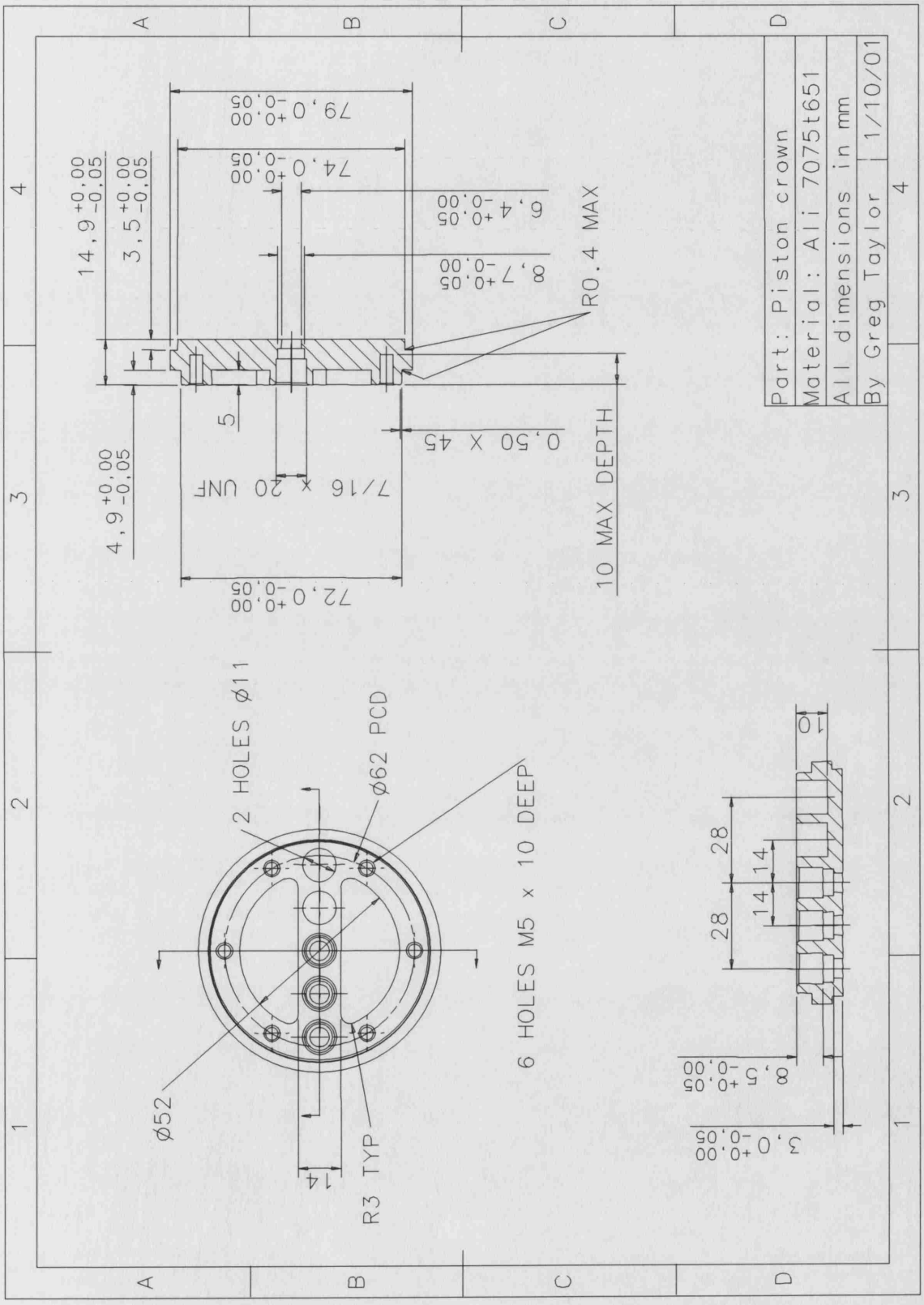
Part: Piston crown
Material: Al 7075t651
All dimensions in mm
By Greg Taylor 1/10/01
79,0 +0.00 -0.05
74,0 +0.00 -0.05
72,0 +0.00 -0.05
14,9 +0.00 -0.05
3,5 +0.00 -0.05
4,9 +0.00 -0.05
6,4 +0.05 -0.00
8,7 +0.05 -0.00
R0.4 MAX
10 MAX DEPTH
0,50 X 45
7/16 x 20 UNF
5
2 HOLES Ø11
Ø62 PCD
6 HOLES M5 x 10 DEEP
Ø52
R3 TYP
14
28
14
28
8,5 +0.05 -0.00
3,0 +0.00 -0.05
10
1

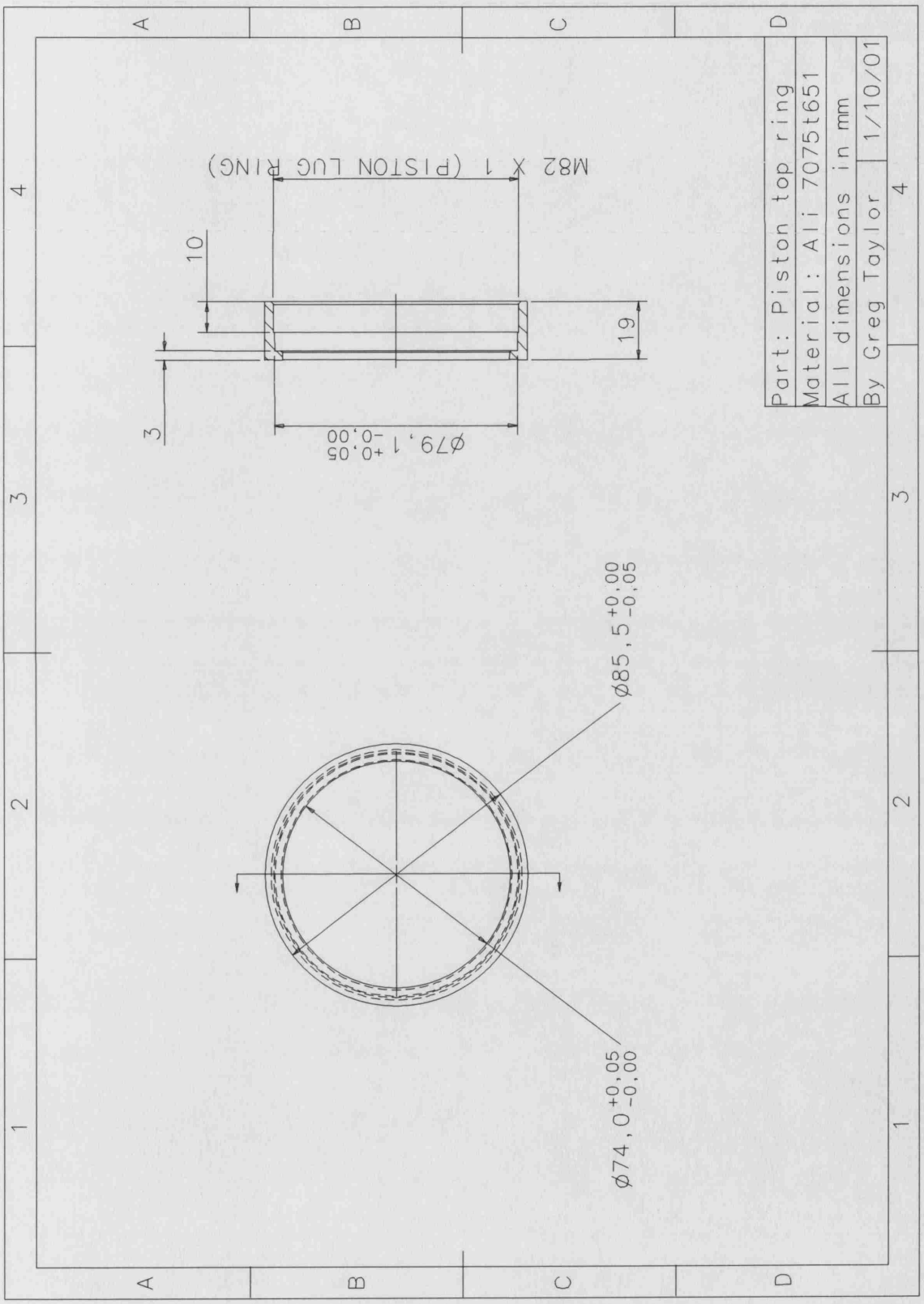
A
B
C
D
1
2
3
4
M82 X 1 (PISTON LUG RING)
10
19
3
Ø79,1 +0,05 -0,00
Ø85,5 +0,00 -0,05
Ø74,0 +0,05 -0,00
Part: Piston top ring
Material: Ali 7075t651
All dimensions in mm
By Greg Taylor
1/10/01

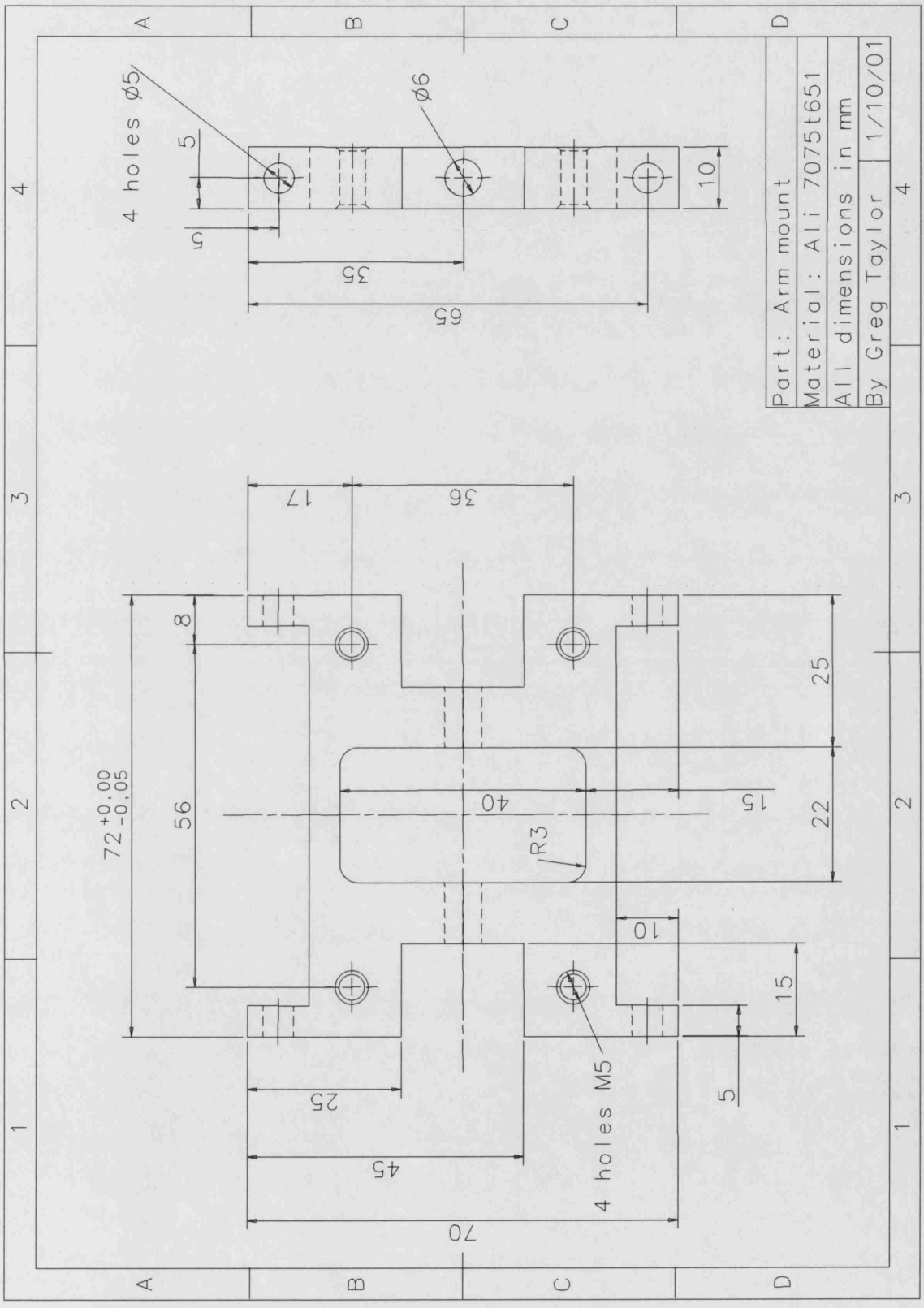
A
B
C
D
1
2
3
4
4 holes ø5
ø6
5
5
35
65
10
Part: Arm mount
Material: Al 7075t651
All dimensions in mm
By Greg Taylor
1/10/01
17
36
8
56
72 +0.00 -0.05
40
R3
15
25
22
10
15
5
4 holes M5
25
45
70

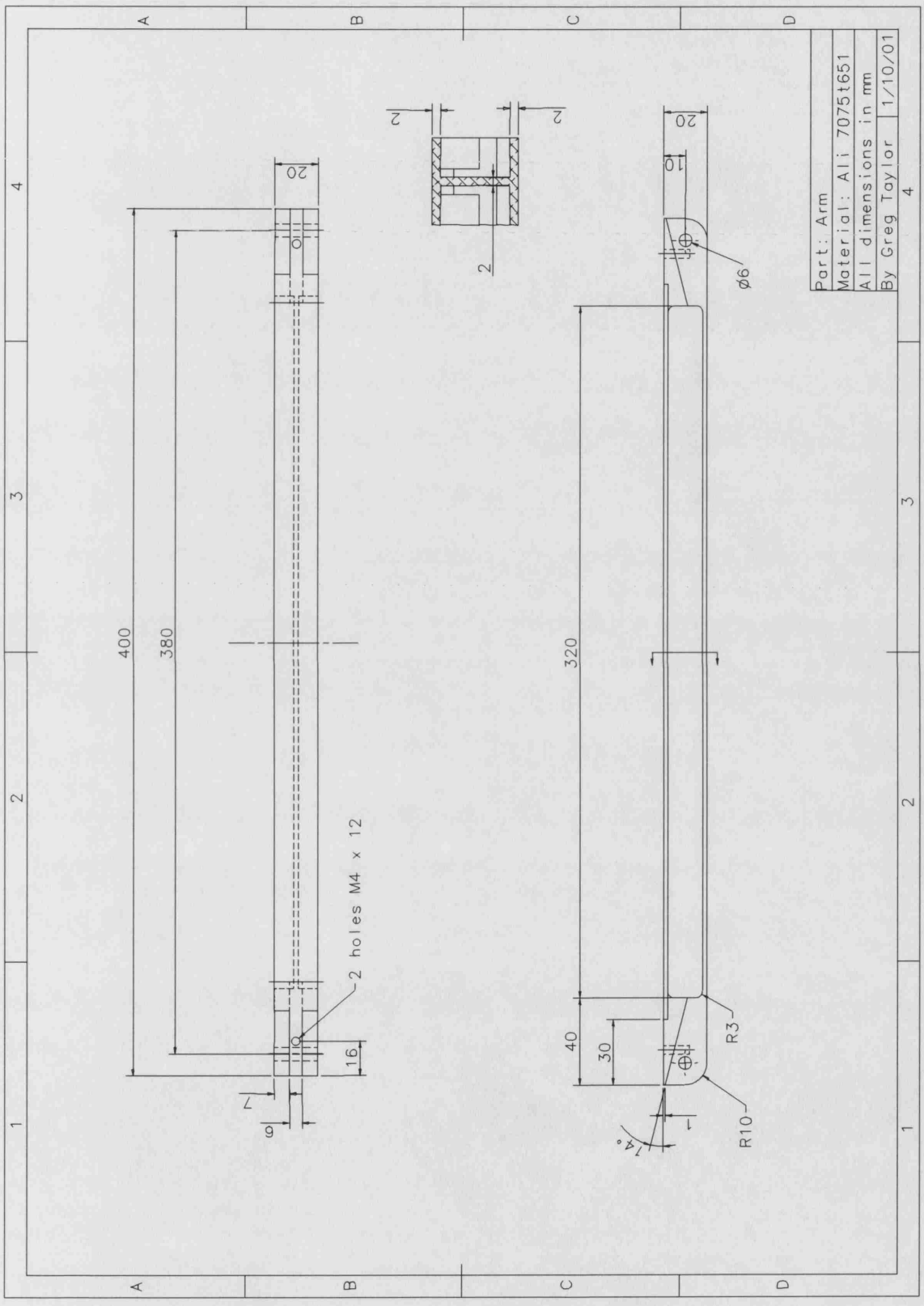
Part: Arm
Material: Ali 7075t651
All dimensions in mm
By Greg Taylor 1/10/01
400
380
320
20
16
2 holes M4 x 12
Ø6
R3
R10
40
30
14°

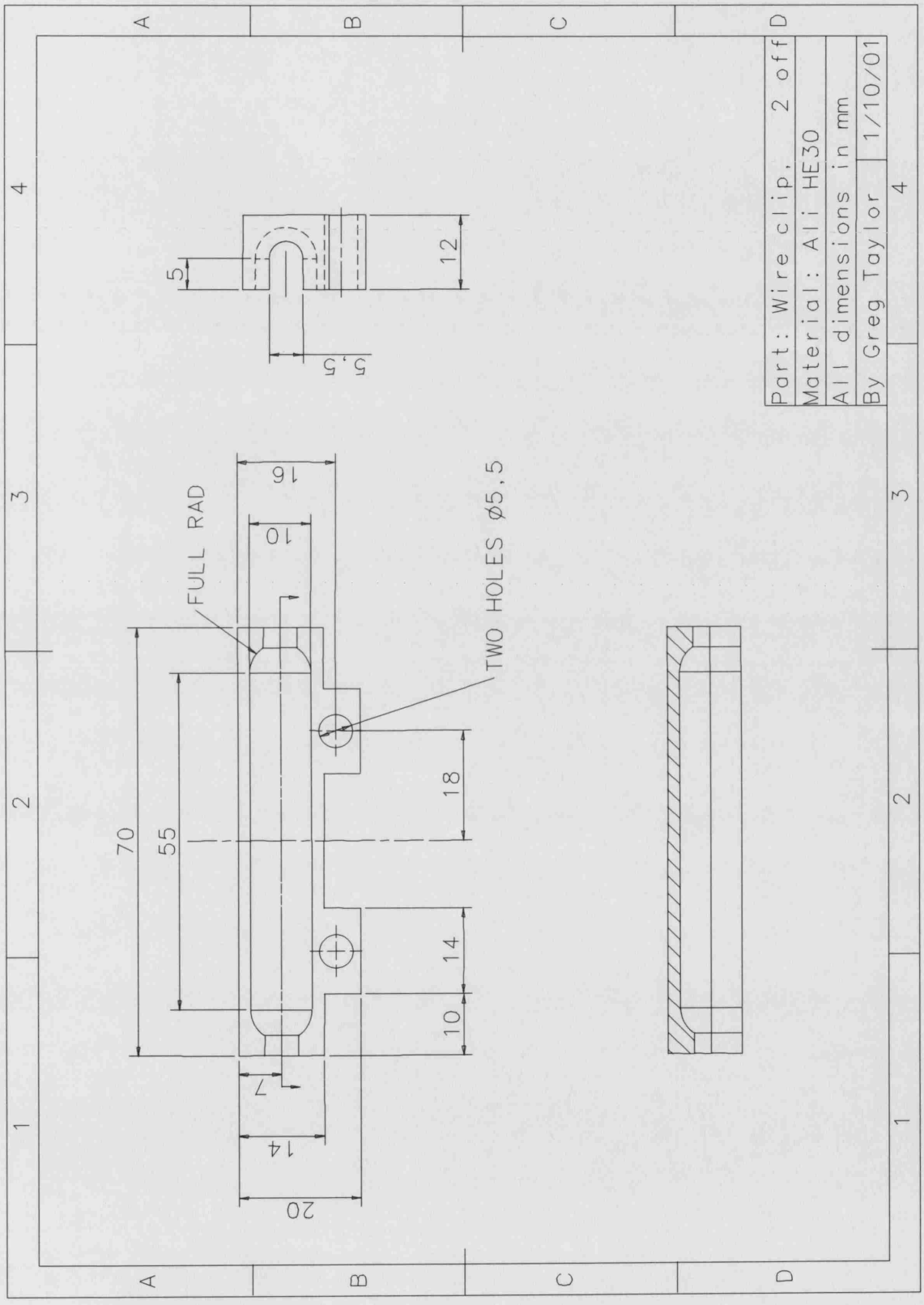
A
B
C
D
1
2
3
4
Part: Wire clip, 2 off
Material: Ali HE30
All dimensions in mm
By Greg Taylor 1/10/01
5
12
5,5
16
10
FULL RAD
TWO HOLES Ø5,5
70
55
18
14
10
7
14
20

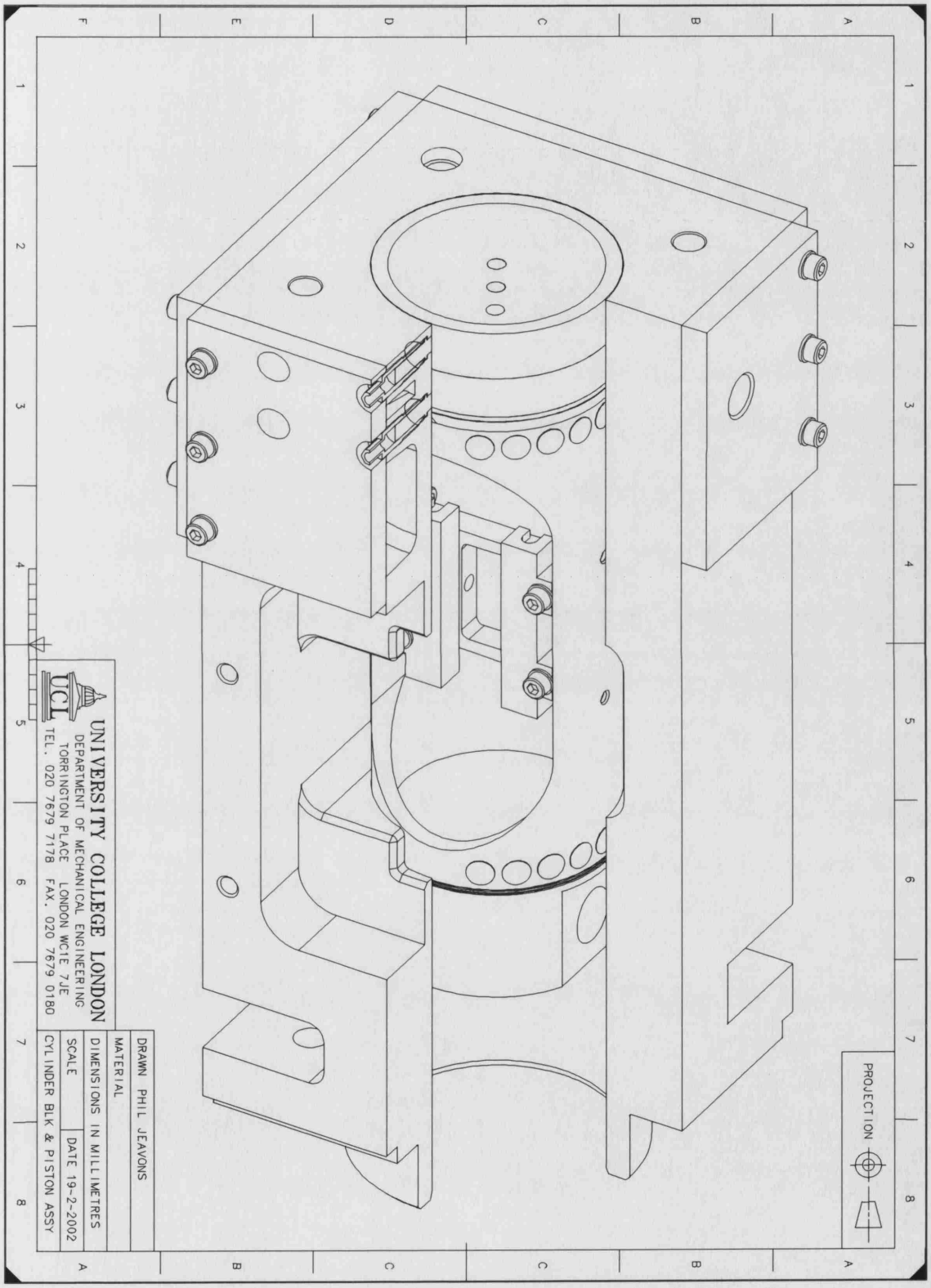
PROJECTION
UNIVERSITY COLLEGE LONDON
DEPARTMENT OF MECHANICAL ENGINEERING
TORRINGTON PLACE LONDON WC1E 7JE
TEL. 020 7679 7178 FAX. 020 7679 0180
UCL
DRAWN PHIL JEAVONS
MATERIAL
DIMENSIONS IN MILLIMETRES
SCALE
DATE 19-2-2002
CYLINDER BLK & PISTON ASSY

APPENDIX III

ENGINE BALANCE ANALYSIS

III-1 Engine balance analysis

The engine used in this work was to use the same Lister bottom-end and mountings as that successfully used by Ioannou (2000). To ensure vibration free operation, it was decided that the combined mass of the piston, mechanism and sensors used in this work should not exceed that of the piston used by Ioannou (Table III-a).

	Mass with two sensors and one fake sensor (g)	Mass with three fake sensors (g)
Piston body	991	991
Piston lug ring	80	80
Piston top ring	41	41
Piston crown	150	150
Gudgeon pin	100	100
Piston rings	5	5
M4 screws (11 off)	35	9
Arm	85	-
Arm mount	60	-
Pin/bush	10	-
Sensor clips (2 off)	36	-
Sensors (2 off)	50	-
Extension wire	25	-
Fake sensor/nut	18	54
Total mass	**1686**	**1430**
Compared to Ioannou	**100.0%**	**84.9%**

Table III-a Piston component masses

Since the piston was of the same mass and there were no geometric changes to the conrod length or crankshaft throw, the respective balance analysis provided the same resultant forces as calculated by Ioannou for a maximum engine speed of 1500 rpm.

In the balance analysis, the connecting rod was considered as two masses concentrated at its ends as shown in Figure III-a. By convention [Plint and Martyr (1995)] one third of the connecting rod mass is assumed to reciprocate with the piston and is considered as part of the piston, while the remaining two thirds rotates with the crankpin and is considered to be part of the crankshaft assembly. Figure III-b shows the main forces produced by the mechanism on the bearings when rotating at constant speed. Force F_p acts along the cylinder axis and produces the acceleration of the piston. Force F_{cp} is directed radially inwards towards the centre of the crankshaft. Force F_{cp} produces the

centripetal acceleration of the parts revolving with the crank pin and is balanced by force F_{ct} which is produced by the counterweights on the crankshaft.

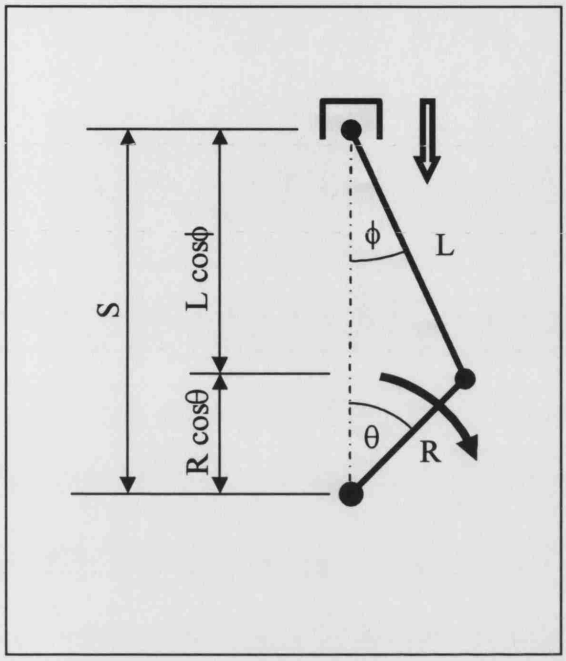

Figure III-a. Schematic of the crank - connecting rod system

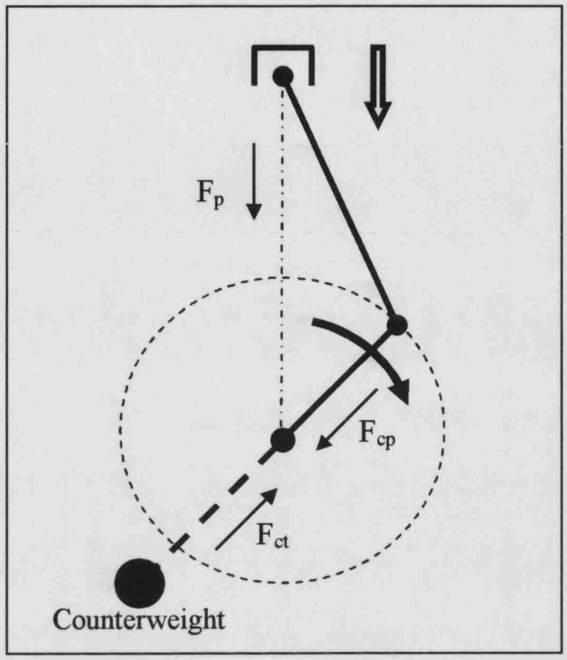

Figure III-b. Force diagram of the crank - connecting rod system

The force on the piston assembly is expressed by [Taylor (1986)]:

$$F_p = M_{pa}\,\omega^2\,R\,(\cos\theta + R/L\,\cos 2\theta) \qquad \ldots(\text{III-a})$$

The net force ($F_{c\,net}$) can be resolved into its horizontal and vertical components:

$$F_{c\,net\,(x)} = M_{ca}\,\omega^2\,R\,\sin\theta \qquad \ldots(\text{III-b})$$

$$F_{c\,net\,(y)} = M_{ca}\,\omega^2\,R\,\cos\theta \qquad \ldots(\text{III-c})$$

Where:

M_{pa} - mass of piston assembly (piston + 1/3 of connecting rod)

M_{ca} - mass of crankshaft assembly (2/3 of conrod plus journal minus the counterweight)

ω - angular velocity

L - connecting rod length

R - crankshaft length

The horizontal and vertical forces acting on the engine bearings are:

From III-a and III-c: $F_{ef(y)} = \omega^2 R \{M_{ca} \cos\theta + M_{pa} (\cos\theta + R/L \cos 2\theta)\}$ ...(III-d)

From III-b: $F_{ef(x)} = M_{ca} \omega^2 R \sin\theta$ ...(III-e)

Component	Symbol	Unit	Design	Lister
Con Rod length	L	(mm)	160	165
Crank length	R	(mm)	44	44
Stroke	S	(mm)	88	88
Maximum engine speed	N	(rev/min)	1500	3000
Angular velocity	ω	(rad/s)	157	314
Piston mass	M_p	(kg)	1.69	1.5
Con rod mass	M_c	(kg)	1.37	1.37
Crank balance mass	M_{cr}	(kg)	2.019	2.019
Piston assembly mass	M_{pa}	(kg)	2.15	1.96

Table III-b Notations and values used in the balance analysis

Figure III–c is a plot in Excel that shows the resultant horizontal and vertical forces for both the design and Lister engines operating at maximum speed. It is apparent that the expected loadings of the designed engine are well within those of the Lister engine.

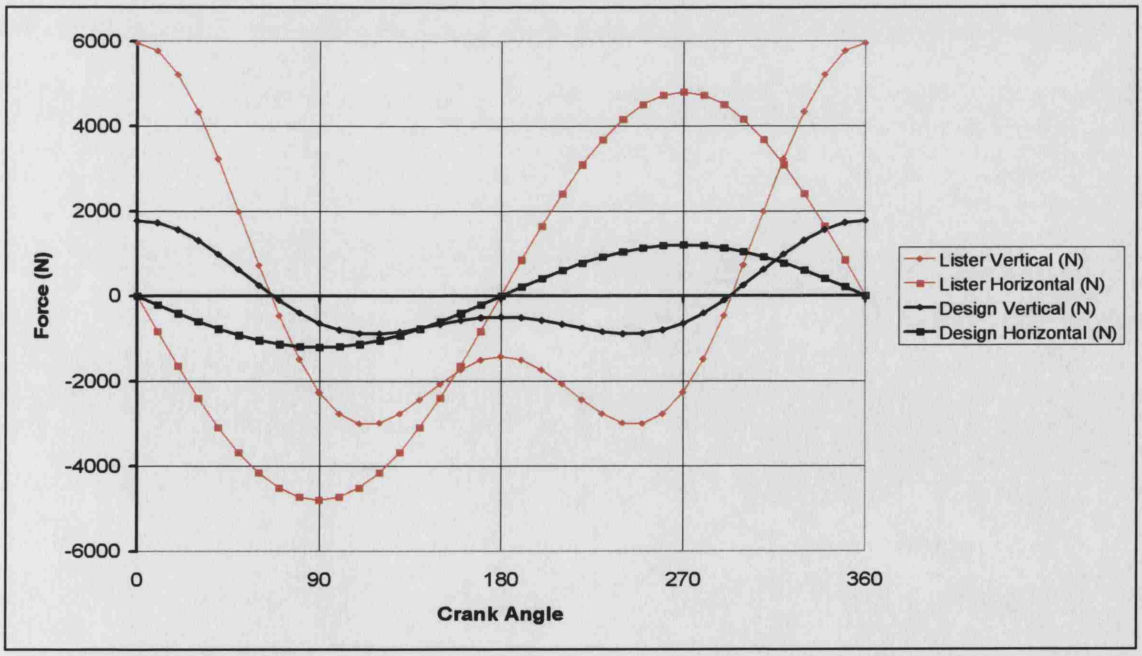

Figure III-c Horizontal and vertical Forces on the engine bearings of the design and Lister engines when operating at maximum speed

APPENDIX IV

ANALYSIS CALCULATIONS

IV-1 Analysis Equations in Microsoft Excel

Many different types of equation were used in the analysis software, ranging from basic arithmetic to complex logic based equations with numerous links to other worksheets or data files. In this appendix, the more complex equations used in the analysis program are presented in the form that they were entered into the PC. The validation of the calculations is also discussed.

Worksheet 'Data'

Column A

The Excel code entered in cell A1 that allowed connection to the other worksheet was:
=Tests!AO4

Data Extraction - Columns G to T:

Point Value Cells - If the user chose 'BLANK' as the filename, the command presented a '0' and did no further tasks. If the user had chosen a filename from the options list, the 'INDIRECT' command would have allowed extraction of data from a closed Excel file, where all of the test data was stored in d:\ADTests\Alltests\. The term "&$B$2&" represented the data file name in the command and "sheet1!" was the standard worksheet name in every data file. Such IF statements were used extensively in this work and can be explained by a simple example. If cell A1 contained "=IF(B1=1,2,3)" and a "1" was entered in cell B1, cell A1 would have shown a "2". If anything else was entered into cell B1, cell A1 would have shown a "3".

=IF($B$2="BLANK",0,INDIRECT.EXT("'d:\ADTests\Alltests\["&$B$2&".xls]Sheet1' !$A$2"))

Direct Drag-Down Value Cells - To allow the cells to be dragged down when creating the analysis program, it was required that the cell reference would be changed slightly. The example below shows the line entered in cell G7 of worksheet 'Data' when 'Data' looked for cylinder pressure in a data file. Since the cylinder pressure was always in column I of the data files, this letter was still held within the last quotation mark. The term F10 related to the counter in column F of the 'Data' worksheet which went from 1 to 720 and allowed 'Data' to look in each of the 720 cells in the data file. Since cell F10 contained a 4, the 4^{th} row of the data column was used.

=IF($B$2="BLANK",0,INDIRECT.EXT("'d:\ADTests\Alltests\["&$B$2&".xls]Sheet1'
!I"&F10))

Optional Drag-Down Value Cells - This more complex command allowed the user to choose one or a number of the 12 File Columns from column C in the 'Data' worksheet. Each of the 12 columns from I to T were referenced to cells C2 to C13 respectively.
=IF($B$2="BLANK",0,INDIRECT.EXT("'d:\ADTests\Alltests\["&$B$2&".xls]Sheet1'
!"&$C$2&F10))

Final Cell Calculation and Averaging – Columns W to AK

Column W - averaged and converted the logged cylinder pressure from voltage to pressure measured in Pascal.
=((SUM(G5:G9)/5)*100000000)/(15.1*20)

Column Y - averaged and converted the logged inlet manifold pressure from voltage to a pressure in Pascal.
=(((SUM(H5:H9)/5)+0.0189)/3.3374)*100000

Column X - This column modified the cylinder pressure data. The user was required to enter the chosen reference crank angle (if a value different to 540° was desired) into cell X6 so that the program could look-up the corresponding inlet manifold pressure from the logged manifold pressure data series at this crank angle. The equation entered in column X for matching cylinder pressure to inlet manifold pressure simply investigated if the cylinder pressure was higher or lower than the manifold pressure and either subtracted or added the respective difference found at 540° to the rest of the values for cylinder pressure in the cycle. The term $V$12 was simply a number in the crank counter column chosen so that the correct row was observed for the 540° pressure values.
=IF(INDIRECT("W"&$X$6+$V$12)>INDIRECT("Y"&$X$6+$V$12),
W7-(INDIRECT("W"&$X$6+$V$12)-INDIRECT("Y"&$X$6+$V$12)),
IF(INDIRECT("W"&$X$6+$V$12)<INDIRECT("Y"&$X$6+$V$12),
W7+(INDIRECT("Y"&$X$6+$V$12)-INDIRECT("W"&$X$6+$V$12)),W7))

Worksheet 'Main'

Worksheet 'Main' contained the main calculations performed in the analysis software. Some calculations were performed as single-cell events and were stored at the top of the worksheet.

Calculating the injected fuel velocity is a typical example of such a single-cell event. In this particular case, the Excel equation rounded the answer to the nearest whole number for convenience in later calculations.

=INT(($A$9/(((2*$A$37)/$A$38)^0.5))/$A$3)

A vast majority of the calculations were performed in the large table on the 'Main' worksheet. These are now presented in column order.

Instantaneous Piston Position – Column B

=($A$6/2)*((COS(RADIANS(A56)))+(((2*$A$7)/$A$6)*
(1-0.5*((($A$6/(2*$A$7))^2)*(0.5-0.5*COS(2*(RADIANS(A56))))))))

Sensor Covering – Column C and D

=IF(B56>($B$56-$A$16),$B$56-$A$16,B56)

=IF(B56>($B$56-$A$17),$B$56-$A$17,B56)

Cylinder volume – Column E

=((((($A$6/2)+$A$7)-B56)*(($A$5/2)^2)*PI())+$A$8

Cylinder pressure – Column F

=Data!X7

Cylinder temperature – Column G

=IF(Data!$J$2=1,300,IF(Data!$J$2=2,IF(AND(A56>=0,A56<$A$20),800,IF(AND(A5
6>=$A$20,A56<$A$20+$A$21),G55-((800-300)/(($A$20+$A$21)-$A$20)),300))))

Inlet manifold pressure – Column H

=Data!Y7

Inlet valve lift – Column I

=IF(OR(A56<($A$19-175),A56>($A$19+175)),0,
IF($A$1=1,IF((INDIRECT("Lifts!B"&A56+362-$A$19)-
0.00045+($A$25/100)*0.00045)<0,0,INDIRECT("Lifts!B"&A56+362-$A$19)-
0.00045+($A$25/100)*0.00045),
IF($A$1=2,IF((INDIRECT("Lifts!D"&A56+362-$A$19)-
0.00045+($A$25/100)*0.00045)<0,0,INDIRECT("Lifts!D"&A56+362-$A$19)-
0.00045+($A$25/100)*0.00045))))

Inlet valve shrouds – Column J

=IF(I56>$A$14,$A$14,I56)

IVO – Column K

=IF(AND(I55=0,I56>0),A56,0)

IcdA – Inlet Coefficient of Discharge and Flow Area – Column L

=1*I56*PI()*0.035

Inlet f/r c/u – Forward or Reverse, Choked or Un-choked Flow – Column M

=IF(I56=0,"0",
IF(F56=H56,"0",
IF(H56>F56,IF(F56/H56>0.528,"FU","FC"),
IF(H56<F56,IF(H56/F56>0.528,"RU","RC")))))

Inlet m f/r c/u – Forward or Reverse, Choked or Un-choked Mass Flow – Column N

This equation used the same logic as the previous column, but calculated actual values.

=IF(I56=0,"0",
IF(F56=H56,"0",
IF(H56>F56,IF(F56/H56>0.528,($A$4*H56*L56*(((2*1.4)/(1.4-
1))*(1/(287*$A$28))*(((F56/H56)^(2/1.4))-((F56/H56)^((1.4+1)/1.4))))^0.5),
($A$4*H56*L56*(((1.4/(287*$A$28))*(2/(1.4+1))^((1.4+1)/(1.4-1)))^0.5))),
IF(H56<F56,IF(H56/F56>0.528,(-$A$4*F56*L56*(((2*1.4)/(1.4-
1))*(1/(287*G56))*(((H56/F56)^(2/1.4))-((H56/F56)^((1.4+1)/1.4))))^0.5),
(-$A$4*F56*L56*(((1.4/(287*G56))*(2/(1.4+1))^((1.4+1)/(1.4-1)))^0.5)))))))

Inlet gas velocity – Column O

=IF(I56=0,0,
IF(F56=H56,0,
IF(H56>F56,IF(F56/H56>0.528,((((2*1.4)/(1-1.4))*(287*$A$28))*(((F56/H56)^((1.4-1)/1.4))-1))^0.5,
(((2*1.4)/(1+1.4))*(287*$A$28))^0.5),IF(H56<F56,IF(H56/F56>0.528,-(((((2*1.4)/(1-1.4))*(287*G56))*(((H56/F56)^((1.4-1)/1.4))-1))^0.5),-
((((2*1.4)/(1+1.4))*(287*G56))^0.5))))))

Exhaust lift, Exhaust shroud, EVO, EcdA, Exhaust f/r c/u and Exhaust m f/r c/u – Columns P to U

These are identical to their inlet equivalents with the only difference being which cells are observed for lift, MOP and percentage of ramps used.

Injection – Column V

=IF(AND(A56>=($A$33),A56<($A$33+$A$35)),1,0)

All direct wall – Column W

=IF(AND(A56>=($A$33+$A$41+$A$43),A56<=($A$33+$A$35+$A$42+$A$44)),1,0
)

Direct window – Column X

=IF(AND(A56>=($A$20+$A$43),A56<=($A$20+$A$21+$A$44)),1,0)

Direct impact – Column Y

=IF(AND(W56=1,X56=1),1,0)

Gas forward – Column Z

=IF(A56=1,0,IF(AND(Z55=0,O56<=0),0,IF(AND(Z55=0,O56>0),A56,-1)))

Gas impact – Column AA

=IF(AND(A56>=($A$45+$A$48),A56<=($A$20+$A$21+$A$46)),1,0)

IV-2 Analysis Validation Calculations

Due to the intricate nature of the LabVIEW data logging software and the Excel analysis program, the calculations had to be checked methodically to ensure the final results were correct. The basic approach was to check each new section as it was created, rather than just check the final program. This incremental approach made it easier to locate mistakes and then correct them.

There were not many calculations performed within LabVIEW, since this mostly just logged data. The only calculated items were the standard deviation and conversion from voltages to meaningful heat flux and temperature values. These were easily checked by logging both the raw data and converted values and then comparing these results to similarly calculated results in Excel, where any differences instantly indicated a mistake.

The very nature of the Excel spreadsheet allowed complete access to all of the values at all times, which not only helped the user understand the heat flux results, but also indicated if any mistakes or omissions had occurred in its creation. In a similar way, some key columns of the Excel program acted as diagnostic features that indicated what the program was doing in addition to the events within the actual engine. This was especially useful for the numerous logic based statements, which were relatively simple calculations that would have a big influence on the final results. A good example was the flow through the valves, which could be forward or reverse and choked or unchoked flow. The spreadsheet would for example present 'fc' for choked forward flow or 'ru' for unchoked reversed flow through the valves in one column and then calculate the numerical value in the neighbouring column. This method helps confirm that the logic and numerical result was correct.

The few remaining columns and cells within Excel were checked manually by calculator.

APPENDIX V

INJECTOR COMPARISON

V-1 Injector comparison

A comparison between the spray characteristics of the two injectors was performed on behalf of the author by a fellow researcher Zane van Romunde, which provided the author with otherwise unobtainable information. The two injectors compared were the green Denso side fed injector from the AJ26 cylinder head and the blue 12-hole Denso injector used on the AJ33 AP and CP cylinder heads. In this appendix they will simply be referred to as the green and blue injectors.

Several aspects of injector performance were compared, including penetration distance, penetration rate, cone angle and droplet size. By setting the injection duration of both injectors at 5 ms, a thorough study of initial spray development, main spray and final spray could be performed. Images were then taken every 0.5 ms after the SOI trigger pulse up to 10 ms after SOI, enabling a movie to be generated when the images were shown in quick succession. This movie is included in the CD attached at the end of this thesis. Figure V-a illustrates the quality of the two sprays by showing images of the two sprays at four different times during the injection event. The green injector produced a poor quality spray containing visually large droplets, while the blue injector produced a spray with many tiny droplets that were too small to measure visually. By scaling distances from the injector tip that was visible in the images, calculation of distances could be performed. To further the study, the pressure across the injector was also varied. The working pressure of the green injector was 3 bar and the injector was tested at pressures of 2.75, 3, 3.25 and 3.5 bar. The working pressure of the blue injector was 3.8 bar and the injector was tested at pressures of 3.5, 3.8 and 4.1 bar. Figures V-b and V-c show the penetration distance and penetration rate of the sprays from the two injectors. The penetration distance of the spray, was the distance from the injector tip to the leading edge of the spray, where an increase in pressure increased the penetration distance. The penetration rate was interesting as it showed the leading droplets from the blue injector accelerated quickly, but were slowed down by air resistance due to their small size. The larger leading droplets of the green injector were not measurably affected by the air resistance and continued at their initial velocity due to their higher momentum. Since neither injector produced a clear cone spray, measurement of the cone angle was found to be extremely difficult and the results are not reported here.

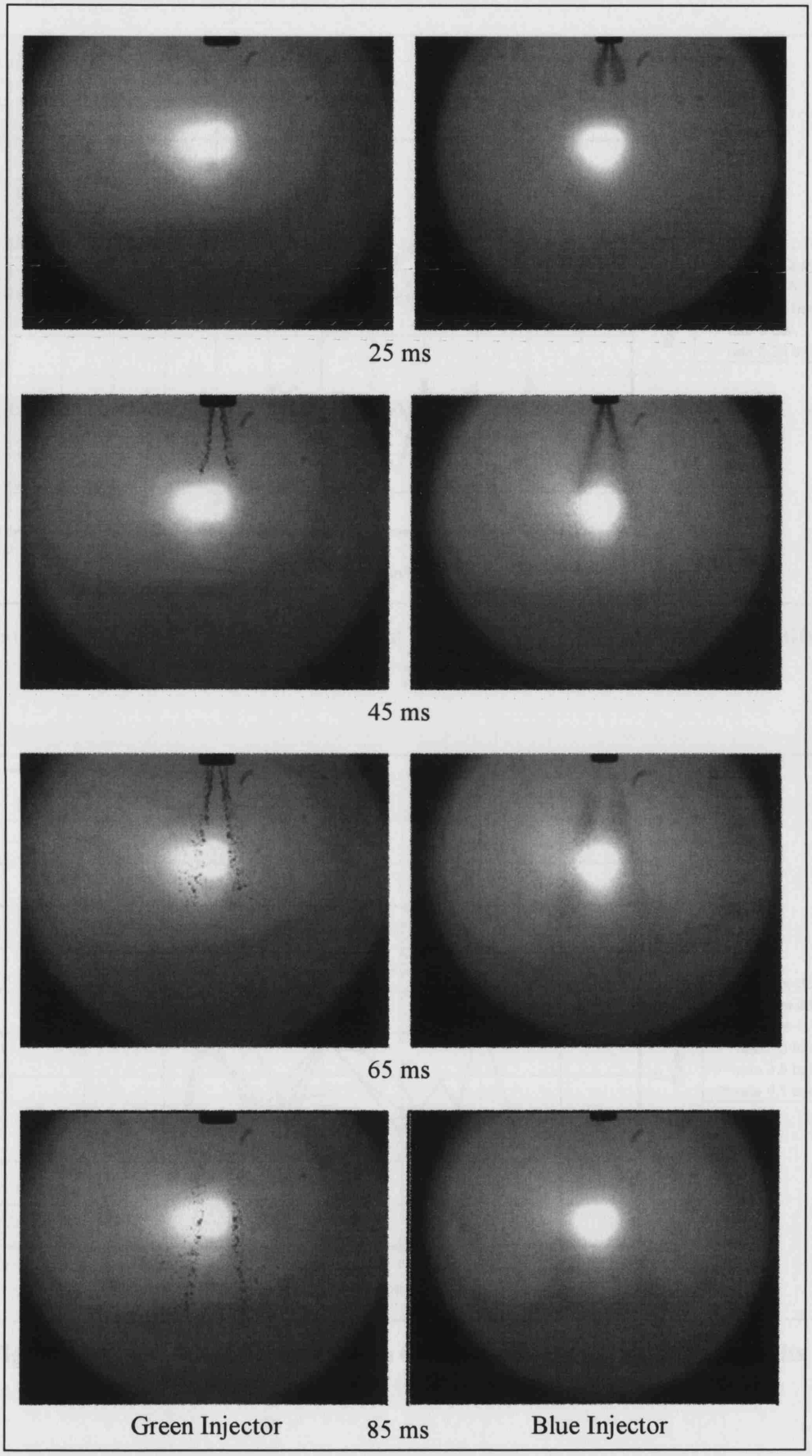

Figure V-a Propagation of the green and blue injector spays with gasoline at four ASOI timings

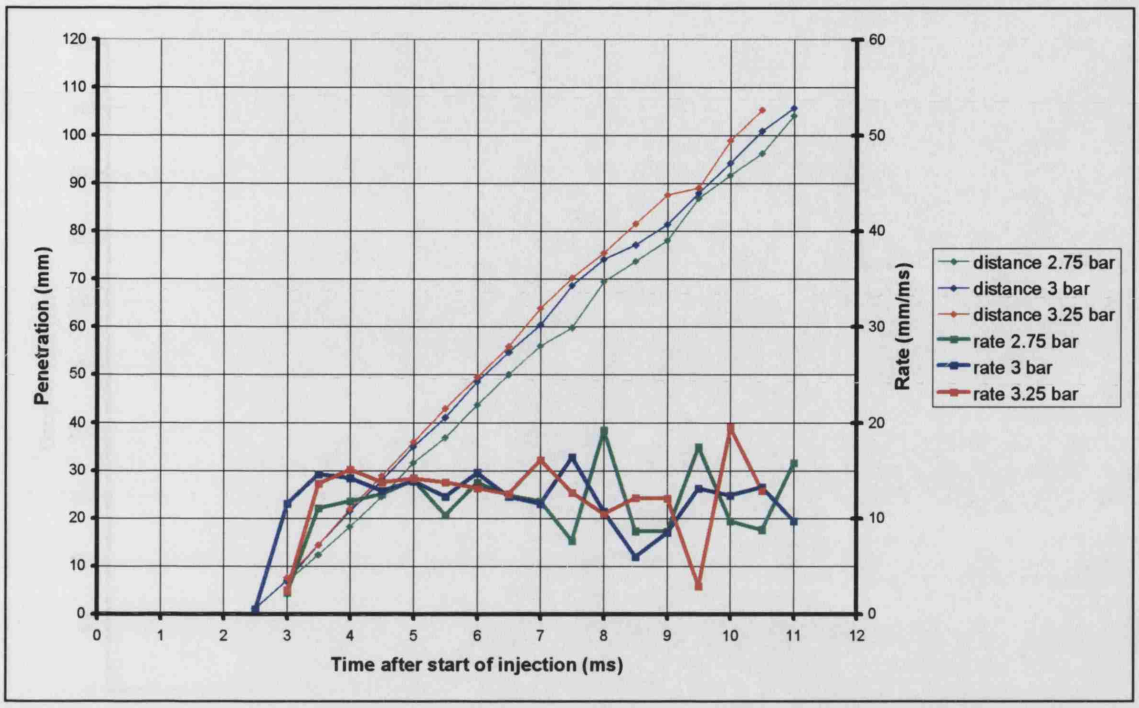

Figure V-b Green injector penetration distance and penetration rate results

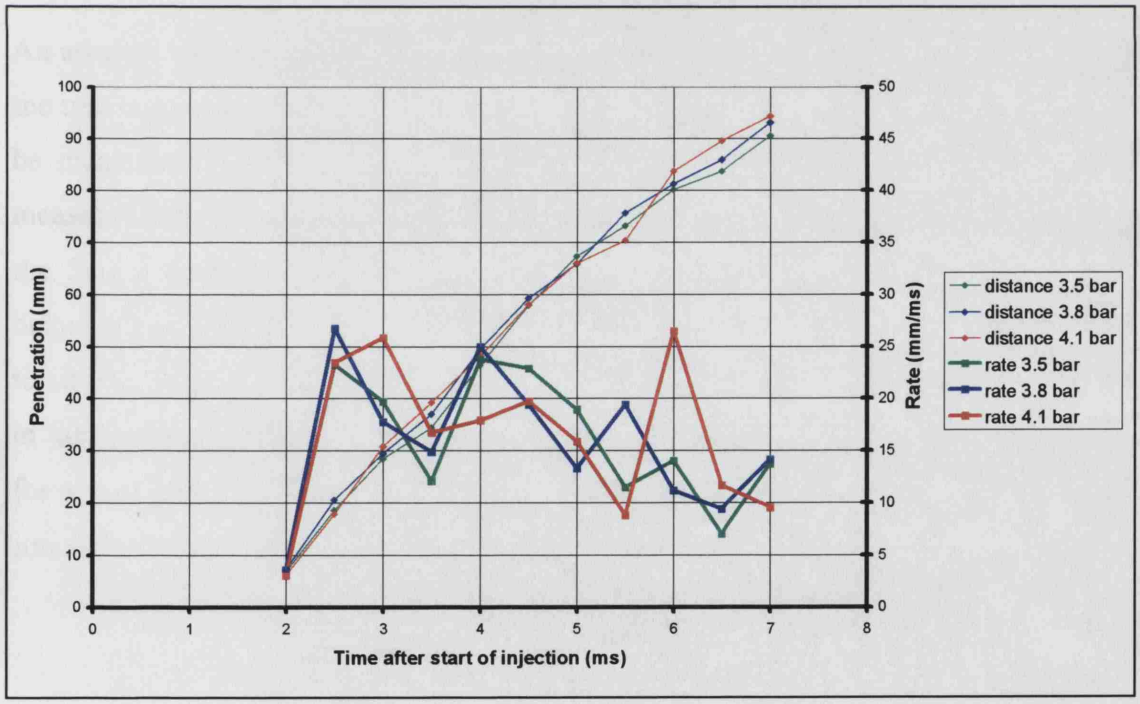

Figure V-c Blue injector penetration distance and penetration rate results

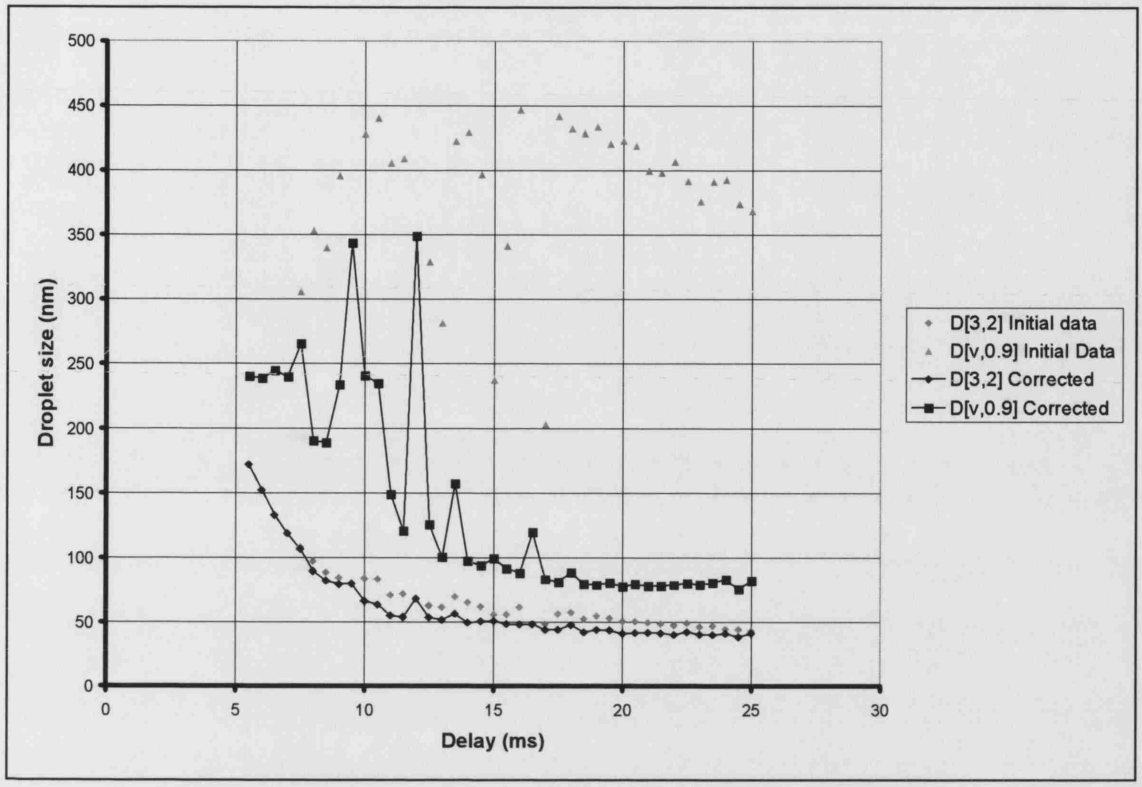

Figure V-d Blue injector droplet sizing results with gasoline

An attempt was made by Romunde to measure the droplet size distribution produced by the two injectors. It was found that the droplets from the green injector were too large to be measured by the particle sizer, but the droplets from the blue injector could be measured and the results are shown in Figure V-d. The two sizing parameters used were the Sauter mean diameter of the droplets as denoted by D[3,2] and the droplet size below which 90% of the droplet population lies, as denoted by D[v,0.9]. The data used to obtain the presented results was adjusted to compensate for the effect of evaporation in the measured spray [Williams (1994)]. The results show extremely good atomisation for a port fuel injector at such low fuel pressure, with the Smd of the spray around 50 μm and the corresponding D[v,0.9] below 100 μm.